EFFECT OF SPEED ON TIRE-SOIL INTERACTION AND DEVELOPMENT OF TOWED PNEUMATIC TIRE-SOIL MODEL

Leslie L. Karafiath, et al

Grumman Aerospace Corporation

Prepared for:

Army Tank-Automotive Command

October 1974

UNCLASSIFIED

SECURITY CLASSIFICATION OF THIS PAGE (When Data Entered)

REPORT DOCUMENTATION PAGE	READ INSTRUCTIONS BEFORE COMPLETING FORM
1. REPORT NUMBER: Technical Report 11997 (LL151)	2. GOVT ACCESSION NO. / 3. RECIPIENT'S CATALOG NUMBER: AD-A003 985
4. TITLE (and Subtitle): Effect of Speed on Tire-Soil Interaction and Development of Towed Pneumatic Tire-Soil Model	5. TYPE OF REPORT & PERIOD COVERED: Final
	6. PERFORMING ORG. REPORT NUMBER: RE-500
7. AUTHOR(s): Leslie L. Karafiath, Frank S. Sobierajski	8. CONTRACT OR GRANT NUMBER(s): DAAE07-74-C-0002, DAAE07-74-C-0204
9. PERFORMING ORGANIZATION NAME AND ADDRESS: Grumman Aerospace Corporation, Research Department, Bethpage, New York 11714	10. PROGRAM ELEMENT, PROJECT, TASK AREA & WORK UNIT NUMBERS: 6.11.02A, 1T161102B52A, 347EH
11. CONTROLLING OFFICE NAME AND ADDRESS: US Army Tank-Automotive Command, RD&E Directorate, Engineering Science Division, Warren, Michigan 48090	12. REPORT DATE: October 1974
	13. NUMBER OF PAGES: 285 / 197
14. MONITORING AGENCY NAME & ADDRESS (If different from Controlling Office)	15. SECURITY CLASS. (of this report): UNCLASSIFIED
	15a. DECLASSIFICATION/DOWNGRADING SCHEDULE

16. DISTRIBUTION STATEMENT (of this Report)
Approved for public release; distribution unlimited.

17. DISTRIBUTION STATEMENT (of the abstract entered in Block 20, if different from Report)

18. SUPPLEMENTARY NOTES
None

19. KEY WORDS (Continue on reverse side if necessary and identify by block number)
Mathematical Models.
Tire-Soil Interaction.

20. ABSTRACT (Continue on reverse side if necessary and identify by block number)

The role of soil inertia forces and the effects of strain rate in tire-soil interaction are analyzed. The differential equations of plasticity for soils are expanded to include soil inertia forces. Two methods are developed for the determination of inertial accelerations in tire-soil interaction. In the first method the theory of velocity fields is applied for the determination of accelerations imparted to soil particles by a tire traveling at

DD FORM 1 JAN 73 1473 EDITION OF 1 NOV 65 IS OBSOLETE

UNCLASSIFIED

SECURITY CLASSIFICATION OF THIS PAGE (When Data Entered)

constant velocity. An iterative scheme is developed that successively updates the geometry of slip line fields for velocity increments and associated inertia forces. In the second method soil particle accelerations are computed on the basis of particle path geometry. An analytical form of the particle path is assumed and related to the time events of tire travel. Computations by both methods indicate that the solution of the differential equations of plasticity for soil becomes multivalued at a relatively low travel velocity. Up to this velocity, tire-soil interaction is not significantly affected by soil inertia forces. Beyond this velocity the multivaluedness of solutions of the differential equations indicates a condition that has not been explored yet for its effect on soil behavior and cannot be treated by present theories.

The effect of strain rate of soil strength properties is analyzed and recognized as the major contributor to the improvement of tire performance with speed.

A mathematical model for towed pneumatic tires and soil is developed for the simulation of towed tire-soil interaction. Towed force coefficient predictions are compared with experimental results.

RE-500

EFFECT OF SPEED ON TIRE-SOIL INTERACTION
AND
DEVELOPMENT OF TOWED PNEUMATIC TIRE-SOIL MODEL

by

Leslie L. Karafiath

and

Frank S. Sobierajski

Prepared Under Contracts

DAAE07-74-C-0002 and DAAE07-74-C-0204

for

United States Army Tank-Automotive Command
Warren, Michigan

by

Research Department
Grumman Aerospace Corporation
Bethpage, New York 11714

October 1974

Approved by: Charles E. Mack

Charles E. Mack, Jr.
Director of Research

FOREWORD

Simulating the interaction of terrain, vehicle, and man is essential to improving land mobility technology — a goal of the U.S. Army Tank-Automotive Command (TACOM) and the U.S. Army Corps of Engineers Waterways Experiment Station (WES). Under TACOM contract, Grumman has been actively supporting this effort and completed the development of a first generation mathematical model for driven rigid wheel and pneumatic tire-soil interaction. This model, conceived as an alternate submodel in the terrain-vehicle-man simulation, called the AMC Vehicle Mobility Model, allows the computation of tire performance in both purely frictional or cohesive and frictional-cohesive soils.

This first generation mathematical model is based on the concept of "steady state" in the soil that assumes a low and constant velocity of travel. Observations in the laboratory and in the field indicate that tire performance improves with travel velocity under certain conditions.

To take this factor into account in mobility evaluation and take advantage of it in off-road vehicle development it is necessary to analyze the effects of soil inertia and loading rates on tire-soil interaction. In a follow-on program to the development of a first generation pneumatic tire-soil model, the results of which are presented in this program, the model was expanded to include soil inertia forces. The effects of the loading rate were analyzed by adjusting the strength properties of soil for the strain rate corresponding to the travel velocity of the tire. The expanded model was also shown to be suitable for the determination of spring constants that can be applied in vehicle dynamic models.

For the analyses of cross country mobility of trailer-mounted weapons, a towed tire-soil model is needed that predicts the motion resistance and sinkage of towed pneumatic tires. The basic concepts of tire-soil interaction were applied to the case of towed tire and an appropriate model, described in the second part of this report, has been developed.

ABSTRACT

The role of soil inertia forces and the effects of strain rate in tire-soil interaction are analyzed. The differential equations of plasticity for soils are expanded to include soil inertia forces. Two methods are developed for the determination of inertial accelerations in tire-soil interaction. In the first method the theory of velocity fields is applied for the determination of accelerations imparted to soil particles by a tire traveling at constant velocity. An iterative scheme is developed that successively updates the geometry of slip line fields for velocity increments and associated inertia forces. In the second method soil particle accelerations are computed on the basis of particle path geometry. An analytical form of the particle path is assumed and related to the time events of tire travel. Computations by both methods indicate that the solution of the differential equations of plasticity for soil becomes multivalued at a relatively low travel velocity. Up to this velocity, tire-soil interaction is not significantly affected by soil inertia forces. Beyond this velocity the multivaluedness of solutions of the differential equations indicates a condition that has not been explored yet for its effect on soil behavior and cannot be treated by present theories.

The effect of strain rate of soil strength properties is analyzed and recognized as the major contributor to the improvement of tire performance with speed.

A mathematical model for towed pneumatic tires and soil is developed for the simulation of towed tire-soil interaction. Towed force coefficient predictions are compared with experimental results.

ACKNOWLEDGMENT

The work reported herein was performed for the Mobility Systems Laboratory of the U.S. Army Tank-Automotive Command (TACOM), Warren, Michigan, under the general supervision of Dr. Jack G. Parks, Chief of the Engineering Science Division and Mr. Zoltan J. Janosi, Supervisor, Research and Methodology Function. Mr. Zoltan J. Janosi was also technical monitor. Their help and valuable suggestions in carrying out this work are gratefully acknowledged.

In the development of the towed tire-soil model use was made of computer techniques, developed in an independent research program, that allows running of large programs on minicomputers. Acknowledgment is due to Mr. R. McGill, head of the Grumman Research Department's Computer Sciences Group, who made the necessary provisions in the program for its accommodation on the minicomputer.

TABLE OF CONTENTS

LIST OF ILLUSTRATIONS

LIST OF TABLES

LIST OF SYMBOLS

A	singular point
A,B,C,D,E	characteristic points along particle paths and slip line field boundaries
$a_{x,z}$	acceleration in the x,z direction
a	constant in particle path equation
B,b	width of tire
c	cohesion
c_1, c_2	constants in particle path equation
CGR	cone index gradient
CI	cone index
D,d	diameter
e	base of natural logarithm
F_δ	ratio of max. interface friction angle to friction angle
F_τ	factor in towed tire model
h	height of tire cross section
i,j	slip line and nodal point designations
k	constant in slip - developed friction equation [Eq. (15)]
ℓ	length of contact area
L	load, length of passive zone of slip line field, travel distance
N_c	clay numeric
N_s	sand numeric

p_i	inflation pressure
p_l	limit pressure
q	normal stress
R	radius of undeflected tire
r	radius of deflected tire
s	slip
s'	contact slip
s_o	constant in slip-developed friction angle equation [Eq. (15)]
t	time
t_o	initial time
v	velocity
v_f	forward velocity
v_n	normal component of velocity
v_p	peripheral velocity (perpendicular to radius)
v_t	tangential velocity
v^α, v^β	velocity vector along α,β lines
v^s	velocity of soil particle
x,z	coordinates
α	central angle (measured from vertical)
α_e	entry angle
α_m	angle of separation
α_o	angle of zero shear stress
α_r	rear angle
α'	angle defining start and end of tire deflection

γ	unit weight of soil
δ	angle of inclination of resultant stress to normal, angle of shear mobilization, deflection in Waterways Experiment Station terminology
ϵ	deflection coefficient
θ	angle between x axis and major principal stress
$\varkappa$	$1 - 2\delta/d$
μ	$\pi/4 - \varphi/2$
ρ_1, ρ_2	constants in particle path equation
ζ	ρ_1/ρ_2
σ	$(\sigma_1 + \sigma_3)/2 + \psi$
σ_n	normal stress
$\sigma_{1,3}$	principal stresses
τ	shear stress/shear strength
τ_{max}	maximum available shear strength
τ_{mob}	mobilized shear strength
φ	angle of internal friction
ψ	c cot φ
ω	angular velocity, parameter in particle path equation

I. SCOPE OF WORK

The scope of work as described in the RFP work statements for Contracts DAAE07-74-Q-0004 and C-0204 was twofold: investigate the effect of speed on tire-soil interaction and develop a towed pneumatic tire-soil model. Within this general scope emphasis was placed on the following items:

- Expansion of plasticity theory for soils to include soil inertia forces
- Development of methods for the determination of inertia accelerations of soil particles caused by tire travel
- Analysis of soil inertia and strain rate effects on tire-soil interaction
- Development of a towed tire-soil model with consideration of interface stress distributions resulting in zero torque condition
- Verification of the towed tire-soil model by comparisons of predicted towed force coefficients with available experimental data.

II. EFFECT OF SPEED ON TIRE-SOIL INTERACTION

At present, tire-soil interaction theories are based on a quasi-static model that assumes a steady state of the tire-soil system. The tire is assumed to travel at a sufficiently low velocity so that velocity effects are negligible. Yet experiments performed under controlled conditions at WES (Ref. 1) show that even in the low velocity range of off-road travel, velocity effects are far from negligible. In the higher velocity range of aircraft landing gear-soil interaction velocity is one of the main controlling factors that affects the drag load as experiments indicate (Refs. 2 and 3).

Velocity affects tire-soil interaction primarily in the following two ways:

- Soil inertia forces are generated in the soil during the passage of a tire. The magnitude of these inertia forces depends on the velocity of the tire and is approximately proportionate with the square of the velocity of the tire.
- The strength of the soil that controls the interface stresses is affected by the rate of loading that is directly proportionate to the velocity of travel.

Secondary effects of velocity on tire-soil interaction may include the increase of tire stiffness with an increase of the angular velocity of tire, the effects of velocity on interface friction development, etc. No study of these effects was made in the present research project.

III. EFFECT OF SOIL INERTIA FORCES ON TIRE-SOIL INTERACTION

The concept of tire-soil interaction presented in Ref. 4 for driven tires and Section VIII of this report for towed tires assumes that the soil is in the plastic state of equilibrium, characterized by slip line fields, whenever the normal stress corresponding to this plastic state of stresses is less than the limiting pressure characteristic of the tire. The geometry of the zones of plastic equilibrium and the stress states in these zones are defined by solutions of the differential equations of plasticity for soils. These differential equations are derived from the combination of the differential equations of static equilibrium with the Mohr-Coulomb yield criterion.

The passage of a tire, even if it travels at a constant velocity, displaces soil particles within the affected soil mass. The end result of soil particle displacement is the formation of a rut behind the tire. Thus, during the passage of the tire a soil particle moves from its original position at rest to a new one where it comes to rest again. This particle motion involves acceleration and deceleration of the particle and, as a consequence, inertia forces are generated in the soil. To consider these inertia forces in the differential equations of plasticity for soil, the Mohr-Coulomb yield criterion has to be combined with the differential equations of motion instead of those of static equilibrium. This combination, after the same manipulation of the equations is performed as in the static case, yields the following differential equations:

$$dz = dx \tan(\theta \mp \mu) \tag{1}$$

$$d\sigma \mp 2\sigma \tan \varphi d\theta = \frac{\gamma}{g}\left[\left(a_x \mp (a_z + g)\tan \varphi\right)dx + (a_x + g \pm a_z \tan \varphi)dz\right]$$

In these equations x and z refer to a coordinate system that moves with the tire, whereas a_x and a_z denote soil particle accelerations that refer to a fixed coordinate system. The motion of soil particles as well as their accelerations are closely related to the geometry of slip line fields. Since this latter itself depends on the particle accelerations, as Eq. (1) indicates, therefore, there is an interdependence between the accelerations and other variables in Eq. (1). Even if a functional relationship could be established among these variables, the direct numerical solution of Eq. (1) would be a formidable task because of the inherent nonlinearities in these relationships. In an attempt to develop a method that yields an acceptable approximate solution of Eq. (1), two approaches have been followed and investigated in detail. In the first, essentially theoretical approach the theory of velocity fields associated with the slip line fields is applied to the determination of particle accelerations. The second approach is based on an analytical simulation of observed particle path geometries and is, therefore, a semi-empirical one. A detailed discussion of these approaches together with an evaluation of the numerical computational procedures developed for their application to the tire-soil interaction problem is given in the following sections.

IV. DETERMINATION OF SOIL INERTIA FORCES BY THE THEORY OF VELOCITY FIELDS

Theoretical Background

Originally, the theory of velocity fields was developed in connection with the application of the theory of plasticity to metal forming processes. For metals the angle of internal friction is zero and the characteristics obtained from the solutions of the differential equations for both the velocities and the stresses coincide. In the plastic state, frictionless materials actually slip along the characteristic line; hence the term "slip line field."

The theory of velocity fields was later extended for materials exhibiting friction, such as soils. The purpose of this extension was, however, not so much to determine the flow of the material, as in the case of metal forming processes, but to enable researchers to apply the limit theorems of plasticity to various problems of the plastic equilibrium in soils. The limit theorems of plastic equilibrium state that a statically admissible stress field, derived from the differential equations of the plasticity theory, yields a lower bound for the collapse load, while collapse loads computed for various kinematically admissible velocity fields yield upper bound solutions. The true solution is when the lower and upper bounds coincide.

The significance of the limit theorems of plasticity in engineering applications is that the collapse load (or failure stresses) may be higher than that computed from stress fields if the geometry of the stress fields is kinematically inadmissible.

Derivation of the differential equations of velocity fields is based on the assumption that the strain rate is proportional to

the time rate of stress (Refs. 5 through 12). A system of partial differential equations similar to that of the stress equations can then be derived. The solutions of this set of hyperbolic differential equations are the characteristics of the velocity field. Generally, the kinematic boundary conditions are insufficient to define the velocity field and, therefore, the usual procedure is to analyze the geometries of stress fields for kinematic admissibility. If, however, for a frictional material the characteristics of the velocity field are assumed to coincide with those of the stress field, the strain rates associated with the velocity fields require a rate of dilation of the soil that is unrealistic. Various theories have been proposed to deal with this problem but none of them is completely satisfactory. It is outside the scope of this report to discuss these controversial issues in detail; regarding the use of velocity fields for the determination of soil inertia forces in tire-soil interaction problems the following considerations apply:

- If the stress boundary conditions are such that they uniquely determine the stress field then the problem is statically determinate, the characteristics of the velocities coincide with those of the stresses. The solution is the true solution since upper and lower bounds are identical (Ref. 11).

- In tire-soil interaction problems boundary conditions completely define the stress field, therefore, the solution is statically determinate and it is the true solution. However, the assumption of a uniform development of interface friction along the contact area, although to some extent supported by experiments, is an arbitrary one.

Since interface friction depends on the kinematic boundary conditions at the interface, the solution of Eq. (1) is the true solution only, if the assumed interface friction distribution is compatible with the kinematic boundary conditions. The establishment of the kinematic boundary conditions at the interface is also necessary for the computation of velocities and is discussed in detail under that heading.

- In the following analyses it is assumed that the characteristics of stress and velocity fields coincide. Although this assumption is associated with an unrealistic rate of dilation, in the case of tire-soil interaction problems the velocity field is an instantaneous one, and the dilation prevails only for an infinitesimal time. Also, the tire-soil models used for the calculation of tire performance assume a steady state in soil where the soil is already compacted by the tire action to a significant degree. Therefore, the soil is likely to dilate under the yield stresses.

In summary, flow fields in tire-soil interaction are maintained for an infinitesimal time, therefore, the rate of dilation is not a critical consideration and the characteristics of stress and velocity fields may be assumed to coincide. If the geometry of the characteristics is computed from the equations for the stress field then the velocities can be computed from the following equations (Ref. 10).

$$dv^{\alpha} + (v^{\alpha} \tan \varphi + v^{\beta} \sec \varphi) d\theta^{\alpha} = 0^{\dagger}$$

$$dv^{\beta} - (v^{\alpha} \sec \varphi + v^{\beta} \tan \varphi) d\theta^{\beta} = 0 \qquad (2)$$

The above equations define the variation of velocities along characteristic lines. The velocity vectors v^{α} and v^{β} are components (projections) of the velocity vector $\bar{v}$ in the direction of the "j" and "i" lines, respectively. It is noted that the vectorial sum of v^{α} and v^{β} is not $\bar{v}$ (Fig. 1).

The v_x and v_z components of the velocity vector, $\bar{v}$, are related to v^{α} and v^{β} as follows

$$v^{\alpha} = v_x \sin \theta^{\alpha} - v_z \cos \theta^{\alpha}$$

$$v^{\beta} = v_x \sin \theta^{\beta} - v_z \cos \theta^{\beta} \qquad (3)$$

Since it is assumed that the velocity and stress characteristics coincide, the angles θ_i and θ_j may be determined from the stress field relation

$$\theta^{\alpha} = \theta + \left(\frac{\pi}{4} - \frac{\varphi}{2}\right)$$

$$\theta^{\beta} = \theta - \left(\frac{\pi}{4} - \frac{\varphi}{2}\right) \qquad (4)$$

For the numerical computation of the velocities the geometry of the characteristic lines as well as the θ values are computed for the stress field and the velocities from the following difference equations:

$^{\dagger}\alpha$ and β are superscripts designating slip lines

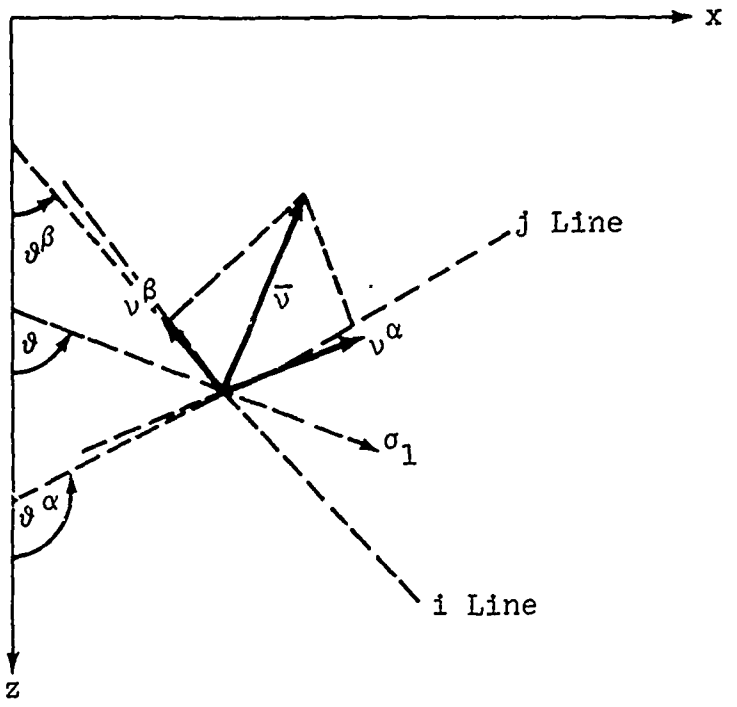

Fig. 1. Velocity Vectors Along Characteristic Lines.

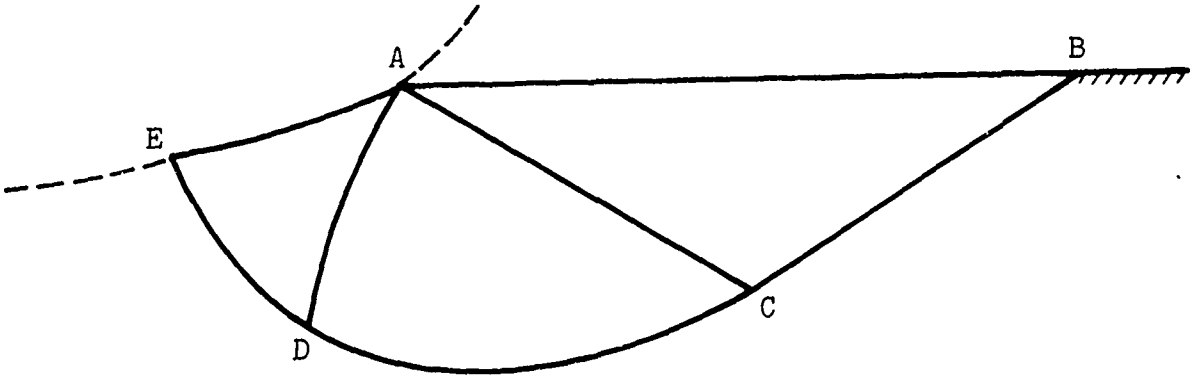

Fig. 2. Boundaries of a Slip Line Field in Tire-Soil Interaction Problems

$$v^{\alpha}_{i,j} = (A - B \cdot C)/(1.0 - B \cdot D)$$

$$v^{\beta}_{i,j} = C - D \cdot v^{\alpha}_{i,j}$$

where

$$A = \frac{v^{\alpha}_{i+1,j} - \frac{1}{2}v^{\alpha}_{i+1,j} \tan \varphi(\theta_{i,j} - \theta_{i+1,j})}{1 + \frac{1}{2} \tan \varphi(\theta_{i,j} - \theta_{i+1,j})}$$

$$B = \frac{\frac{1}{2} \sec \varphi(\theta_{i,j} - \theta_{i+1,j})}{1 + \frac{1}{2} \tan \varphi(\theta_{i,j} - \theta_{i+1,j})} \qquad (5)$$

$$C = \frac{v^{\alpha}_{i,j+1} + \frac{1}{2}v^{\alpha}_{i,j+1} \sec \varphi(\theta_{i,j} - \theta_{i,j+1})}{1 - \frac{1}{2} \tan \varphi(\theta_{i,j} - \theta_{i,j+1})}$$

$$D = \frac{\frac{1}{2} \sec \varphi(\theta_{i,j} - \theta_{i,j+1})}{1 - \frac{1}{2} \tan \varphi(\theta_{i,j} - \theta_{i,j+1})}$$

The difference equations (5) indicate that for given stress field characteristics the velocity for a grid point i,j can be computed if the velocities at two adjacent points ($i+1,j$ and $i,j+1$) are known. The kinematic boundary conditions, discussed under the next heading, provide the initial values of velocities necessary to start the numerical computations.

Kinematic Boundary Conditions

In a slip line field determined by the differential equations of plasticity for soils by methods discussed in detail in Refs. 13 through 18 there are three boundaries where kinematic boundary conditions are to be examined (Fig. 2). At the stress free surface AB it is assumed that there are no kinematic constraints and

points at the surface may be displaced freely. The boundary BCDE is the outermost slip line beyond which the soil is not in the state of failure. Implicit in the use of the Mohr-Coulomb yield criterion is that soil deformations prior to yield are disregarded, therefore, in this concept the soil beyond the outermost slip line acts as a rigid body. Consequently, velocities across this boundary must be zero, resulting in the kinematic boundary condition $v^{\beta} = 0$ for this line. For this boundary condition Eq. (5) is integrable and yields

$$v^{\alpha} = v_o^{\alpha} \cdot e^{\tan \varphi(\theta^{\alpha}-\theta_o^{\alpha})} \tag{6}$$

Note that for the stress computations the state of the soil outside the slip line field is immaterial. The velocity field, however, is profoundly affected by the assumption that the soil adjacent to the outermost slip line is assumed to be rigid. Experimental information on soil displacements along this boundary is scarce. It appears that while the soil mass outside this boundary undoubtedly undergoes some deformation there is an abrupt change in the displacements in a narrow band along the boundary. Thus, the theoretical boundary condition corresponding to the rigid-plastic material idealization may not be too far off from reality.

As stated before, the critical kinematic boundary conditions are those at the tire-soil interface. The distribution of interface friction along this boundary must be consistent with the kinematic conditions there if the slip line field solution is to be the true solution for the yield stresses. As a result of detailed studies of the kinematic conditions at the interface, new concepts of slip and interface friction were developed. These are not only useful for the definition of boundary conditions for velocity fields but

also offer new insight in the not very well understood area of slip-interface friction relationships. The results of these kinematic analyses and the reasoning that led to the development of these new concepts regarding interface friction are presented in the following discussions.

The kinematics of a point attached to the surface of the tire are easily determined if the geometry of the tire centerline and the angular and translational velocities of the tire are known. The trajectory of such a point, in a fixed coordinate system is shown in Fig. 3 for a complete revolution of a slipping tire. The

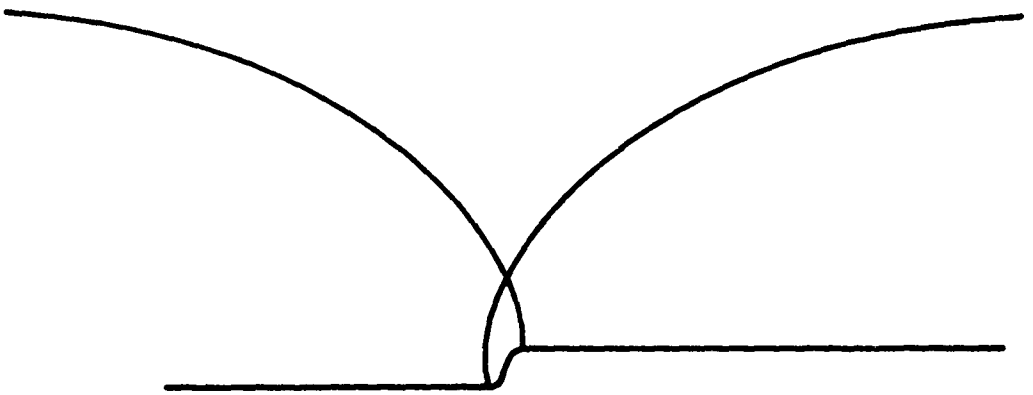

Fig. 3. Trajectory of a Point at the Circumference of a Deformable Tire

point describes a prolate cycloid when its position is in the undeflected part of the tire; otherwise the trajectory is an irregular curve corresponding to the assumed tire deflection. The horizontal and vertical components of the velocity of the point may also be easily determined since both the angular and translational velocities are assumed to be constants.

For the determination of the velocity boundary conditions that apply to the slip line field in the soil the velocities imparted to a soil particle at the interface are needed. These are related to the velocities of a point attached to the tire surface

but are by no means identical. A fundamental aspect of the analysis of the kinematic conditions at the interface is that the interface must be considered as consisting of two faces: one being the surface of the tire, the other that of the soil. It is assumed that these two faces of the interface may slide on, but may not separate from each other. This latter assumption leads to the condition that the normal components of the velocities of the two faces be the same at every point. This condition, however, is by itself insufficient for the determination of soil particle velocities at the interface. The additional assumption is made that the direction of the velocity vector of a soil particle coincides with the direction of the major principal stress in the slip line field. For homogeneous isotropic soils with linear stress-strain relations this assumption follows from the theorems of continuum mechanics; for soils not meeting the above criteria strictly the assumption is only approximately valid. With these assumptions the velocities of soil particles at the interface (that constitute the velocity boundary conditions) can be determined as follows.

The velocity vector for a point at the tire surface may be determined by vectorially adding the forward velocity vector $(\bar{v}_f)$ and the tangential velocity vector $(\bar{v}_t)$ (Fig. 4a). The tangential velocity vector is the component of vector $\bar{v}_p$ (peripheral velocity) in the direction of the deflected surface of the tire

$$v_p = \omega r = v_f/(1 - s)$$

$$v_t = v_p \cos(\alpha - \alpha') \tag{7}$$

The horizontal and vertical components of the resultant velocity vector are

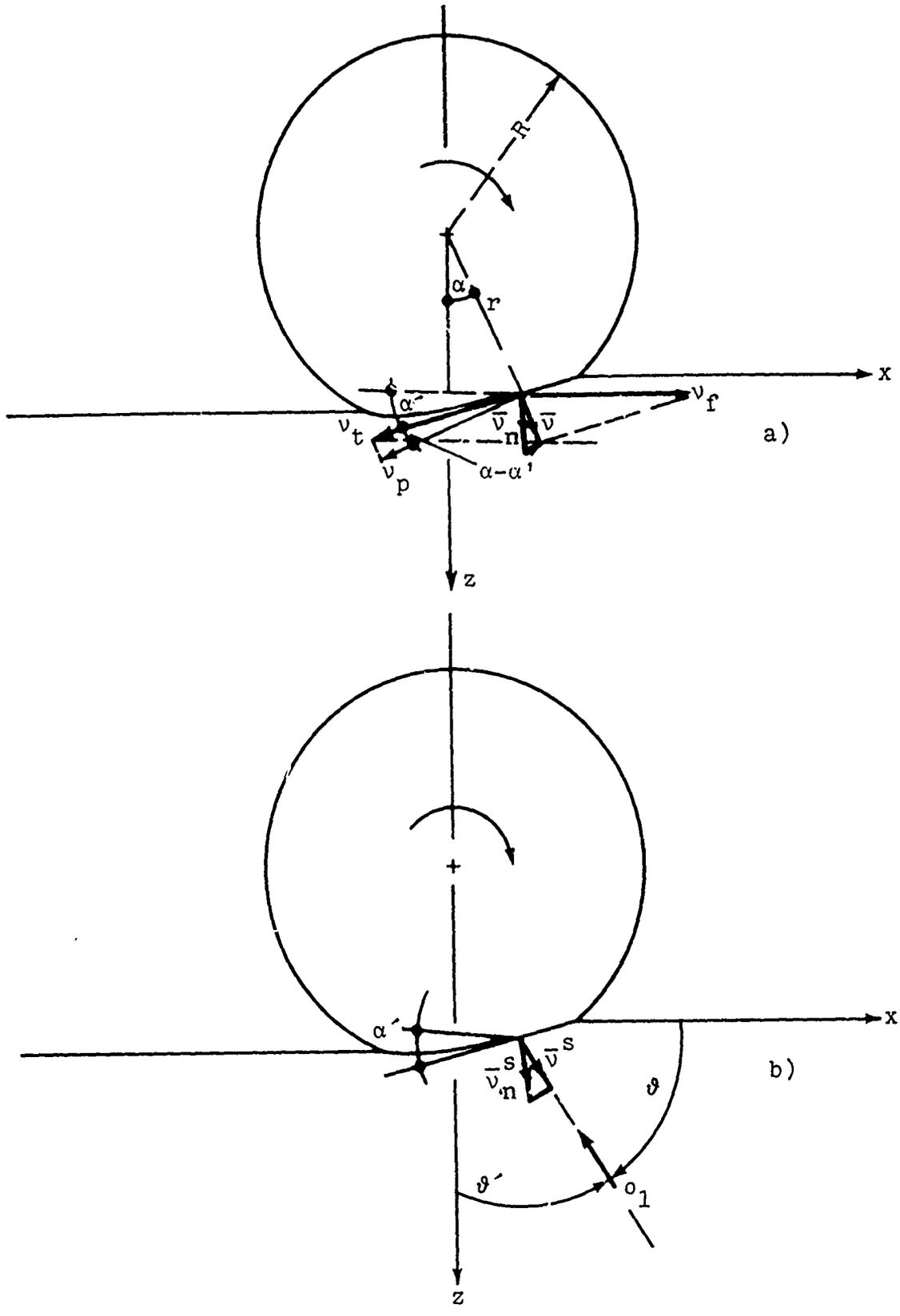

Fig. 4. Kinematic Boundary Conditions at the Tire-Soil Interface.
a) For the Tire b) For Soil

$$v_x = v_f - v_p \cos(\alpha - \alpha')\cos \alpha'$$

$$v_z = v_p \cos(\alpha - \alpha')\sin \alpha' \tag{8}$$

$$v_n = v_x \sin \alpha' + v_z \cos \alpha' = v_f \sin \alpha'$$

This last equation expresses the fact that the component of the velocity vector normal to the deflected surface of the tire depends only on the forward velocity and is independent of slip.

For a soil particle at the interface the normal component of the velocity vector can be computed as (Fig. 4b)

$$v_n^s = v_x^s \sin \alpha' + v_z^s \cos \alpha' = v_f \sin \alpha' \tag{9}$$

$$\frac{v_x^s}{v_z^s} = \tan \theta'$$

From Eq. (8) the horizontal and vertical components of the velocity vector can be expressed as

$$v_x^s = v_f \frac{\sin \alpha'}{\sin \alpha' + \operatorname{cotan} \theta' \cos \alpha'} \tag{10}$$

$$v_z^s = v_x^s \operatorname{cotan} \theta'$$

The velocity vector of a soil particle at the interface can also be thought of as being composed of the forward velocity vector and a tangential velocity vector. This latter can be computed from the following equation:

$$v_t^s = v_f \frac{1}{\sin \alpha' \tan \theta' + \cos \alpha'} \tag{11}$$

---

† Superscript s designates soil particle velocities

The tangential velocity computed by Eq. (11) for a soil particle is in the case of driven tires generally less than the tangential velocity computed by Eq. (7) for a point at the surface of the tire indicating that a relative displacement occurs between the soil and the tire. From the value of the tangential velocity of a soil particle a hypothetical slip value may be computed as

$$s' = 1 - \cos(\alpha - \alpha') \cdot (\sin \alpha' \tan \theta' + \cos \alpha') \qquad (12)$$

It is interesting to note that this hypothetical slip value is independent of the translational velocity of the tire, at least for the assumed steady state concept of tire-soil interaction.

At this point it is worthwhile to consider the meaning of the hypothetical slip value determined by Eq. (12). If the tire actually turned with an angular velocity that resulted in a slip equal to s' then there would be no differential displacement between the surface of the tire and the soil. Therefore, the hypothetical slip s' may be termed as "contact slip." On the other hand, the difference between s and s' is the result of differential displacement between tire surface and soil. The term "spin" conveys the idea of a tire rotating relative to a nonyielding surface and is also expressive of the relative motion between a tire and a yielding surface, therefore it will be used herein to designate the quantity $s - s'$.

To further elucidate the meaning and significance of these terms a track element may be considered (Fig. 5a). If a track element displaces the soil by ΔL but stays in contact with the soil while the vehicle travels a distance L then the "contact slip" is

$$s' = \left(1 - \frac{L - \Delta L}{L}\right) = \frac{\Delta L}{L} \qquad (13)$$

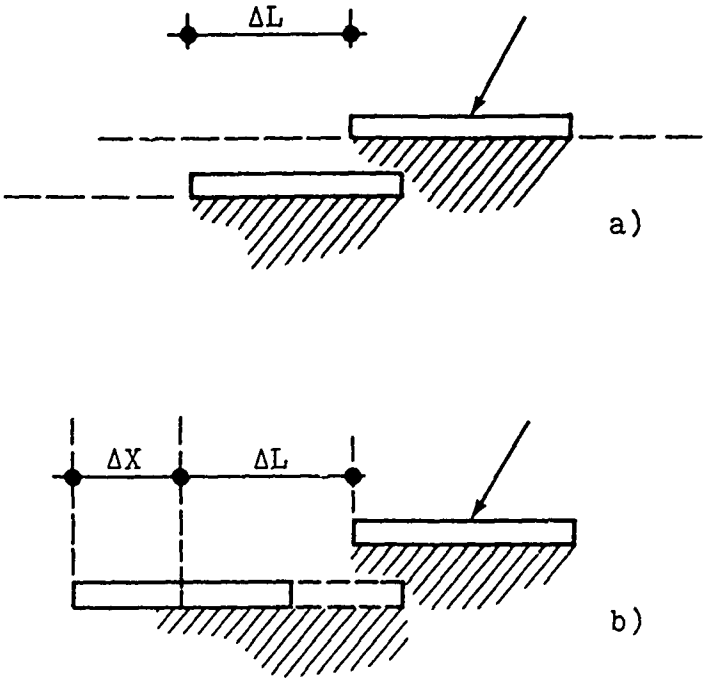

Fig. 5. Contact Slip (a) and Total Slip (b) of a Track Element

However, if the track element slides over the soil and at the end of vehicle travel L is displaced by ΔX relative to its original position (Fig. 5b) then the total slip is

$$s = \frac{\Delta X + \Delta L}{L} \tag{14}$$

In the case of a track element it is easy to visualize the meaning of the two slip values s and s'. In the case of tire-soil interaction the assumption of a steady state in the soil leads to the concept that the slip line fields move with the tire while the soil particles are displaced from their original position with respect to a coordinate system that is fixed to the ground. This concept makes it somewhat difficult to visualize the relative

displacement of the tire surface to the soil. However, the meaning of the terms introduced by Eq. (12) is essentially the same as explained for a track element.

In the foregoing discussions velocities of a point at the surface of tire and soil were defined and compared. On the other hand, the conventional definition of slip relates slip to actual and theoretical distances traveled by the tire. Obviously, the conventional slip value determines an overall slip for the tire. Janosi (Ref. 19) and others have pointed out that the slip for an infinitesimal element of a rigid wheel may vary along the interface. In the case of pneumatic tires infinitesimal elements of the surface of both tire and soil may deform and exhibit different displacements relative to each other. As a result, a variation of slip along the interface may easily develop.

The kinematic boundary conditions and Eq. (12) derived from these conditions allow the computation of contact slip for every point at the interface once the tire centerline geometry and the associated slip line fields have been determined. For the determination of the slip line fields in the tire-soil model the angle of interface friction is assumed, or computed from the modified Janosi-Hanamoto equation

$$\tan \delta = \tan \delta_{max} \left(1 - e^{-(s+s_o)/k}\right) \tag{15}$$

for given slip and slip-shear parameters. Equation (15) refers to the conventional value of slip. In the model, slip and interface friction angle are assumed to be constant along the interface. For these conditions the variation of the contact slip along the interface in the tire-soil model was determined for several loading conditions, tire types, and conventional slip values. It was found

that the variation of the contact slip along the interface was minimal and its value less than the conventional value of slip.

Typical variations of the contact slip along the interface are shown in Fig. 6 as a function of the central angle. The contact slip values were found to vary little along the interface in the cases investigated. Largest deviations from the average value were found near the exit angle where the tire centerline geometry shows an upward curvature. Kinematically this portion of the interface is the most problematic since the kinematic boundary conditions as set forth in the foregoing paragraphs require that the velocity of the soil particle be upward directed so that no separation of soil and tire surface occurs.

The concept of contact slip has important implications for both the theory of tire-soil interaction and the practical aspects of off-road vehicle engineering. The contact slip represents the absolute minimum of slip at which a certain tire performance can be realized. In the tire-soil model the tire centerline geometry as well as the directions of the principal stresses along the interface are computed and from this information contact slip values for every nodal point at the interface can be determined. Since the variation for the contact slip values along the interface is minimal, an average value of the contact slip may be computed and relationships between the development of interface friction angle and the average value of the contact slip may be established for various conditions. Thus a theoretical basis exists for analysis of the relationship between interface friction angle and contact slip. This relationship may be compared with Eq. (15) that represents the relation with the conventional slip value.

The concept of contact slip and the method of analysis that allows its determination for various soil and loading conditions

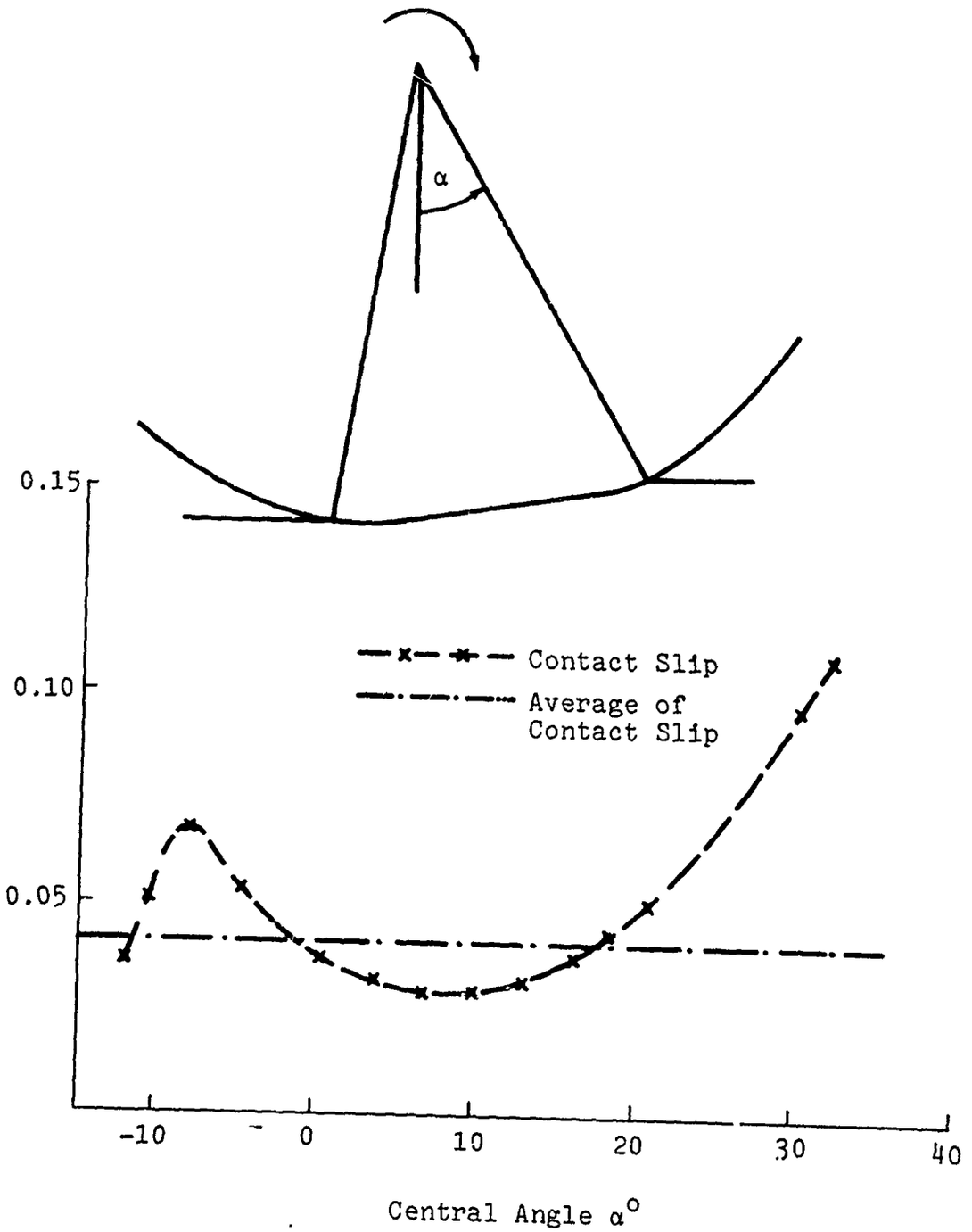

Fig. 6. Variation of Contact Slip Along the Interface of a 9.00-14 Tire in Yuma Sand. Load 620 lbs; Conventional Slip: 15%; Cone Index Gradient: 15 lbs/cu in.

opens new avenues of research that could lead to economics in off-road vehicle engineering. Obviously, spin, the differential displacement between tire and soil surface, is undesirable since it is the primary cause of tire wear and results in a waste of energy. For understanding of the phenomena that causes spin a systematic analysis of the contact slip and its relation to the conventional slip, soil, and loading conditions, preferably coupled with experimental investigations, would be needed. These would include measurements of soil particle displacements at the surface as well as torque rather than slip-controlled performance tests.

Computation of Inertial Accelerations from Velocity Fields

The concept of tire-soil interaction for which the mathematical model was developed (Ref. 13) assumes that steady state conditions exist in the soil. This assumption is equivalent to stating that the slip line fields travel with the tire with the same velocity. For these conditions the computation of accelerations becomes very simple if the velocity fields are known. In an infinitesimal Δt time increment the velocity of a soil particle at any point x,z changes to the velocity at $x - \Delta x,z$ where $\Delta x = v_f \Delta t$. The velocity field computation yields the velocity components for every nodal point in the slip line field. The numerical computation of the accelerations for these nodal points requires the determination of the velocities for a Δx change. This is accomplished by assuming a linear velocity change between the nodal point in question and two adjacent nodal points, one along the "i" and one along the "j" line. At the boundaries of the slip line field, velocities at these points are not always available and other combinations of adjacent nodal points had to be selected for the determination of accelerations.

Computational Scheme for the Consideration of Soil Inertia Forces in Tire-Soil Interaction

For analysis of the effect of soil inertia forces, computed on the basis of velocity fields, a computer program was prepared. This computer program computes the interface stresses for a given entry, rear and separation angles for various translational velocities of the tire. The soil inertia forces considered in the program correspond to a constant translational velocity of the tire.

The program represents a numerical solution method for the differential equations (1). It computes the soil inertia forces by successive iteration. In this iteration the first step is to determine the slip line field geometry without soil inertia forces, i.e., for $v_f = 0$. Then on the basis of this slip line field geometry the velocity fields and accelerations are determined for each nodal point for a selected velocity increment. It is assumed that the accelerations computed for each nodal point are valid when a new slip line field geometry is computed on the basis of these accelerations. This iteracion scheme in the computer program is included in an interactive manner that allows study of the effect of the selection of velocity increments as well as the effect of repeated iterative acceleration computations on the slip line field geometry. A detailed flow chart for the program is given in Appendix A.

Problems Encountered with Development of the Computer Program

Numerous minor problems were encountered with development of the program because initially the same iteration and interpolation schemes were used in the program as in the case without inertia

forces. The consideration of inertia forces in Eq. (1) resulted in a more complex situation where the behavior of soil was often different from that anticipated on the basis of previous experience and, therefore, iteration and interpolation schemes had to be modified. Other problems that have broader significance are discussed below.

The starting point for the development of this computer program was the one prepared for the simulation of tire-soil interaction presented in Ref. 13. In that program an ixj = 48 x 16 grid is set up for the computation of a slip line field, but only as many j lines are computed as are necessary to end up with the boundary j line at a prescribed location at the interface. The boundary j line is obtained by interpolation between evenly spaced j lines. This technique was developed to reduce the computer time that would be necessary to find the required size of the slip line field for a preset number of j lines.

Initial application of the same technique to the present problem created difficulties, because the number of j lines may change in the various slip line fields when inertia forces are taken into account. In the iteration technique where the slip line field geometry is updated for velocity increments a variable number of j lines is undesirable, because for an updated slip line field geometry containing more j lines than the previous field, accelerations for points on the additional j line are not available. For this reason the technique using a variable number of j lines was discontinued in this program and a constant 30 x 10 grid size was adapted. It was found that although the computer time needed to perform the necessary iterations to find the required size of the slip line field increased considerably for the first slip line field, in the subsequent iterative procedure for the updating of the slip line field geometries the

changes in the size of these fields were small and the total computer time was comparable to that needed with variable j lines.

The boundary conditions for the stress field also presented problems when inertia forces were included. The soil surface outside the tire-soil contact area was initially assumed as stress free and the direction of the major principal stress as horizontal even if soil inertia forces were included. Examination of the geometries of slip line fields generated with this assumption clearly showed an abrupt change in the directions of slip lines at the first row of nodal points beneath the free surface. In further analyses the direction of the major principal stress at the surface was assumed to correspond to a hypothetical loading in the direction of the resultant inertial force. Slip line fields generated with this assumption were smooth and this assumption was adapted in the further development.

The singular point (Point "A" in Fig. 2) presents special problems when inertial accelerations are included in the computations. Stresses at this point are computed by the equation

$$\sigma = \sigma_o \, e^{2 \tan \varphi(\theta-\theta_o)} \tag{16}$$

that is the solution of differential equations (1) when both dx and dz vanish. It is seen that the inclusion of inertial accelerations does not affect the validity of Eq. (16) since all inertial terms are multiplied by the vanishing dx or dz differential. The singular point can be regarded as a degenerate j line (with zero length) along which θ changes from its value θ_o at the adjacent free surface to that specified at the adjacent interface. However, for the determination of θ_o the inertial accelerations would have to be known at the singular point considered as part of the free surface. For the computation of these

acceleration velocities at this point, themselves dependent on θ_o, would have to be computed. Since the neighborhood of the singular point and the singular point itself is a critical part of the solution for the whole slip line field, it was necessary to develop and adopt an updating procedure for the computation of θ_o and velocities for this point independently of the updating of the rest of the field. The problem of updating the solution of the differential equations in the neighborhood of the singular point was compounded by the difficulties of applying the numerical techniques to the solution. The assumption of a linear variation of velocities from an i,j point to an i,j+1 and i+1,j point (applied for acceleration computations at an inner i,j point of the velocity field) is clearly inapplicable to the singular point that is the common location of nodal points with various i designations. The assumption of linearity would lead in this case to either infinite, or undetermined accelerations. Thus, it was necessary to compute the theoretical accelerations at the singular point from another combination of points along the next j line. An extensive analysis of the acceleration computation was made using various grid sizes and combinations of two or more points along the j+1 line. From these analyses it was concluded that while different numerical techniques affected the value of acceleration computed for this point the problem is a physical one: with increasing translational velocity the location where accelerations become critical first is that of the singular point. This could be expected since the singular point is also the entry point where the tire "hits" the ground. Accelerations at the singular point are critical when the inclination of the major principal stress associated with these accelerations equals that at which the free surface becomes a slip line. There is no single valued solution for the slip line field when the accelerations at this point exceed this limit.

The geometries of updated slip line fields generated with the iterative procedure for the computation of inertial accelerations were transmitted to a plotting program subroutine that allowed the visual examination of the updated geometries. This examination revealed that in many cases when the numerical end results appeared to be acceptable the numerical solution of the differential equations (1) was multivalued, as evidenced by the overlapping of the slip lines. A slip line field with an appreciable overlap is shown in Fig. 7. In many cases the overlap was hardly noticeable

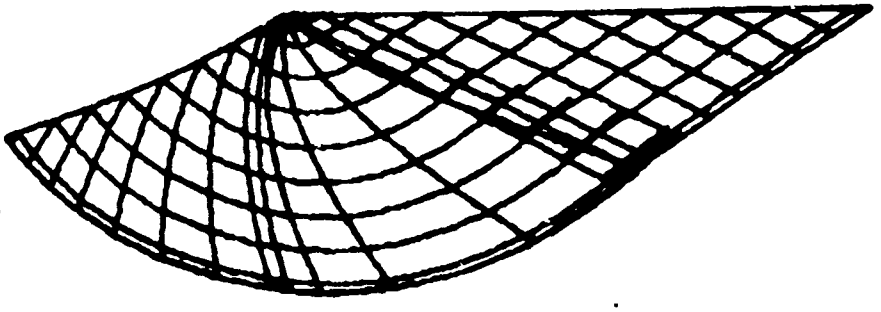

Fig. 7. Overlap of Slip Lines in the Case of a Multivalued Solution of the Governing Differential Equations

upon visual examination of the slip line field, therefore, a provision was made in the program to indicate by a printout if, within the accuracy of calculations, overlap occurs. Overlap indicates that the mathematical solution of the differential equations (1) at a particular location is multivalued, i.e., more than one σ and θ value belongs to the same x,z point in the slip line field.

The importance of an overlap indicating multivaluedness of the mathematical solution is that the solution no longer represents the physical behavior of soil under the applied loads, since it is a physical impossibility to have two different stress states in the soil at the same place and at the same time. Thus, overlap is a limitation to the application of plasticity theory with inertial

forces to the tire-soil interaction problem. Since with the method of velocity fields, overlapping starts to occur at relatively low velocities (in the range of 5 feet/second); this limitation is a serious one. Therefore, an extensive investigation was made to determine the causes of the overlap and especially, whether the overlap is the result of the application of numerical techniques or is inherent in the problem. As a result of these investigations the following conclusions were drawn:

1. Overlap occurs if there is an abrupt change in the magnitude of inertia forces between adjacent nodal points. The geometry of the slip line fields is such that while there are no abrupt changes in the velocities along the slip lines, there are abrupt changes in the derivatives of the velocities at locations where the various zones (active, passive, and radial) are joined together. This is evident in the case of Prandtl fields for weightless soil where straight slip lines are joined with logarithmic spirals at the zone boundaries. Numerical computation techniques can aggravate this problem if at the zone boundaries a different set of nodal points is used for the acceleration computation than inside the field. Numerical computation techniques can alleviate the problem by using schemes that tend to smooth these abrupt changes.

2. Overlap usually occurs first in the neighborhood of the singular point. Bow waves change the geometry of free surface in a way that the effect of inertia forces in the neighborhood of the singular point is counterbalanced.

3. The velocities determined by the theory of velocity fields are based on a two dimensional model of the tire-soil interaction. Implicit in the model is that soil particles may move only in the plane of travel. In actuality the movement of soil particles is not restricted to the plane of travel and, as a consequence, the actual velocities and accelerations are less than predicted by the two dimensional theory.

Results of Sample Computations

For the evaluation of the effect of inertia forces on tire performance sample computations were made within the velocity limits imposed by the criterion that the solution should be single valued. The results of these sample computations were surprising in that the effect of inertia forces was minimal even though the computed inertial accelerations often exceeded g by a factor of 10 or more. Figure 8 shows a comparison of normal stresses computed with and without inertia forces generated at a translational velocity of 5 feet/second. There is a slight, almost imperceptible rise in the normal stresses in the front and a very slight decrease of them in the rear of the tire when inertia forces are accounted for. Table 1 shows the pertinent input and performance data.

Figure 9 shows the geometries of front slip line fields determined for 0, 3, and 6 feet/second translational velocities, respectively. Although changes in the geometry with the velocity appear to be minor, closer observations of the "i" lines shows their approaching each other in the vicinity of the boundary between the passive and radial zone, an indication of an impending overlap situation.

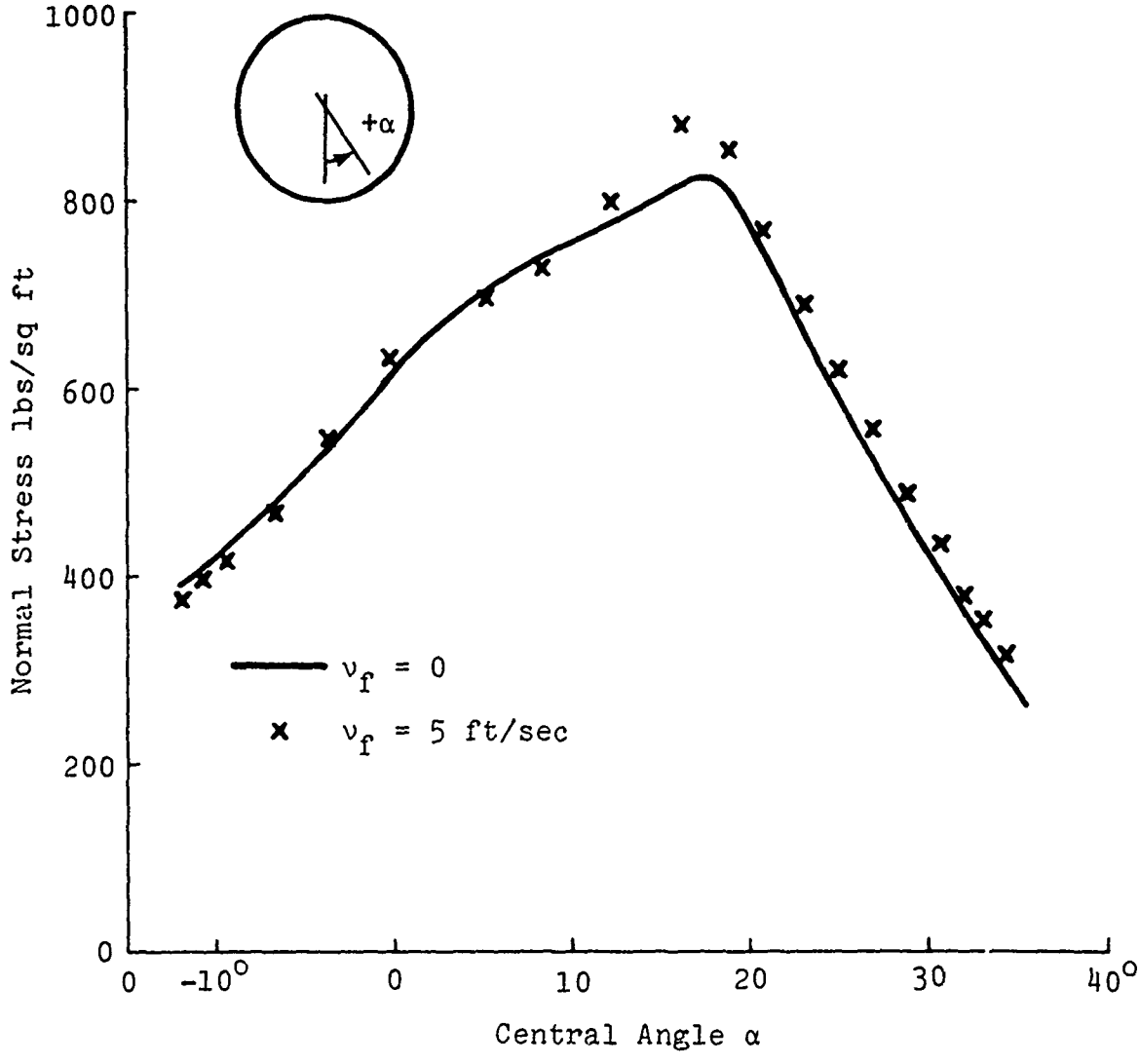

Fig. 8. Normal Stress Distribution With/Without Soil Inertia Forces for Tire Loading and Soil Conditions Shown in Table 1.

Summary Discussion of the Method of Velocity Fields and Conclusions

A computer program has been developed that takes soil inertia forces in tire-soil interaction into account by computing the velocity fields associated with the slip line fields and the accelerations therefrom. It was found that the method can be used up to about 5 feet/second velocity with 9.00-14 tires (for larger tires probably up to proportionately higher velocities)

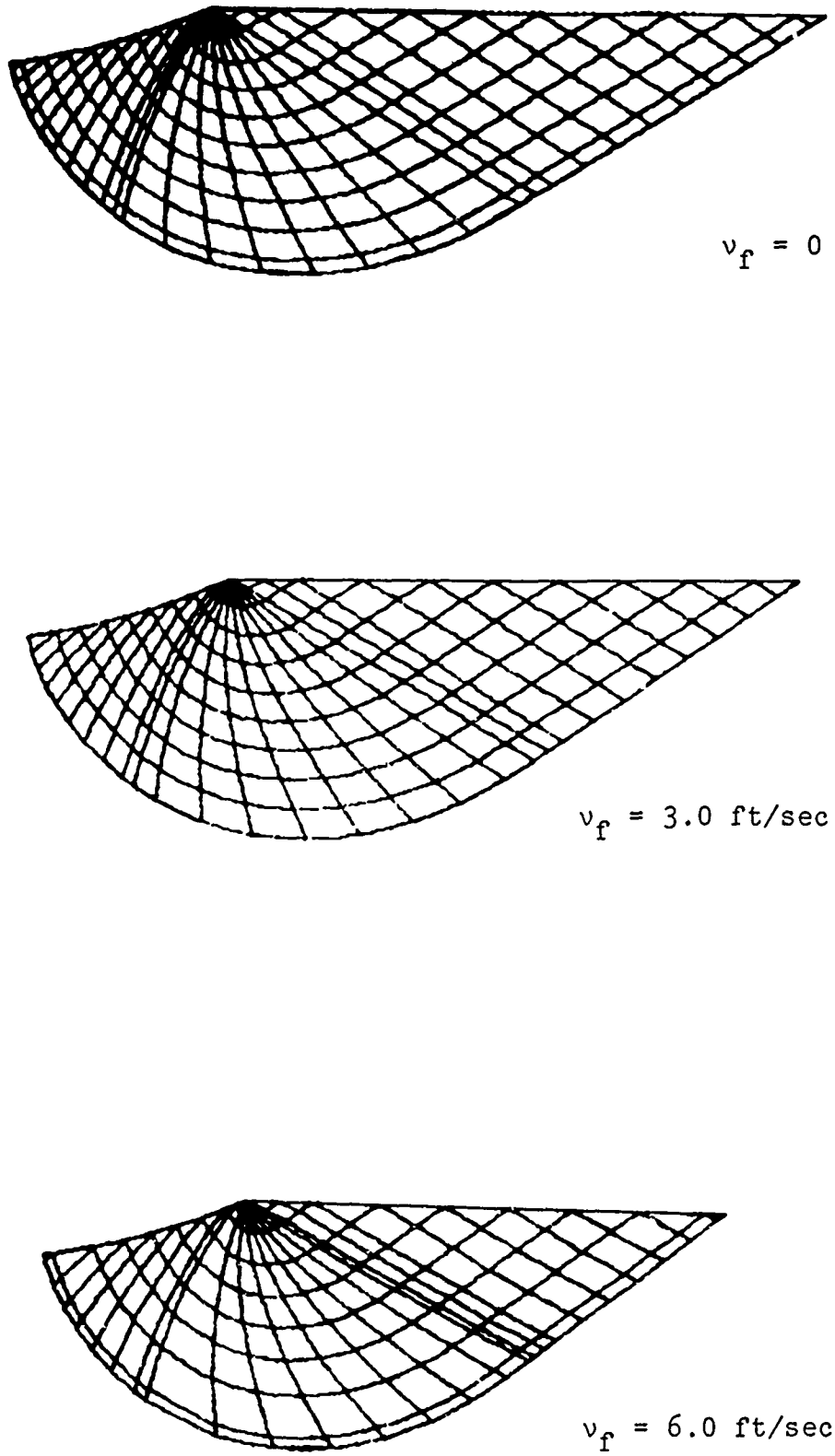

Fig. 9. Geometry of Front Slip Line Fields Computed For v_f = 0 (No Soil Inertia Forces) and v_f = 3 and 6 ft/sec

TABLE 1 TIRE PERFORMANCE WITH AND WITHOUT SOIL INERTIA FORCES

(Method of Velocity Fields)

Tire Size:	9.00-14
Tire Radius (nominal):	1.18 ft
Tire Width:	0.70 ft
Inflation Pressure (p_i):	12.5 psi
Slip:	15%
Angle of Interface Friction:	15.7°

	Front Field	Rear Field
Cohesion	15 lbs/sq ft	30 lbs/sq ft
Friction Angle	24°	28°
Unit Weight	100 lbs/cu ft	105 lbs/cu ft
Translational Velocity	v_f = 0 ft/sec	v_f = 5 ft/sec
Load	408 lbs	410 lbs
Drawbar Pull	48 lbs	53 lbs
Torque	129 ft-lb	135 ft-lb
Sinkage	2.03 in.	1.81 in.
Pull Coefficient	0.119	0.129

when the solution of the differential equations becomes multivalued. Because of the two dimensionality of the velocity fields, velocities and associated inertial accelerations are overestimated by this method. It was found that abrupt changes in inertia forces occur inherently in this method because derivatives of slip line directions that control the velocity field are discontinuous at the joint boundaries of the active, passive, and radial zones.

There is no experimental information on the physical phenomenon that occurs when the plasticity solution becomes multivalued. Speculatively, one may assume that failure in the classical Coulomb sense cannot occur and a so-called "rigid" soil zone exists within the bounds of overlap. It is also likely that the soil adjusts itself and seeks to fail along slip lines with continuous curvature. Upper bound solutions based on the characteristics of the differential equations for velocities would have to be considered rather than solutions based on stress characteristics. A possible solution would be a slip line field with only one zone and continuous curvature of the slip lines.

Inertia forces appear to have little effect on tire performance as long as the plasticity solution is single valued. A slight rise in the normal stresses in the front field increases tire deflection thus resulting in a slightly better tractive performance. It should be noted that even though the calculations were made for a low translational velocity the calculated inertia forces inside the field were in the range of several, often more than 10 g-s.

An incidental but important result with this method is the introduction of a new concept, that of "contact slip" in the tire soil interaction problem. For determination of the contact slip in any interaction problem, only a small portion of the computer program, dealing with the kinematic boundary conditions, is needed. The new concept can be the basis of further theoretical research in the area of slip, mobilized shear, and traction development.

V. DETERMINATION OF SOIL INERTIA FORCES BY THE PARTICLE PATH METHOD

Introduction

Soil inertia forces are generated by the acceleration and deceleration of soil particles during the passage of a tire. The motion of soil particles follows a particle path that defines the geometry of particle motion in a coordinate system fixed to the ground. Velocities and accelerations are time derivatives of the coordinate vectors of particle path.

Experimental Information on Particle Path Geometry

Measurements of particle paths beneath rigid wheels were performed by several researchers under laboratory conditions (Refs. 20 through 22) using the flash X-ray technique. These experiments show the same general pattern and dependence of the particle path on slip, as shown, for example, in Fig. 10. Although not pointed out in the referenced publications that describe these particle path measurements, theoretical considerations indicate that for a constant velocity the particle path geometry must not change with the x coordinate, the direction of travel. Any variation in particle path geometry in the x direction obtained in experiments must be the result of experimental error, inhomogeneities in the soil bed preparation, etc. The invariability of the particle path geometry with respect to the direction of travel also follows from the "steady state" concept of tire-soil interaction.

The experiments show, on the other hand, that the size of particle paths diminishes with the depth beneath the wheel and there is a certain limit depth below which the soil is unaffected by the passage of the wheel.

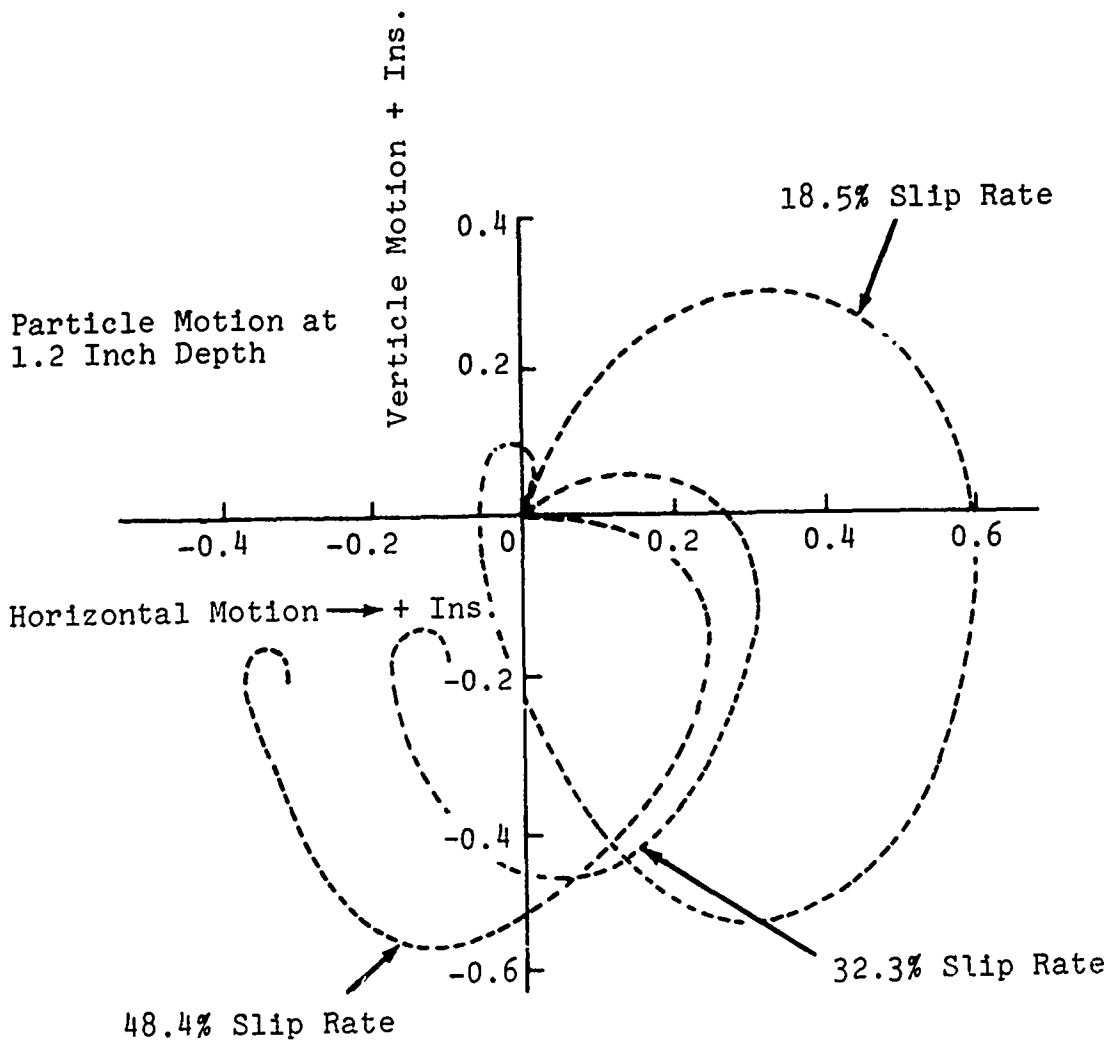

Fig. 10. Particle Motion as Influenced by Slip Rate (From Ref. 21)

There are some conditions that define the end points of the path of particles that were originally at the surface. After the passage of the tire these particles wind up in the rut at some depth, that evidently equals the vertical distance between the end points of the path. Experiments also show that the horizontal position of a particle at the surface is changed by the action of the wheel as it passes over the particle. In the case of a slipping

wheel, the particle at the surface is pushed backward from its original position; in the case of a skidding wheel, or negative slip, the particle at the surface is pushed in the forward direction. Figure 11 shows the displacement of dyed sand particles

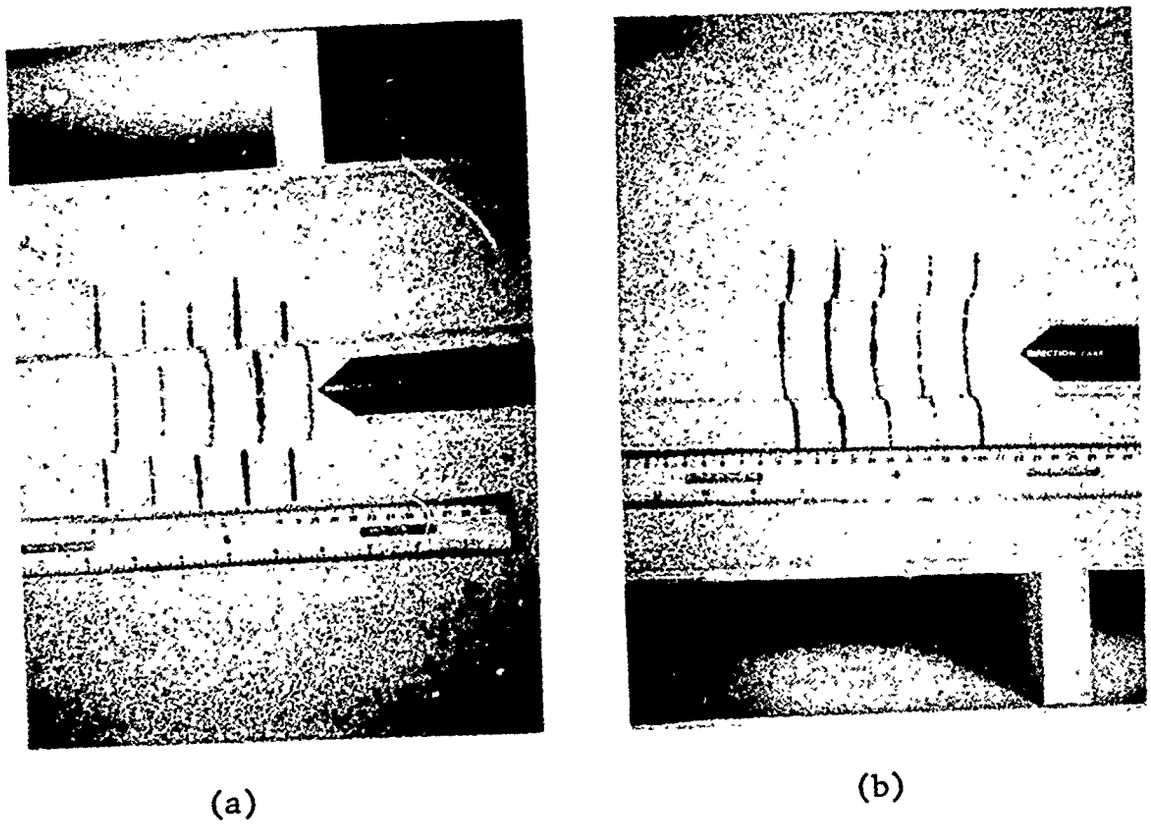

(a) (b)

Fig. 11. Displacement of Sand Particles Under a Slipping Wheel (a, s = 55%) and a Skidding Wheel (b, s = -40%)

beneath a skidding and a slipping wheel determined in the mobility bin at Grumman. Thus, a particle at the surface is generally displaced both in the horizontal and vertical direction; the displacement equals the difference between the origin and the terminus of the path of a particle at the surface.

Idealization of Particle Path Geometry

For the intended use of particle path geometries it is desirable to describe these geometries by analytical functions. Experimentally determined particle paths have some resemblance to

cardioids and in some publications they are referred to as such. The parametric equation of a cardioid is (Fig. 12)

$$x = 2a \sin \omega - a \sin 2\omega$$

$$z = 2a \cos \omega - a \cos 2\omega \qquad (17)$$

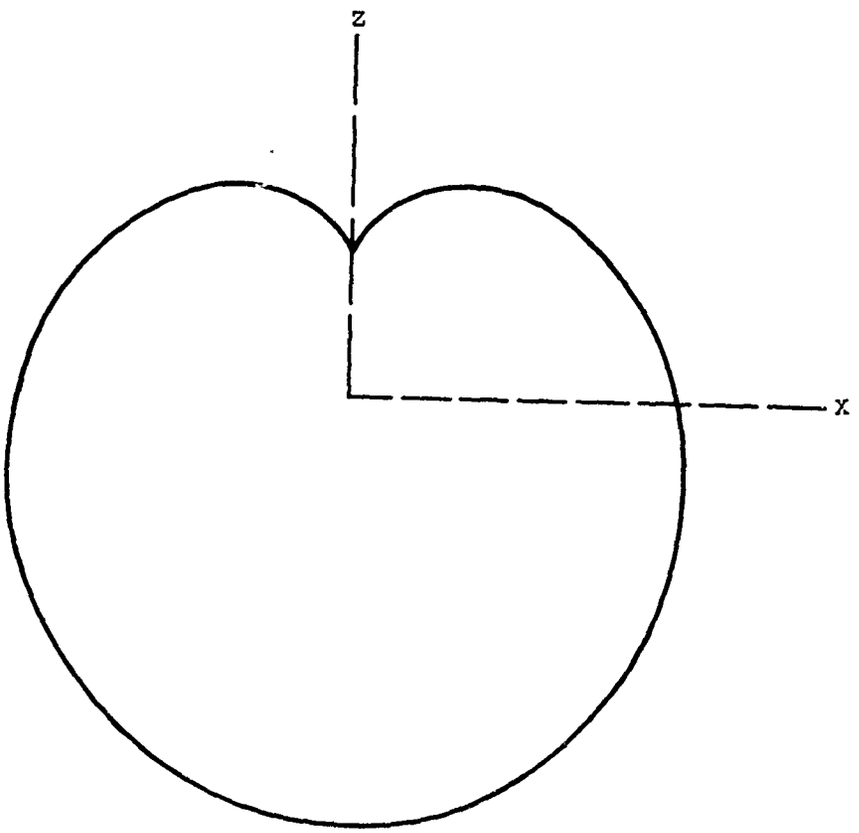

Fig. 12 Cardioid Geometry

Obviously, a cardioid is not a suitable curve to describe the parcicle path when constraints are set for the displacement of the end point in both the horizontal and vertical direction.

Another curve that has a shape similar to the observed particle paths is the nephroid. The parametric equation is (Fig. 13)

$$x = 3a \sin \omega - a \sin 3\omega$$

$$z = 3a \cos \omega - a \cos 3\omega \qquad (18)$$

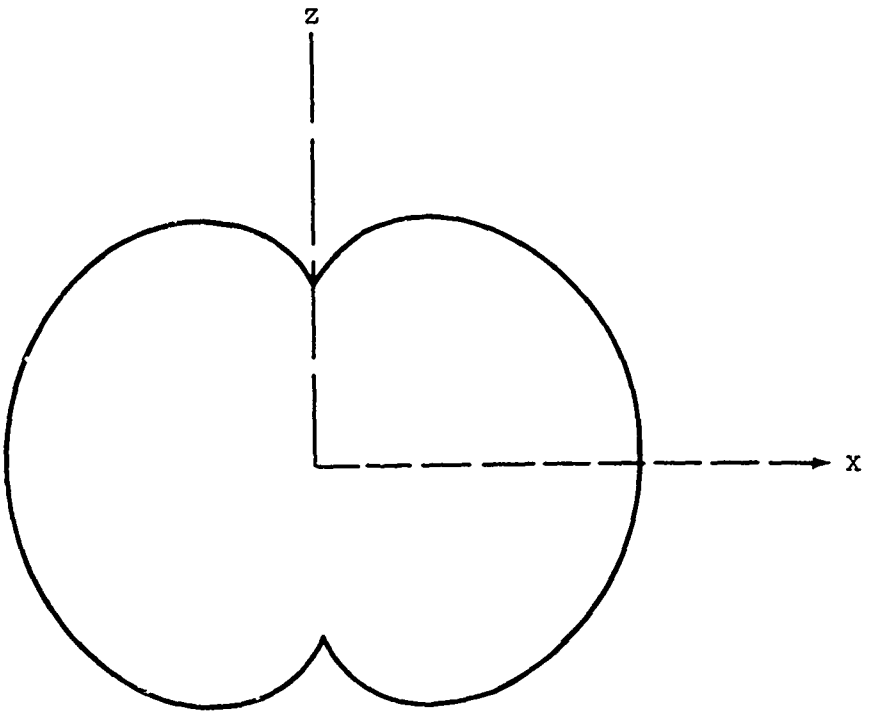

Fig. 13 Nephroid Geometry

A study of the shape of these curves showed that even if the constraints for the end conditions could be met by selecting only a portion of these curves for particle path simulation, more freedom is needed to describe particle paths under the wide variety of soil and tire loading conditions. Also, the experimental information is restricted to the case of rigid wheels and it can be assumed that the simulation of the effect of tire deflection on particle path geometry would require more freedom in the analytical expression. This freedom is achieved by allowing the constants in the above expressions to vary as

$$x = a[\rho_1 \sin \omega - \sin \rho_1\omega]$$

$$z = a[\rho_2 - 1 - \rho_2 \cos \omega + \cos \rho_2\omega] \qquad (19)$$

Equation (19) refers to a coordinate system with its origin coinciding with the initial at rest position of the particle. The expansion of the expression in parentheses for z by the term $(\rho_2 - 1)$ serves this purpose.

Equation (19) contains parametric expressions of the particle path that represents a family of curves of various shapes. Figure 14 shows variations of the geometry as defined by Eq. (19) for various values of the parameters ρ_1 and ρ_2. Equation (19) also represents the geometry of the particle path in parametric form. Time derivatives of the coordinates x and z yield the velocities and accelerations of the particle at the time the particle is at point x,z. To calculate these time derivatives the parameter ω has to be related to time, t, preferably by a differentiable function. If

$$\omega = f(t) \tag{20}$$

then the time derivatives of the coordinates of the particle path are

$$\begin{aligned}
\dot{x} &= a\rho_1\dot{\omega}(\cos\omega - \cos\rho_1\omega) \\
\dot{z} &= a\rho_2\dot{\omega}(\sin\omega - \sin\rho_2\omega) \\
\ddot{x} &= a\rho_1\ddot{\omega}(\cos\omega - \cos\rho_1\omega) + a\rho_1(\dot{\omega})^2(-\sin\omega + \rho_1\sin\rho_1\omega) \\
\ddot{z} &= a\rho_2\ddot{\omega}(\sin\omega - \sin\rho_2\omega) + a\rho_2(\dot{\omega})^2(\cos\omega - \rho_2\cos\rho_2\omega)
\end{aligned} \tag{21}$$

To compute the accelerations from Eq. (21) the relationship between the parameter ω and time, t, has to be defined. To this end it is useful to consider the changes in the direction of the particle movement that can be associated with the relative position of the tire. The direction of the particle at any point

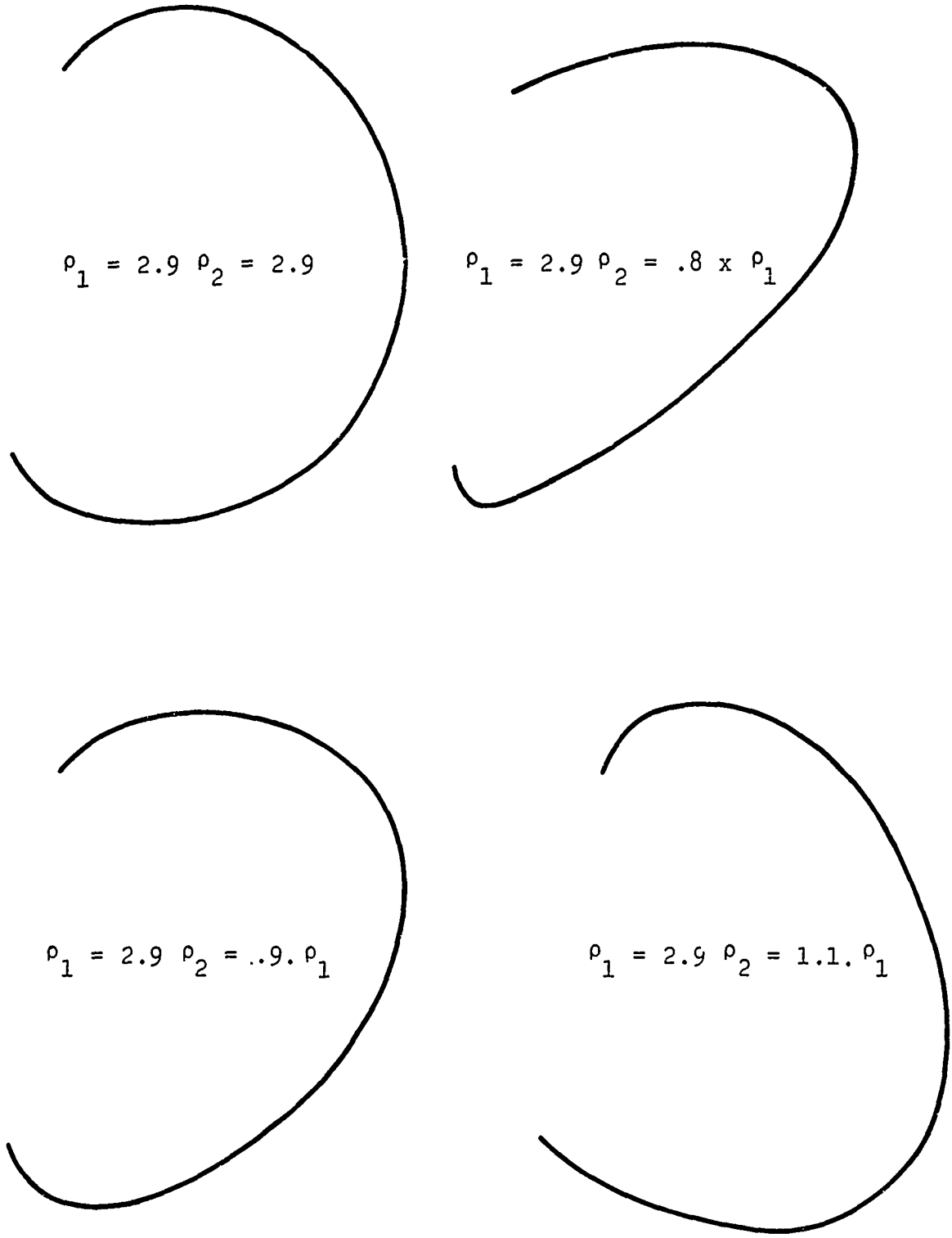

Fig. 14. Particle Path Simulation by Eqs (19)

along the particle path is given by the tangent of the path at that point. From Eq. (19) the tangent of the particle path can be calculated as

$$\frac{dz}{dx} = \frac{\frac{dz}{d\omega}}{\frac{dx}{d\omega}} = \frac{\rho_2}{\rho_1} \frac{\sin \omega - \sin \rho_2 \omega}{\cos \omega - \cos \rho_1 \omega} \tag{22}$$

The points along the particle path that may be associated with various positions of the tire are shown in Fig. 15. The value of the parameter at these points may be determined from the condition that the tangent of the particle path is either horizontal or vertical. The following tabulation shows the ω values at these points.

TABLE 2 VALUES OF THE PARAMETER ω AT VARIOUS POINTS OF PARTICLE PATH

Point	Tangent	ω
A	Vertical	0
B	Horizontal	$\pi/(1 + \rho_2)$
C	Vertical	$2\pi/(1 + \rho_1)$
D	Horizontal	$3\pi/(1 + \rho_2)$
E	Vertical	$2\pi/(\rho_2 - 1)$

The position of the tire that may be associated with the above points and the time elapsed while the tire passes from one point to another is shown in the lower part of Fig. 15. Obviously, there is no rigorous time relation between these particle locations and tire travel positions and these considerations serve primarily as a guide for the mathematical formulation of the $\omega = f(t)$ relationship.

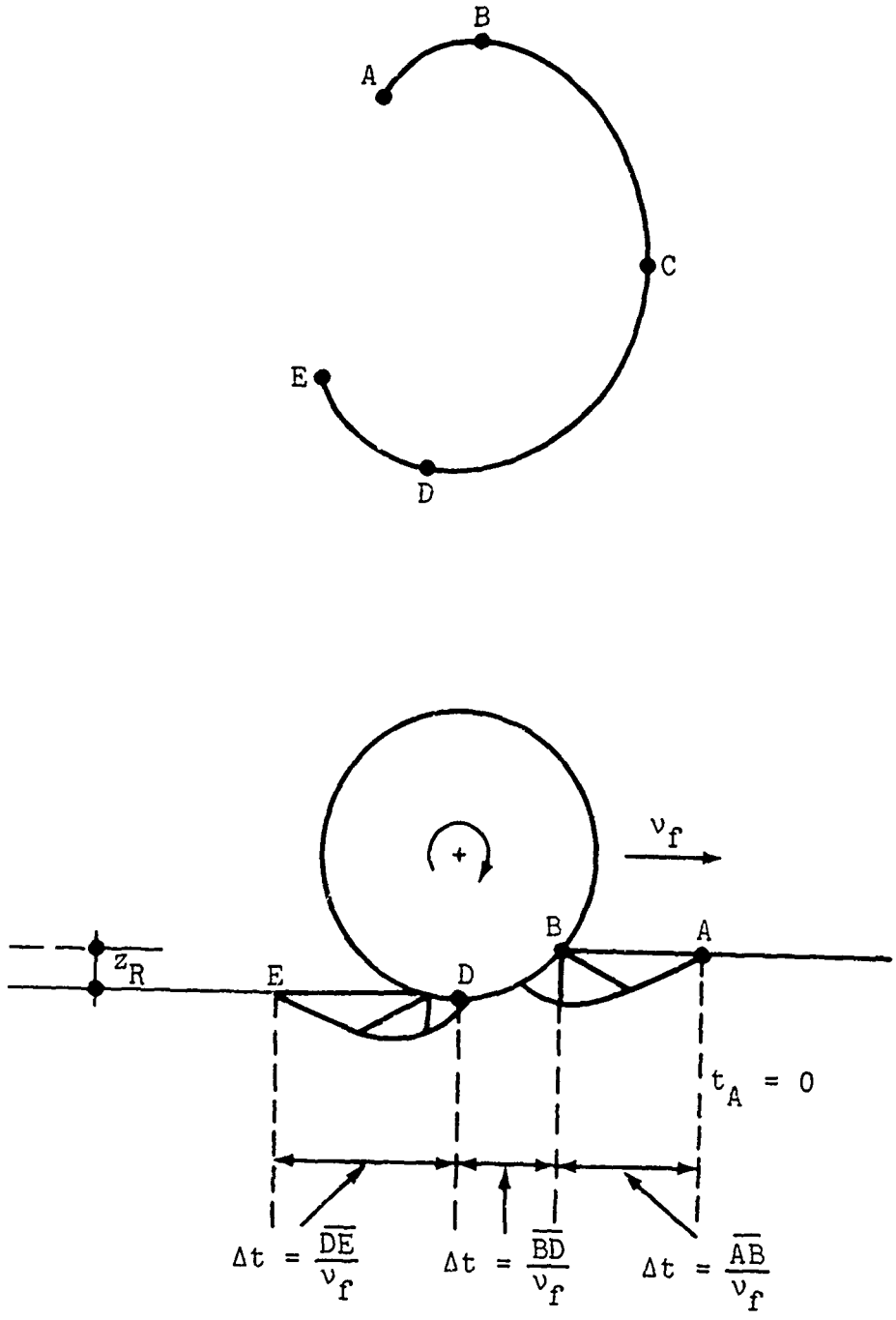

Fig. 15. Relation Between Position of Tire and Characteristic Points of Particle Path

As mentioned before, for a particle at the surface the end points also have to meet certain conditions. First, the vertical distance between the end points must equal the rut depth, i.e.,

$$z_E - z_A = z_r \tag{23}$$

The constant "a" in Eq. (19) is selected so that this condition be met.

Second, the assumption is made that the horizontal distance between the end points equals the contact slip times the rut depth, or

$$\frac{x_E - x_A}{z_E - z_A} = s' \tag{24}$$

If in Eq. (19) the x,z values are substituted with the values given by Eqs. (23) and (24) and with the appropriate value of the ω parameter given in Table 2 then a relationship between ρ_1 and s' can be obtained. This relationship is shown in Figure 16 for ρ_2 values varying from $0.75\ \rho_1$ to $0.95\ \rho_1$. It is seen that within these limits the value of ρ_1 is affected but little by the value of ρ_2, and Fig. 16 could be used for the estimation of ρ_1 for any value of the contact slip s'. On the basis of the available experimental information on particle paths, it appears that a ρ_2 value of about $0.9\ \rho_1$ is a reasonable assumption. Should further information on particle paths become available, any other value of ρ_2 that allows a good simulation of particle path may be selected. In this case the value of ρ_1 may be computed from the following polynomial determined as best fitting the curves shown in Fig. 16.

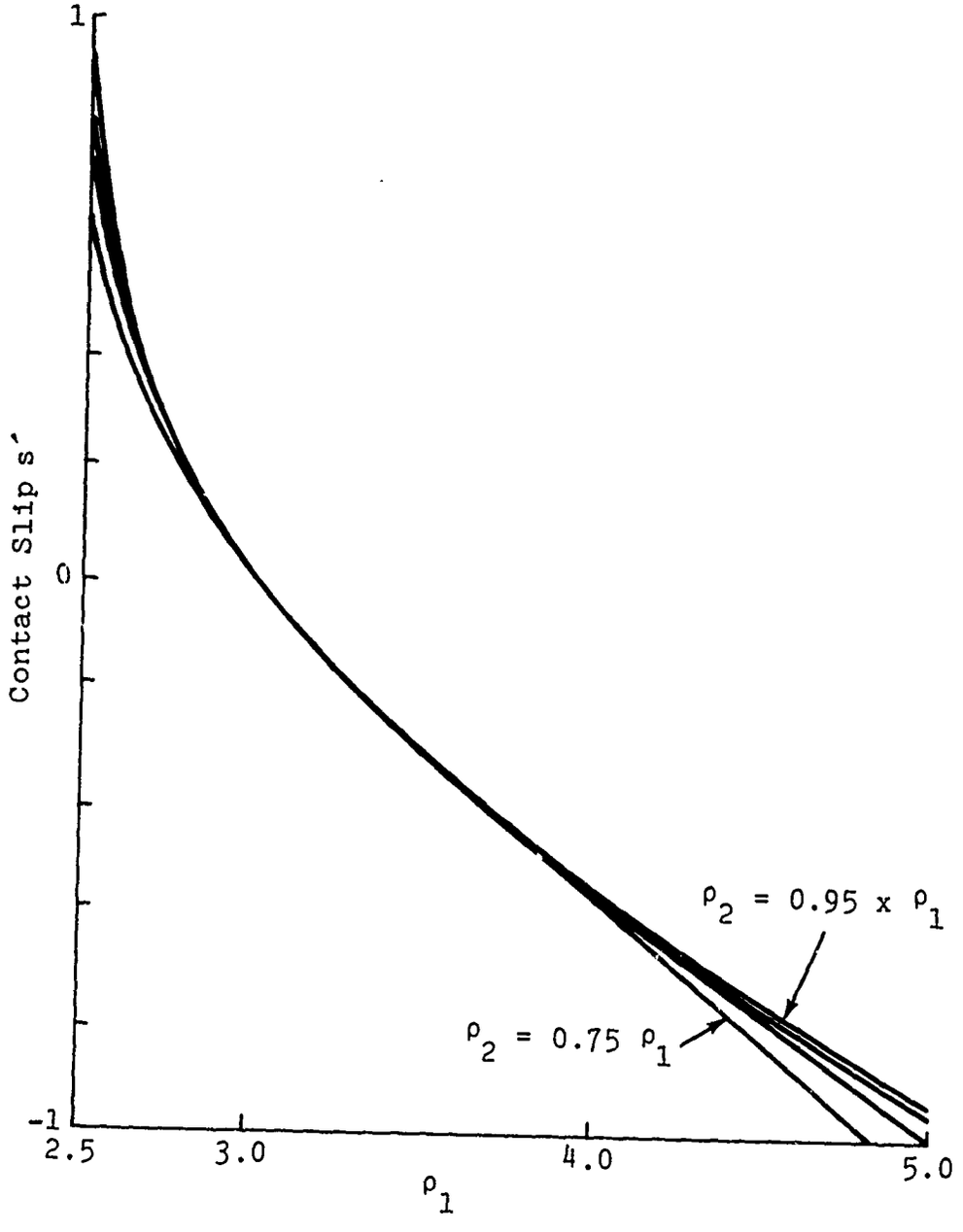

Fig. 16. Relationship Between ρ_1 and s´ for ρ_2 Varying Between $0.75\ \rho_1$ and $0.95\ \rho_1$

$$\rho_1 = a_3 s'^3 + a_2 s'^2 + a_1 s' + a_o$$

where

$$\begin{aligned} a_3 &= -\ 717.661\ \xi^4 + 2504.05\ \xi^3 - 3253.0\ \xi^2 \\ a_2 &= -\ 10.986\ \ \xi^3 + 24.6844\ \xi^2 - 17.6294\ \xi + 4.71601 \\ a_1 &= \quad .273714\ \xi^2 + 1.05039\ \xi\ \ - 2.0157 \\ a_0 &= -\ 1.40114\ \xi^2 + 2.37218\ \xi\ \ + 2.01924 \end{aligned} \tag{25}$$

$$\xi = \frac{\rho_2}{\rho_1}$$

The parameters ρ_1, ρ_2 and a completely define the particle path and the accelerations if $\omega = f(t)$ is known. Various functional forms for this relationship have been assumed and investigated for suitability to fit the time constraints established previously for the various points along the path. Polynomials generally did not meet the requirement that ω should increase monotonically with t. An analytical study of various logarithmic and exponential expressions showed that if the requirement for a monotonic increase of ω with t was satisfied then, in some instances, it was not possible to meet the time constraints. Finally, the following expression was chosen

$$\omega = c_1 \arctan\left(c_2(t + t_o)\right) + \omega_o \tag{26}$$

The constants c_1, c_2 in Eq. (26) are determined from the ratios of the elapsed time between particle path locations A,B,D, and E. The value of ω_o in Eq. (25) may be tentatively chosen as $0.5 \times \omega_E$.

Use of the Idealized Particle Path Geometry in the Tire-Soil Model

The analytical expression for the particle path geometry is convenient for the determination of accelerations. To use this analytical expression for the calculation of inertia forces in the tire-soil model it is necessary to determine the constants in that expression. To this end it is assumed that the constants in the particle path equation may be determined from the $v_f = 0$ case. An alternative to this assumption is that the particle path remains unchanged for small increments of velocity and the particle path geometry for a given translational velocity would be determined by an updating procedure. Analysis of a few cases indicated that, in view of the approximate nature of the particle path concept, an elaborate updating procedure would be justified only if more experimental information on the geometry of particle paths were available.

For the assumption chat the particle path geometry may be determined from the $v_f = 0$ case, computations of accelerations become a simple matter. They require the addition of a short subroutine named "ACCE" to the program that was developed for the computation of tire performance for given tire and soil input data. (Main program "KTIRE" and subroutine "SLFI," developed for tire-soil interaction simulation, are described in TACOM Tech. Report No. 11900 (LL147) (Ref. 4). The subroutine "ACCE" is called from subroutine "SLFI" after the first approximation of the coordinates x,z is computed for each nodal point of the slip line field. The accelerations computed by the subroutine "ACCE" are then used in the difference equations for the computation of σ and θ and for the computation of the improved values of the x,z coordinates of the nodal point.

A detailed flow chart of the expanded program for the computation of tire performance with consideration of soil inertia force is given in Appendix B.

Problems Encountered with the Development of the Computer Program

These were generally of the same nature as with the program based on velocity fields. However, the analytical simulation of the particle path geometry resulted in continuous time derivatives alleviating the overlap problems at zone transitions encountered with the other program. The critical accelerations occurring at the singular point, that are inherent in the problem, limit the applicability of the method to about 10 to 20 feet/second translational velocity, depending on the tire dimensions.

In cases where the soil and loading conditions are such that there is no slip line field in the front, association of the various points of the particle path with relative positions of the tire is no longer applicable. Experimental information on particle paths generated under such conditions is needed for meaningful simulation of the geometry of particle paths and the motion of particles in the time frame of tire passage.

Results of Sample Computations

For evaluation of the effect of soil inertia forces on tire performance by this method, computations were performed for a few typical cases. Results of these computations are shown in Tables 3 and 4.

In the computations for the performance calculations shown in Tables 3 and 4 no overlap was experienced for the translational velocities indicated, i.e., all slip line field solutions were

TABLE 3 TIRE PERFORMANCE AT VARIOUS VELOCITIES

Tire Size:	9.00-14
Tire Radius:	R = 1.18 ft
Tire Width:	B = 0.74 ft
Load:	L = 614 lbs
Inflation Pressure:	p_i = 10.9 psi
Limit Pressure:	p_ℓ = 11.0 psi
Deflection Coefficient:	ϵ = 0.9
Slip:	s = 10%
Cone Index Gradient:	CGR = 15 pci
Interface Friction Angle:	δ = 22.8°

Translational Velocity ft/sec	Pull Coefficient	Sinkage in.	Contact Slip	Entry Angle (°)	Rear Angle (°)
0	0.3268	0.724	0.0738	26.06	12
5	0.3334	0.599	0.0614	23.90	10
8	0.3340	0.593	0.0600	23.84	10
10	0.3346	0.588	0.0618	23.77	10
12	0.3352	0.583	NA	23.71	10

single valued. The highest velocities shown in these tables are approximately the limits above which the solution becomes multi-valued.

It is seen that the increase of tire performance due to soil inertia forces are minimal in these cases and, for all practical purposes, negligible.

TABLE 4 TIRE PERFORMANCE AT VARIOUS VELOCITIES

Tire Size:	4.00-7
Tire Radius:	R = 0.59 ft
Tire Width:	B = 0.40 ft
Load:	L = 225 lbs
Inflation Pressure:	p_i = 10.3 psi
Limit Pressure:	p_ℓ = 10.6 psi
Deflection Coefficient:	ϵ = 0.85
Slip:	s = 30%
Cone Index Gradient:	CCR = 19.6 pci
Interface Friction Angle:	δ = 27.8°

Translational Velocity ft/sec	Pull Coefficient	Sinkage in.	Contact Slip	Entry Angle (°)	Rear Angle (°)
0	0.3217	1.11	0.089	42.3	22
5	0.3270	1.08	0.093	42.0	22
8	0.3291	1.07	0.131	41.9	22
10	0.3508	0.93	0.135	39.3	20

Summary Discussion of the Particle Path Method and Conclusions

The consideration of soil inertia forces by the particle path method is simpler than with the method of velocity fields. The analytical simulation of particle path geometries results in smooth changes of velocities and accelerations from one nodal point to another in the slip line field. As a result, the limitation imposed by the multivaluedness of the solution of the differential equations defining the slip line fields is less severe than the velocity field method, and analysis of tire performance at higher velocities becomes possible.

The drawback of the particle path method is that its empirical basis includes only a few tests. Therefore, it was unavoidable to make somewhat arbitrary assumptions in the analytical simulation of the particle path geometry to attain a usable method. However, there is enough freedom in the analytical simulation of particle paths to allow for adjustments should more experimental information become available.

The most interesting and important result of the analyses performed by the method of particle paths is that, in agreement with the results obtained with the method of velocity fields, the effect of soil inertia forces on tire performance is minimal for the translational velocities investigated. An explanation for this finding, that is somewhat contrary to expectations, is that in the cases analyzed tire performance was governed by failure conditions in the soil. Even though soil inertia forces affected the geometry of slip line fields, the stresses in the soil were controlled by its strength; therefore, soil inertia forces had little effect on the interface stresses and, consequently, on tire performance. A logical amplification of this explanation is that soil inertia forces are very likely to have appreciable effect on tire performance if they affect the mode of failure in the soil. Multivaluedness of the solution of Eq. (1) is an indication that the soil may not fail according to the concepts of soil plasticity. At this time neither theory nor experiments are available that would apply to the problem.

Another result of the sample calculations worth noting is that the computed average value of contact slip changes with velocity. The improvements in tire performance with speed reported in Ref. 1 refer to a constant slip of 20 percent. The question may be raised whether the improvement in tire performance with speed

would manifest itself over the entire slip range, including the maximum pull performance, or whether the observed improvements signify only an accelerated development of the interface shear stresses with slip as the travel velocity increased. Tire performance experiments at various velocities over the entire slip range are needed to clarify this problem.

VI. EFFECT OF LOADING RATE ON SOIL STRENGTH AND TIRE-SOIL INTERACTION

Introduction

In tire-soil interaction the soil is loaded at a rate that is directly proportional to the translational velocity of the tire. The rate of loading affects the strength of soil in many ways. In civil soils engineering practice consolidation and creep theories deal with the long term effects of loading rates on soil strength; the loading rates encountered in tire-soil interaction problems fall into the category termed as "rapid" or "quick" loading and the soil strength referred to as "undrained" indicating that during such rapid loading there is no drainage of the soil. For the purposes of civil soils engineering, laboratory tests aimed at determining the strength of soil under rapid loading conditions are performed so as to reach the maximum load in a matter of minutes.

In tire-soil interaction the loading rate is generally faster than that considered "rapid" in civil soil engineering. Soil behavior at loading rates comparable to those encountered in tire-soil interaction has not been investigated until recently, since laboratory investigations at these loading rates require special equipment, referred to as "dynamic" triaxial testing apparatus. In dynamic tests, loads are applied in fractions of seconds. Dynamic tests are generally strain controlled and investigations relate strength properties to the strain rate.

Indirect information on the effect of loading rate on the strength properties of soils is also available from various sources where the resistance of soil to the penetration of plates, blades, or cones is measured at various rates of penetration.

Physical Causes of Strain Rate Dependent Strength Properties of Soils

The physical causes of the strain rate dependent behavior of soils are manifold and some of them are not clearly understood. The rate of strain affects soil behavior on the microlevel through its effect on the physicochemical and electrochemical bonding forces between the soil particles. On the macrolevel, moisture redistribution during shearing and plastic flow of contacting particle asperities are the major time-dependent phenomena that affect soil strength and tire-soil interaction. Since these phenomena affect the results of the various types of laboratory and field strength tests and tire-soil interaction in a different way, it is important to consider the mechanism underlying these phenomena when strain rate effects are analyzed. In the following discussion many aspects of these very complex phenomena are omitted so that the essential mechanism may be clearly presented. For the purposes of this discussion it is convenient to group soils in three categories: saturated cohesive type soils, cohesionless soils, and partially saturated frictional-cohesive soils.

In saturated cohesive type soils, such as the Buckshot clay, moisture redistribution during loading is the most important single factor responsible for the increase of soil strength with the rate of strain. The phenomenon of moisture redistribution can be best explained by considering a triaxial test (Fig. 17). Loading of the sample in a triaxial test results in a stress state ultimately leading to the development of a failure surface where shear stresses exceed the shear strength of the material. In the process of straining the sample, high shear stresses along the potential failure surface tend to dilate the soil. This tendency to dilate reduces the pore water pressures along the potential failure

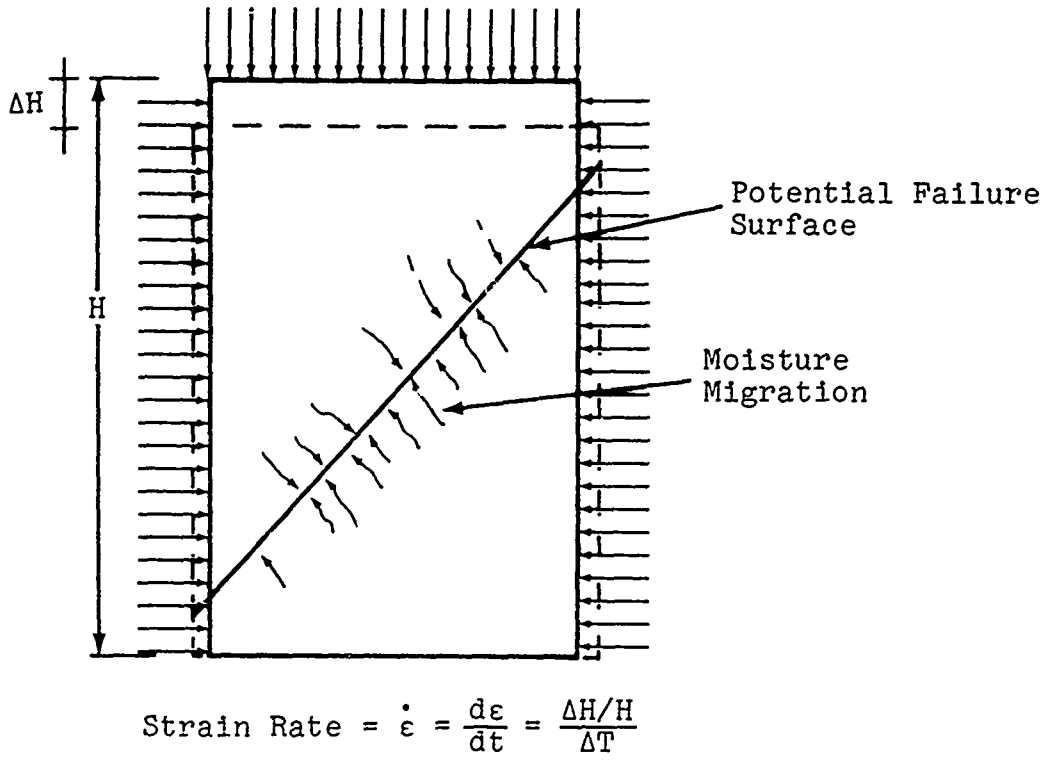

Fig. 17. Moisture Migration in Triaxial Test

surface relative to the rest of the sample. The reduced pore water pressures suck moisture toward the failure surface, therefore increasing the moisture content locally. Thus, a moisture redistribution occurs in the sample during the test and the actual strength of the sample corresponds to the moisture content in the immediate vicinity of the failure surface. Experiments confirm that moisture redistribution takes place in dynamically tested triaxial samples (Ref. 23).

The rate of moisture migration depends on the permeability of the clay. The total amount of moisture that migrates during a test depends on the rate of migration and the time available for migration. Obviously, this latter depends on the strain rate and hence dependence of the strength on the strain rate. It should be noted that this moisture migration occurs even though the test is of the

"undrained" type, i.e., no water is going in or out to the sample during the test and the total water content of the sample has not changed.

The process of moisture redistribution is extremely complex and its analytical treatment would require the knowledge of stress states in the specimen for the deformed geometry as well as pore water pressure response of the soil to these stress states. From the viewpoint of tire-soil interaction, a significant feature of this complex redistribution process is that the rate of moisture migration toward a potential failure surface depends not only on the properties of soil, but also on the stress states in the vicinity of that surface and the distance from the impervious boundaries (the sealed bottom and the rubber membrane in the triaxial test) of the specimen. These conditions are different in tire-soil interaction from those in a triaxial or a field test, therefore, strength-strain rate relations found by such tests are not immediately applicable to tire-soil interaction problems.

In cohesionless soils the experimental evidence concerning the effect of strain rate on their strength is inconclusive. Early experiments by Casagrande and Shannon (Ref. 24) showed a small increase in strength with an increase of the strain rate, while Whitman and Healy found the shear strength of sands unaffected by the strain rate (Ref. 25). Larew and Atakol (Ref. 26) found that the rate of shear strain affected the strength of cohesionless soils. These experimental results indicate that the response of cohesionless soils to dynamic loading is not uniform and the mineral composition of the grains and arrangement of the particles also play a role. The strain rate may affect this response by delaying the force transmission from particle to particle due to the inertia of the individual particles and the plastic deformation of the contacting surfaces.

In partially saturated frictional-cohesive soils the effect of strain rate on strength properties is diverse. In the three-phase solid-water-air system pressures of pore water, as well as of pore air, may be generated and moisture redistribution during loading may be prevented by pore air pressures. Also, if there are open channels, the pore air pressure may be relieved; the time rate of this relief would depend on the air permeability of soil. In summary, the effect of strain rate on the strength properties of partially saturated frictional-cohesive soils is exceedingly complex and cannot be evaluated, even qualitatively, on the basis of theoretical and experimental information available at present.

Correlation of Strain-Rate Effects in Laboratory and Field Tests for Strength Property Determination and in Tire-Soil Interaction

Dynamic triaxial tests performed under controlled laboratory conditions are the best source of information on the relationship between strain rate and strength in various types of soils. Even so, the measured resistance of the soil sample to the applied loading includes the effects of soil inertia. Only in the most recent experiments (Ref. 27) has an attempt been made to separate inertia effects in the triaxial test from the shearing resistance.

In the dynamic triaxial tests the applied strain rate is constant and controlled during the test. Thus, experimental relationships between strain rate and strength can be clearly formulated; these relationships may be approximated by a logarithmic relationship between strain rate and strength. Figure 18, from Ref. 28, shows such a relationship for normally and overconsolidated clays.

Indirect experimental information on the effect of strain rate on the strength properties of soils has also been obtained from dynamic plate bearing and cone penetration tests (Refs. 29 through 31). In these experiments the total force required to

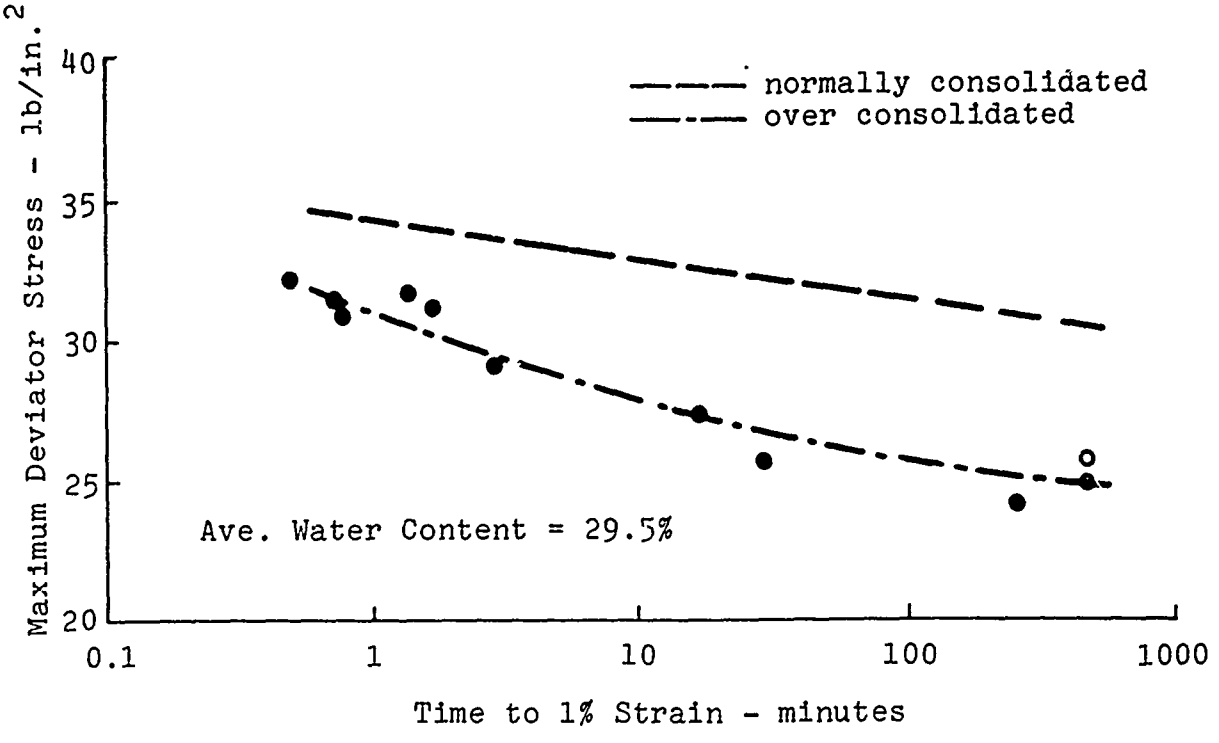

Fig. 18. Soil Strength - Strain Rate Relationships for Normally and Overconsolidated Clays (From Ref. 28)

force the plate or cone into the soil was measured at various rates of penetration. While these experiments provide useful information on the behavior of the soils tested under these conditions there is no theoretical basis for the generalization of these findings to other types of soils. Also, the evaluation of the strength properties of soils from these tests is difficult for two reasons. First, the effect of soil inertia forces would have to be accounted for separately. Second, the strain and the strain rate in the soil volume affected varies, and, therefore, any observed effect of the penetration rate on the load is the cumulative effect of various strain rates in the soil.

To compare, at least approximately, results of cone penetration tests and dynamic triaxial tests, an average strain rate was calculated for cone penetration tests performed in Buckshot clay on the following basis. Slip line fields for cone penetration in

clay show that a soil volume of a radius of about $R = (5 \text{ to } 6) * r$ (r = radius of the base of the cone) is affected by the penetration of the cone. If the initial void ratio of the soil is e_o and $R = 5r$ is assumed, then the change of void ratio due to the volume displaced by the cone (assuming no surface heave) is

$$\Delta e = \frac{e_o^2 - e_o + 1}{24(1 + e_o)} \tag{27}$$

The corresponding strain is

$$\epsilon = \frac{\Delta e}{1 + e_o} \tag{28}$$

The average strain rate depends on the average strain and the rate of penetration. For the WES cone the strain rate is

$$\dot{\epsilon} = \epsilon \frac{v_z}{h} \tag{29}$$

where $h = 3.77$ cm, the height of the cone. For the standard rate of cone penetration (3.05 cm/sec)

$$\dot{\epsilon} = .8 \times \epsilon (\text{sec}^{-1}) \tag{30}$$

In the tire tests conducted in Buckshot clay the cone index varied from 16 to 62. According to experiments reported in Ref. 32 this cone index variation corresponds to a variation in moisture content from 40 to 33 percent. The corresponding initial void ratios vary from 1.37 to 0.97, the average strains from 1.2 to 1.0 percent, and the average strain rates from 0.8 to 1.0 percent sec^{-1}.

In tire-soil interaction a crude approximation for the average strain ratio may be computed by the assumption that the depth of

soil affected by the interaction equals the radius of the tire. For two-dimensional conditions the average strain rate may be estimated as

$$\dot{\epsilon} = \frac{z_r}{R} \cdot \frac{v_f}{\ell} \tag{31}$$

This formula was used to compute the average strain rate for the test series on 9.00-14 tires reported in Table 8 of Ref. 1. For the tests performed at the standard velocity of 5 feet/second, the average strain rate computed by Eq. (31) varied from 5 to 34 percent sec^{-1}, appreciably higher than the average strain rate in a standard cone penetration test. For the tests performed at velocities from 0.5 to 18 feet/second, the average strain rate computed by Eq. (31) varied from 1 to 58 percent sec^{-1}.

Consideration of Strain Rate Effects in the Tire-Soil Model

In the test series on 9.00-14 tires mentioned previously the soil was characterized by its cone index obtained in cone penetration tests performed at the standard penetration rate. For the purpose of model validation, a relationship between the Coulomb strength parameters and the cone index was established for the Buckshot clay in Ref. 4, that was found to yield good prediction for the tire tests performed in Buckshot clay. The slip-interface shear parameters needed in the prediction were established by an empirical optimization technique.

In order to take strain rate effects in consideration in the model it would be desirable to establish the strength properties of the Buckshot clay as a function of the strain rate, determine the strain rate for a particular case, and apply in the model the strength parameters adjusted for the strain rate. Since the

strain rate is not known a priori, additional iterations would have to be performed in the model for its determination. Also, the inconsistency of the average strain rate being different in a standard cone penetration test from that in a standard tire test, such an approach would be unworkable. Instead, the experimental data reported for the test series on 9.00-14 tires in Buckshot clay were analyzed by adjusting the cone index values obtained at the standard penetration rate for the variations of the translational velocity. The cone penetration resistance was found to vary with the rate of penetration according to the following relation (Ref. 30)

$$CI_v = CI_s \left(\frac{v}{v_s}\right)^{0.092} \tag{32}$$

Since strain rates are proportional to the penetration rate in cone penetration and to the translational velocity in tire-soil interaction, the v/v_s ratio in the above equation may be substituted by the ratio of the actual translational velocity to the standard translational velocity in tire tests (5 feet/second).

An analysis of tire performance was made where the Coulomb strength parameters were determined for the CI values adjusted for the translational velocity by Eq. (32). Results of this analysis are shown in Fig. 19 where predicted pull coefficients are shown against measured ones. Indicated by various symbols are the ranges of adjustment factors for the CI values used in the computation.

It is seen from Fig. 19 that pull coefficients are generally overpredicted by the tire-soil model if adjustments in the strength properties for the strain rate are made on the assumption that the

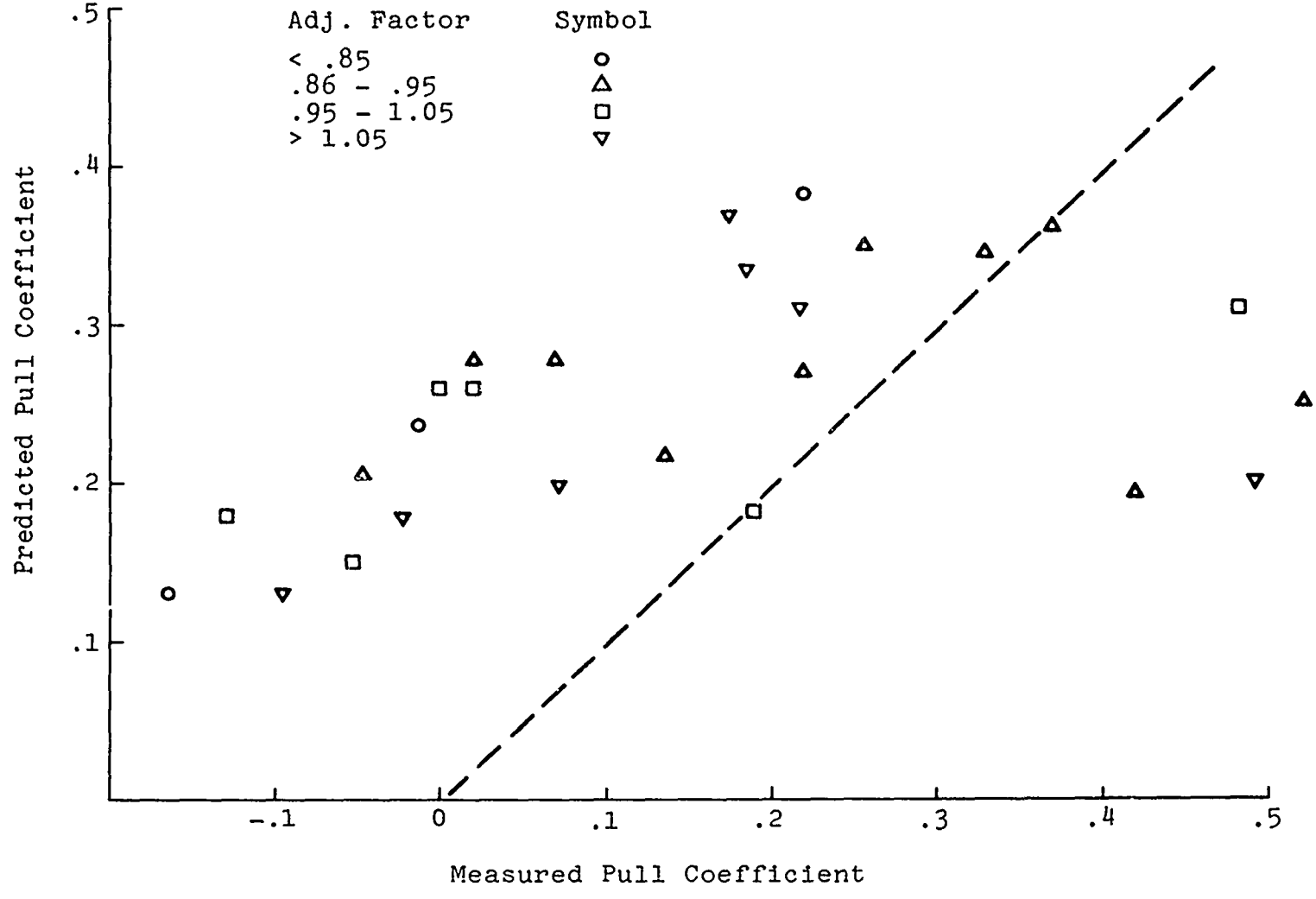

Fig. 19. Comparison of Measured and Predicted Pull Coefficients for Various Translational Velocities. Predictions Based on Cone Index Adjusted for the Ratio of Translational Velocity to the Standard Velocity (5 ft/sec) of Tire Tests

cone strength varies with the translational velocities as indicated by Eq. (32).

There are several reasons why this procedure has not resulted in a better approximation of the pull performance. These can be summed up as follows:

- In the computations for Fig. 19 the interface friction-slip parameters were assumed on the basis of unadjusted CI values. These parameters may vary with the translational velocity of the tire.
- In the tire-soil model the soil properties are assumed to be uniform throughout the affected soil mass. In tire-soil interaction, strains and strain rates vary from point to point. Thus, if variation of strength properties with strain rate is to be properly considered in the model, then the model would have to be expanded to allow for the variation of the strength properties at every nodal point. This variation would have to be determined on the basis of strain rate computations. The two methods for the computation of soil inertia forces presented in Sections IV and V lend themselves readily applicable to the computation of strain rates. Velocity fields as well as particle path geometries may be used for strain rate computations.
- The crude approximation of the average strain rate by Eq. (31) shows that strain rates are

proportional to the translational velocity for the same tire-soil geometry but vary significantly with the rut depth even if the translational velocity remains the same. Thus, an adjustment in the CI values based solely on translational velocities cannot reflect the effect of strain rate on the strength properties in tire-soil interaction.

Summary Discussion of the Effects of Strain Rate on Tire-Soil Interaction and Conclusions

Strain rate significantly affects the strength properties of certain soils and thereby tire-soil interaction. The experimental information on the effect of strain rate on soil strength behavior is limited to a few types of soil. The complexity of the physics of strain rate effects and the lack of a theory prohibit generalization of the results of experiments for other types of soils. Specifically, clay soils saturated to a lesser degree than in the experiments performed on Buckshot clay are likely to exhibit different behavior. More basic research is needed for the interpretation of strain rate effects observed in the experiments.

Theoretically, the most valuable information on the effect of strain rate on soil behavior is that obtained in dynamic triaxial tests where the strain rate is constant and controlled. Indirect information on the effects of strain rate has been obtained from cone penetration and plate sinkage tests performed at various rates of penetration. Interpretation of the results of these tests is difficult and the general validity of correlations with tire performance are questionable for the following reasons. First, soil inertia effects in these tests are not separated from strain rate

effects. Second, the strain rate varies in the affected soil mass and, therefore, measured changes in penetration resistance reflect the cumulative effect of strain rate variation in the affected soil volume. Theoretical and experimental research is needed to establish strain rate patterns for these experiments.

Soil strain rates also vary in tire-soil interaction. To take their effect properly into account in the tire-soil model it is necessary to determine the strain rate distribution in the soil. Of the various ways to accomplish this the evaluation from particle path geometries appears to be the most practical. More experimental information on particle path geometries is needed to determine the parameters in the analytical simulation presented in Section V.

VII. USE OF TIRE-SOIL MODEL IN VEHICLE RIDE DYNAMICS SIMULATION

In the simulation of tire-soil interaction by the tire-soil model it is assumed that tire load and travel velocity are constant and a steady state exists in the soil. With these assumptions the fundamental relationships governing tire-soil interaction may be formulated and compared with laboratory experiments without undue interference from interactions between tire and vehicle.

Another important area in mobility research is the simulation of ride dynamics of off-road vehicles. In the first generation dynamic models of off-road vehicles it is assumed that the ground is rigid and the motions of the vehicle are two dimensional. With these assumptions it is possible to analyze the dynamics of off-road vehicles under idealized conditions and validate the model for such conditions.

Ideally, in both vehicle performance and ride dynamics, simulation of the interaction between running gear and vehicle should be taken into account. Even though in the model expansion reported in Sections IV through VI velocity effects have been considered only in a very preliminary way, the model may be used to demonstrate its potential use in vehicle dynamic models. To this end sample computations were performed to determine axle height-load relationships for a 9.00-14 tire predicted by the model for the conditions shown in Table 5.

Figure 20 shows the results of computations for Cases 1 and 2. The difference between the two cases is in the value of the assumed drawbar pull. In this case the 100 pounds difference in drawbar pull does not appear to affect the axle height-load relationship appreciably. However, in other types of soils,

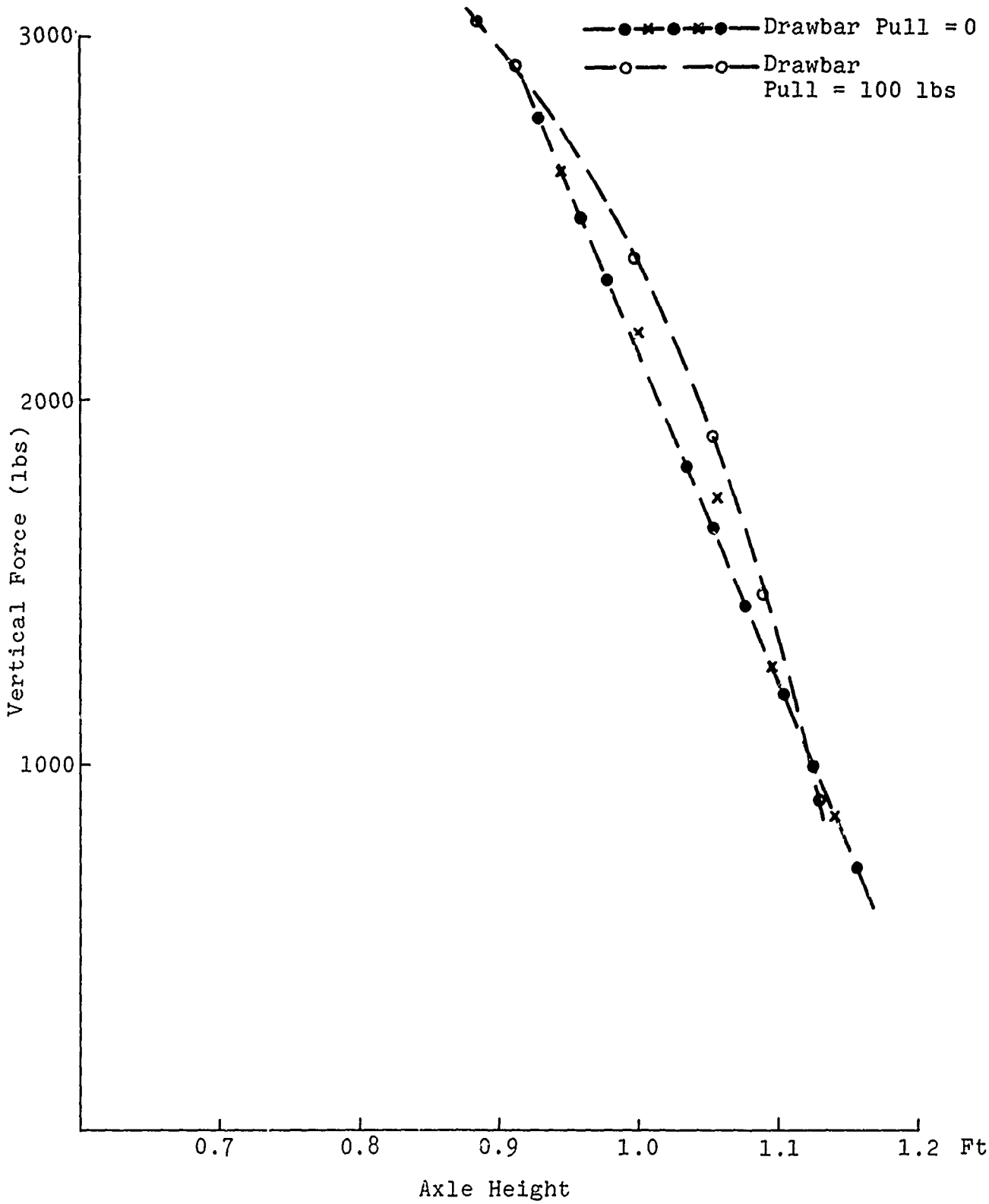

Fig. 20. Vertical Force - Axle Height Relationships for Cases No. 1 and 2 Shown in Table 5

TABLE 5 AXLE HEIGHT-LOAD RELATIONSHIPS

Tire Size: 9.00-14
Nominal Radius: 1.18 ft
Nominal Width: 0.74 ft
Soil: Buckshot Clay

Case No.	1	2	3	4
Tire Inflation Pressure psi	38	38	11.8	11.8
Limit Pressure psi	29	29	11.6	11.6
Deflection (WES Term.)	25%	25%	25%	25%
Deflection Coefficient (ε)	0.9	0.9	0.9	0.9
Translational Velocity ft/sec	5	5	5	10
Drawbar Pull lbs	0	100	0	0
Cone Index at Standard Penetration Rate	37	37	43	43
Cone Index Adjusted for Velocity	37	37	43	46

especially in cohesionless soils, it is likely that the effect of the drawbar pull on the vertical force-axle height relationship will be significant. Note that the relationship shown in Fig. 20 could be closely approximated by a linear spring model.

Figure 21 shows the same relationship for Cases 3 and 4 shown in Table 5. These two cases differ in soil strength since in Case 4 the cone index was adjusted for the strain rate corresponding to the 10 feet/second translational velocity. The obtained axle height-load relationships are almost identical, probably due to the controlling influence of the limiting pressure that governs the normal pressure over a large portion of the contact area in both cases. The soil strength comes into play only in a limited

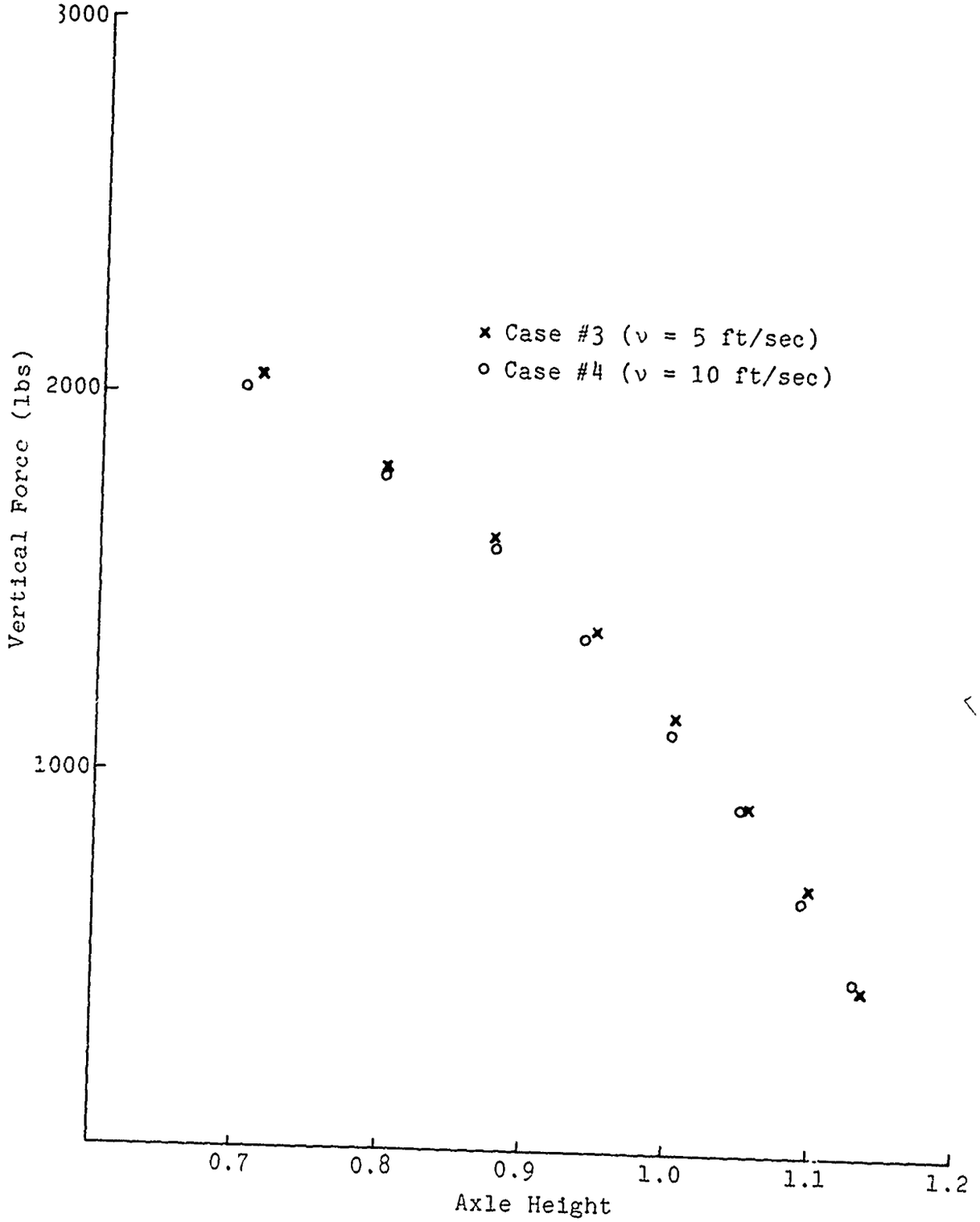

Fig. 21. Vertical Force - Axle Height Relationships for Cases No. 3 and 4 Shown in Table 5

portion of the contact area, hence the almost identical axle height-load relationships. This relationship is not as close to a linear one as the one shown in Fig. 20. Nevertheless, considering all other idealizations in vehicle dynamic models, a linear spring model would be an acceptable approximation.

These sample computations show that the tire-soil model, in addition to performance predictions, may also be used for the determination of realistic spring constants representing both tire deflection and ground deformation in vehicle dynamic models. Once such constants are determined for given tire and soil parameters, their inclusion in a dynamic model is simple. The main advantage of this procedure is that in the spring constants determined by the tire-soil model, the deformability of soil is included allowing thereby a more realistic simulation of off-road ride dynamics.

VIII. TOWED PNEUMATIC TIRE-SOIL MODEL

Introduction

For the analysis of cross country mobility of all wheel drive vehicles, determination of the drawbar pull that a tire can develop under various soil and terrain conditions is of prime importance. The driven pneumatic tire-soil model developed under Contract DAAE07-73-C0115 serves this purpose. However, it is often necessary to evaluate the performance of off-road vehicles towing trailers or of all wheel drive vehicles when the front wheel drive is disengaged or inoperative. For this purpose it is necessary to determine the towing force needed to move a pneumatic tire in various soils.

For the determination of the towing force a pneumatic towed tire model was developed by Janosi in 1960 (Ref. 33) using soil parameters from plate sinkage tests. Many features of this model were incorporated in the tire-soil model for driven tires. The accuracy of performance predictions achieved by the driven tire model, the need to use uniform soil parameters in both driven and towed tire models, and the desire to incorporate the results of more recent experimental information on tire geometry and interface stresses into the model, prompted the development of a towed tire-soil model described herein.

Experimental Information on Towed Pneumatic Tire Behavior

Numerous towed tire tests have been performed by various researchers over the years. Most of these were restricted to the measurement of towing force and sinkage. For the development of a towed tire-soil model those tire tests are especially of interest

where tire geometry and interface stresses were measured (Refs. 33 through 40).

The tire geometry measurements on towed tires (Refs. 36 through 40) show that for towed tires the same qualitative relationships among tire stiffness, soil stiffness, sinkage, and deflection hold as this general relationship is shown schematically in Fig. 22 for driven tires.

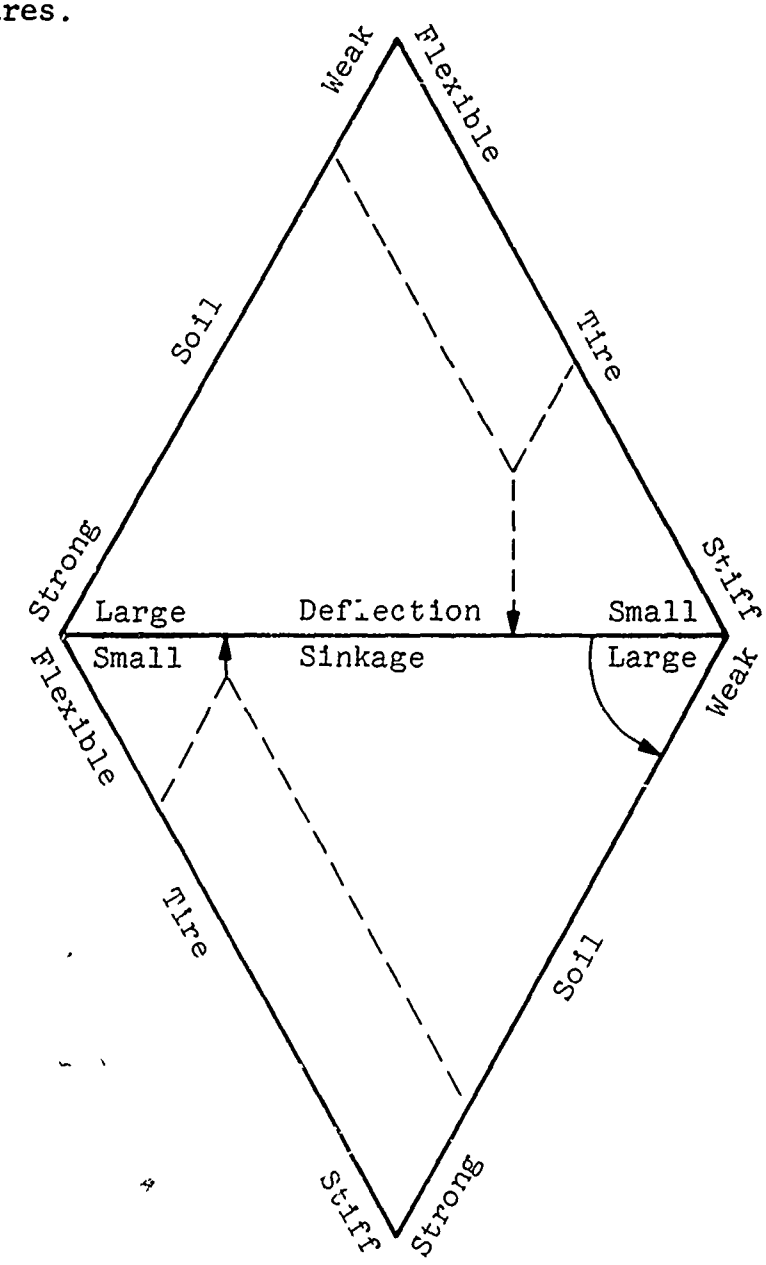

Fig. 22. Schematic Representation of Tire-Soil Behavior (Based on WES Experiments)

Experimental information on stresses measured at the interface of towed tires is meager and restricted to the measurement of normal stresses. Since the salient difference between driven and towed tires is in the magnitude and distribution of interface shear stresses, this lack of experimental information presented a serious drawback for the formulation of interface shear stress criteria. In lieu of anything better, these were formulated on the basis of interface shear stress measurements on towed rigid wheels. Figure 23 shows a typical result of such measurements by Krick (Ref. 40).

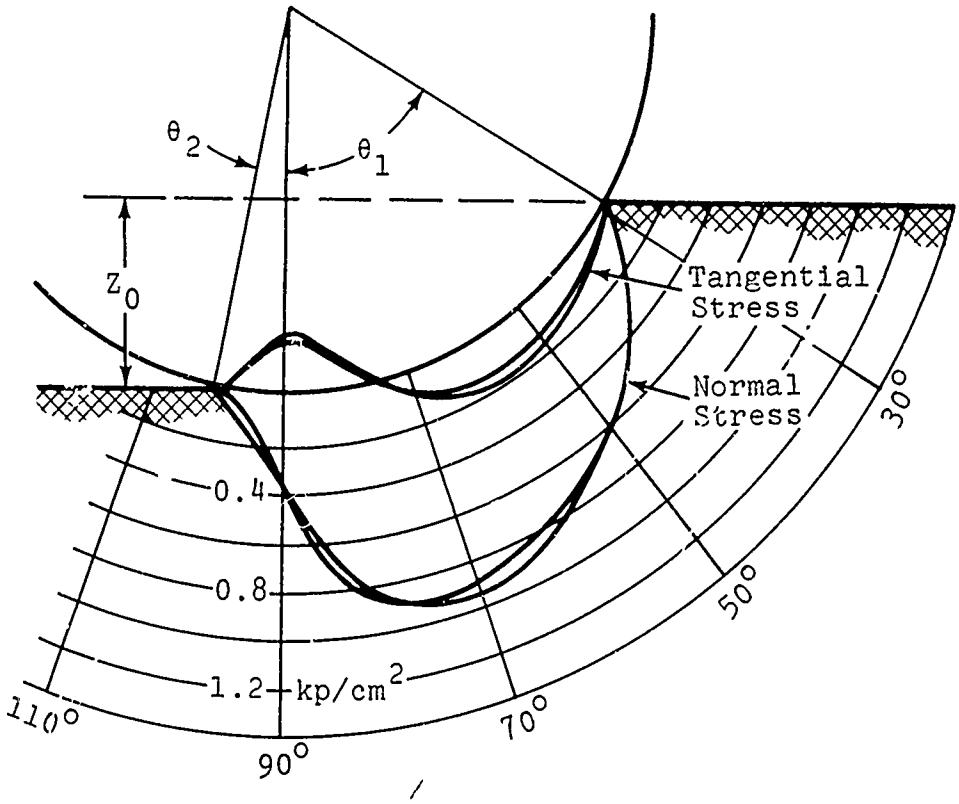

Fig. 23. Distribution of Normal and Shear Stresses Beneath a 0.88 in. Diameter Rigid Wheel (Averaged Over the Width for Two Tests) Wheel Load: 640 kg (From Ref. 40)

Concept of Towed Tire-Soil Interaction

In the conceptual development of the towed tire-soil model the inferences drawn from the study of experimental information were incorporated in the following way.

- Tire deflection was related to the arc length of the front slip line field in the same way as in the driven tire-soil model.
- The interface friction coefficient, δ, that governs the shear stress distribution, was assumed to vary linearly from the entry and exit points to a central angle, α_o, where its sign changes. This assumption results in a shear stress distribution similar to that obtained for rigid wheels and shown in Fig. 23.
- For the shear stresses the criterion was adopted that their moment about the tire axis be zero. While at first glance this criterion appears to be self-evident for a towed tire where the applied torque is zero, it should be brought to mind that in the case of a deflecting tire normal stresses may also produce moments about the axis. In such a case the moment produced by the normal stresses would have to be balanced by the shear stresses resulting in a different shear stress distribution. It is in this respect that the lack of experimental information on interface shear stresses beneath towed tires hindered the development of a towed tire model that

would be responsive to this contingency in shear stress distribution.

- For the driven tire-soil model, relationships were developed between slip and the interface friction angle. For towed tires, skid or negative slip is of less importance since it does not affect travel efficiency or power consumption. Therefore, skid-interface friction relationships were not analyzed and included in the model.

Development of Towed Tire-Soil Model

The concepts of towed tire-soil interaction described previously were incorporated in the towed tire-soil model shown in Fig. 24. The tire centerline geometry consists of logarithmic spirals and straight lines, as in the driven tire model. Tire deflection is assumed to start ahead of the entry point and ceases after the exit point. This assumption is incorporated in the model by the angle α' (see Fig. 24) that defines the end points of the logarithmic spirals in the front and rear. The normal stresses are controlled by plastic equilibrium conditions in the soil whenever they are less than the limit pressure p_ℓ that depends on the tire inflation pressure. The shear stresses and the interface friction angle δ are assumed to vanish at the central angle α_o. A linear variation of δ from the entry and exit points results in a shear stress distribution as shown in Fig. 24.

For towed tire-soil interaction, the soil model is the same as for driven tire-soil interaction. Soil behavior is represented by its Coulomb strength parameters and its unit weight. The gen-

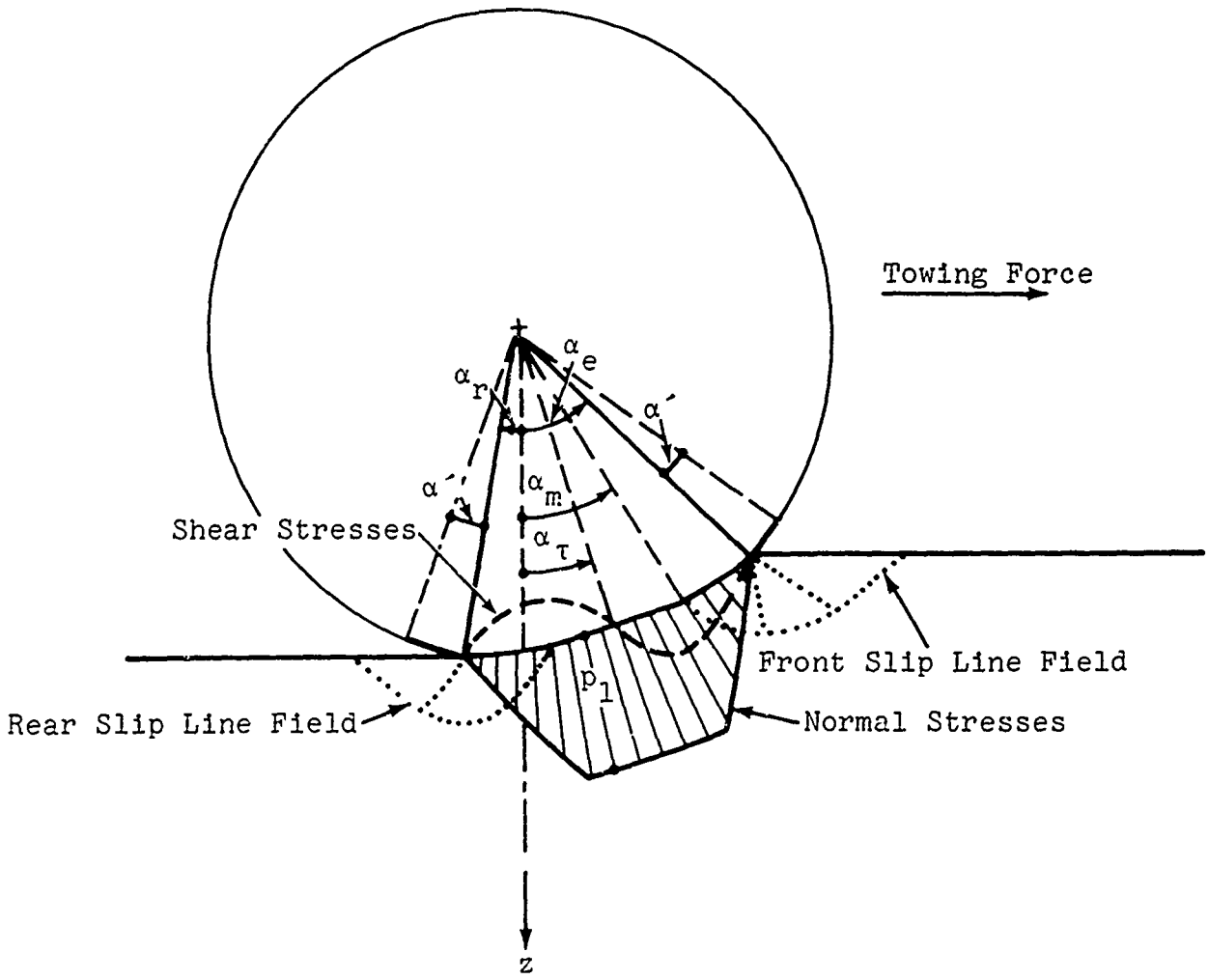

Fig. 24. Towed Tire-Soil Model

eral concept of towed tire-soil interaction as incorporated in the towed tire-soil model shown in Fig. 24 does not, in itself, uniquely define the geometry of the tire-soil interface. The condition that the normal stress, q_m at the assumed angle, α_m, be equal to the limit pressure p_ℓ defines the entry angle, since it is by the variation of the entry angle that this condition is met. However, the rear angle α_r is undefined. Experimental information on the geometry of towed tires shows that the rear angle varies with the load and the entry angle. To define a general relationship

for a wide variaty of soil and loading conditions the same approach was followed as for the development of the driven tire-soil model. A computer program was written for the towed tire-soil model and towing force computations were made for a variety of assumptions regarding the rear angle. The towed force computations were performed for tire sizes and soil conditions for which experimental data were reported in Ref. 1. These towed tire tests were selected for validation of the model because soil strength parameters for the two types of soils used in the tests were already established in Report No. 11900 (LL147) (Ref. 4).

Since the cost of the large number of computer runs required to perform the contemplated systematic analysis of the effect of the various assumptions on the towed force is high, the computer program was adapted to the General Data Corporation Nova Minicomputer owned by the Research Department. Running time of the computer program on the minicomputer is about 4-8 times that on large computers but the running cost is nominal. Arrangements were made for input and output data reading from, and recording on, data files so that results for a large number of selected cases could be obtained overnight.

The computer analyses of a large number of cases served the dual purpose of comparing results with experimental data and checking on tolerance limits and convergency criteria of various iteration schemes adopted in the computer program. In connection with the latter, some new problems arose that are discussed below.

Problems Encountered

In the development of the computer program for towed tire-soil interaction the experiences gained with the driven tire-soil model were heavily relied upon. One of the tasks that had to be solved

in both models is that of finding the size of the slip line field that matches a prescribed normal stress at the interface at its end point. All iteration schemes developed for the driven tire-soil model were based on the assumption that the normal stresses computed for any slip line field increase from the edge point adjoining the free surface toward the inner points. While this is generally true for a constant δ angle of interface friction assumed for driven tires, it is not necessarily so when the angle decreases from the edge toward the inner point. It was found that in certain cases in cohesive soils with a low friction angle the normal stress is unchanged or even decreases from the edge point for a certain rate of decrease in the δ angle. Measurements of normal stresses at the interface of a rigid wheel towed in clay reported by Uffelmann (Ref. 41) and shown in Fig. 25 indicate that in highly cohesive soils this is, indeed, possible.

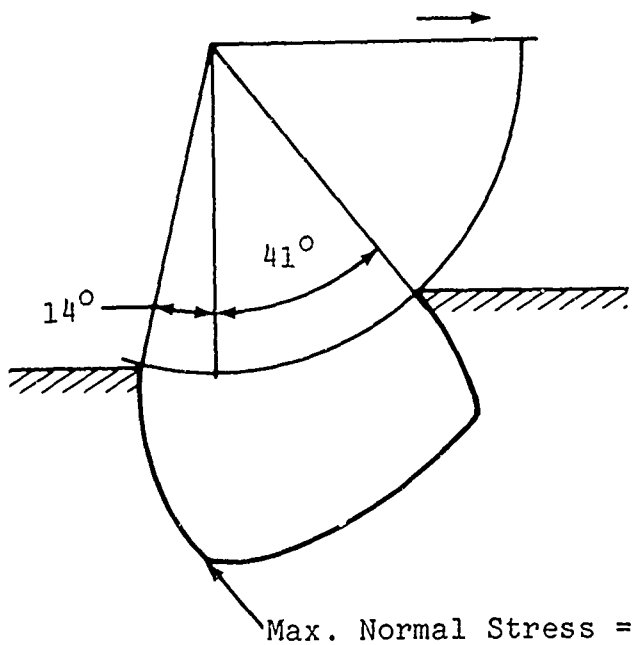

Fig. 25. Distribution of Normal Stresses Beneath a 54-in. Diameter Rigid Wheel Towed in Heavy Clay. Load: 6720 lbs; Slip: = 27%, (From Ref. 41)

This feature of the normal stress distribution in cohesive soils made it necessary to make provisions in the program that account for this situation. The main problem that had to be resolved was the determination of the size of the front slip line field for nearly constant normal stresses. In principle, this problem was resolved by assuming that the size of the front field for entry angles between 30 and 60 degrees is determined by the condition that the vertical components of all stresses be equal to the load. The rear angle is assumed as 10 degrees for the variations of the entry angle from 30 to 60 degrees. For entry angles less than 30 degrees the rear angle is reduced by half of the difference between the entry angle and 30 degrees. A computational scheme corresponding to these assumptions was incorporated in the computer program. Results of the towing force computations were compared with experimental data and were found to yield acceptable approximations within the limitations of a two dimensional model.

Results of the Analyses of Experimental Data

The systematic analyses of the experimental data were directed primarily toward determination of the best assumption as to the relative positions of the front and rear slip line field controlled by the angle of separation and rear angle. The effects of other assumptions, such as the relationship between the limiting and inflation pressures, the value of the interface friction angle at the entry and exit point, and the location of zero shear stress were also investigated. In the course of these systematic analyses performed on the minicomputer over 3000 cases were investigated, all representing different combinations of the input data and assumptions. The cost of this systematic investigation, if carried out

on large computers at commercial rates, would have amounted to more than half of the contract cost. Even though the number of cases investigated appears to be large, only a limited number of all possible combinations of input variables and assumptions are covered. Nevertheless, it was possible to establish approximate relationships that define the towed tire-soil model completely and result in acceptable prediction accuracy. Although further systematic analyses could have resulted in refinements in the model, the time spent would have been prohibitive. Also, the systematic analyses showed that prediction accuracy could not be improved significantly unless three dimensional conditions were considered in the model.

The following assumptions were incorporated in the final computer program on the basis of these systematic analyses:

Initial value of rear angle $\alpha_r = 10°$

Initial value of separation angle $\alpha_m = 20°$

Relationship between rear and separation angle =

$$\alpha_m = 1.5 \times \alpha_r + 5° \tag{33}$$

The effects of limiting pressure on the prediction of towing forces were also investigated. In the case of towed tires the following relationship was found to yield good simulations

$$p_\ell^{(psi)} = 0.82 \times p_i + 6 \tag{34}$$

The interface friction angle δ is assumed to vary from a maximum value at the entry and exit points to 0 at some inner point. The variation of δ along the interface is thus defined by its maximum value and the angle α_o at which its value becomes zero. This angle was defined in the program as

$$\alpha_o = F_\tau \alpha_m \tag{35}$$

where the value of the factor F_τ was to be determined by the condition that the moment of the shear stresses about the tire axis be zero. The systematic analyses were run with various values of the F_τ factor. It was found that a value of $F_\tau = 0.5$ generally yielded a negligible moment of the shear stresses. Although it would have been possible to set up an iteration scheme whereby the moment of the shear stresses was made less than a specified tolerance by an appropriate variation of the F_τ value, it was found that the prediction accuracy would not have been improved in a significant degree to warrant the additional computer time required for these iterations. If, however, for any reason, the moment of shear stresses appears to be unacceptably high, an appropriate change in the input F_τ value would bring it to an acceptable level.

The maximum value of the interface friction angle was assumed as

$$\delta_{max} = F_\delta \cdot \varphi \tag{36}$$

In the systematic analysis the effect of the factor F_δ on the towed force coefficient was investigated by assuming various values for F_δ. It was found that for good simulation F_δ may vary between 0.25 and 0.50. These values are in the range of F_δ values evaluated from experimental data on rigid wheels. Shear stress measurements on towed pneumatic tires in various soils would be needed to firm up the value of the F_δ factor. A detailed flow chart of the computer program incorporating these features is given in Appendix C.

A comparison of measured and predicted towed force coefficients is given in Tables 6 through 10 for various tire sizes, loading, and soil conditions. The experimental data were reported in Ref. 1 where more detailed information on the performance of experiments may be found.

As shown in the tabulations, in addition to the towed force coefficient actually measured in the experiment, the one computed from the best fitting curve for all experiments performed in the same soil, as reported in Ref. 1, is also given. Since all experimental measurements necessarily contain some experimental error, differences in predicted and measured towed coefficients may arise from errors or inaccuracies in either value. In the course of the systematic analyses of the experimental data it became evident, in some instances, that efforts to simulate individual experiments may be antiproductive if that experiment contains a significant error. A comparison of measured towed coefficients with that obtained from a best fitting curve is an indication of whether that may be the case.

The predicted towed force coefficients were obtained with $F_\tau = 0.5$ and $F_\delta = 0.25$ and deflection coefficients ϵ established for driven tires in Ref. 4 and shown in Table 11.

Figures 26 and 27 show typical centerline geometries and interface stress distributions predicted by the model for the following conditions:

	Fig. 26	Fig. 27
Tire Size:	9.00-14	4.00-20
Tire radius:	1.18 ft	1.17 ft
Tire Width:	0.73 ft	0.37 ft
Inflation Pressure:	12.0 psi	40.0 psi
Deflection Coefficient ϵ:	0.905	0.945
Soil:	Yuma Sand	Buckshot Clay
Cone Index:	----	18 psi
Cone Index Gradient:	3.5 pci	----

TABLE 6 COMPARISON OF PREDICTED AND MEASURED TOWED FORCE COEFFICIENTS
TIRE SIZE: 6.00-16

SOIL: YUMA SAND

Case Code No.	WES Identification No.	Cone Index (psi) (in clay) or Cone Index Gradient (pci) (in sand)	Load lbs	Inflation Pressure psi	WES Deflection δ/h	Towed Force Coefficient		
						Measured	Averaged From Best Fitting Curve	Predicted
1	164 802A	5.8	213	8.5	0.15	0.155	0.114	0.088
2	164 805A	12.1	215	8.5	↓	0.070	0.058	0.081
3	164 809A	15.6	222	8.5	↓	0.059	0.048	0.075
4	164 808A	12.4	293	11.4	↓	0.065	0.073	0.085
5	164 807A	10.4	458	17.2	↓	0.131	0.139	0.121
6	165 35A	4.0	650	29.0	↓	0.449	2.3	0.203
7	164 816A	13.5	240	4.5	0.25	0.042	0.0395	0.078
8	165 37A	15.0	223	4.5	↓	0.063	0.035	0.083
9	164 818A	15.6	455	10.3	↓	0.040	0.057	0.092
10	165 33A	2.3	429	10.3	↓	0.424	0.604	0.238
11	164 812A	13.8	865	21.0	↓	0.088	0.116	0.127
12	164 817A	9.5	863	21.0	↓	0.200	0.179	0.155
13	164 803A	5.8	225	2.5	0 35	0.116	0.055	0.111
14	164 813A	16.4	239	2.5	↓	0.046	0.029	0.078
15	164 814A	17.3	446	7.0	↓	0.018	0.040	0.092
16	165 34A	3.5	674	10.3	↓	0.365	0.331	0.217
17	164 811A	15.0	870	13.0	↓	0.055	0.077	0.125
			SOIL: BUCKSHOT CLAY					
164	321C	20	238	8.5	0.15	0.059	0.061	0.087
165	323C	63	237	8.5	↓	0.013	0.023	H.S.F.
166	329C	40	238	8.5	↓	0.021	0.031	H.S.F.
167	325C	20	430	17.2	↓	0.144	0.142	0.124
168	351C	55	461	17.2	↓	0.033	0.042	H.S.F.
169	327C	20	631	29.0	↓	0.254	0.367	0.157
170	339C	40	688	29.0	↓	0.112	0.093	0.086
171	344C	37	877	38.0	↓	0.155	0.170	0.125
172	359C	54	875	38.0	↓	0.114	0.089	H.S.F.
173	322C	20	243	4.5	0.25	0.037	0.047	H.S.F.
174	324C	61	234	4.5	↓	0.004	0.097	H.S.F.
175	330C	42	237	4.5	↓	0.021	0.051	H.S.F.
176	326C	19	444	10.3	↓	0.119	0.107	0.135
177	357C	51	460	10.3	↓	0.022	0.036	H.S.F.
178	354C	50	662	15.3	↓	0.050	0.051	H.S.F.
179	338C	22	688	15.3	↓	0.222	0.179	0.165
180	362C	50	716	16.2	↓	0.052	0.056	H.S.F.
181	337C	21	848	21.0	↓	0.292	0.355	0.183
182	345C	37	893	21.0	↓	0.127	0.111	H.S.F.
183	360C	52	889	21.0	↓	0.066	0.069	H.S.F.
184	331C	20	240	2.5	0.35	0.038	0.040	H.S.F.
185	342C	37	226	2.5	↓	0.027	0.024	H.S.F.
186	355C	53	223	2.5	↓	0.045	0.019	H.S.F.
187	332C	20	457	7.0	↓	0.074	0.081	0.092
188	343C	37	448	7.0	↓	0.033	0.040	H.S.F.
189	356C	53	447	7.0	↓	0.034	0.0295	H.S.F.
190	341C	36	672	10.3	↓	0.042	0.063	H.S.F.
191	358C	50	673	10.3	↓	0.022	0.044	H.S.F.
192	340C	39	878	13.0	↓	0.071	0.079	H.S.F.
193	361C	52	873	13.0	↓	0.046	0.056	H.S.F.

TABLE 7 COMPARISON OF PREDICTED AND MEASURED TOWED FORCE COEFFICIENTS
TIRE SIZE: 9.00-14

SOIL: YUMA SAND

Case Code No.	WES Identification No.	Cone Index (psi) (in clay) or Cone Index Gradient (pci) (in sand)	Load lbs	Inflation Pressure psi	WES Deflection δ/h	Towed Force Coefficient		
						Measured	Averaged From Best Fitting Curve	Predicted
71	164 778A	8.1	230	7.5	0.15	0.052	0.065	0.075
72	164 779A	6.3	225	7.5		0.093	0.079	0.082
73	164 780A	13.8	230	7.5		0.074	0.043	0.065
74	164 786A	17.9	232	7.5		0.026	0.036	0.063
75	164 777A	8.9	460	16.4		0.113	0.114	0.108
76	164 782A	12.4	458	16.4		0.068	0.081	0.092
77	164 783A	5.2	436	16.4		0.216	0.203	0.137
78	164 785A	17.6	460	16.4		0.046	0.060	0.083
79	164 781A	12.1	871	36.7		0.177	0.161	0.123
80	164 784A	17.0	864	36.7		0.086	0.109	0.097
81	165 5A	10.7	144	5.5	0.25	0.049	0.028	0.067
82	165 4A	11.2	225	6.0		0.031	0.035	0.088
83	165 7A	22.5	216	6.0		0.028	0.024	0.072
34	165 6A	12.4	446	8.8		0.063	0.052	0.098
86	165 28A	3.5	656	11.6		0.386	0.315	0.201
87	165 3A	13.8	850	14.5		0.035	0.081	0.115
88	165 24A	15.0	862	14.5		0.041	0.076	0.114
89	1-65-64	13.3	156	5.5		0.013	0.027	0.067
90	1-65-65	11.8	144	5.5		0.035	0.027	0.061
91	1-65-66	12.7	243	6.4		0.021	0.034	0.086
92	1-65-67	11.6	237	6.4		0.025	0.035	0.087
93	1-65-68	13.2	650	11.3		0.029	0.066	0.109
94	1-65-69	10.3	821	14.0		0.069	0.105	0.136
95	1-65-70	13.2	348	7.5		0.017	0.041	0.093
104	1-65-71	9.7	286	6.9		0.024	0.045	0.089
97	1-65-72	10.3	163	5.7		0.001	0.031	0.064
98	1-65-74	11.0	450	8.8		0.028	0.058	0.108
99	165 9A	20.7	243	2.0	0.35	0.074	0.023	0.071
100	165 11A	13.0	226	2.0		0.058	0.027	0.080
101	165 12A	24.2	668	7.5		0.033	0.034	0.090
102	165 13A	3.7	653	7.5		0.198	0.180	0.195
103	165 10A	12.4	892	10.6		0.044	0.069	0.123
	SOIL: BUCKSHOT CLAY							
135	297C	17	227	7.5	0.15	0.040	0.056	0.087
136	304C	32	231	7.5		0.017	0.031	H.S.F.
137	308C	54	238	7.5		0.013	0.022	H.S.F.
138	298C	17	434	16.4		0.161	0.135	0.123
139	303C	51	444	16.4		0.027	0.036	H.S.F.
140	305C	32	459	16.4		0.033	0.060	0.068
141	301C	16	621	25.4		0.308	0.374	0.176
142	306C	30	653	25.4		0.110	0.102	0.100
143	313C	57	652	25.4		0.063	0.046	H.S.F.
144	307C	31	866	36.7		0.136	0.155	0.123
145	418C	32	882	36.7		0.088	0.072	H.S.F
146	299C	16	431	7.5	0.25	0.128	0.098	0.124
147	310C	34	436	7.5		0.025	0.041	H.S.F.
148	312C	57	441	7.5		0.034	0.027	H.S.F.
149	308C	16	817	16.4		0.379	0.410	0.254
150	311C	35	867	16.4		0.092	0.086	H.S.F.
151	419C	51	886	16.4		0.047	0.056	H.S.F.
152	314C	36	243	2.0	0.35	0.025	0.023	H.S.F.
153	414C	55	225	2.0		0.062	0.017	H.S.F.
154	417C	25	233	2.0		0.047	0.028	H.S.F.
155	390C	40	451	4.4		0.042	0.032	H.S.F.
156	408C	23	449	4.4		0.042	0.053	H.S.F.
157	410C	51	442	4.4		0.023	0.026	H.S.F.
158	409C	22	646	7.5		0.082	0.087	0.161
159	411C	52	658	7.5		0.021	0.035	H.S.F.
160	412C	39	658	7.5		0.030	0.046	H.S.F.
161	413C	39	883	10.6		0.041	0.062	H.S.F.
162	415C	56	864	10.6		0.032	0.042	H.S.F.
163	416C	23	880	10.6		0.127	0.131	0.124

TABLE 8 COMPARISON OF PREDICTED AND MEASURED TOWED FORCE COEFFICIENTS
TIRE SIZE: 4.00-7

SOIL: YUMA SAND

Case Code No.	WES Identification No.	Cone Index (psi) (in clay) or Cone Index Gradient (pci) (in sand)	Load lbs	Inflation Pressure psi	WES Deflection "/h	Towed Force Coefficient		
						Measured	Averaged From Best Fitting Curve	Predicted
44	164 198A	17.3	85	16.2	0.15	0.259	0.085	0.068
45	164 824A	15.8	106	16.2		0.113	0.117	0.082
46	164 825A	9.8	123	33.2		0.171	0.258	0.250
47	164 800A	13.0	210	33.2		0.305	0.377	0.175
48	164 827A	17.6	121	6.2	0.25	0.025	0.073	0.107
49	164 828A	19.6	122	6.2		0.033	0.067	0.104
50	164 831A	25.1	185	17.0		0.130	0.077	0.098
51	164 822A	13.0	216	17.0		0.139	0.188	0.161
52	164 829A	19.6	234	17.0		0.107	0.126	0.131
53	164 826A	12.1	348	26.0		0.210	0.434	0.229
54	164 833A	18.7	109	2.5	0.35	0.119	0.049	0.100
55	164 834A	18.7	152	5.5		0.086	0.064	0.109
56	164 1A	22.8	145	5.5		0.103	0.052	0.100
57	164 830A	19.6	224	10.1		0.076	0.085	0.132
58	164 832A	19.9	455	12.7		0.125	0.174	0.157
			SOIL: BUCKSHOT CLAY					
21	363C	56	113	16.2	0.15	0.027	0.034	H.S.F.
22	368C	45	117	16.2		0.117	0.040	H.S.F.
23	371C	26	97	16.2		0.093	0.062	0.079
24	365C	46	226	33.2		0.137	0.087	0.077
25	383C	66	228	33.2		0.083	0.056	H.S.F.
26	373C	41	335	51.8		0.188	0.212	0.125
27	380C	66	340	51.8		0.109	0.092	H.S.
28	375C	42	439	63.5		0.237	0.427	0.143
29	385C	66	451	63.5		0.146	0.141	H.S.F.
30	364C	46	117	6.2	0.25	0.026	0.033	H.S.F.
31	372C	26	103	6.2		0.068	0.050	H.S.F.
32	367C	62	217	17.0		0.134	0.044	H.S.F.
33	370C	44	229	17.0		0.074	0.068	H.S.F.
34	374C	42	330	26.0		0.148	0.122	H.S.F.
35	384C	66	340	26.0		0.097	0.067	H.S.F.
36	376C	37	436	35.0		0.287	0.292	0.166
37	386C	65	446	35.0		0.108	0.097	H.S.F.
38	378C	34	221	10.4	0.35	0.104	0.073	H.S.F.
39	387C	66	222	10.4		0.072	0.037	H.S.F.
40	379C	36	322	17.0		0.208	0.115	H.S.F.
41	388C	66	336	17.0		0.042	0.055	H.S.F.
42	377C	38	446	21.9		0.197	0.192	H.S.F.
43	389C	68	448	21.9		0.083	0.074	H.S.F.

TABLE 9 COMPARISON OF PREDICTED AND MEASURED TOWED FORCE COEFFICIENTS
TIRE SIZE: 4.00-20

SOIL: YUMA SAND

Case Code No.	WES Identification No.	Cone Index (psi) (in clay) or Cone Index Gradient (pci) (in sand)	Load lbs	Inflation Pressure psi	WES Deflection δ/h	Towed Force Coefficient		
						Measured	Averaged From Best Fitting Curve	Predicted
59	164 791A	7.5	218	24.7	0.15	0.211	0.198	0.107
60	164 793A	16.4	221	24.7	↓	0.118	0.084	0.062
61	164 788A	12.1	426	48.2	↓	0.246	0.252	0.119
62	164 794A	12.7	440	48.2	↓	0.227	0.246	0.109
63	164 795A	16.1	446	48.2	↓	0.195	0.181	0.093
64	165 14A	27.7	227	11.4	0.25	0.079	0.038	0.076
65	165 15A	14.4	238	11.4	↓	0.046	0.065	0.091
66	165 19A	16.1	338	18.2	↓	0.062	0.079	0.100
67	165 16A	13.0	450	24.7	↓	0.156	0.131	0.123
68	165 21A	25.6	233	6.7	0.35	0.064	0.034	0.084
69	165 22A	25.6	350	11.0	↓	0.029	0.058	0.091
70	165 20A	16.4	442	15.0	↓	0.048	0.074	0.111
		SOIL: BUCKSHOT CLAY						
105	401C	48	305	82.0	0.08	0.056	0.065	H.S.F.
106	402C	22	307	82.0	0.08	0.156	0.251	0.123
107	269C	20	204	24.7	0.15	0.059	0.086	0.099
108	275C	48	221	24.7	↓	0.023	0.036	H.S.F.
109	279C	32	228	24.7	↓	0.048	0.055	0.067
110	271C	18	388	40.0	↓	0.255	0.427	0.177
111	273C	46	456	48.2	↓	0.070	0.081	0.085
112	287C	32	448	48.2	↓	0.127	0.139	0.125
113	286C	48	629	61.0	↓	0.097	0.122	0.099
114	270C	22	204	11.4	0.25	0.044	0.057	0.099
115	276C	52	228	11.4	↓	0.022	0.028	H.S.F.
116	280C	33	225	11.4	↓	0.044	0.042	H.S.F.
117	272C	19	377	18.2	↓	0.207	0.171	0.162
118	274C	48	450	24.7	↓	0.038	0.056	H.S.F.
119	288C	33	447	24.7	↓	0.103	0.089	0.114
120	281C	47	645	37.5	↓	0.095	0.090	0.099
121	291C	40	664	37.5	↓	0.130	0.121	0.125
122	293C	54	637	37.5	↓	0.055	0.073	H.S.F.
123	277C	50	211	6.7	0.35	0.038	0.025	H.S.F.
124	283C	29	236	6.7	↓	0.021	0.042	H.S.F.
125	289C	19	236	6.7	↓	0.021	0.067	0.110
126	278C	50	433	15.0	↓	0.035	0.044	H.S.F.
127	284C	30	454	15.0	↓	0.077	0.084	0.125
128	295C	19	421	15.0	↓	0.140	0.156	0.181
129	282C	45	651	23.0	↓	0.060	0.078	H.S.F.
130	292C	35	664	23.0	↓	0.092	0.115	0.136
131	294C	52	628	23.0	↓	0.033	0.062	H.S.F.
132	285C	52	696	23.0	↓	0.052	0.070	H.S.F.
133	400C	48	660	16.1	0.45	0.055	0.063	H.S.F.
134	403C	22	635	16.1	↓	0.228	0.210	0.183

TABLE 10 COMPARISON OF PREDICTED AND MEASURED TOWED FORCE COEFFICIENTS

Tire Size: 31 x 15-13

Soil: Yuma Sand

Case Code No.	WES Identification	Cone Index Gradient (pci)	Load (lbs)	Inflation Pressure (psi)	WES Deflection δ/h	Towed Force Coefficient Measured	Towed Force Coefficient Averaged From Best Fitting Curve	Towed Force Coefficient Predicted
18	A68-0111-1	17.5	455	5.6	0.15	0.009	0.031	0.073
19	A68-0107-1	9.8	1200	9.7	0.25	0.059	0.063	0.118
20	A68-0110-1	13.1	890	4.0	0.35	0.044	0.033	0.104

TABLE 11 ESTIMATION OF THE DEFLECTION COEFFICIENT ϵ FOR VARIOUS SIZE TIRES

Tire Size	Relationship for Estimation of ϵ
9.00-14	$1.24\kappa - 0.195$
6.00-16	$1.62\kappa - 0.59$
4.00-7	$1.14\kappa - 0.115$
4.00-20.0	$0.91\kappa + 0.085$
31 x 15-13	$0.98\kappa + 0.065$

$$\kappa = 1 - \frac{2\delta}{d}$$

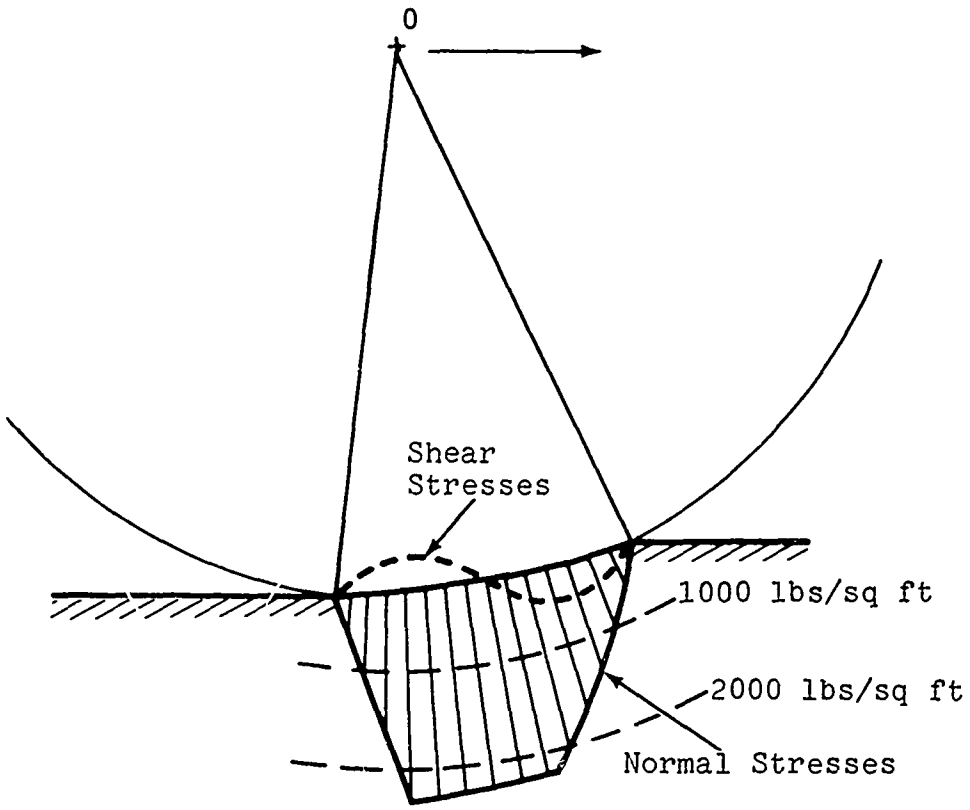

Fig. 26. Interface Normal and Shear Stress in Sand Predicted by the Towed Tire-Soil Model

Evaluation of the Towed Tire-Soil Model

In Tables 6 through 10 towed force coefficients predicted by the model are compared with experimental data. The soil strength parameters used in these predictions are those established for Yuma sand and Buckshot clay in Ref. 4 as functions of cone penetration values. Considering that the soil strength parameters determined on this basis are approximate ones the prediction accuracy achieved by the towed tire-soil model is generally very good.

A review of towed force coefficient predictions was made with the objective of determining causes of differences between predictions and experiments. As a result of this review the following conclusions were reached.

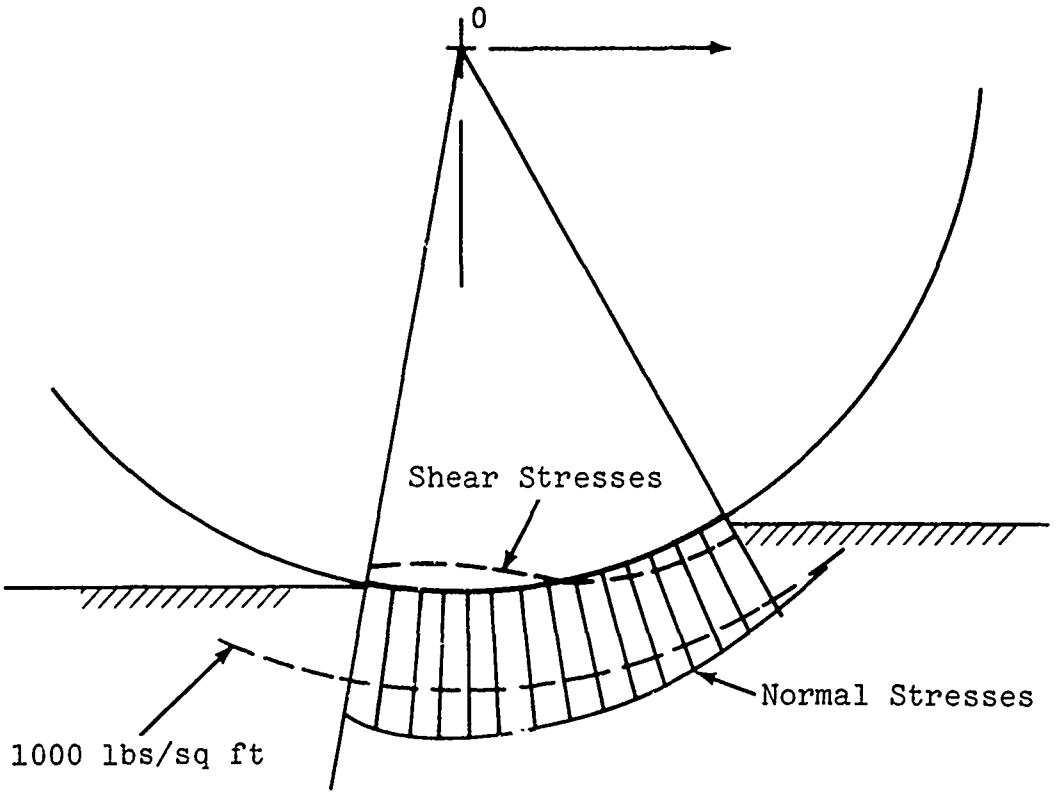

Fig. 27. Interface Normal and Shear Stresses in Clay Predicted by the Towed Tire-Soil Model

- Underpredictions of the towed force coefficient occurred when the measured coefficient was very high (higher than about 0.3). The major cause of this underprediction was that three dimensional effects were disregarded in the two dimensional model. Soil failure in the third (lateral) dimension would limit normal stresses in the transverse direction beneath the tire and result in a reduction of normal stresses toward the side edges of the tire, especially in the front field. Because of this reduction of the normal stresses the contact area would have to increase to balance the load resulting in higher entry angle, sinkage and towed force coefficient.

- Bow waves, unaccounted for in the model, may also cause an increase in the towed force coefficient.

- In cohesive soils, the towed force coefficient is very sensitive to small changes in soil strength. This may be best illustrated by the summary plot of the WES tire tests (Fig. 28) where test results were plotted against the dimensionless number

$$N_c = CI \cdot \frac{b \cdot d}{W} \left(\frac{\delta}{h}\right)^{\frac{1}{2}} \cdot \frac{i}{1 + b/2d} \cdot$$

When N_c is less than about three, the towed force coefficient curve becomes very steep indicating that very small changes in the cone index result in large changes in the towed force coefficient. Under these conditions it would be unrealistic to expect that the towed force coefficient could be determined by any method very accurately.

- The towed tire-soil model is based on the concept that soil failure conditions govern the towed tire-soil interaction. In strong cohesive soils, soil failure does not occur under the tire load and the concept of tire-soil interaction does not apply. In the computer program this situation is recognized by an approximate calculation that computes the failure stresses for an infinitesimally small slip line field and compares these

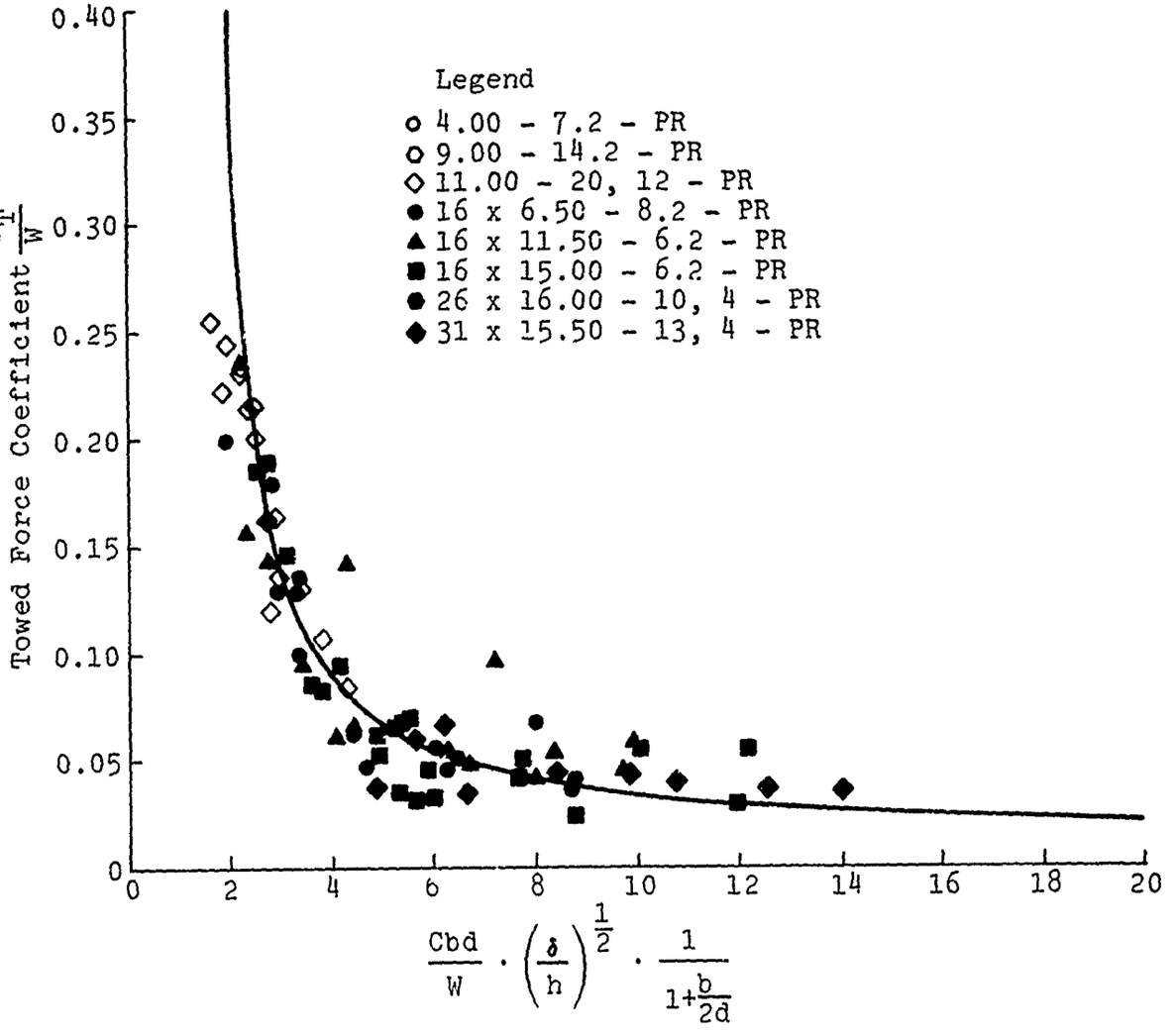

Fig. 28. Variation of Towed Force Coefficients with N_C in Fat Clay (From Ref. 1)

with the limit stress. If these computed failure stresses are larger than the limit stress then no failure occurs in the soil, and therefore, soil failure is not the controlling factor in tire-soil interaction. The computer message for this condition is "use hard surface formula" indicated by "H.S.F." in the tabulation.

In the towed tire tests on Buckshot clay, hard surface condition is frequently indicated in the predicted towed force coefficient column. An examination of these cases showed that in the majority of the cases the measured towed force coefficient was in the range of 0.02-0.05. Since the rolling resistance of tires on concrete or asphaltic surface is in the lower limit of this range, the hard surface designation appears to be appropriate. The measured sinkage in these cases is very small indicating that the soil actually behaved as a stiff rather than a plastic material.

Tire-soil interaction in these cases is governed by the deformation rather than by the strength properties of soil. For the simulation of tire-soil interaction under such conditions, the soil model would have to be modified accordingly. Since this situation is not critical in off-road mobility the development of such a model was not attempted.

IX. CONCLUSIONS AND RECOMMENDATIONS

Methods have been developed to estimate soil inertia forces generated by a tire traveling at various velocities and to take these inertia forces into account in the solutions of the differential equations of plasticity for soils. These methods have been incorporated in the computer program simulating tire-soil interaction. From the analysis of the effect of soil inertia forces on tire-soil interaction the following conclusions were drawn.

As long as the inertia forces generated in the soil by the traveling tire result in single-valued solutions for the front and rear slip line field, the effect of soil inertia forces on tire-soil interaction is minor. At a relatively low velocity (in the range of 10 feet/second) solution of the differential equations of plasticity becomes multivalued indicating that soil behavior must be different from that described by plasticity theory. The effect of such stress states on soil behavior is unexplored and cannot be analyzed by present state of the art methods.

It is recommended that both theoretical and experimental research be started to gain insight in soil behavior under such conditions and a theory be developed that could be applied to tire-soil interaction at high speeds.

In tire-soil interaction the rate of loading of the soil and the rate of strain is directly affected by the velocity of travel. The strength properties of certain soils are appreciably affected by changes in the rate of strain, while other soils are relatively insensitive to strain rate variations. The increase of soil strength with strain rate is probably the major contributor to the improvement of tire performance with speed.

Strain rates vary in the affected soil mass in both tire-soil interaction and in the various field tests used for soil property determination. In order to approach the problem of strain rate effects in a logical way, it is necessary to develop methods for the determination of strain rates in tire-soil interaction as well as in the various field tests.

Strain rates are directly related to particle path geometry. It is recommended that methods be developed for the determination of strain rates from particle paths and experimental determination of particle path geometries be extended to tire-soil interaction, cone penetration, and plate sinkage tests under a variety of soil conditions. More experimental information on particle path geometries would also be useful to improve the computation of soil inertia forces in tire-soil interaction.

An important new concept, that of the contact slip, was developed in connection with soil particle acceleration determination by the velocity field method. This concept establishes a relation between the shear stresses at the tire-soil interface and the minimum value of slip that is necessary to develop these shear stresses. Slip that exceeds the value of contact slip is a waste in energy and tire wear.

It is recommended that the theory of contact slip be further developed and general relationships between contact slip and interface friction be established. It is also recommended that in all tire tests the horizontal displacement of selected soil particles at the surface be routinely determined and compared with the measured conventional slip value. The horizontal displacement of a soil particle at the surface is a measure of the contact slip. Its measurement is a simple way to obtain experimental information that could lead to economies in off-road vehicle usage.

A towed pneumatic tire-soil model has been developed that predicts towed force coefficients with good accuracy. For improvement of the model it is recommended that three dimensional conditions be taken into account in the model. The consideration of three dimensional conditions is also essential for the prediction of towed force in the case of dual tires.

X. REFERENCES

1. Turnage, G. W., "Performance of Soils Under Tire Loads," U.S. Army Corps of Engineers, Waterways Experiment Station, Technical Report No. 3-666, Report No. 8, September 1972.

2. Crenshaw, B. M. and Butterworth, C. K., "Aircraft Landing Gear Dynamic Loads from Operation on Clay and Sandy Soil," AF Flight Dynamics Laboratory Technical Report AFDL-TR-69-51, February 1971.

3. Crenshaw, B. M., "Aircraft Landing Gear Dynamic Loads Induced by Soil Landing Fields," AF Flight Dynamics Laboratory Report TR-70-169, June 1972.

4. Karafiath, L. L., "Development of Mathematical Model for Pneumatic Tire-Soil Interaction," U.S. Army Tank Automotive Command Mobility Systems Laboratory Tech. Report No. 11900(LL147), July 1974.

5. Besdo, D., "Principal- and Slip-Line Methods of Numerical Analysis in Plane and Axially Symmetric Deformations of Rigid/Plastic Media," J. Meth. Phys. Solids, Vol. 19, 1971.

6. Butterfield, R. and Harkness, R. M., "The Kinematics of Mohr-Coulomb Materials," Proc. of the Roscoe Memorial Symposium on Stress-Strain Behavior of Soils, Cambridge University, March 1971.

7. Soil Mechanics-Selected Topics, edited by I. K. Lee, American Elsevier Pub. Co., New York, 1968, "Theories of Plasticity and the Failure of Soil Masses" (E. H. Davis).

8. Hill, R., Lee, E. H., and Tupper, S. J., "The Theory of Wedge Indentation of Ductile Materials," Proc. Roy. Soc. A., Vol. 188, 1946.

9. Mandl, G. and Fernandez, L. R., "Fully Developed Plastic Shear Flow of Granular Materials," Geotechnique, Vol. 20, No. 3, September 1970.

10. Roscoe, K. H., "The Influence of Strains in Soil Mechanics," Geotechnique, Vol. 20, No. 2, June 1970.

11. Shield, R. T., "Mixed Boundary Value Problems in Soil Mechanics," Q. Appl. Math., Vol. xi, No. 1, 1953.

12. Spencer, A. J. M., "A Theory of the Kinematics of Ideal Soils Under Plane Strain Conditions," J. Mech. Phys. Solids, Vol. 12, 1964.

13. Karafiath, L. L., Nowatzki, E. A., Ehrlich, I. R., and Capin, J., "An Application of Plasticity Theory to the Solution of the Rigid Wheel-Soil Interaction Problem," U.S. Army Tank Automotive Command Mobility Systems Laboratory Technical Report No. 11758(LL141), March 1973.

14. Karafiath, L. L. and Nowatzki, E. A., "Stability of Slopes Loaded Over a Finite Area," Highway Research Board Record No. 323, November 1970.

15. Karafiath, L. L., "Plasticity Theory and Stress Distribution Beneath Wheels," J. of Terramechanics, Vol. 8, No. 2, 1971.

16. Nowatzki, E. A. and Karafiath, L. L., "Effect of Cone Angle on Penetration Resistance," Highway Research Record No. 405, 1972.

17. Nowatzki, E. A. and Karafiath, L. L., "General Yield Conditions in a Plasticity Analysis of Soil-Wheel Interaction," J. of Terramechanics, Vol. 11, No. 1, 1974.

18. Karafiath, L. L., "On the Effect of Pore Pressures on Soil-Wheel Interaction," Proc. Fourth International Conference for Terrain Vehicle Systems, Stockholm, April 1972.

19. Janosi, Z., "An Analysis of Pneumatic Tire Performance on Deformable Soils," Proc. of the 1st Int. Conf. on the Mechanics of Soil-Vehicle Systems, Torino, 1961.

20. Wilson, N. and Krzywicki, h., "Soil Mechanics As it Affects Vehicle Performance," Canadian Geotechnical Journal, Vol. III, No. 4, November 1966.

21. Yong, R. and Webb, G., "Energy Dissipation and Drawbar Pull Prediction in Soil-Wheel Interaction," Proc. of the Third International Conference for Terrain Vehicle Systems, Vol. 1, July 1969, Haus der Technik, Essen, West Germany.

22. Windisch, E. and Yong, R., "The Determination of Soil Strain Rate Behavior Beneath a Moving Wheel," J. of Terramechanics, Vol. 7, No. 1, 1970.

23. Whitman, R. V., Richardson, A. M., and Nasim, N. M., "The Response of Soils to Dynamic Loadings," MIT Dept. of Civil Engineering Research Report R62-22, June 1962.

24. Casagrande, A. and Shannon, W. L., "Stress Deformation and Strength Characteristics of Soils Under Dynamic Loads," 2nd Int. Conf. on Soil Mech. and Found. Eng., Rotterdam, 1948.

25. Whitman, R. V. and Healy, K. A., "Shear Strength of Sands During Rapid Loading," Proc. of ASCE, Vol. 88, No. 2, April 1962.

26. Larew, H. G. and Atakol, K., "The Effect of Rate of Shearing Deformation on the Shearing Resistance of a Cohesionless Soil," Sandia Laboratories Report SC-CR-67-2658, June 1967.

27. Yong, R. N. and Japp, R. D., "Stress-Strain Behavior of Clays in Dynamic Compression," Symposium on Vibration Effects of Earthquakes on Soils and Foundations, San Francisco, ASTM Special Publication 450, June 1968.

28. Richardson, A. M. and Whitman, R. V., "Effect of Strain Rate Upon Undrained Shear Resistance of a Saturated Remolded Clay," Geotechnique, Vol. XIII, No. 4, December 1963.

29. Truesdale, W. B. and Nelson, R. D., "Soil Tests and Soil Response Studies," AFFDL Tech. Report 70-169, Vol. 11, June 1972.

30. Turnage, G. W., "Resistance of Fine Grained Soils to High Speed Penetration," Report No. 5, Technical Report No. 3-652, U.S. Army Engineers Waterways Experiment Station, June 1973.

31. Turnage, G. W., "Resistance of Coarse Grained Soils to High Speed Penetration," Report No. 6, Tech. Report No. 3-652, U.S. Army Engineers Waterways Experiment Station, July 1974.

32. "Strength-Moisture-Density Relations of Fine Grained Soils in Vehicle Mobility Research," U.S. Army Engineers Waterways Experiment Station, Technical Report No. 3-639, January 1969.

33. Bekker, M. and Janosi, Z., "Analysis of Towed Pneumatic Tires Moving on Soft Ground," U.S. Army OTAC Report No. RR-6, March 1960.

34. Murphy, N. R., Jr. and Green, A. J., Jr., "Stresses Under Moving Vehicles - Distribution of Stresses Beneath a Towed Pneumatic Tire in Air-Dry Sand," U.S. Army Corps of Engineers Waterways Experiment Station, Technical Report No. 3-545, Report No. 5, July 1965.

35. Freitag, D. R., Green, A. J., and Murphy, N. R., Jr., "Normal Stresses at the Tire-Soil Interface in Yielding Soils," Highway Research Record No. 74, 1965.

36. Trabbie, G., Lask, K., and Buchele, W., "Measurement of Soil-Tire Interface Pressures," Agricultural Engineering, November 1959.

37. Smith, M. E. and Freitag, D. R., "Deflection of Moving Tires - Centerline Deflection Studies through July 1963," U.S. Army Corps of Engineers Waterways Experiment Station, Technical Report No. 3-516, Report No. 3, May 1965.

38. Freitag, D. R. and Smith, M. E., "Centerline Deflection of Pneumatic Tires Moving in Dry Sand," J. of Terramechanics, Vol. 3, No. 1, 1966.

39. Krick, G., Die Wechselbeziehungen Zwischen Starren Rad, Luftreifen und Nachgiebigem Boden, Dissertation, Technische Universität Munchen, 1971.

40. Krick, G., "Radial and Shear Stress Distribution Under Rigid Wheels and Pneumatic Tires Operating on Yielding Soils with Consideration of Tire Deformation," J. of Terramechanics, Vol. 6, No. 3, 1969.

41. Uffelmann, F. L., "The Performance of Rigid Cylindrical Wheels in Clay," Proc. of the 1st International Conference on the Mechanics of Soil-Vehicle Systems, Torino, 1961.

APPENDIX A

COMPUTER PROGRAM FLOW CHART FOR ANALYSIS OF EFFECT OF SOIL INERTIA FORCES ON TIRE PERFORMANCE BY METHOD OF VELOCITY FIELDS

(Pages 11, 20, and 24 omitted)

CHART TITLE - INTRODUCTORY COMMENTS

MAIN PROGRAM

THIS PROGRAM COMPUTES TIRE CENTERLINE
GEOMETRY, INTERFACE STRESSES AND PERFORMANCE
PARAMETERS FOR GIVEN TIRE CHARACTERISTICS.
SOIL STRENGTH PROPERTIES WITH CONSIDERATION
OF SOIL INERTIA FORCES GENERATED AT VARIOUS
TIRE TRANSLATIONAL VELOCITIES.

THE PROGRAM CONSISTS OF FOUR PARTS

MAIN PROGRAM
SUBROUTINE SLFIA
SUBROUTINE VCOMP
SUBROUTINE ACOMP
INPUT VARIABLES ARE READ IN THE MAIN
PROGRAM FROM DATA FILES IN THE FOLLOWING ORDER

AFD (ENTRY ANGLE IN DEGREES)
AFN (SEPARATION ANGLE IN DEGREES)
DA (NOMINAL TIRE DIAMETER IN FEET)
BO (NOMINAL TIRE WIDTH IN FEET)
LO (LOAD IN LBS)
PO (LIMIT PRESSURE IN PSI)
DE (DEFLECTION COEFFICIENT EPSILON)
SL (SLIP IN DECIMAL)
SJ (SLIP PARAMETER J ZERO)
SKK (SLIP PARAMETER K)
CF (COHESION IN FRONT FIELD, LBS/SQFT)
CR (COHESION IN REAR FIELD, LBS/SQFT)
FF (FRICTION ANGLE IN FRONT FIELD, DEGREES)
FR (FRICTION ANGLE IN REAR FIELD, DEGREES)
GF (UNIT WEIGHT IN FRONT FIELD, LBS/CUFT)
GR (UNIT WEIGHT IN REAR FIELD, LBS/CUFT)
AD (ANGLE ADDED TO ENTRY AND REAR ANGLE TO MARK
END OF DEFLECTION)
AR (REAR ANGLE IN DEGREES)

ENTRY, REAR, AND SEPARATION ANGLES ARE TO BE
OBTAINED FROM THE STANDARD TIRE-SOIL INTERACTION
PROGRAM.

DESIGNATION OF MAIN VARIABLES IN THE PROGRAM ARE

AAO ENTRY ANGLE IN RADIANS
AAN SEPARATION ANGLE IN RADIANS
BI BETA COEFFICIENT FOR LOG SPIRAL
DI INTERFACE FRICTION ANGLE (DELTA) IN RADIANS
PL LIMITING PRESSURE IN LBS/SQFT

CHART TITLE - INTRODUCTORY COMMENTS

RO DEFORMED TIRE RADIUS
RMF COMPUTED LOAD
RTF COMPUTED DRAWBAR PULL
RTT TOTAL TORQUE
TMS TORQUE FROM NORMAL STRESSES
SMK SINKAGE
MM(N) CENTRAL ANGLE AT POINT N IN DEGREES
QQ(N) NORMAL STRESSE AT POINT N IN LBS/SQFT
FF(N) SHEAR STRESS AT POINT N IN LBS/SQFT
UU(N) X COORDINATE OF POINT N WITH REFERENCE TO TIRE AXIS
VV(N) Z COORDINATE OF POINT N WITH REFERENCE TO TIRE AXIS

SUBROUTINE SLFIA

THIS SUBROUTINE COMPUTES COORDINATES, SIGMA AND THETA VALUES FOR SLIP LINE FIELDS

DESIGNATIONS OF MAIN VARIABLES ARE

X(I,J) X COORDINATE OF POINT I,J
Z(I,J) Z COORDINATE OF POINT I,J
S(I,J) SIGMA AT POINT I,J
T(I,J) THETA AT POINT I,J
ACCX(I,J) X COMPONENT OF INERTIAL ACCELERATION
ACCZ(I,J) Z COMPONENT OF INERTIAL ACCELERATION
GG GRAVITIONAL CONSTANT
UX(I,J) X COMPONENT OF VELOCITY
UZ(I,J) Z COMPONENT OF VELOCITY
A(J) TANGENT OF CENTERLINE AT POINT J
D(J) DELTA ANGLE AT POINT J

SUBROUTINE VCOMP

THIS SUBROUTINE COMPUTES THE VELOCITY FIELD FOR SLIP LINE FIELD GEOMETRIES COMPUTED IN SUBROUTINE SLFIA.

DESIGNATIONS OF THE MAIN VARIABLES ARE

UX(I,J) X COMPONENT OF VELOCITY AT POINT I,J
UZ(I,J) Z COMPONENT OF VELOCITY AT POINT I,J
AJ(I,J) VELOCITY COMPONENT ALONG J LINE
AI(I,J) VELOCITY COMPONENT ALONG I LINE

SUBROUTINE ACOMP

THIS SUBROUTINE COMPUTES THE ACCELERATIONS AT I,J

CHART TITLE INTRODUCTORY COMMENTS

POINT FROM VELOCITIES DETERMINED IN SUBROUTINE
V COMP.

DESIGNATIONS OF THE MAIN VARIABLES ARE

VTRANS TRANSLATIONAL VELOCITY
ACCEE(,J) X COMPONENT OF INERTIAL ACCELERATION
ACCZE(,J) Z COMPONENT OF INERTIAL ACCELERATION

CHART TITLE PROCEDURES

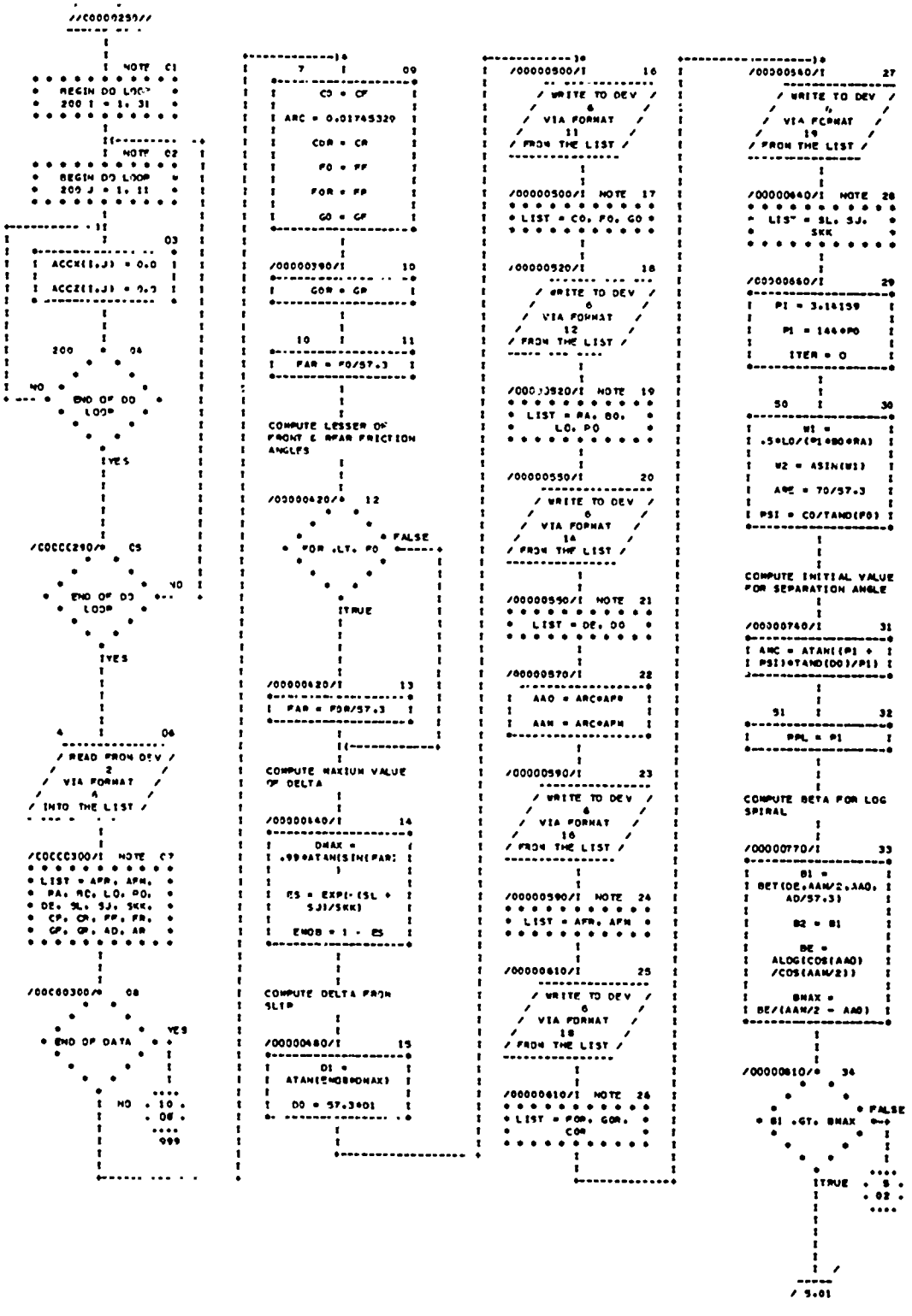

CHART TITLE PROCEDURES

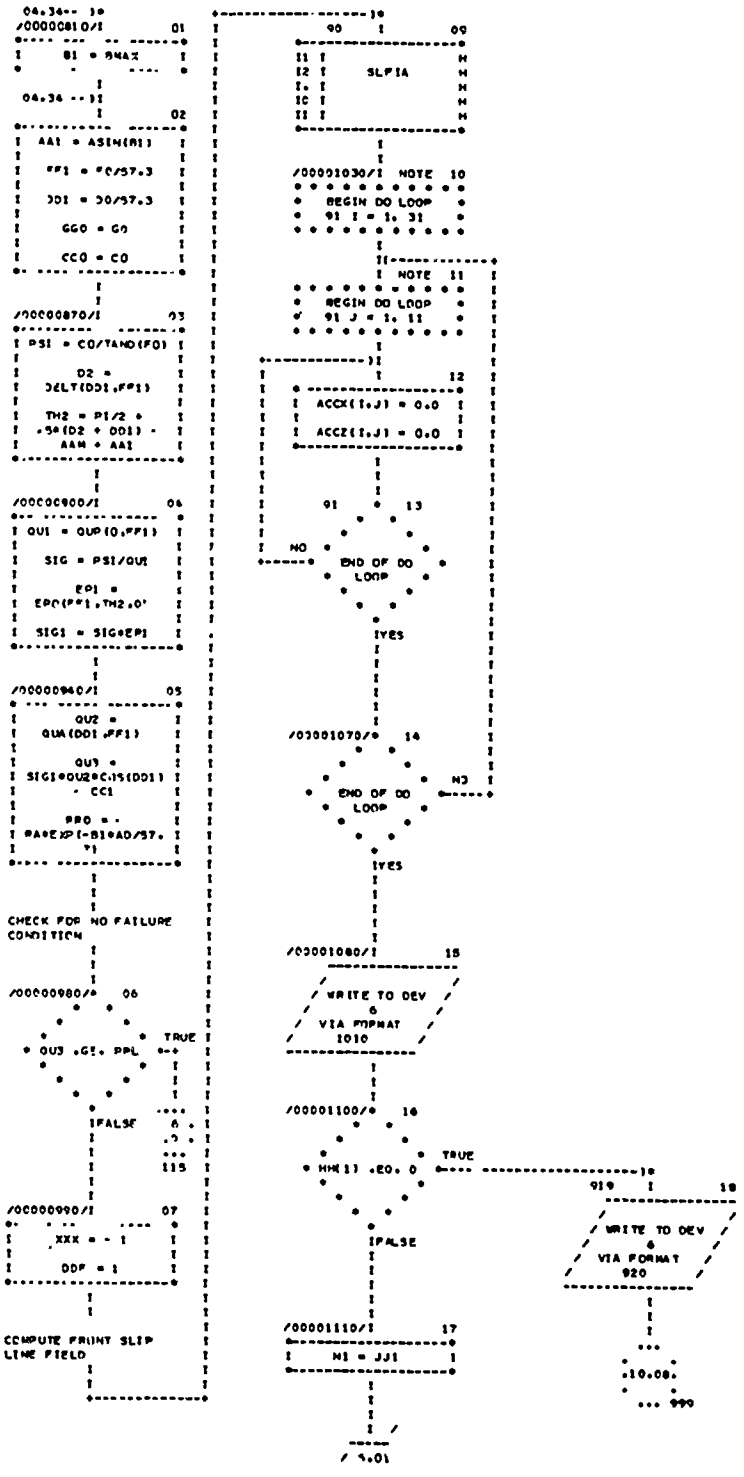

CHART TITLE PROCEDURES

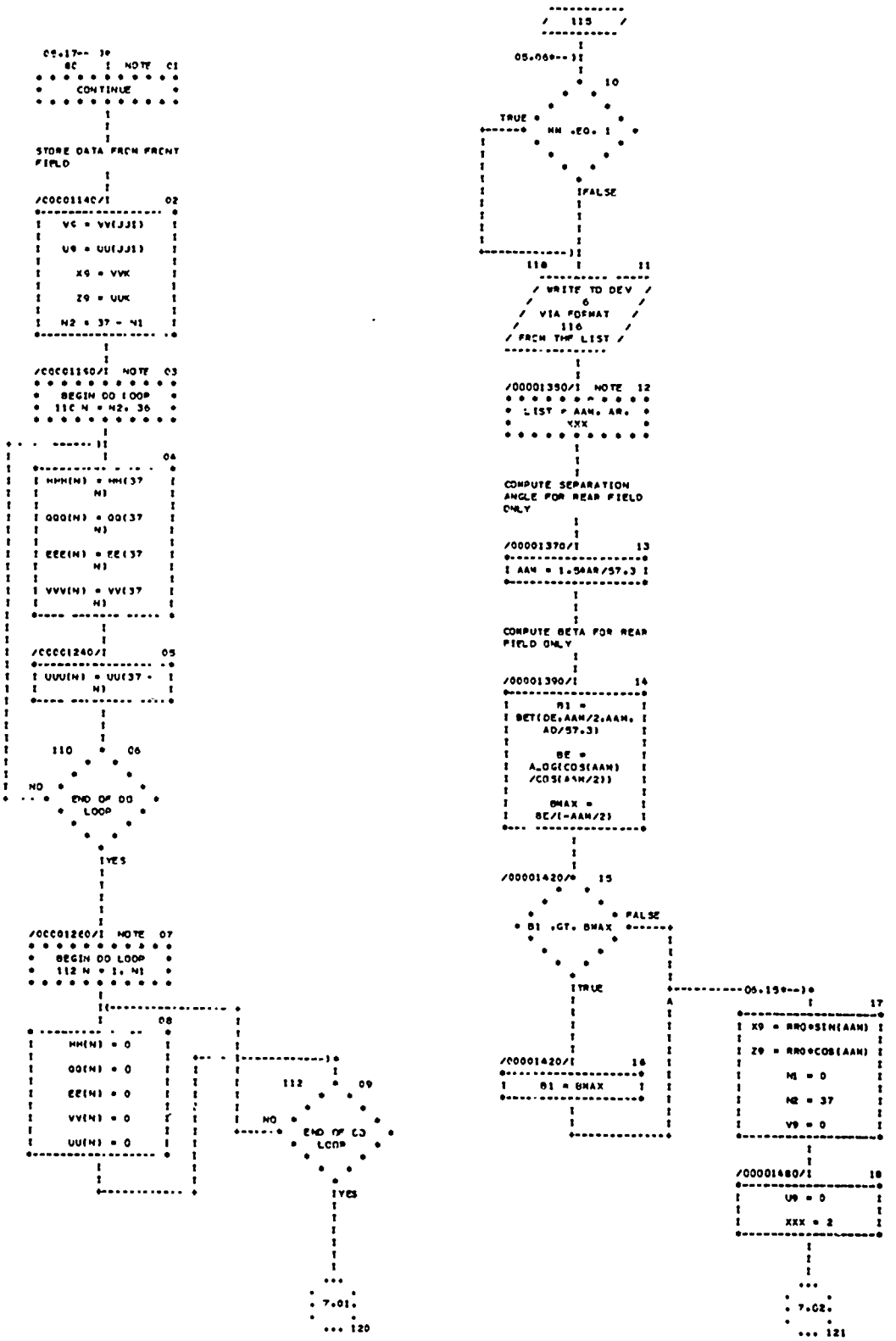

CHART TITLE PROCEDURES

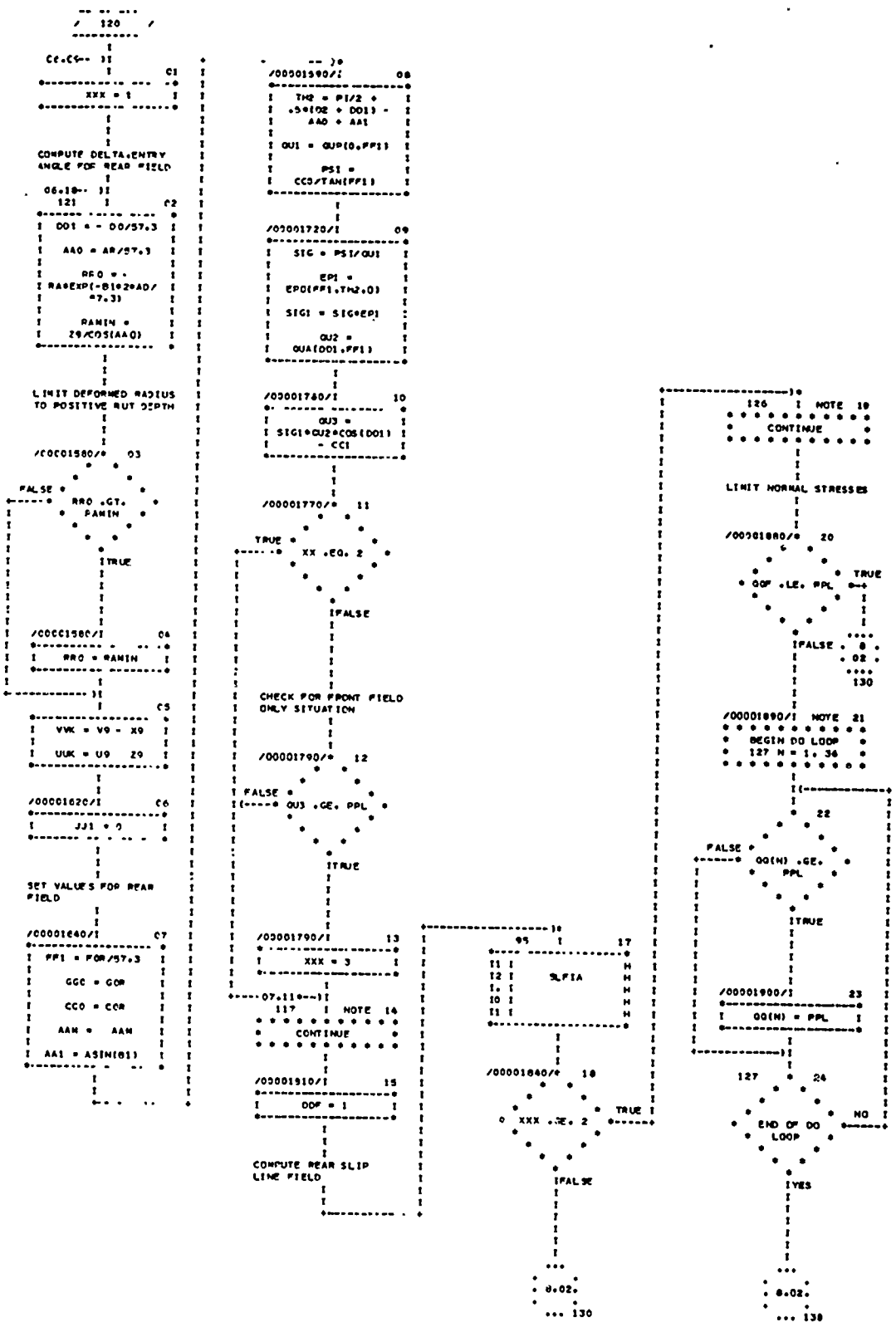

CHART TITLE - PROCEDURES

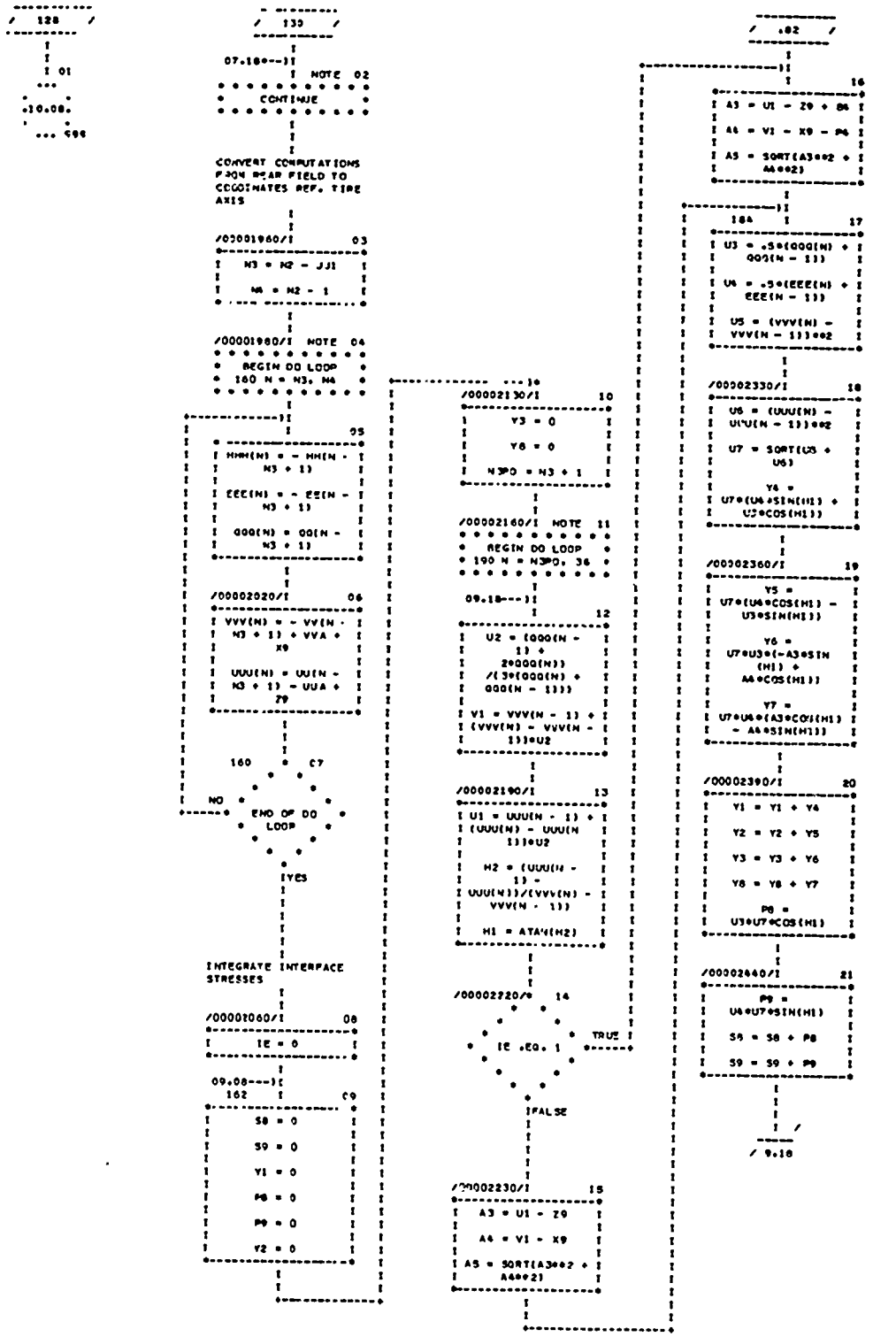

CHART TITLE PROCEDURES

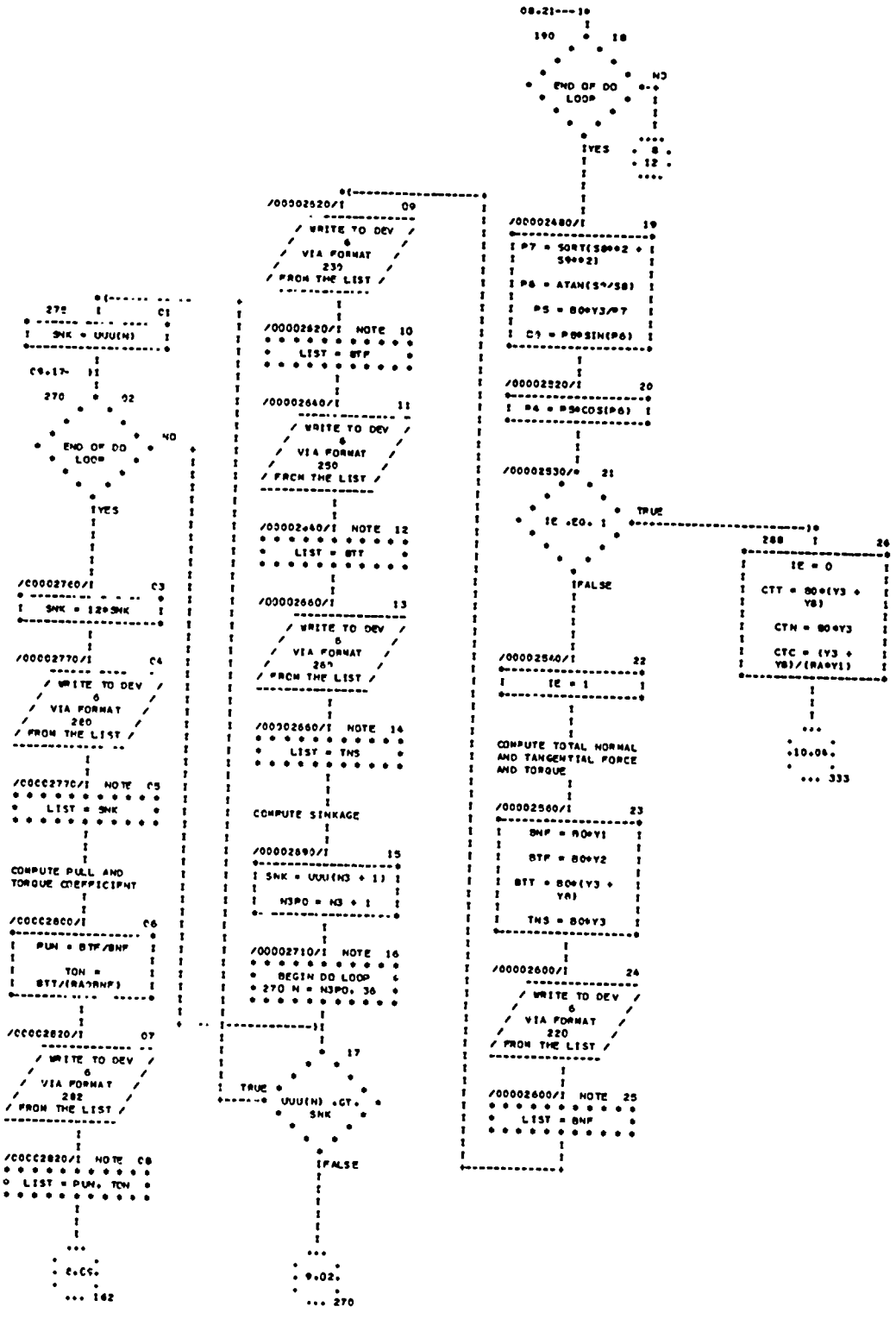

CHART TITLE PROCEDURES

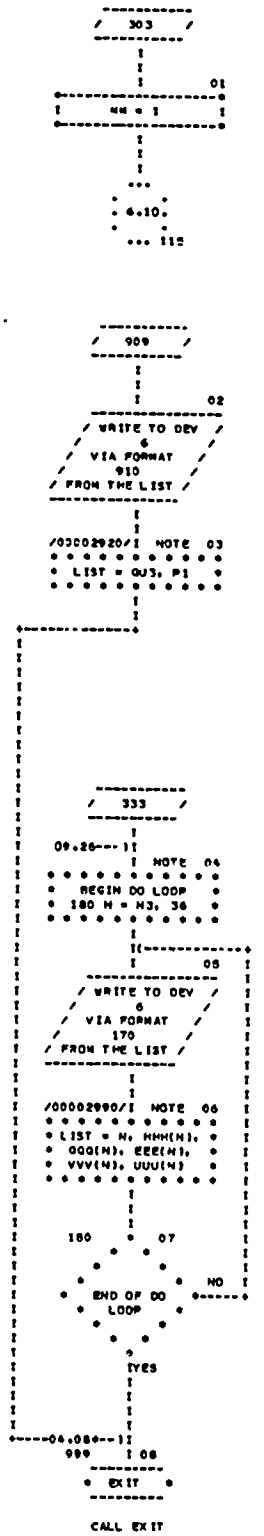

CHART TITLE SUBROUTINE SLPIA

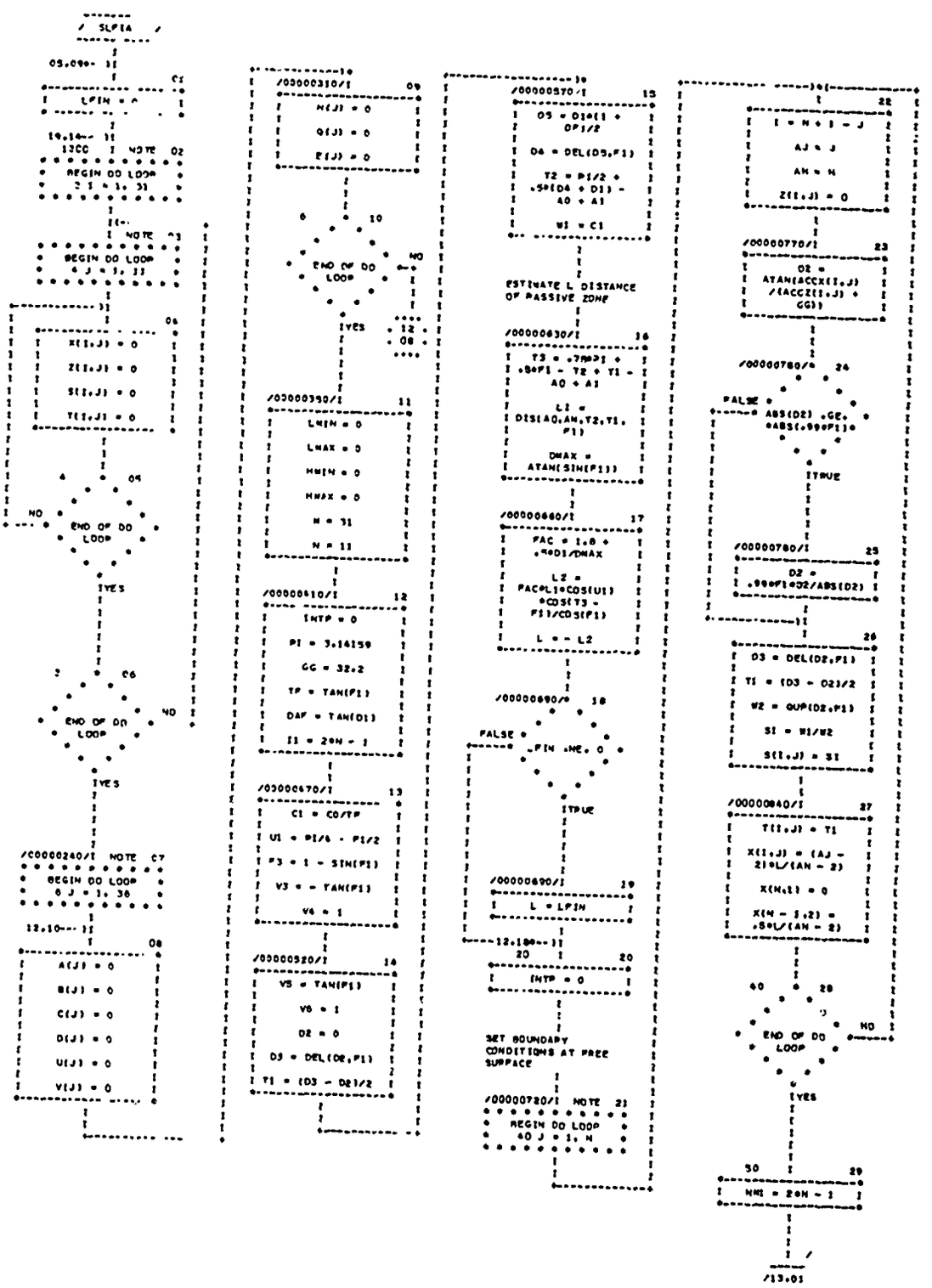

CHART TITLE - SUBROUTINE SLP1A

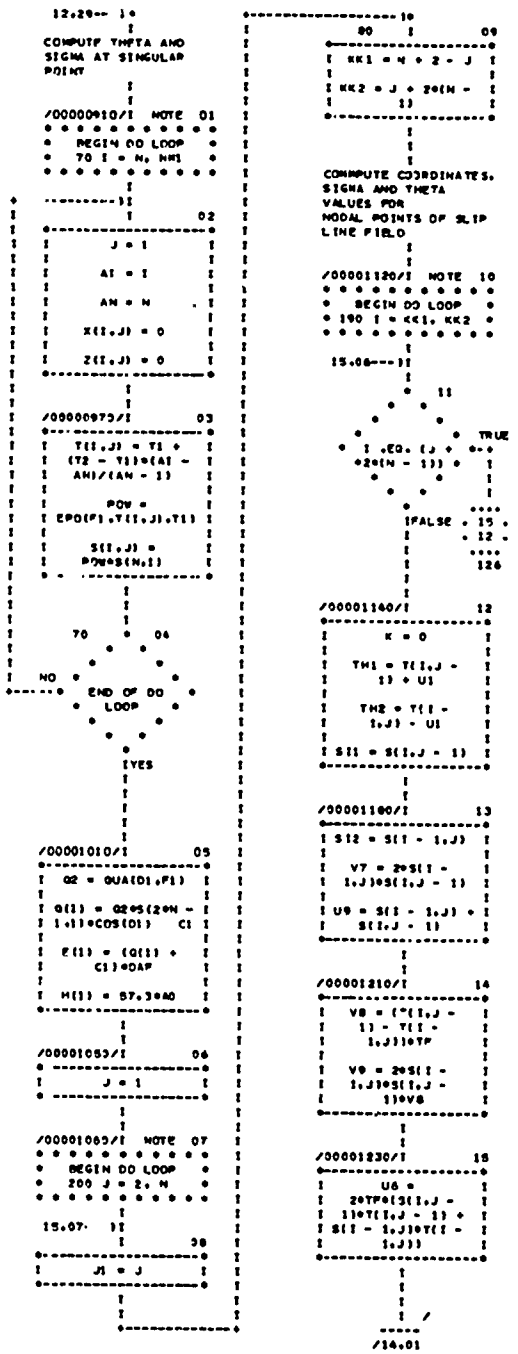

CHART TITLE - SUBROUTINE SUF1A

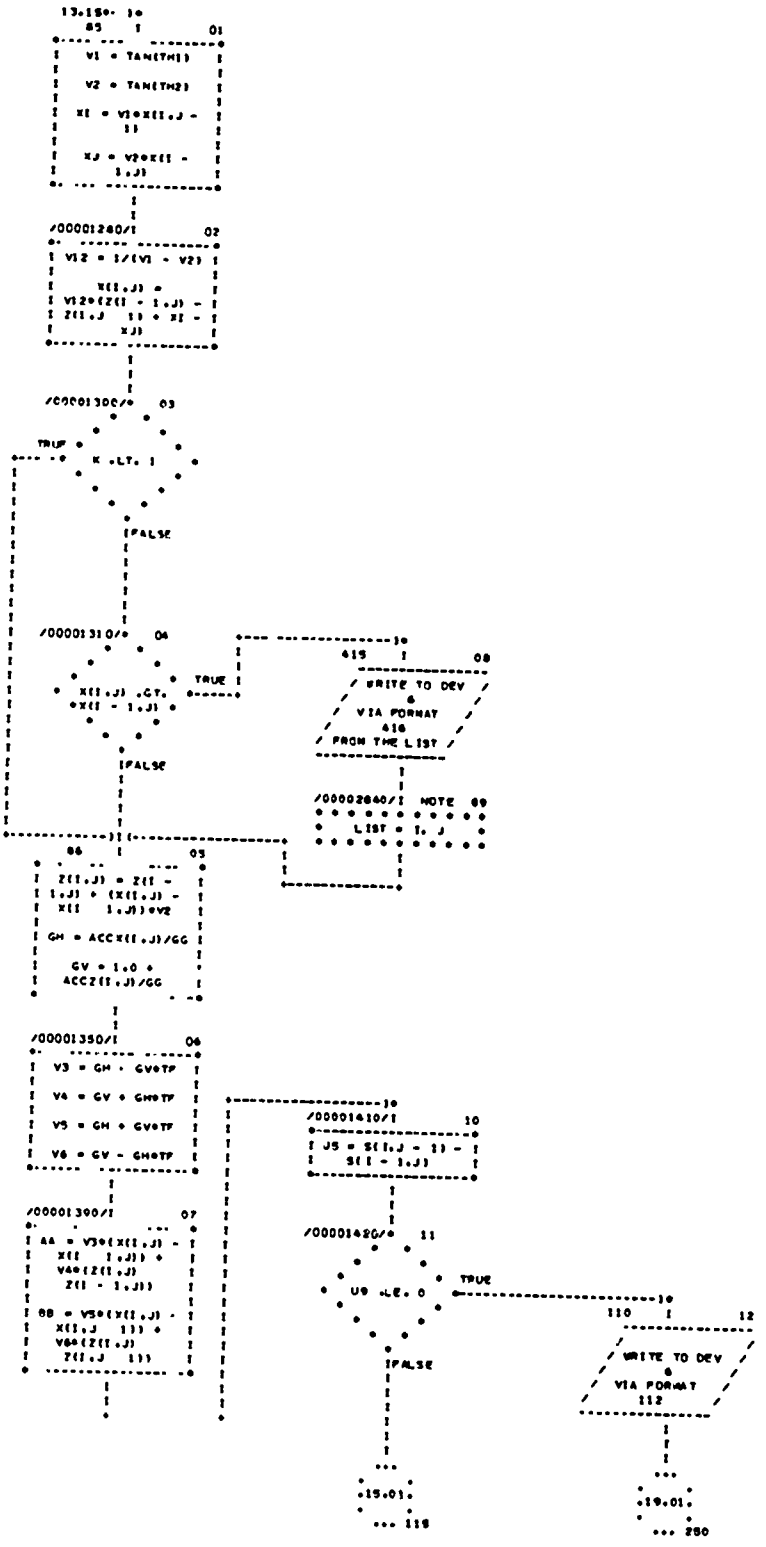

CHART TITLE SUBROUTINE SLPIA

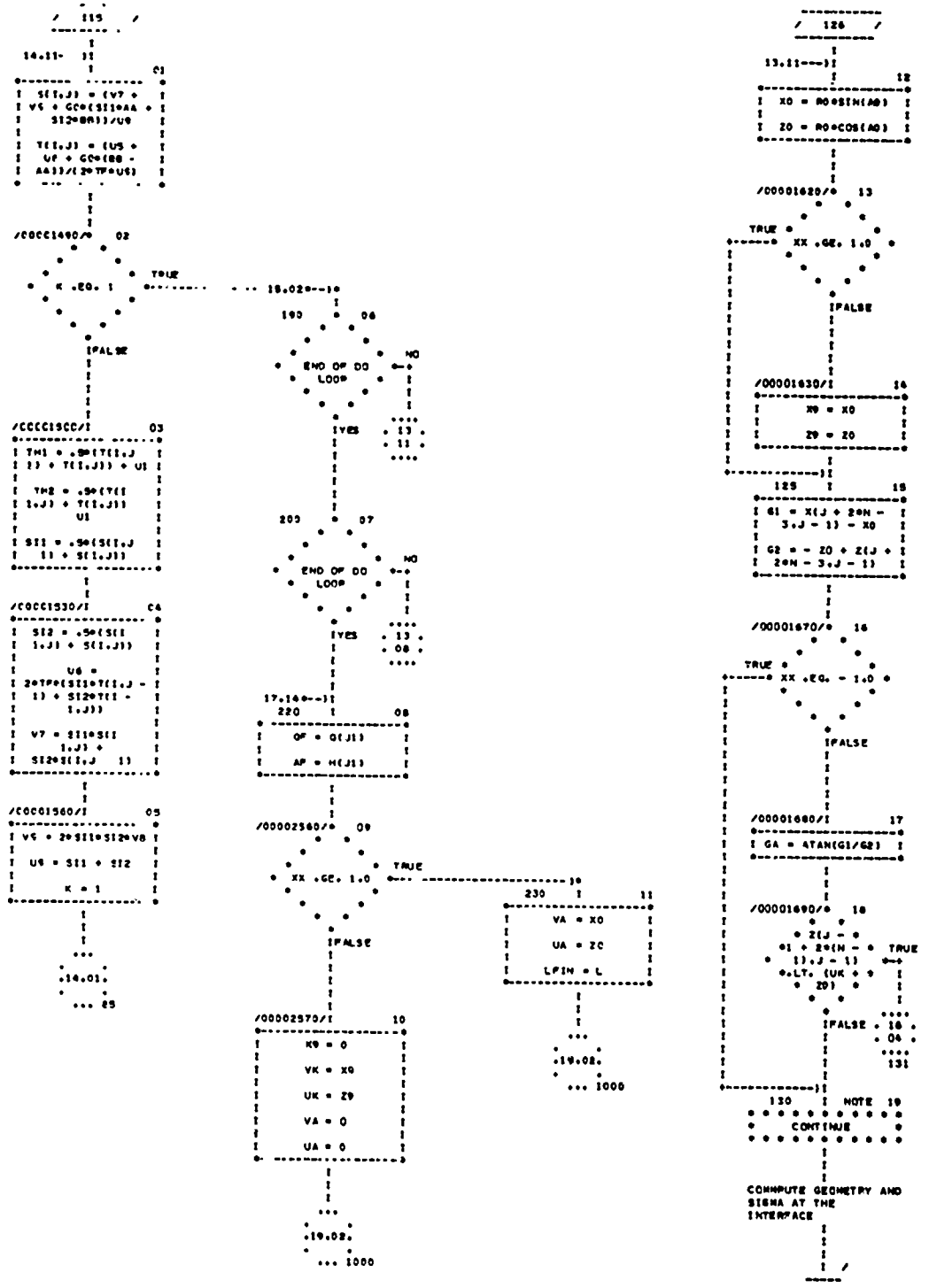

CHART TITLE SUBROUTINE SLPIA

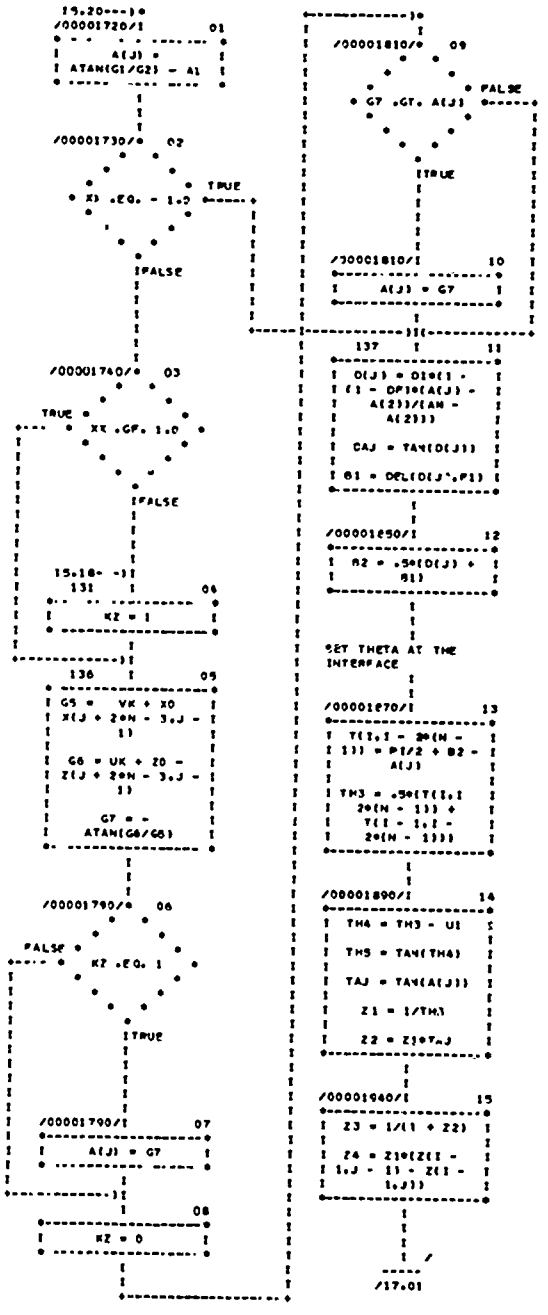

CHART TITLE SUBROUTINE SUF1A

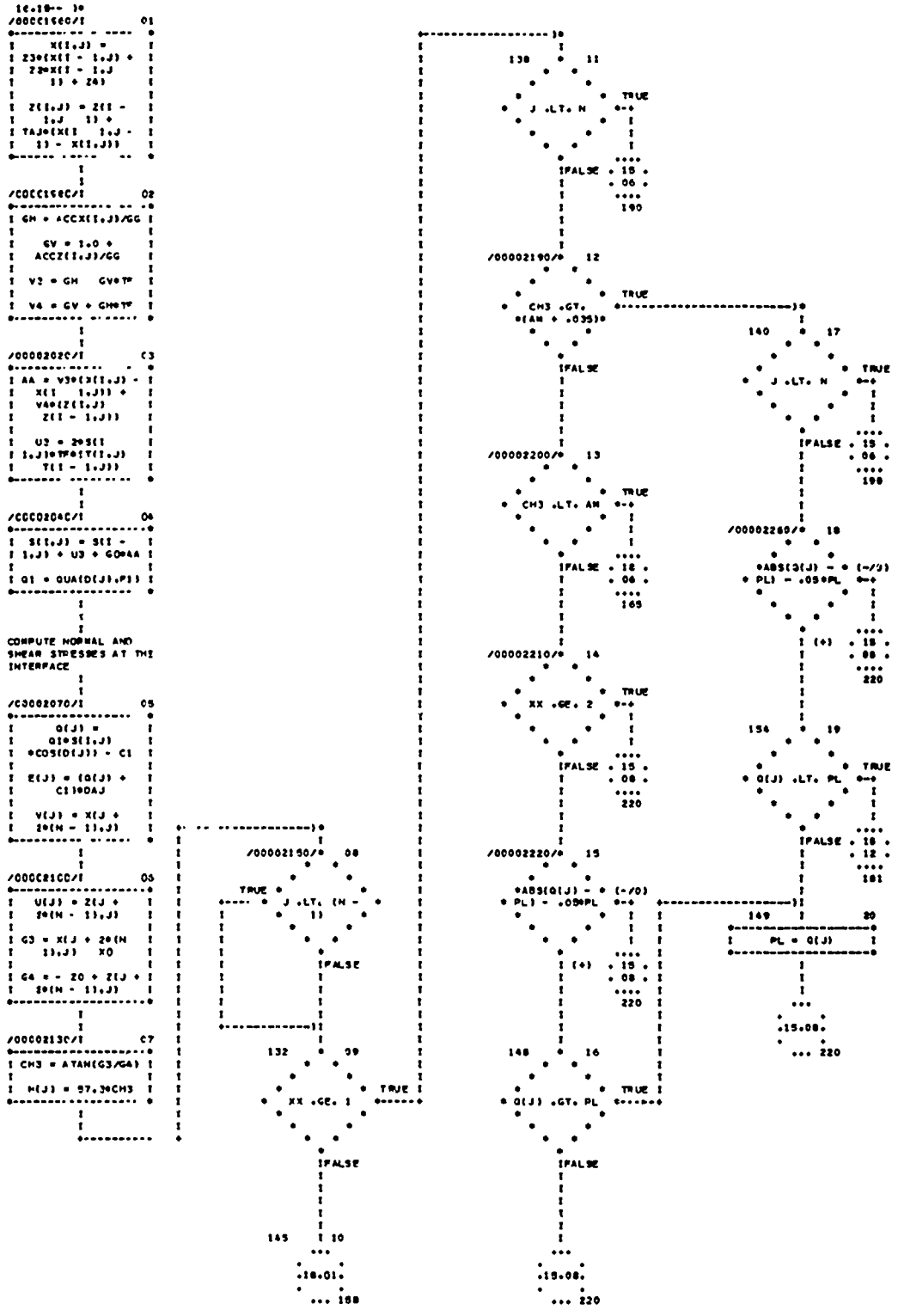

CHART TITLE - SUBROUTINE SLPIA

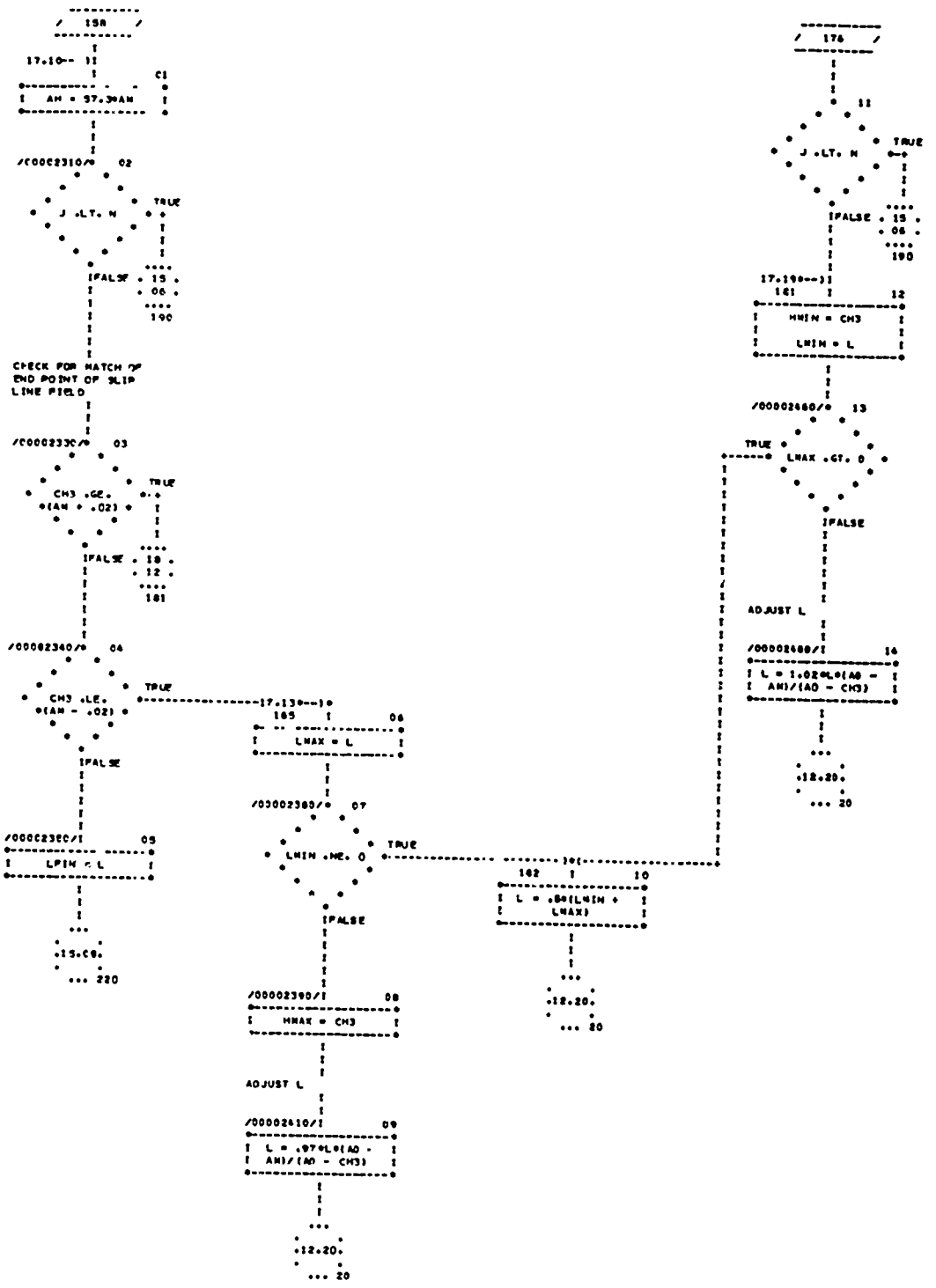

'HART TITLE SUBROUTINE SLPIA

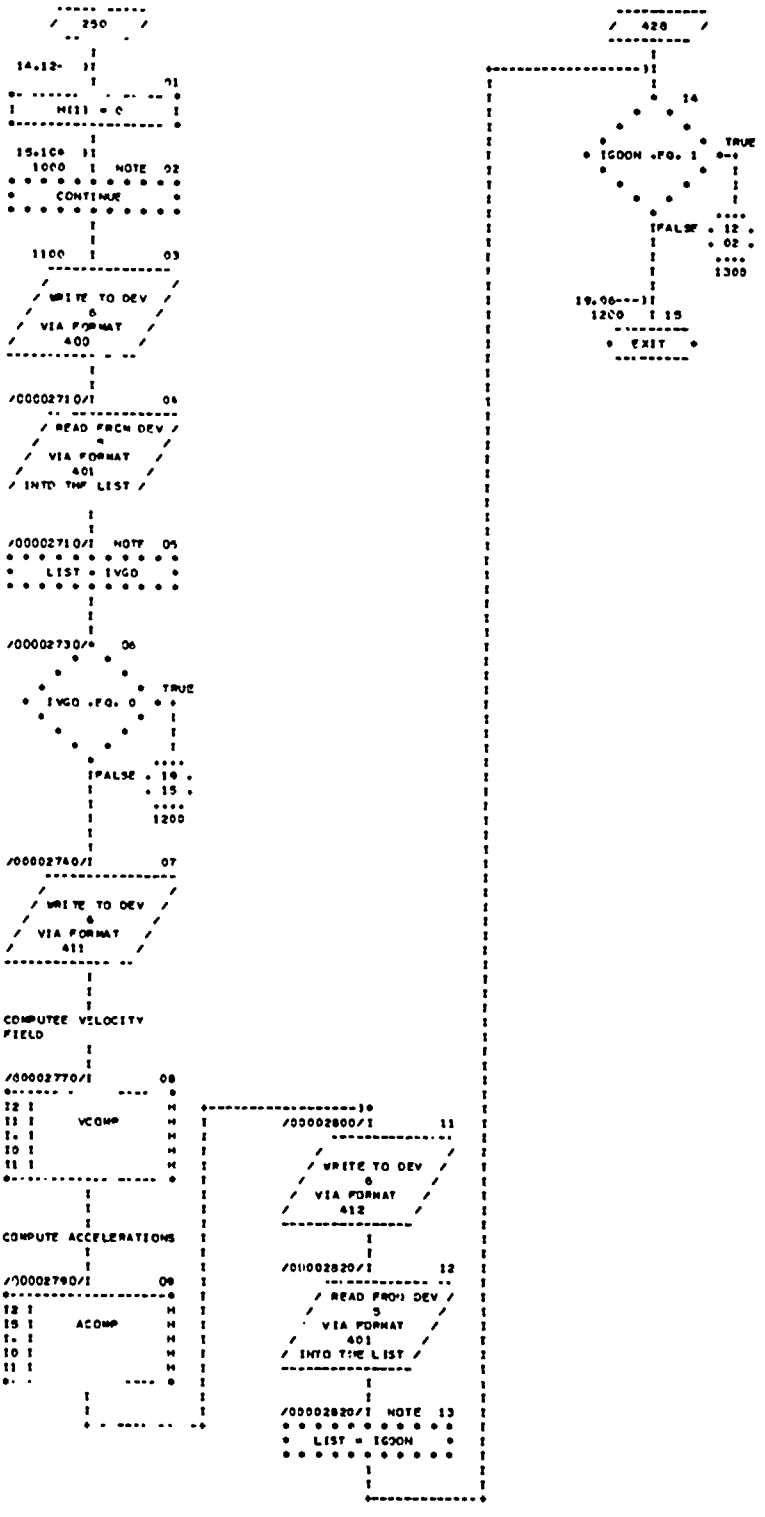

CHART TITLE SUBROUTINE VCOMP

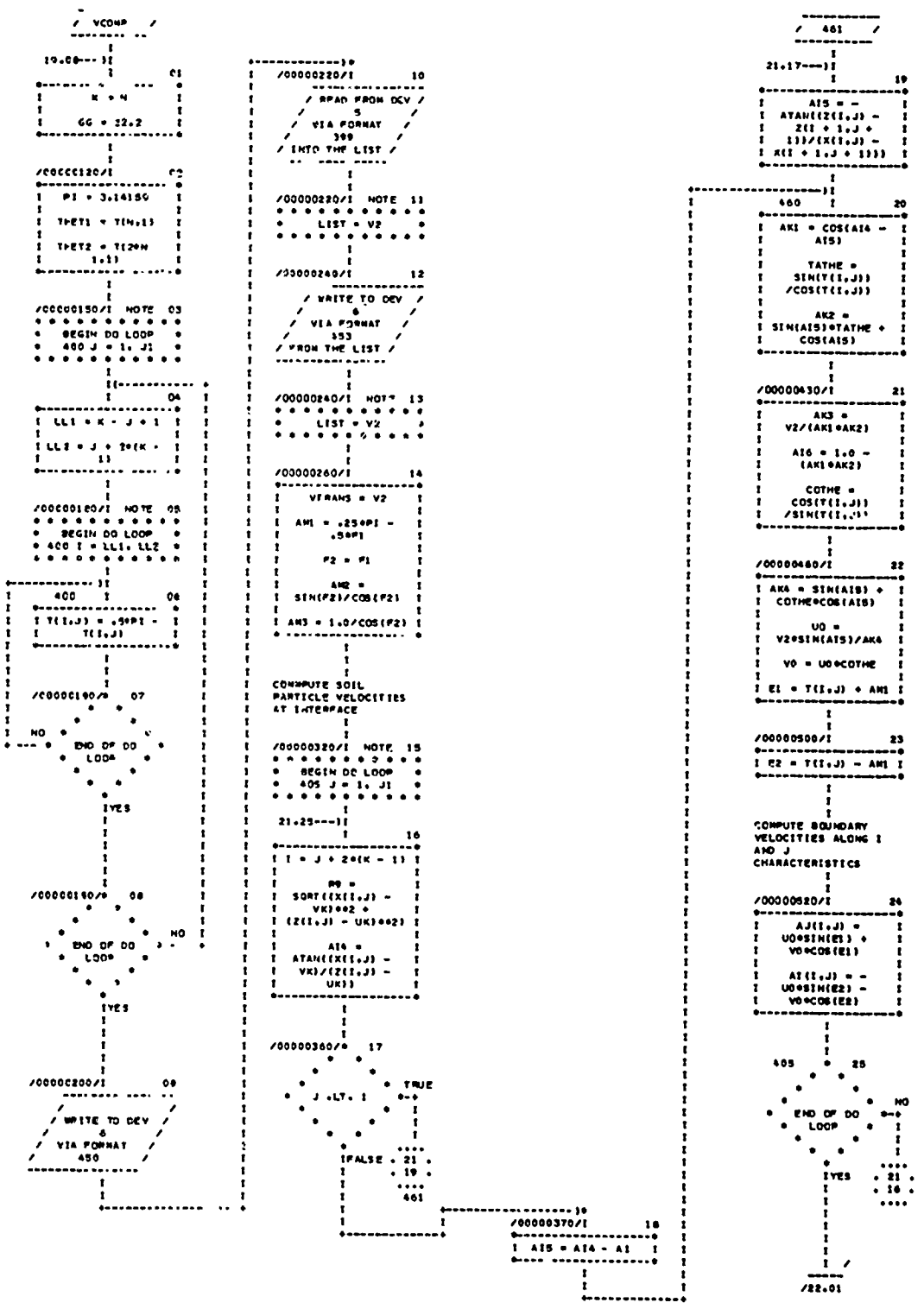

CHART TITLE - SUBROUTINE VT[illegible]

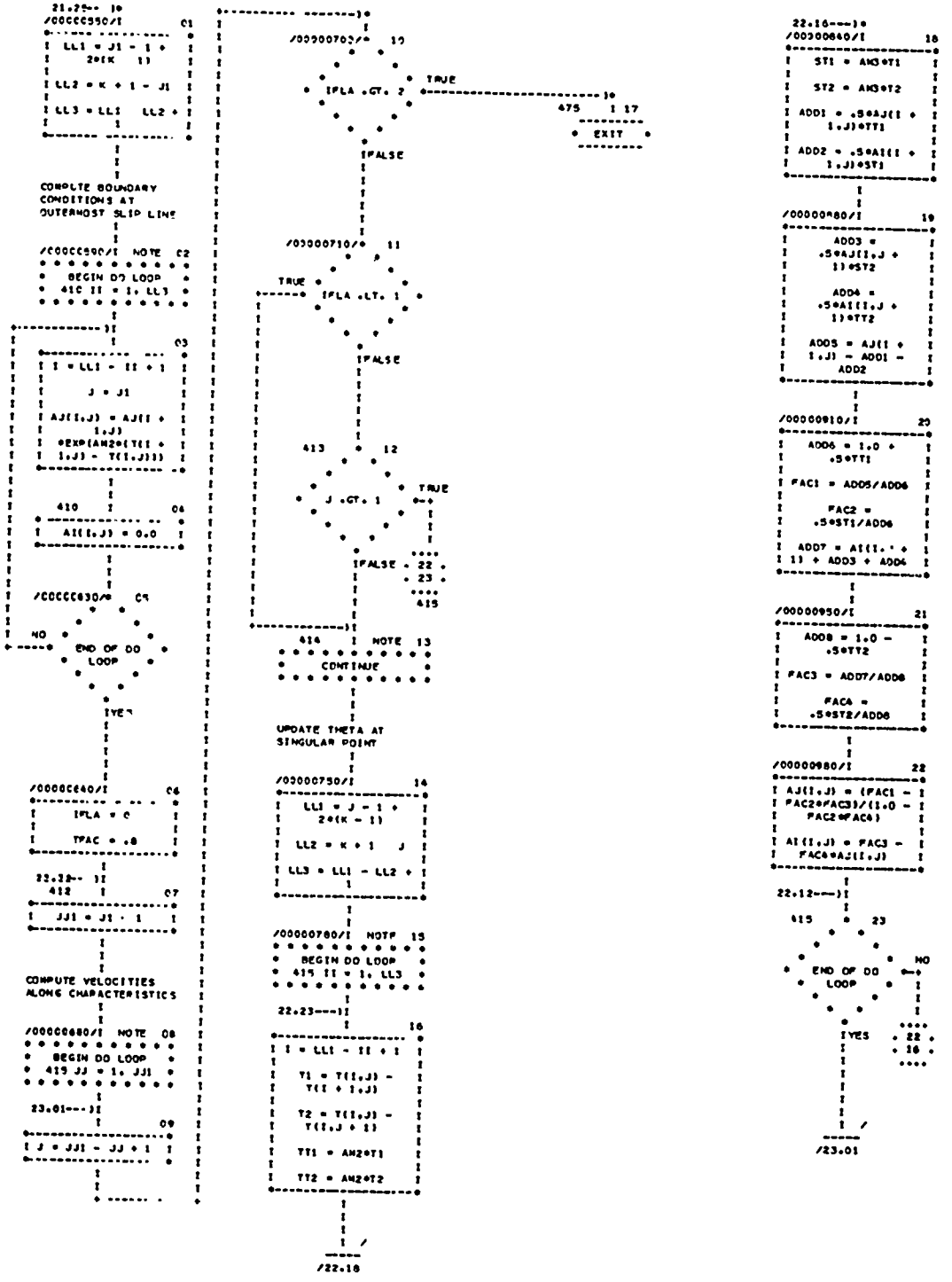

CHART TITLE SUBROUTINE VCOMP

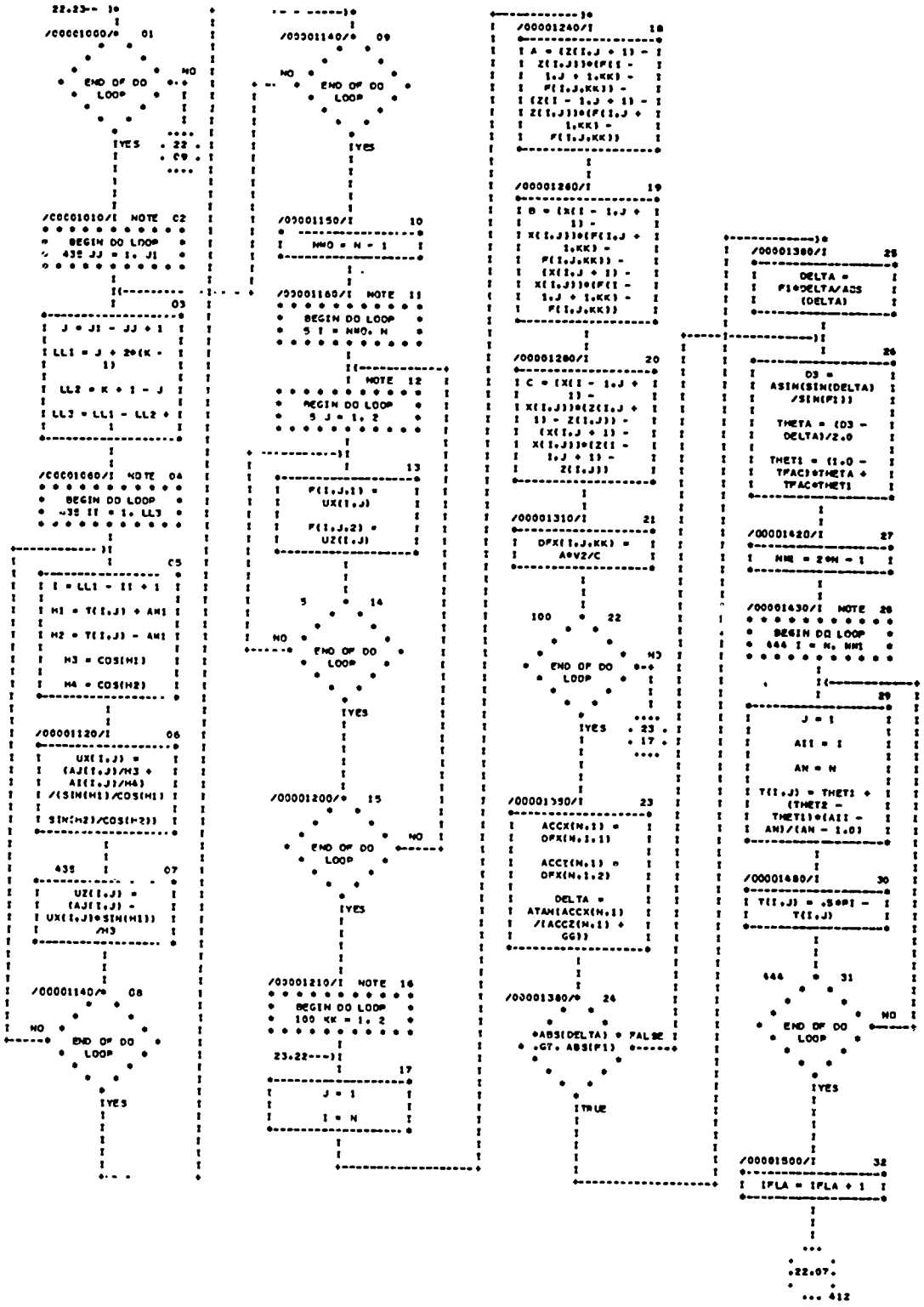

CHART TITLE SUBROUTINE ACOMP

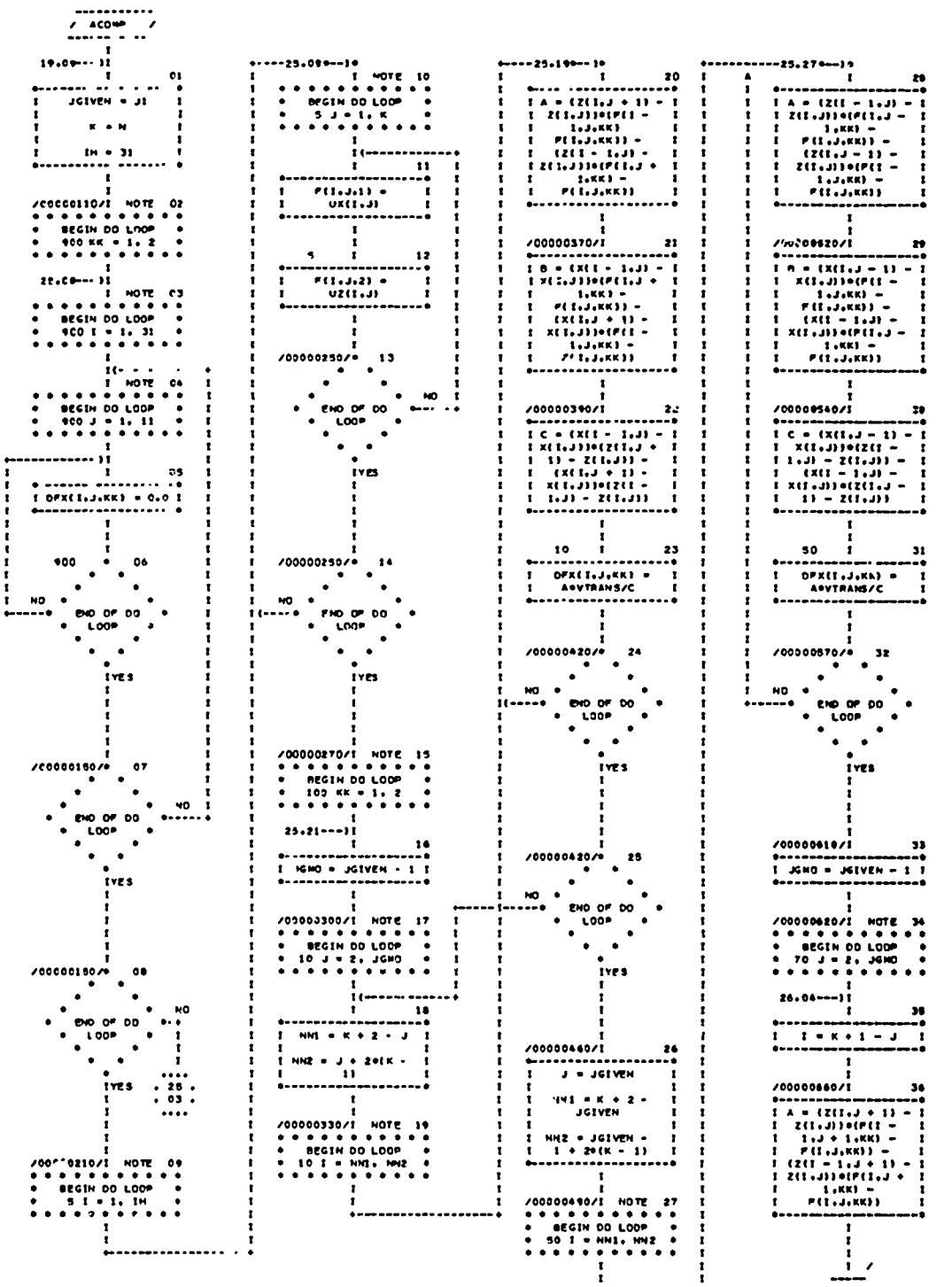

CHART TITLE - SUBROUTINE ACOMP

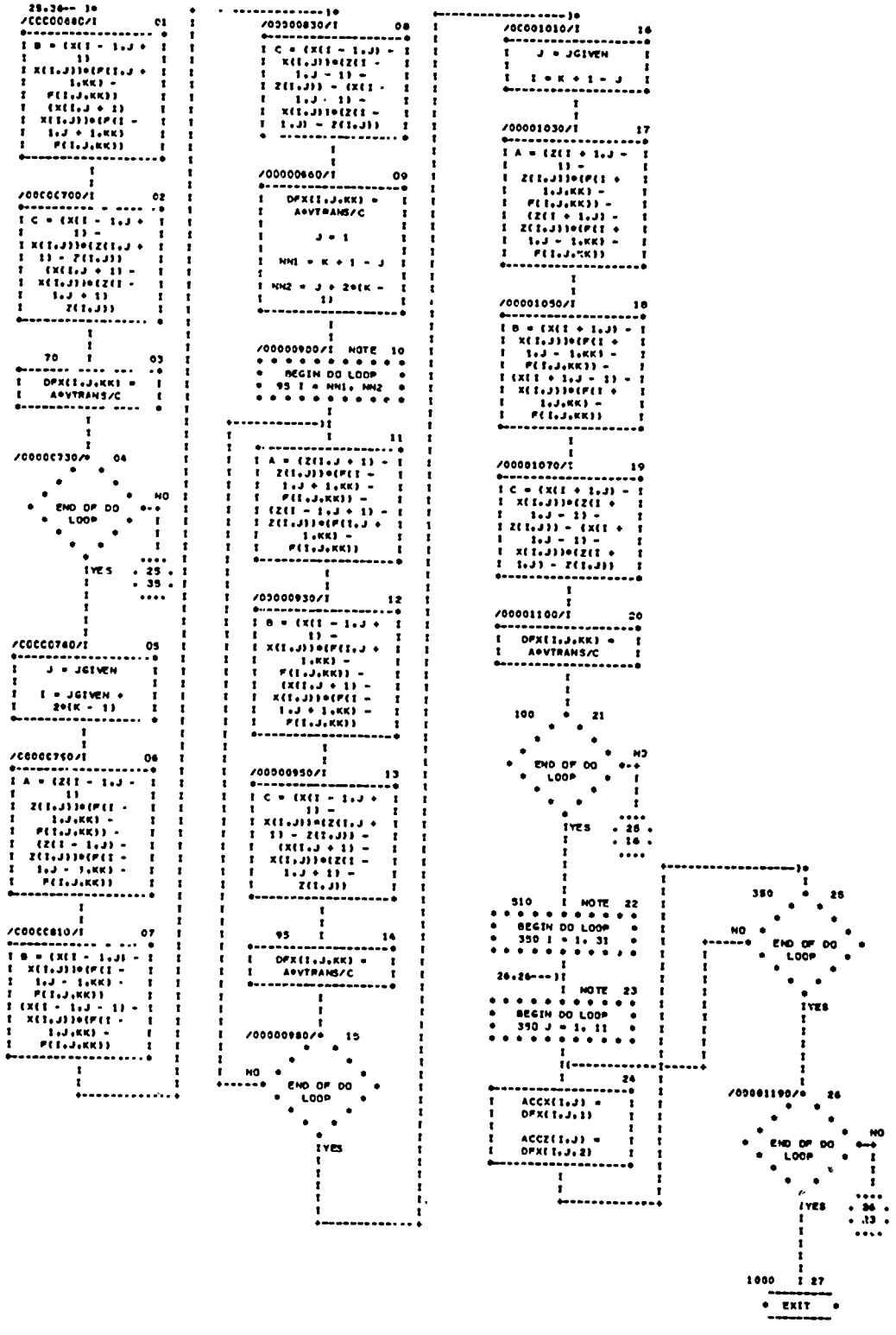

APPENDIX B

COMPUTER PROGRAM FLOW CHART FOR COMPUTATION OF TIRE PERFORMANCE WITH CONSIDERATION OF INERTIA FORCES BY PARTICLE PATH METHOD

(Pages 16, 17, and 27 omitted)

CHART TITLE - INTRODUCTORY COMMENTS

```
      THIS PROGRAM COMPUTES OFF-ROAD TIRE PERFORMANCE
      AT VARIOUS VELOCITIES WITH CONSIDERATION OF
      SOIL INERTIA FORCES COMPUTED BY THE PARTICLE
      PATH METHOD.  THE PROGRAM CONSISTS OF THE
      FOLLOWING PARTS
           MAIN PROGRAM (KTIRE)
           SUBROUTINE (SLFIC)
           SUBROUTINE (KACC)
           SUBROUTINE (PLOTSL)
      INPUTS IN THE MAIN PROGRAM ARE READ
      FROM DATA FILE TYR.DAT IN THE FOLLOWING
      ORDER

          CGR=CONE INDEX GRADIENT(LBS/CU IN)
          CI=CONE INDEX (LBS/SQ FT)
          RA=TIRE RADIUS (FT)
          BO=TIRE WIDTH (FT)
          LO=LOAD (LBS)
          PO=LIMIT PRESSURE (LBS/SQ IN)
          DE=DEFLECTION COEFF. EPSILON
          SL=SLIP (DECIMAL)
          SJ=SLIP PARAMETER J ZERO
          SKK=SLIP PARAMETER K
          CF=COHESION IN FRONT FIELD (LBS/SQ FT)
          CR=COHESION IN REAR FIELD (LBS/SQ FT)
          FF=FRICTION ANGLE IN FRONT FIELD (DEGREES)
          FR=FRICTION ANGLE IN REAR FIELD (DEGREES)
          GF=UNIT WEIGHT IN FRONT FIELD (LBS/CU FT)
          GR=UNIT WEIGHT IN REAR FIELD (LBS/CU FT)

      IF THE PROGRAM IS USED WITH CONE PENETRATION
      VALUES, CGR OR CI IS ENTERED WITH THE
      OTHER AS ZERO.  COHESION, FRICTION ANGLE AND
      UNIT WEIGHT IS COMPUTED IN THE PROGRAM AND
      THEIR VALUES IN THE DATA FILE DISREGARDED.
      ALTERNATIVELY, IF THE PROGRAM IS USED WITH
      COHESION, FRICTION ANGLE AND UNIT WEIGHT
      VALUES IN THE LAST SIX PLACES OF THE DATA
      FILE BOTH CGR AND CI MUST BE ZERO.
      THE FOLLOWING INPUT DATA ARE ACCEPTED IN
      THE PROGRAM FROM TYPED IN DATA.
          VEL=TRANSLATIONAL VELOCITY (FT/SEC)
          ZDEPTH=DEPTH OF INFLUENCE (FT) --IF NO OTHER DATA ASSUME
                                           EQUAL TO TIRE RADIUS
          ZETA=FACTOR FOR PARTICLE PATH GEOMETRY--IF NO OTHER DATA
                                                  ASSUME AS 0.9
          AO=ENTRY ANGLE IN RADIANS
      PRINCIPAL VARIABLES IN THE PROGRAM ARE
```

CHART TITLE - INTRODUCTORY COMMENTS

AM=SEPARATION ANGLE IN RADIANS
A1=TANGENT OF LOG. SPIRAL
D1=INTERFACE FRICTION ANGLE IN RADIANS
L=LENGTH OF PASSIVE ZONE AT SURFACE
SSLIP=AVERAGE VALUE OF CONTACT SLIP
AZERO=VERTICLE DISTANCE BETWEEN END POINTS OF PARTICLE PATH
OME1,OME3,OME4=OMEGA VALUES AT B,D,E POINTS OF PARTICLE
TIM1,TIM3,TIM4=ELAPSED TIME ASSOCIATED WITH B,D,E POINTS,
RESPECTIVELY
X(I,J),Z(I,J)=X,Z COORDINATES OF SLIP LINE FIELD WITH
REFERENCE TO ENTRY POINT
S(I,J),T(I,J)=SIGMA, THETA VALUE AT I,J POINT OF SLIP
LINE FIELD
A(J),O(J),E(J)=CENTRAL ANGLE, NORMAL STRESS, SHEAR
STRESS AT POINT J OF INTERFACE
U(J),V(J)=X AND Z COORDINATES OF INTERFACE WITH REFERENCE
TO TIRE AXIS
ACCX(I,J),ACCZ(I,J)=X,Z COMPONENT OF ACCELERATION AT I,J
POINT OF SLIP LINE FIELD

CHART TITLE - PROCEDURES

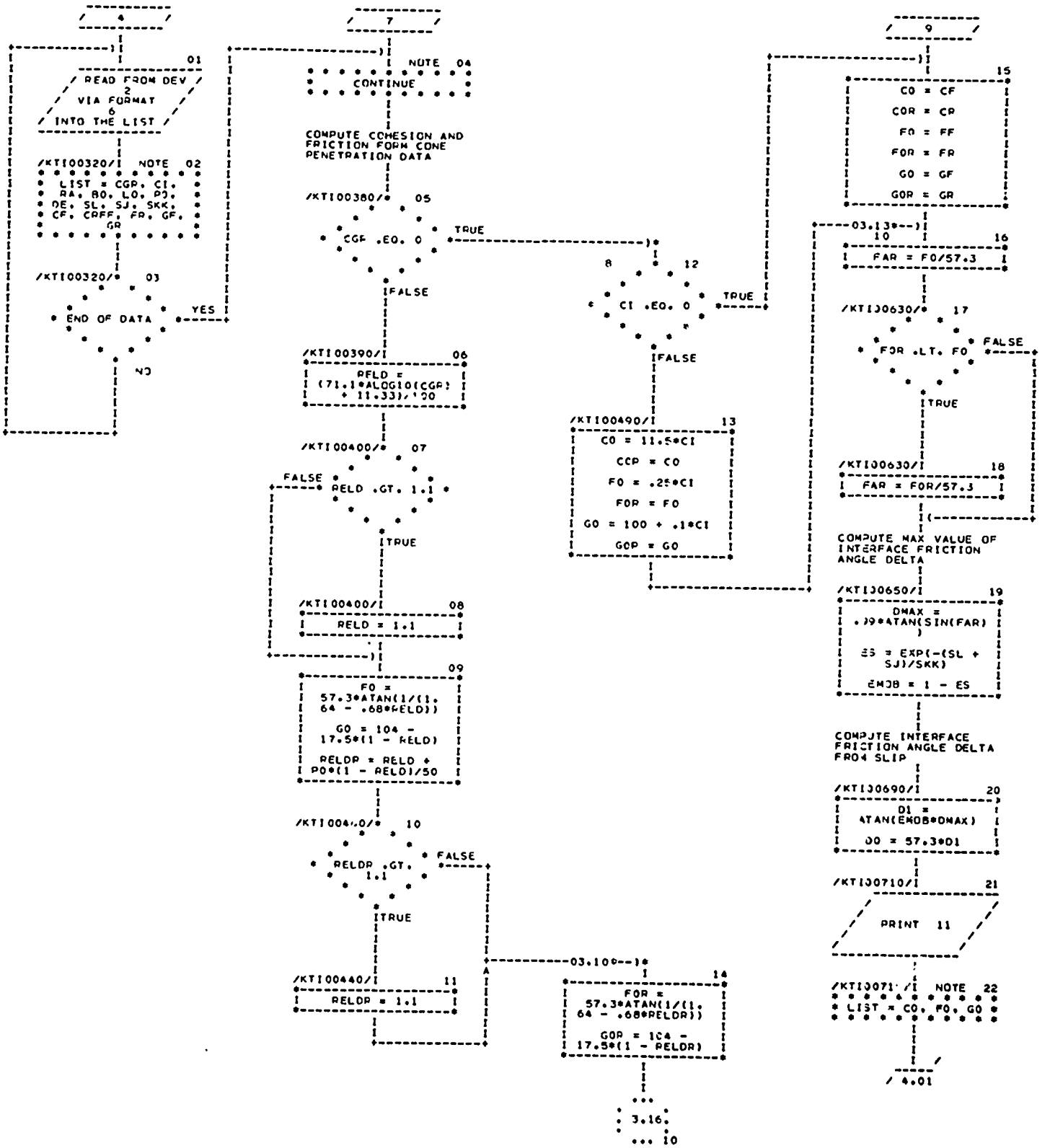

CHART TITLE - PROCEDURES

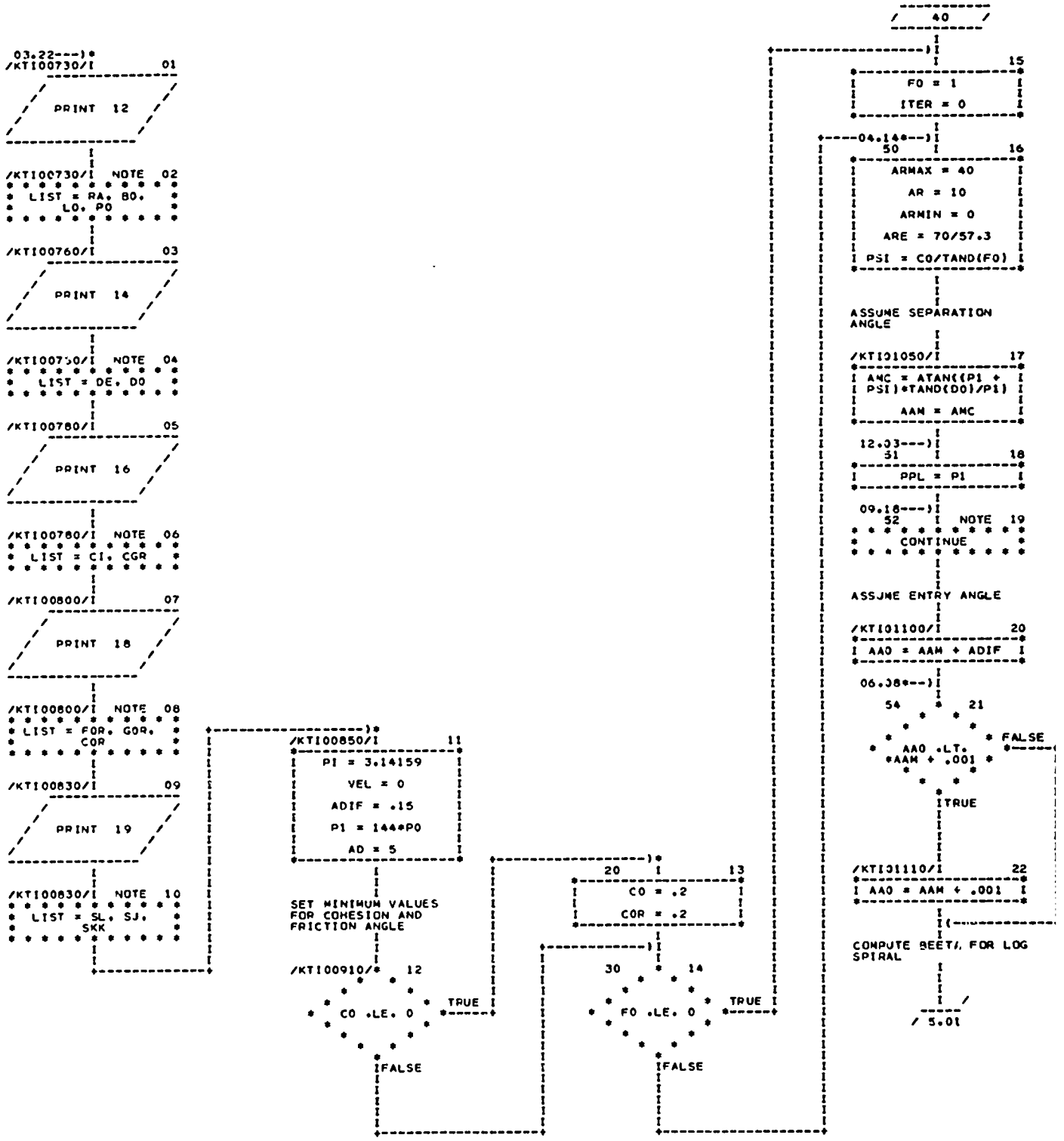

CHART TITLE - PROCEDURES

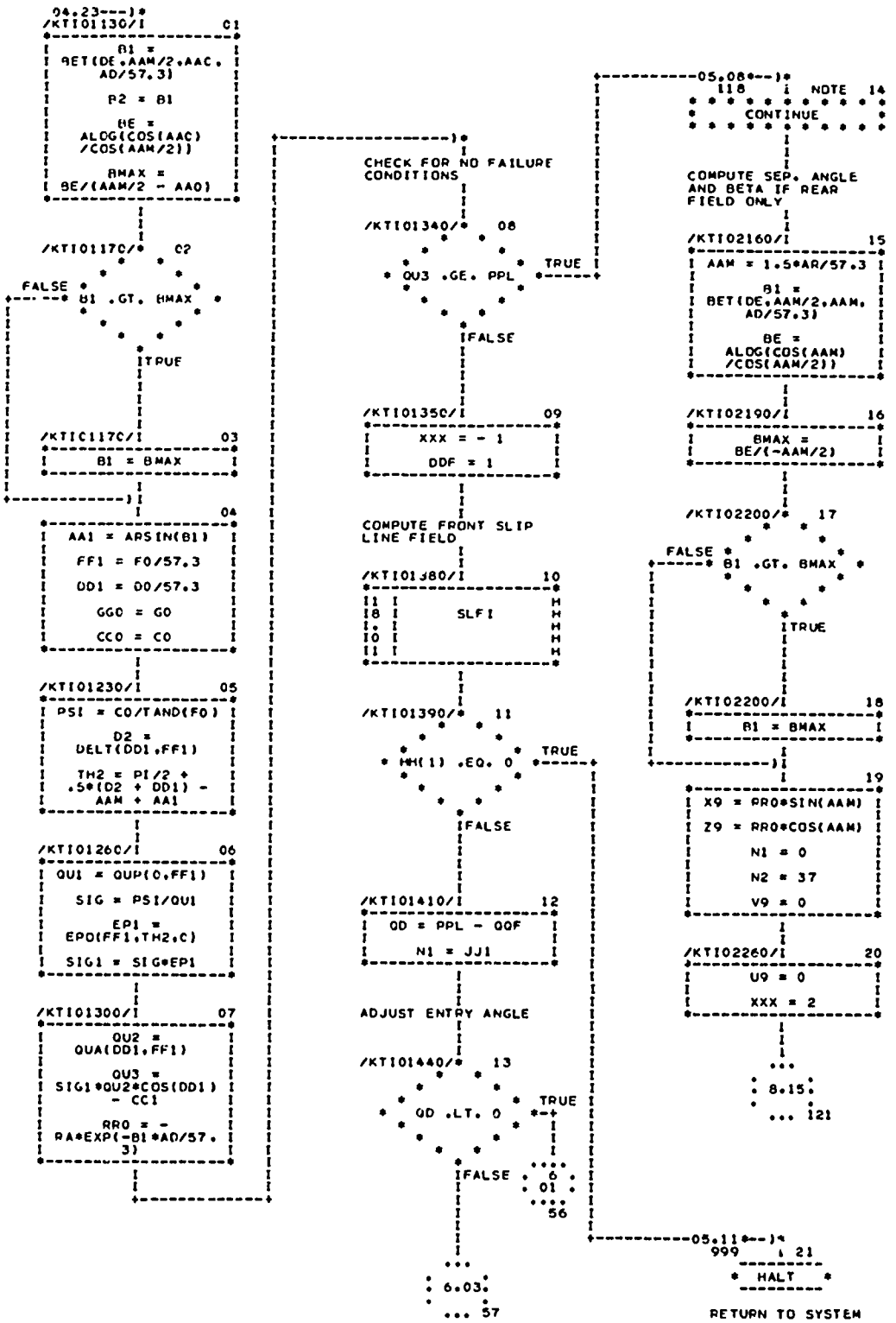

CHART TITLE - PROCEDURES

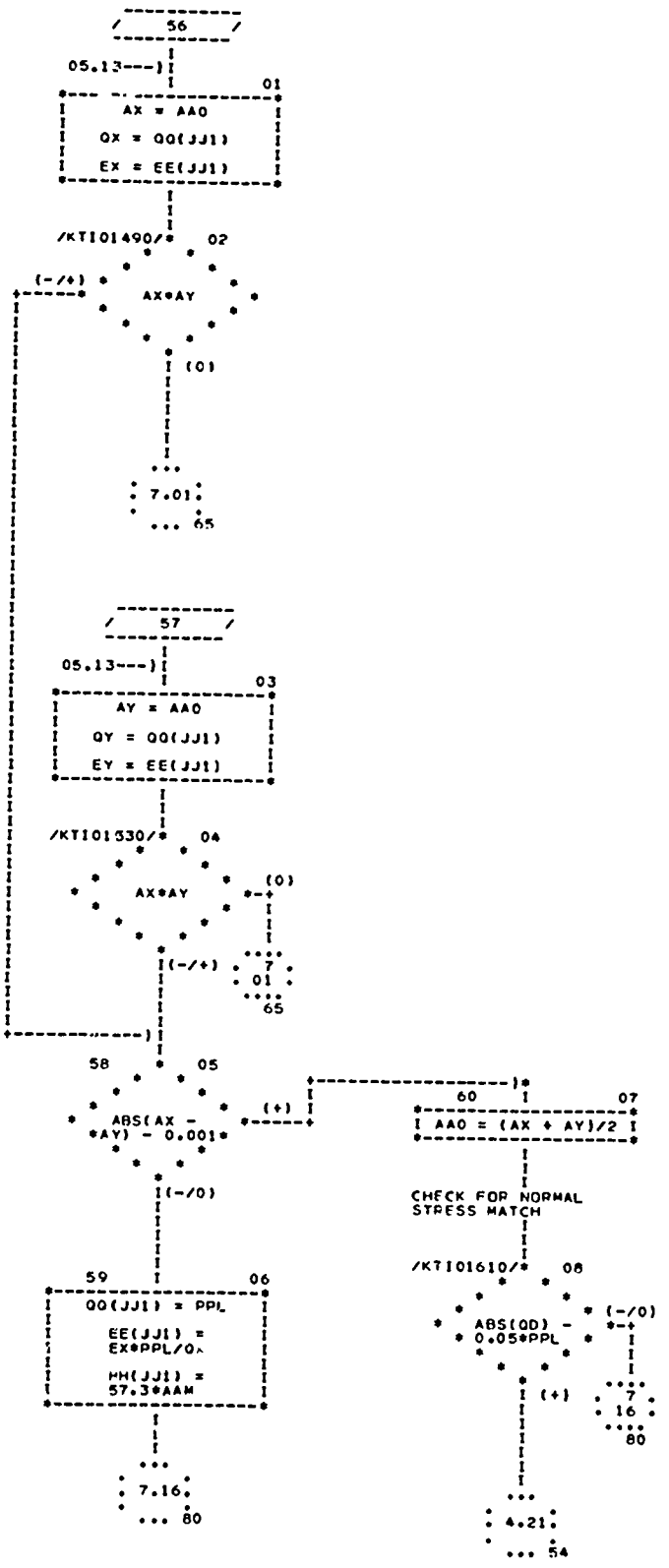

CHART TITLE - PROCEDURES

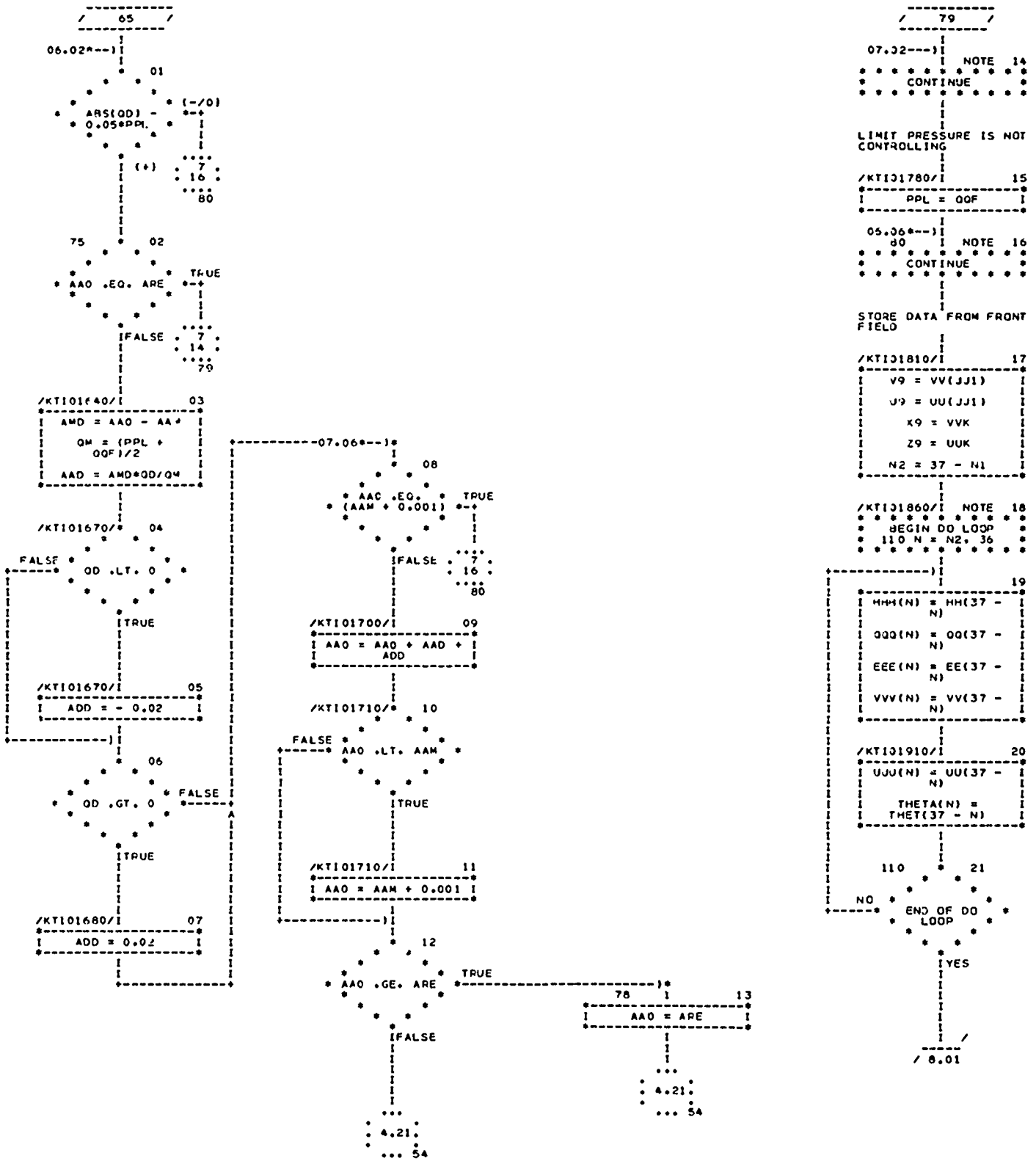

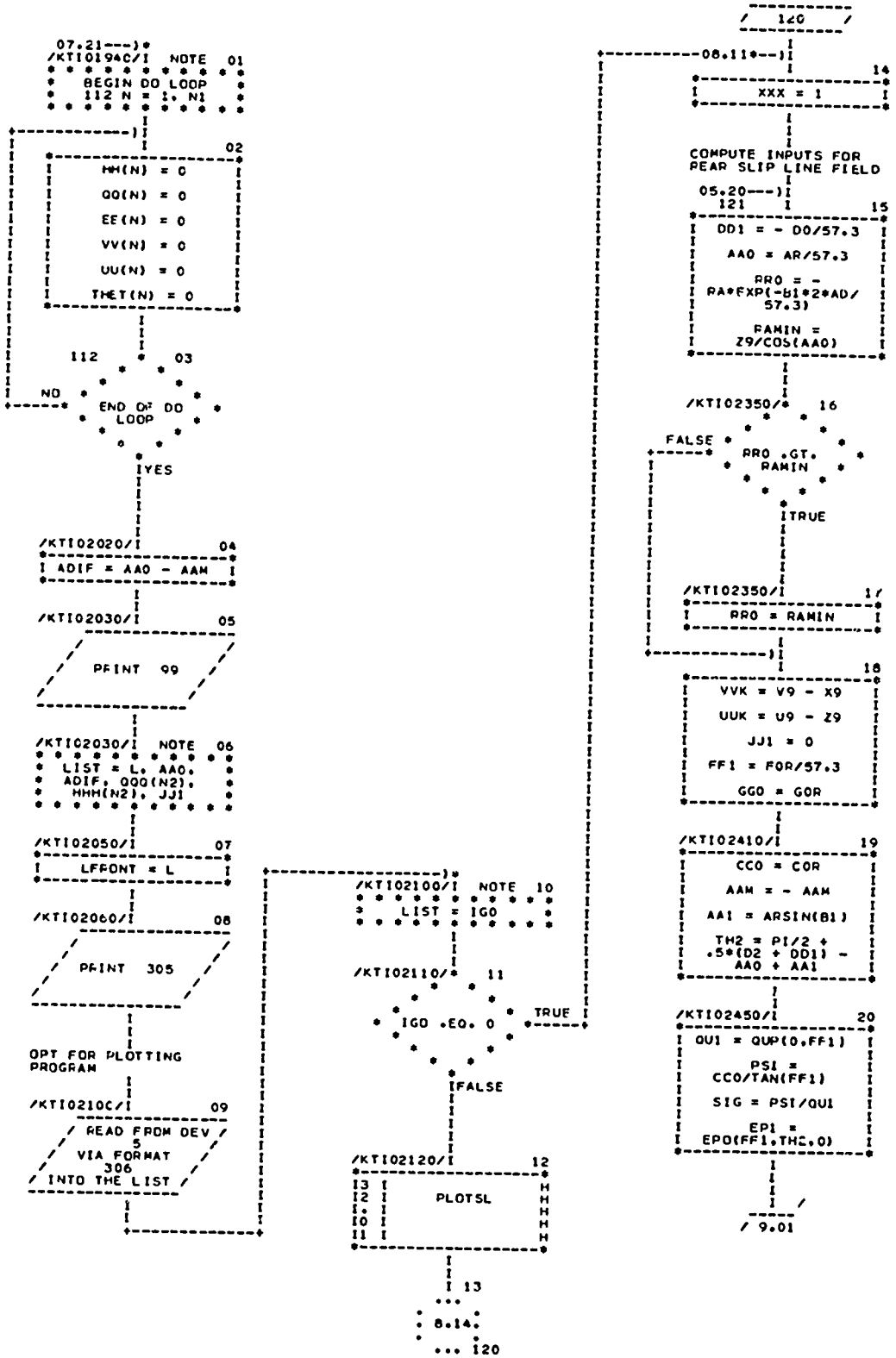
07.21---)
/KTI0194C/I NOTE 01
BEGIN DO LOOP
112 N = 1, N1
02
MM(N) = 0
QQ(N) = 0
EE(N) = 0
VV(N) = 0
UU(N) = 0
THET(N) = 0
112
03
NO
END OF DO LOOP
YES
/KTI02020/I 04
ADIF = AA0 - AAM
/KTI02030/I 05
PRINT 99
/KTI02030/I NOTE 06
LIST = L, AA0, ADIF, QQQ(N2), MMM(N2), JJ1
/KTI02050/I 07
LFRONT = L
/KTI02060/I 08
PRINT 305
OPT FOR PLOTTING PROGRAM
/KTI0210C/I 09
READ FROM DEV 5 VIA FORMAT 306 INTO THE LIST
/KTI02100/I NOTE 10
LIST = IGO
/KTI02110/I 11
IGO .EQ. 0
TRUE
FALSE
/KTI02120/I 12
PLOTSL
13
8.14.
120
120
08.11---)
14
XXX = 1
COMPUTE INPUTS FOR REAR SLIP LINE FIELD
05.20---)
121
15
DD1 = - D0/57.3
AA0 = AR/57.3
RR0 = - RA*EXP(-B1*2*AD/57.3)
RAMIN = Z9/COS(AA0)
/KTI02350/ 16
RR0 .GT. RAMIN
FALSE
TRUE
/KTI02350/I 17
RR0 = RAMIN
18
VVK = V9 - X9
UUK = U9 - Z9
JJ1 = 0
FF1 = FOR/57.3
GG0 = G0R
/KTI02410/I 19
CC0 = C0R
AAM = - AAM
AA1 = ARSIN(B1)
TH2 = PI/2 + .5*(D2 + DD1) - AA0 + AA1
/KTI02450/I 20
QU1 = QUP(0,FF1)
PSI = CC0/TAN(FF1)
SIG = PSI/QU1
EP1 = EP0(FF1,THE,0)
9.01

CHART TITLE - PROCEDURES

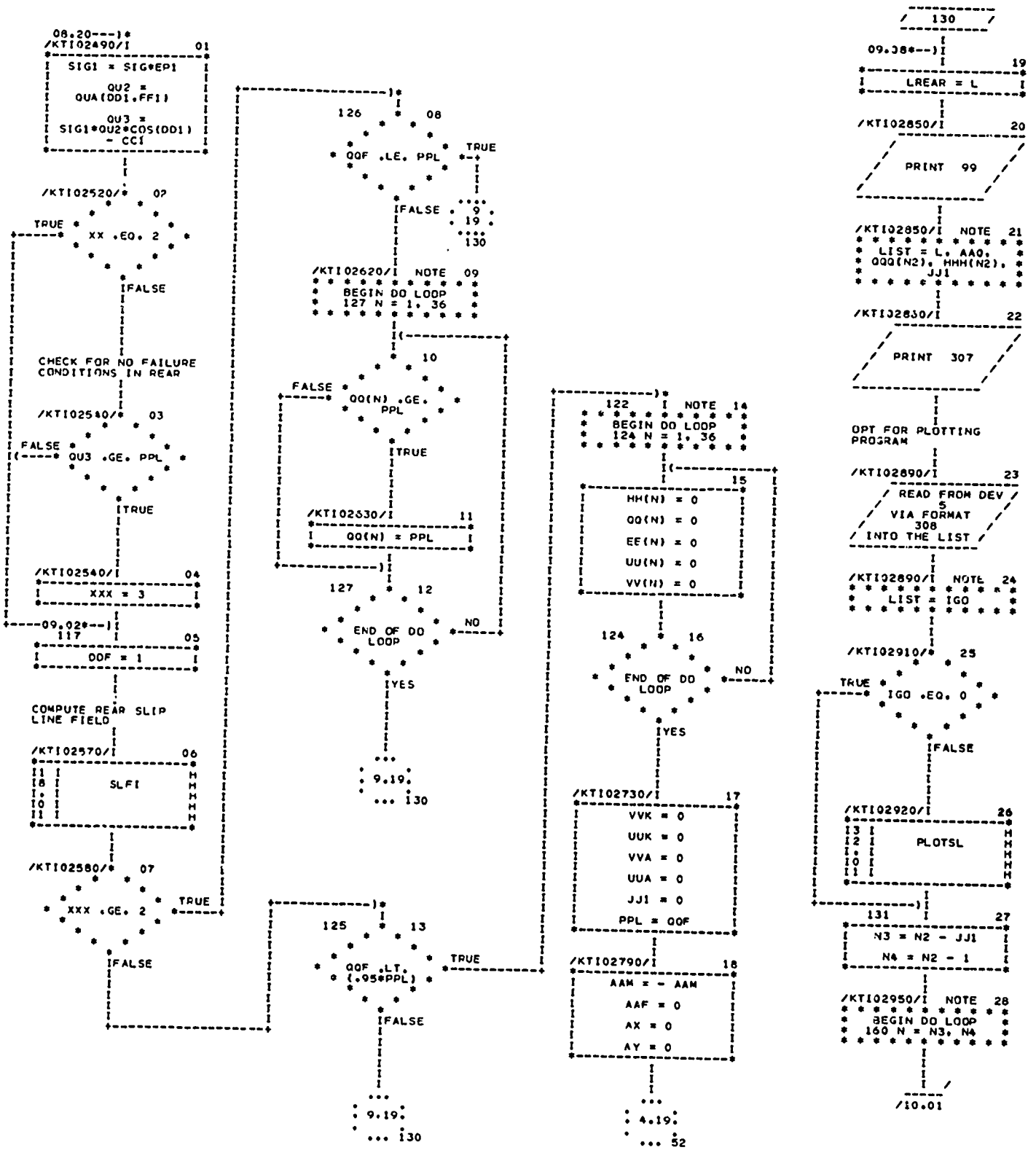

CHART TITLE - PROCEDURES

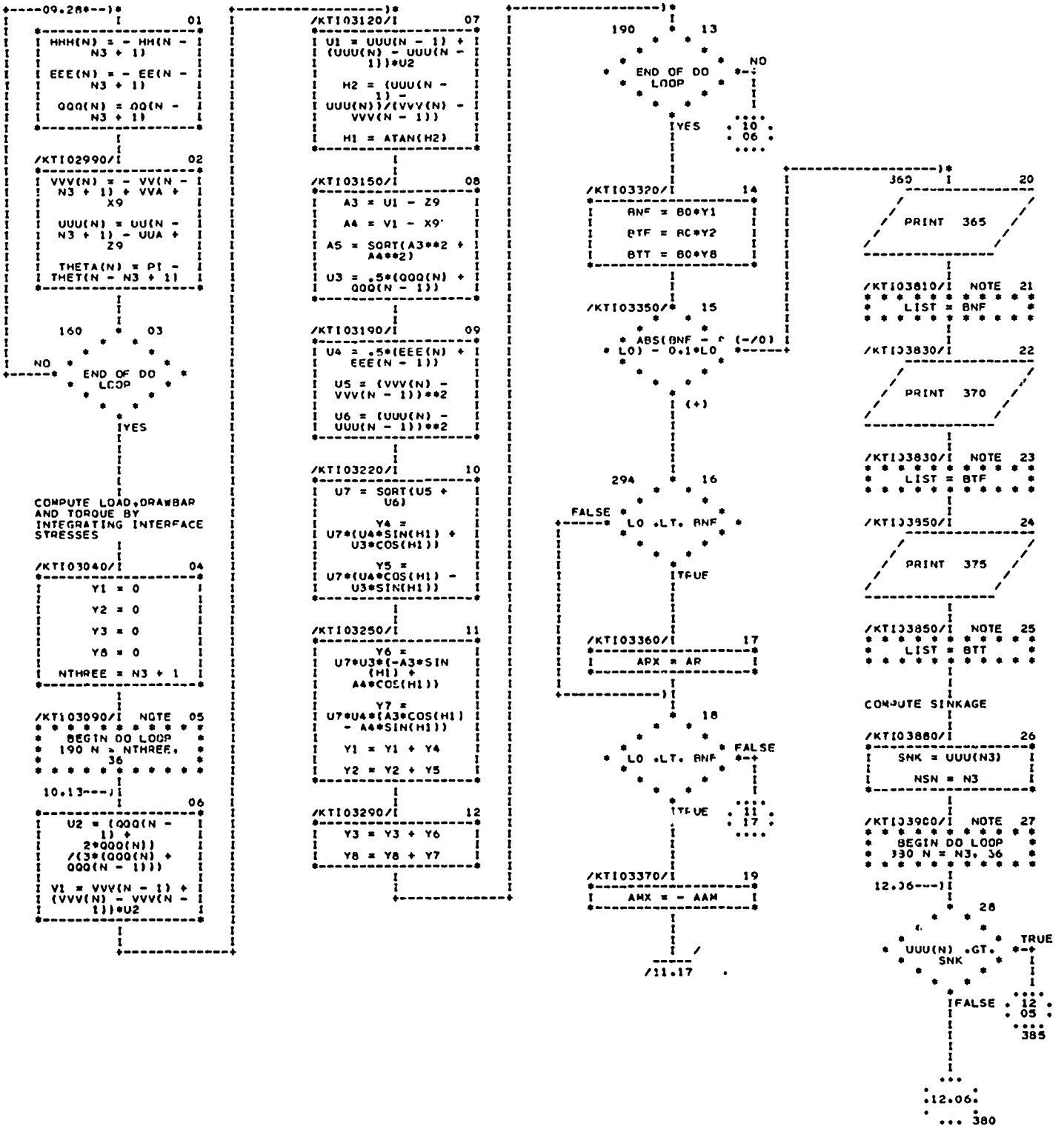

CHART TITLE - PROCEDURES

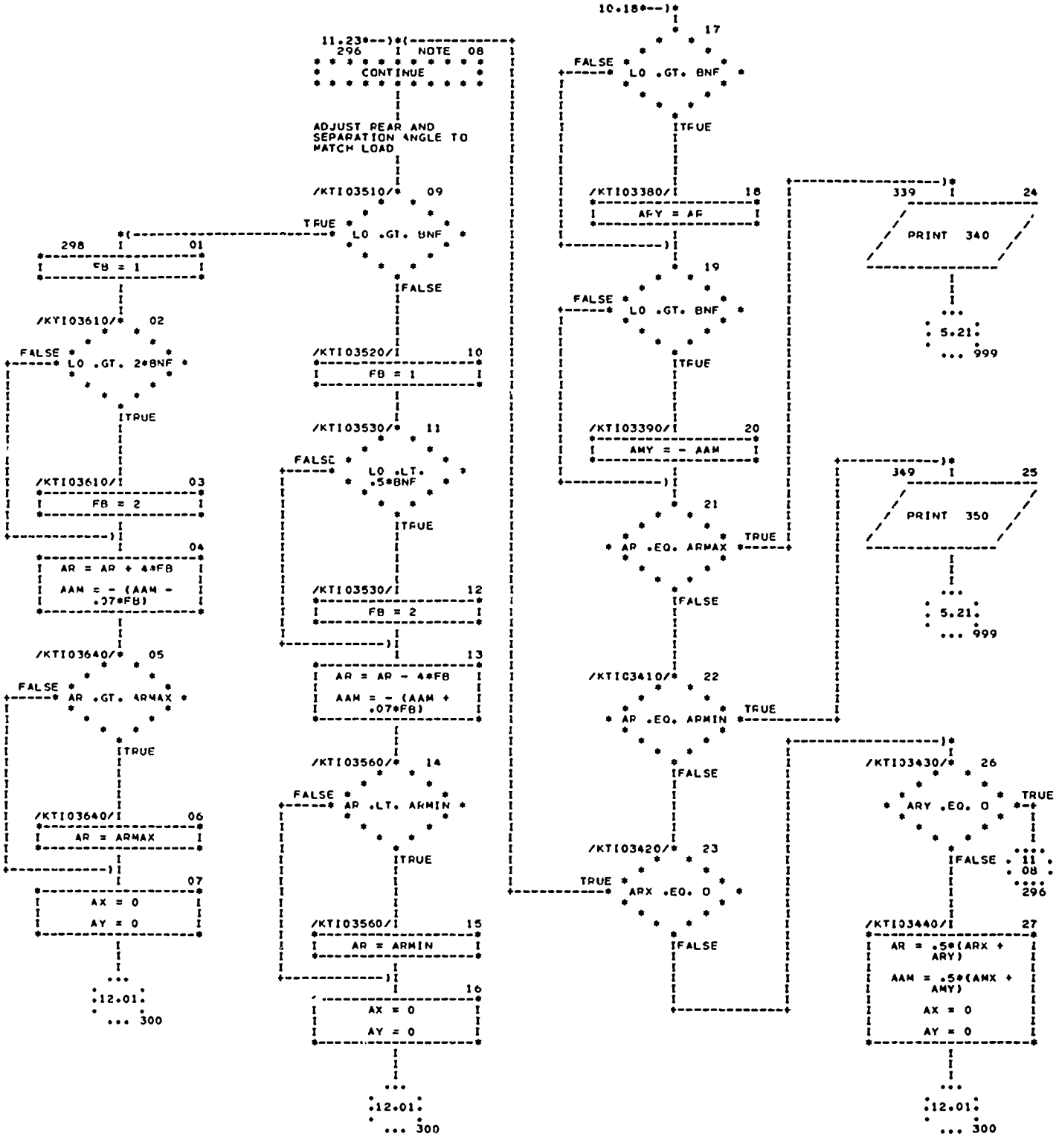

CHART TITLE - PROCEDURES

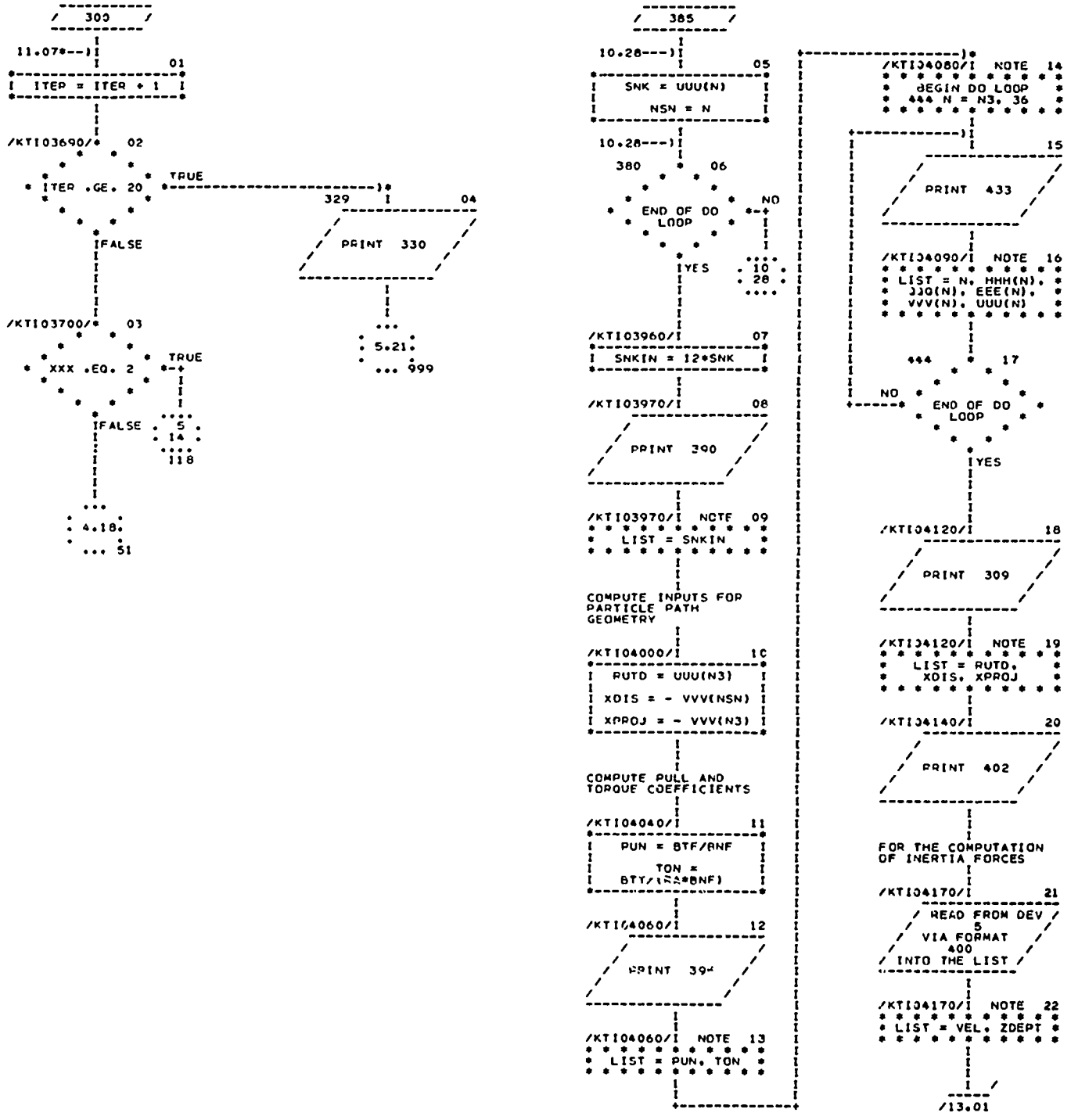

CHART TITLE - PROCEDURES

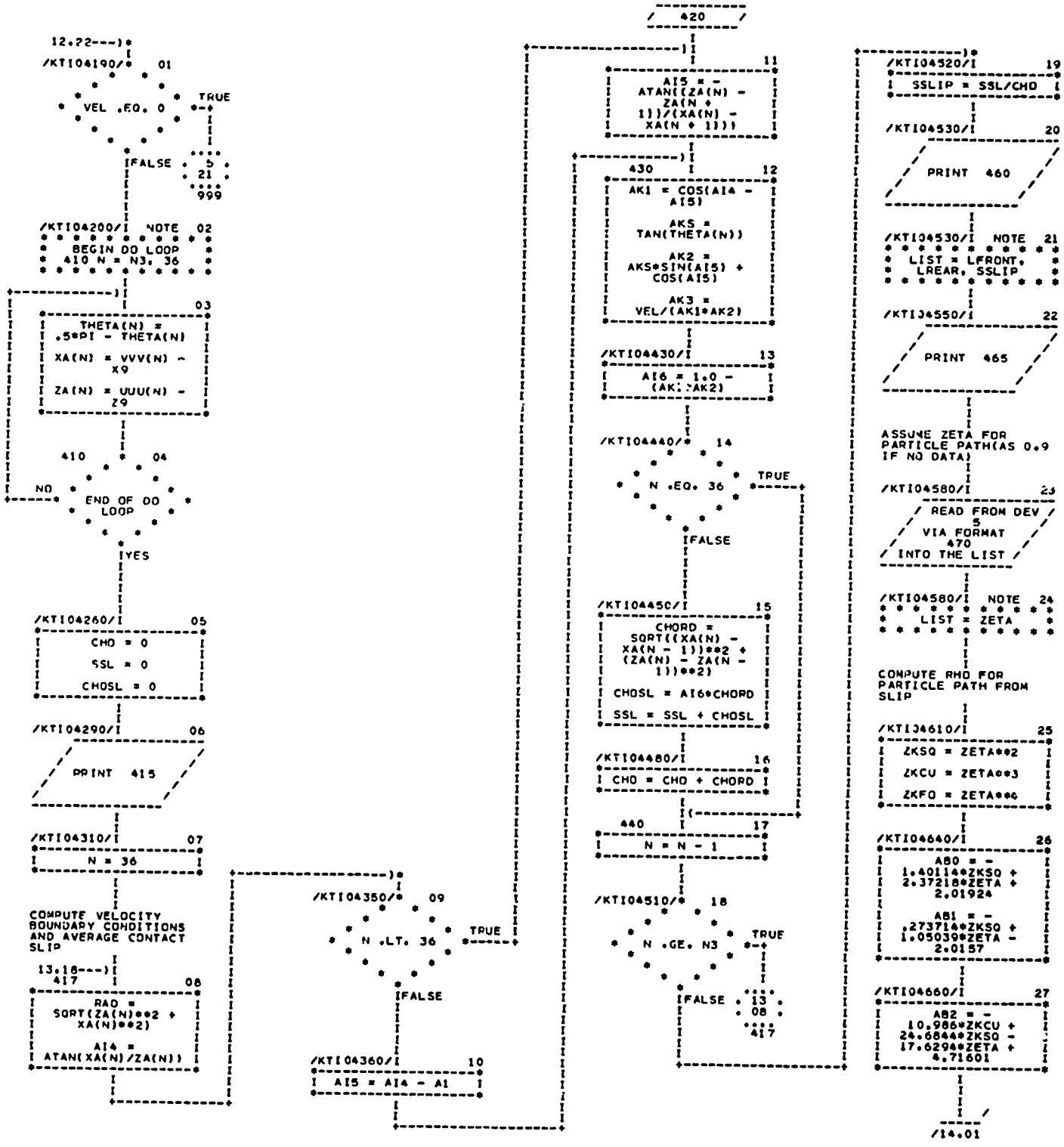

CHART TITLE - PROCEDURES

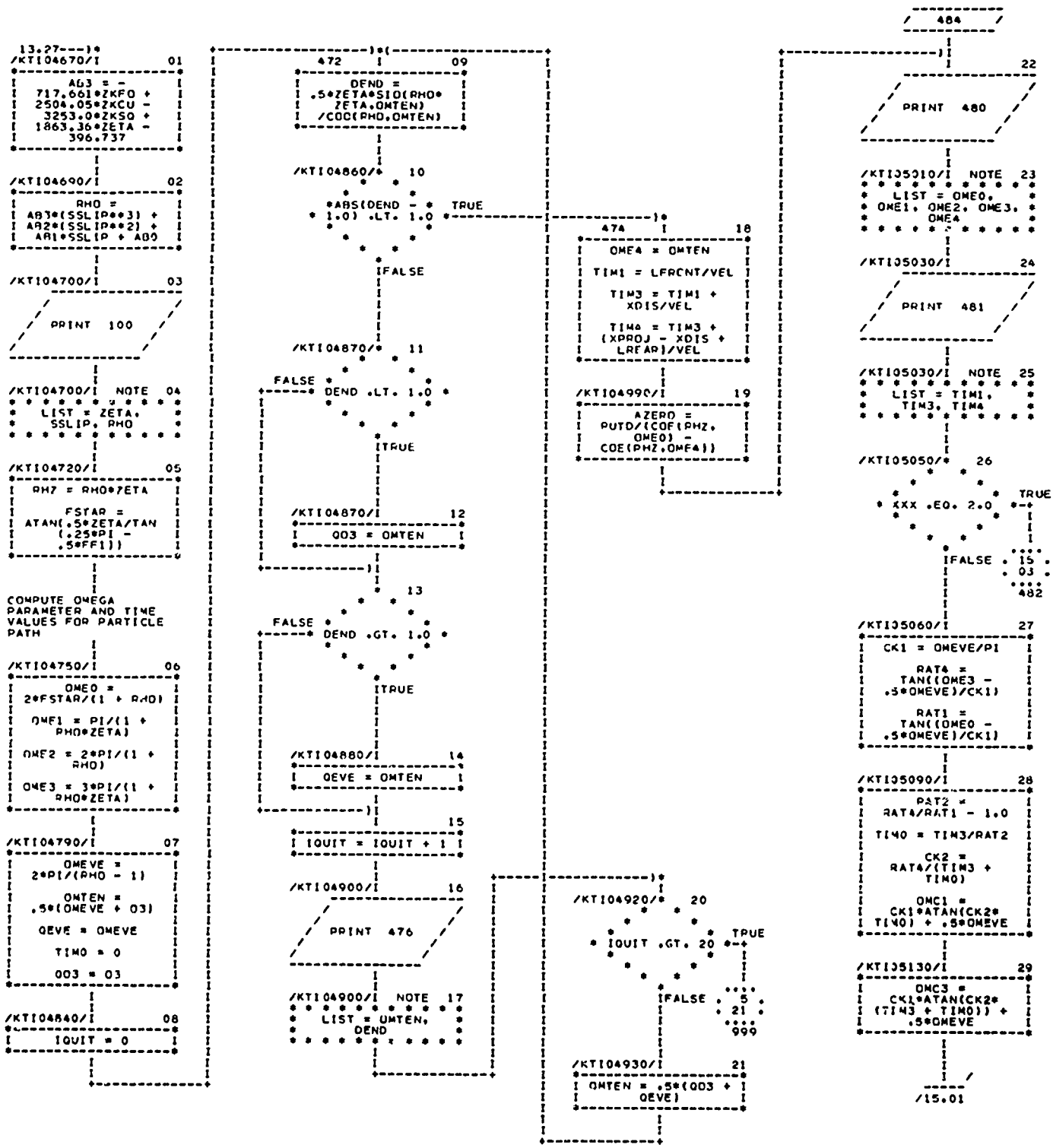

CHART TITLE - PROCEDURES

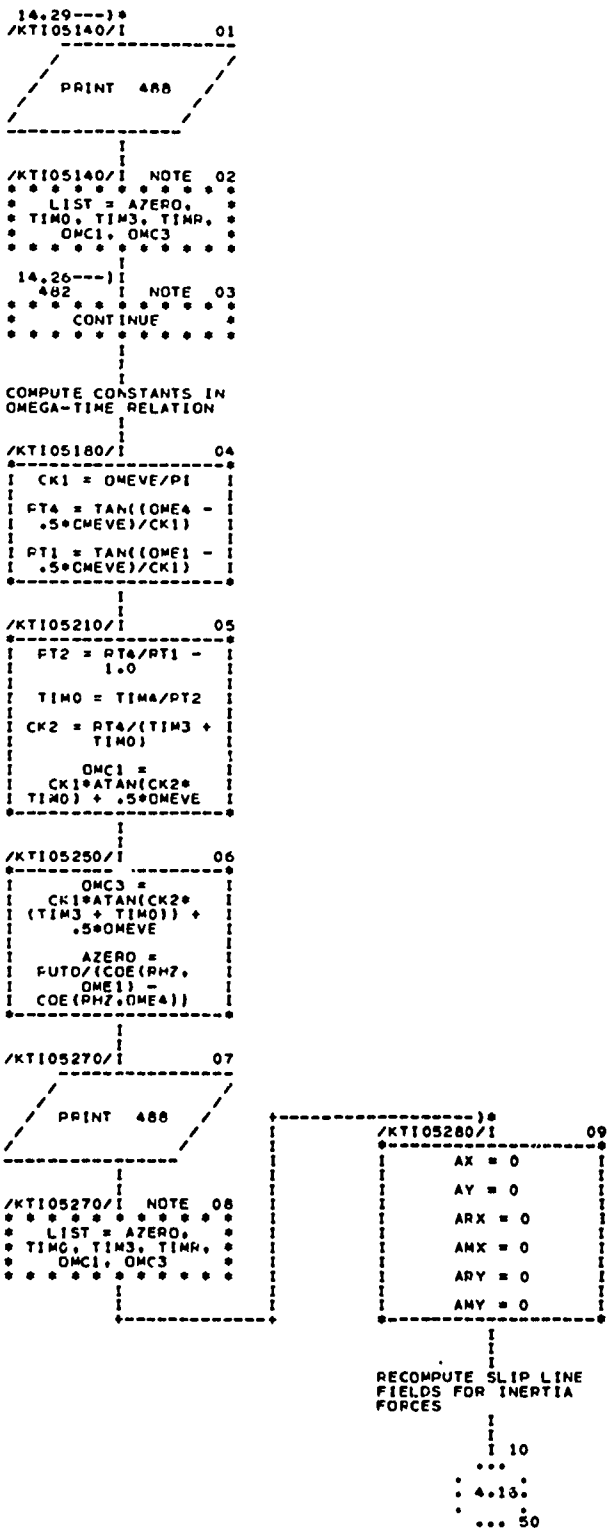

CHART TITLE - SUBROUTINE SLF1

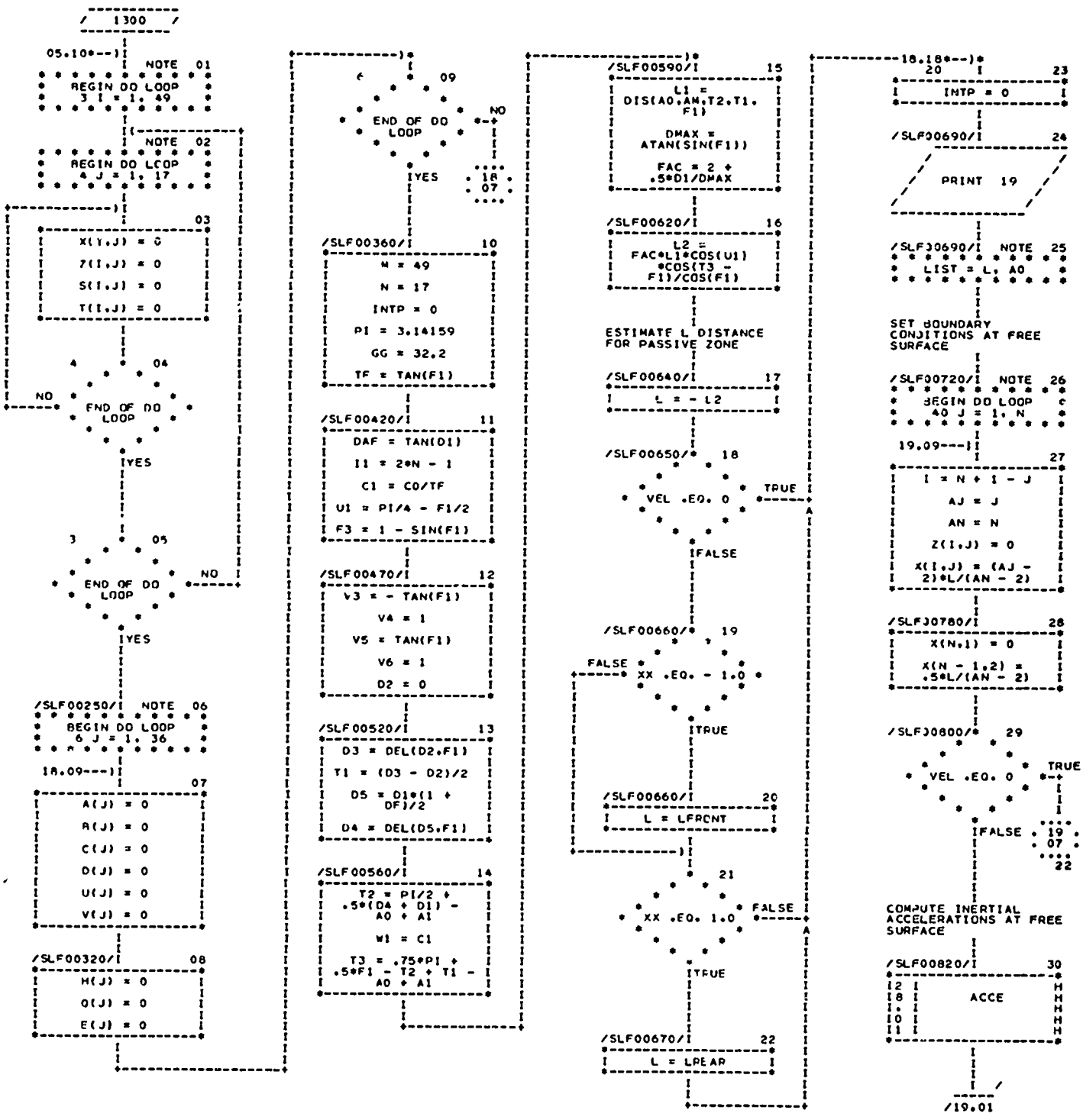

CHART TITLE - SUBROUTINE SLFI

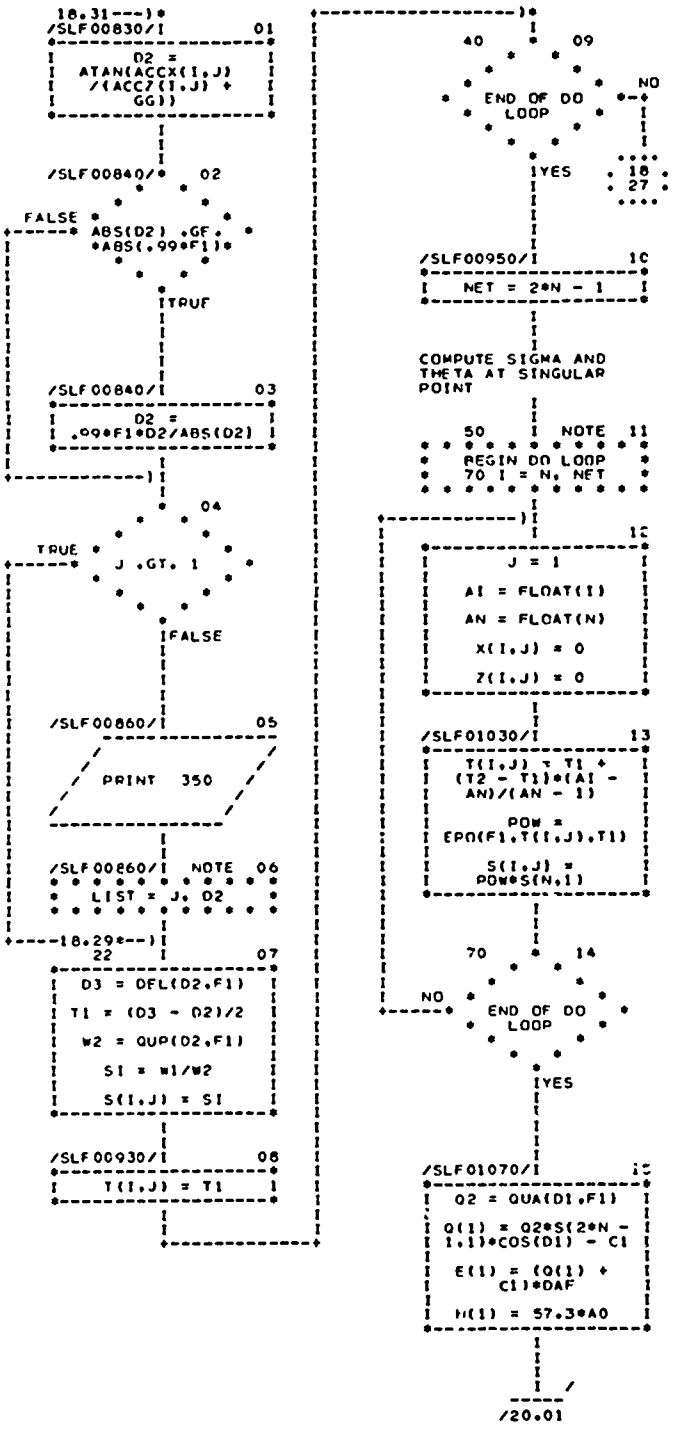

CHART TITLE - SUBROUTINE SLFI

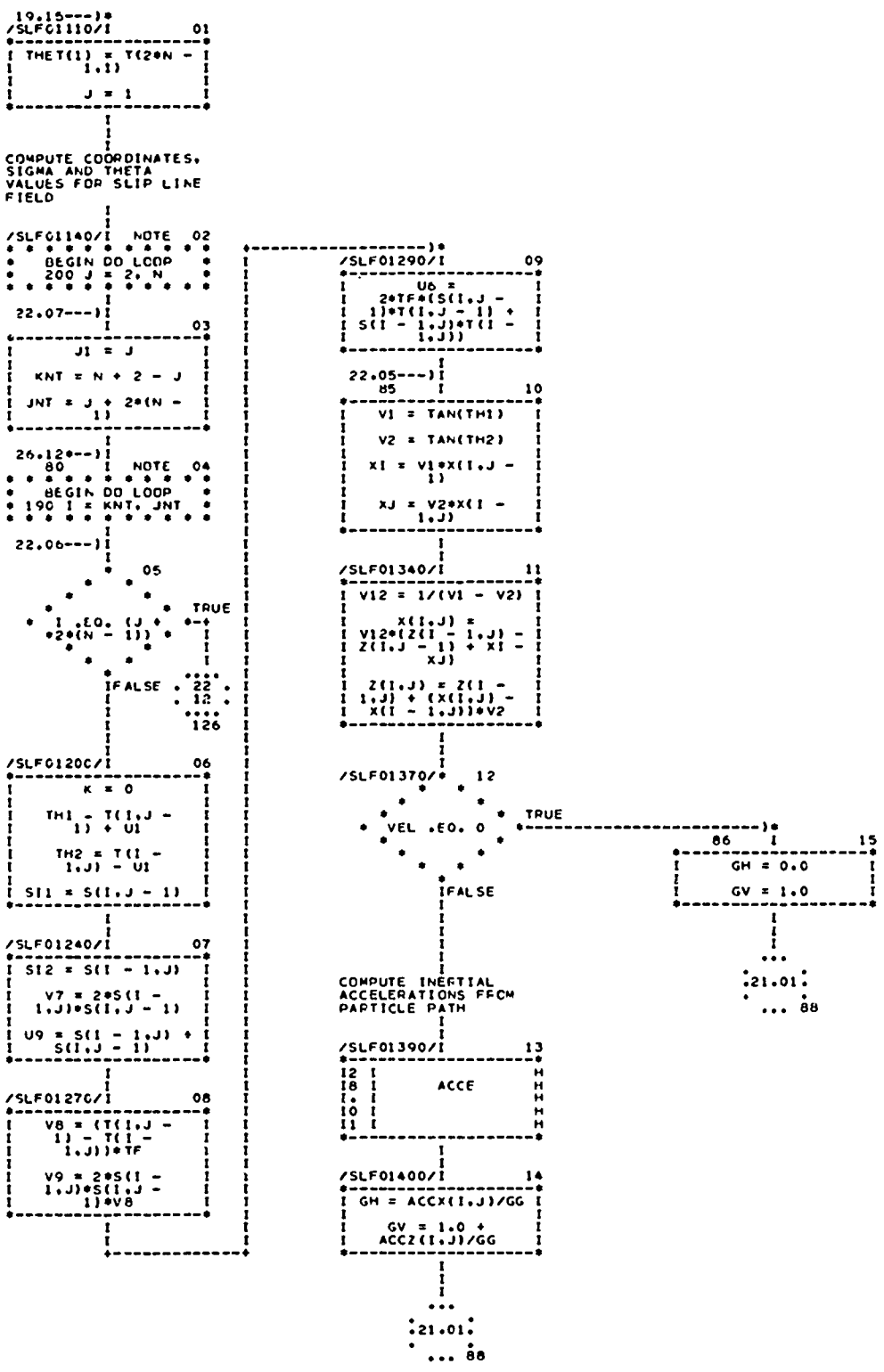

CHART TITLE - SUBROUTINE SLF1

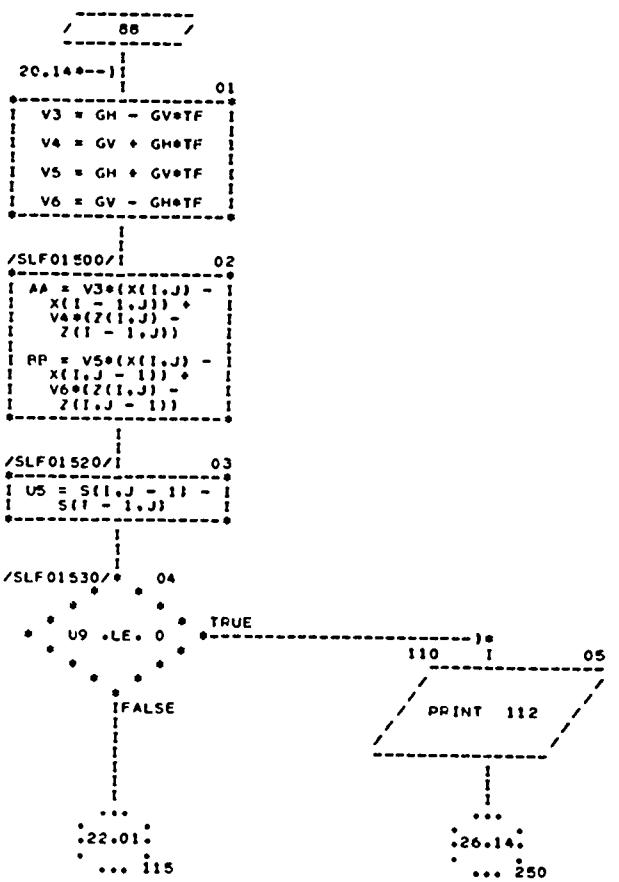

CHART TITLE - SUBROUTINE SLF I

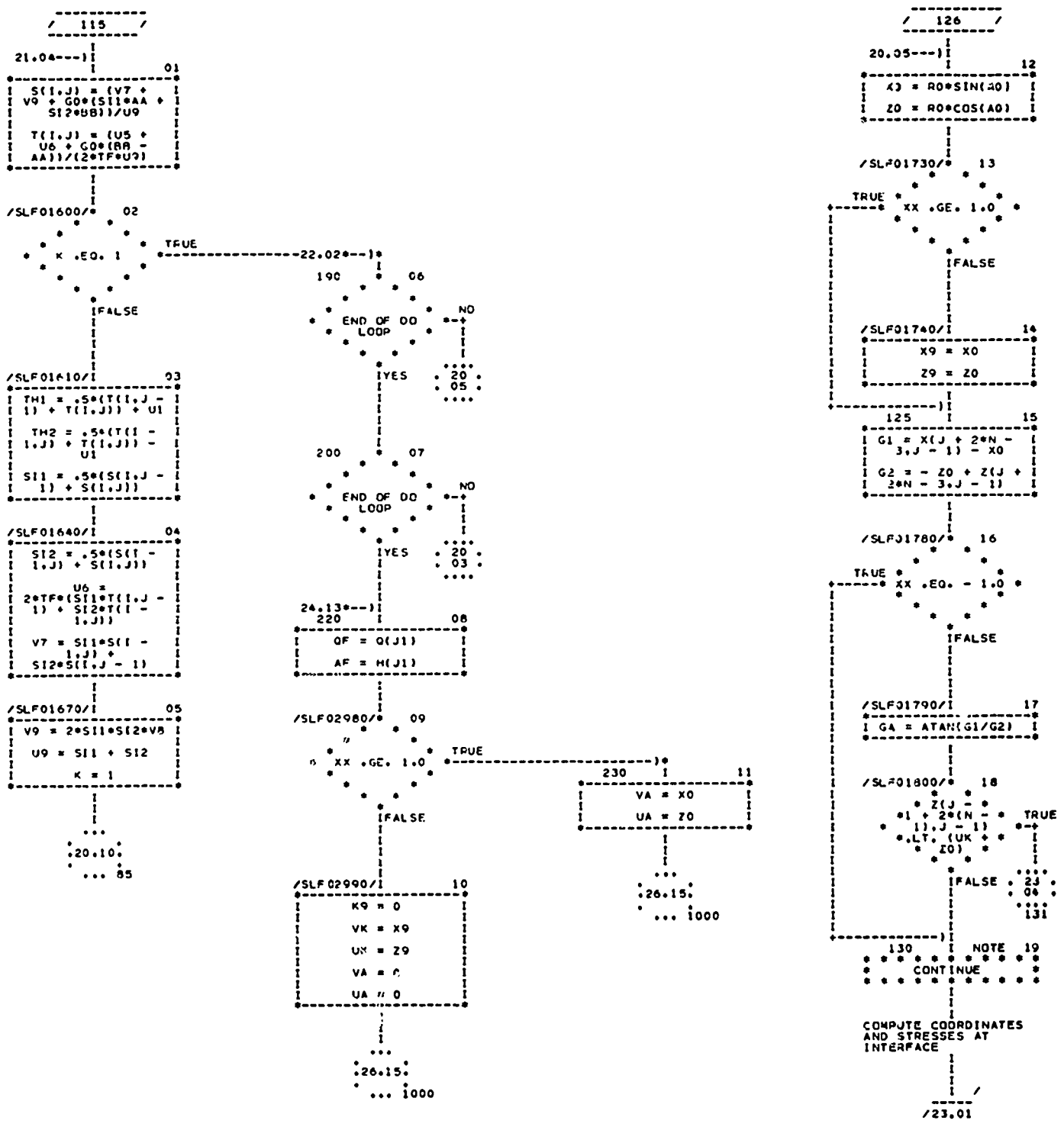

CHART TITLE - SUBROUTINE SLFI

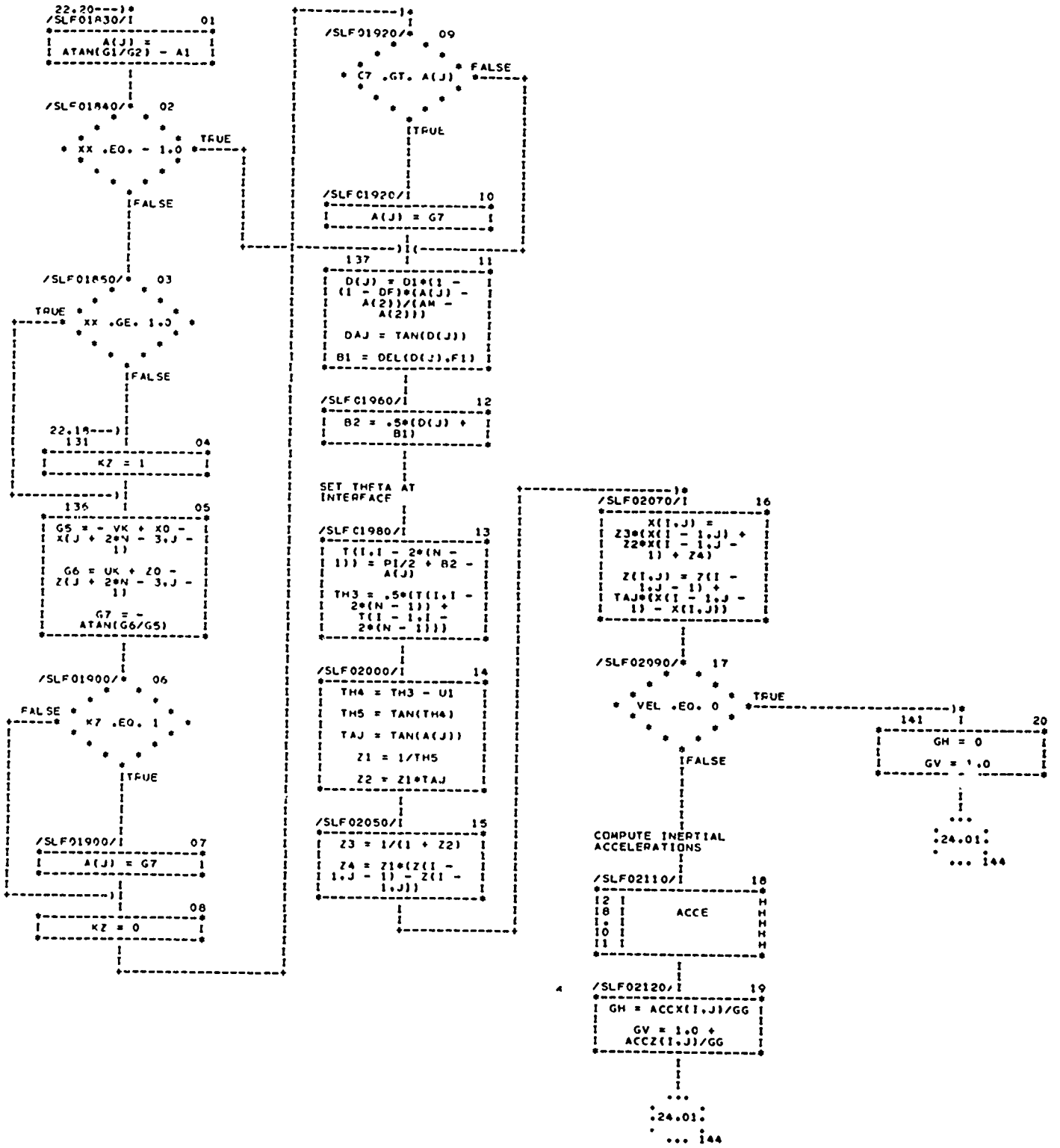

CHART TITLE - SUBROUTINE SLF1

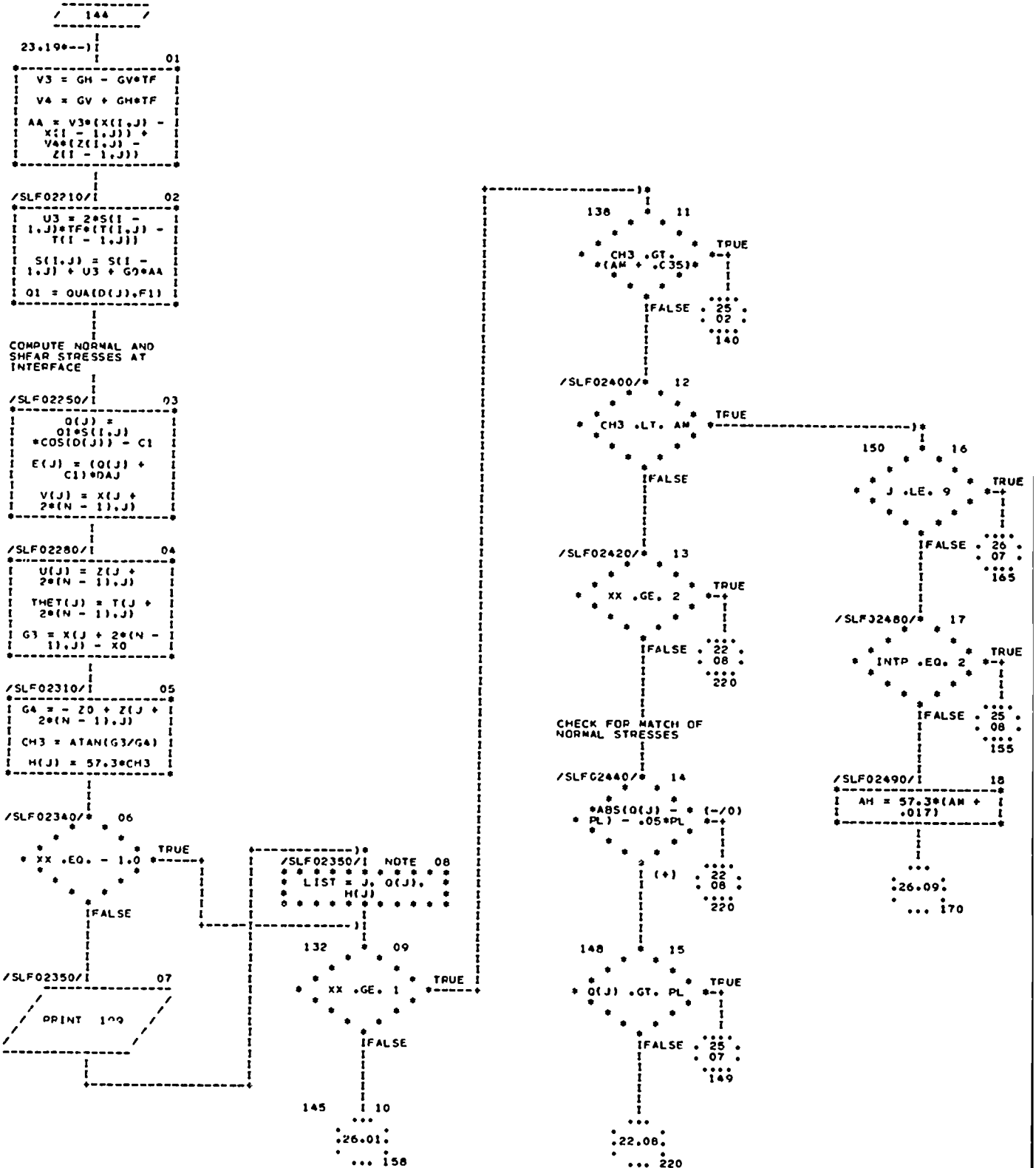

CHART TITLE - SUBROUTINE SLFI

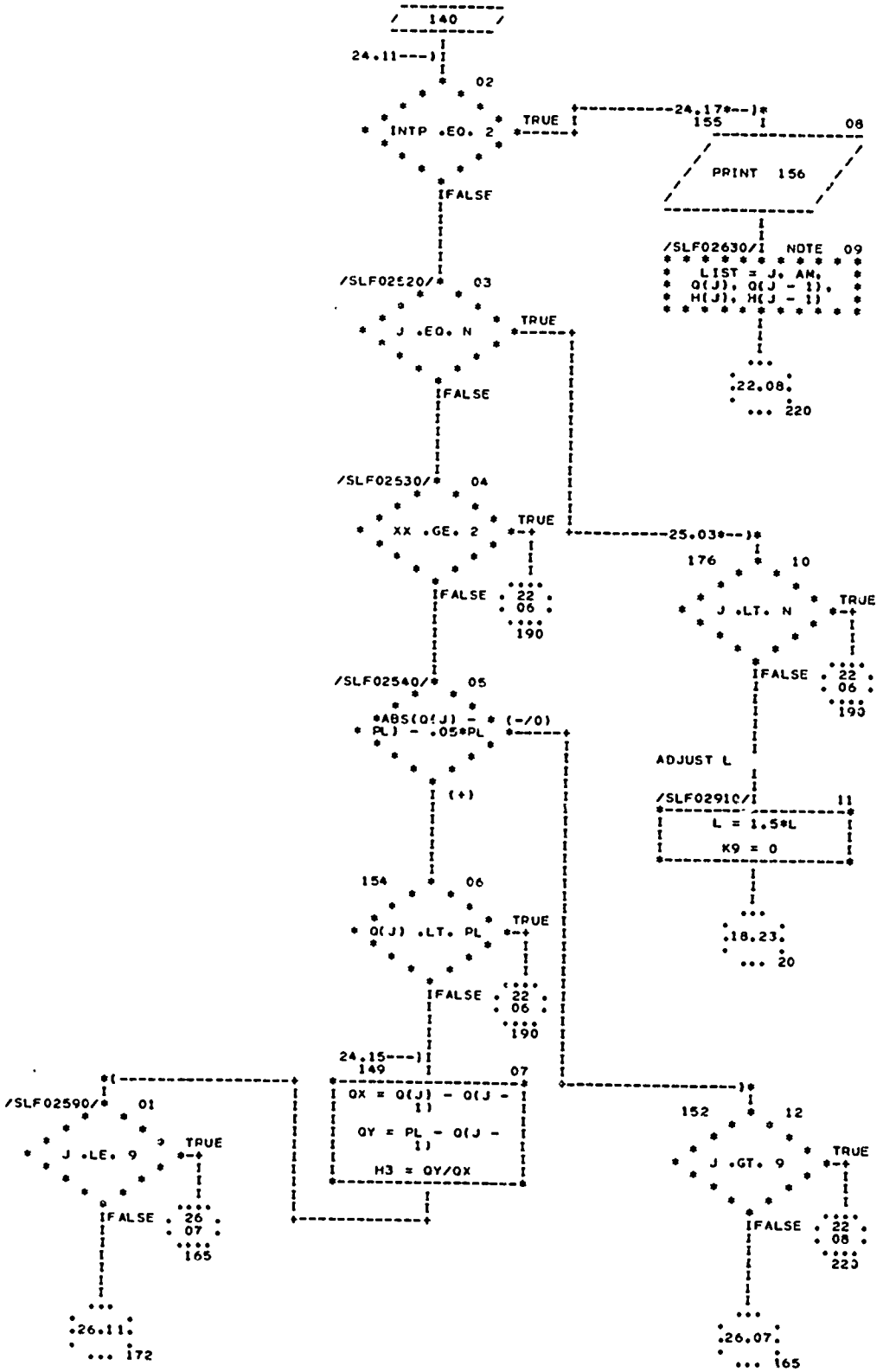

CHART TITLE - SUBROUTINE SLFI

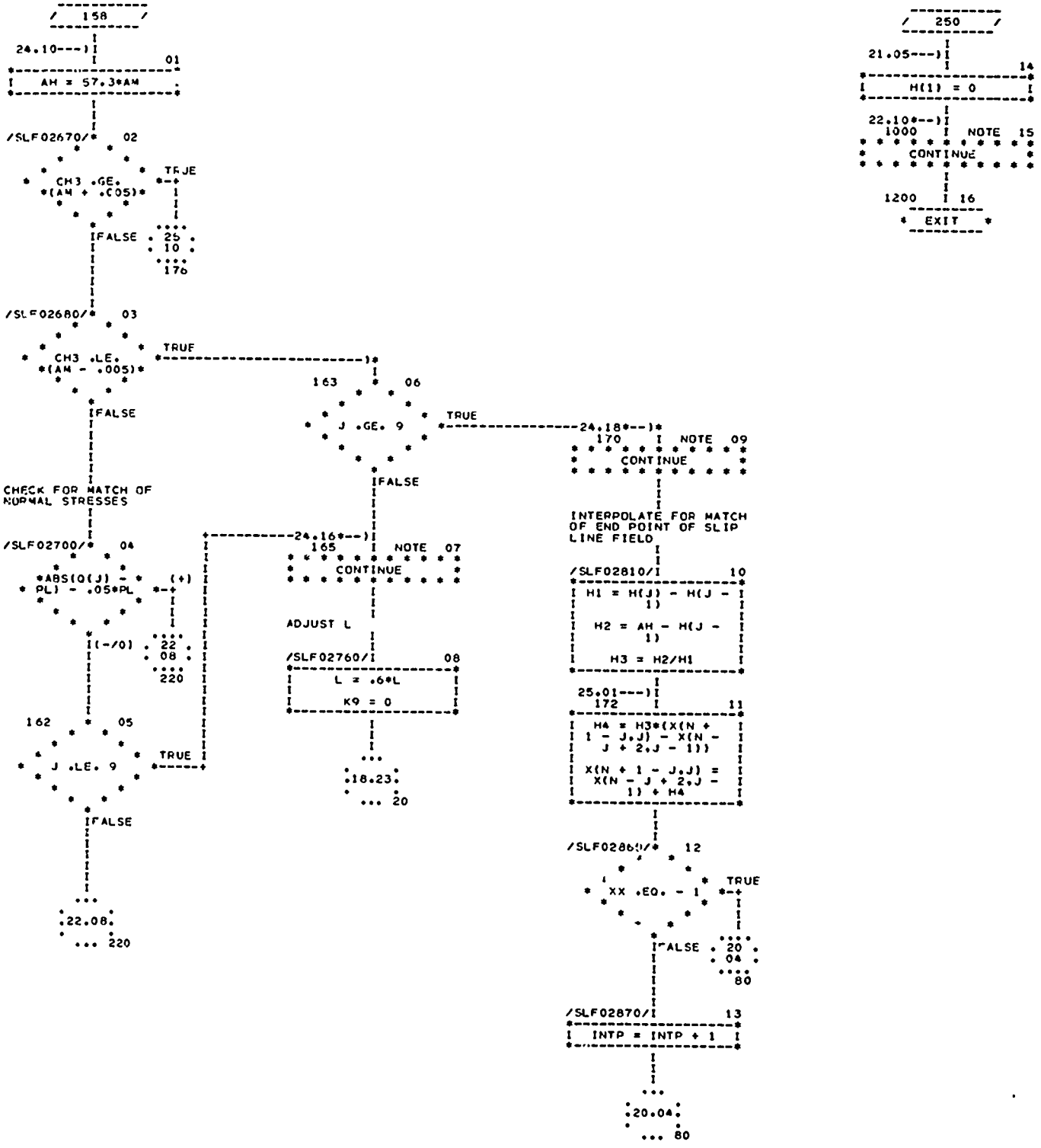

CHART TITLE - SUBROUTINE ACCE

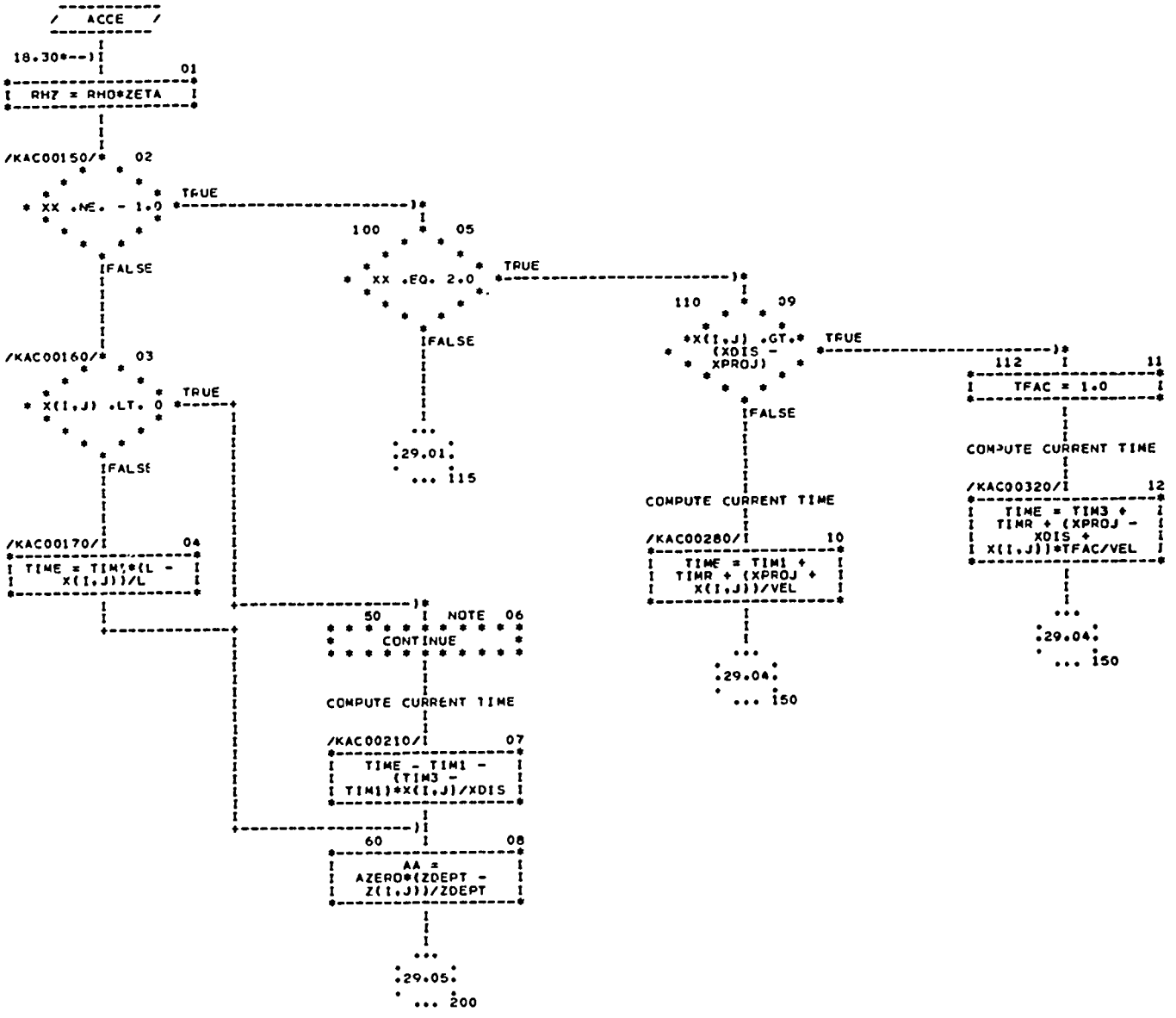

CHART TITLE - SUBROUTINE ACCE

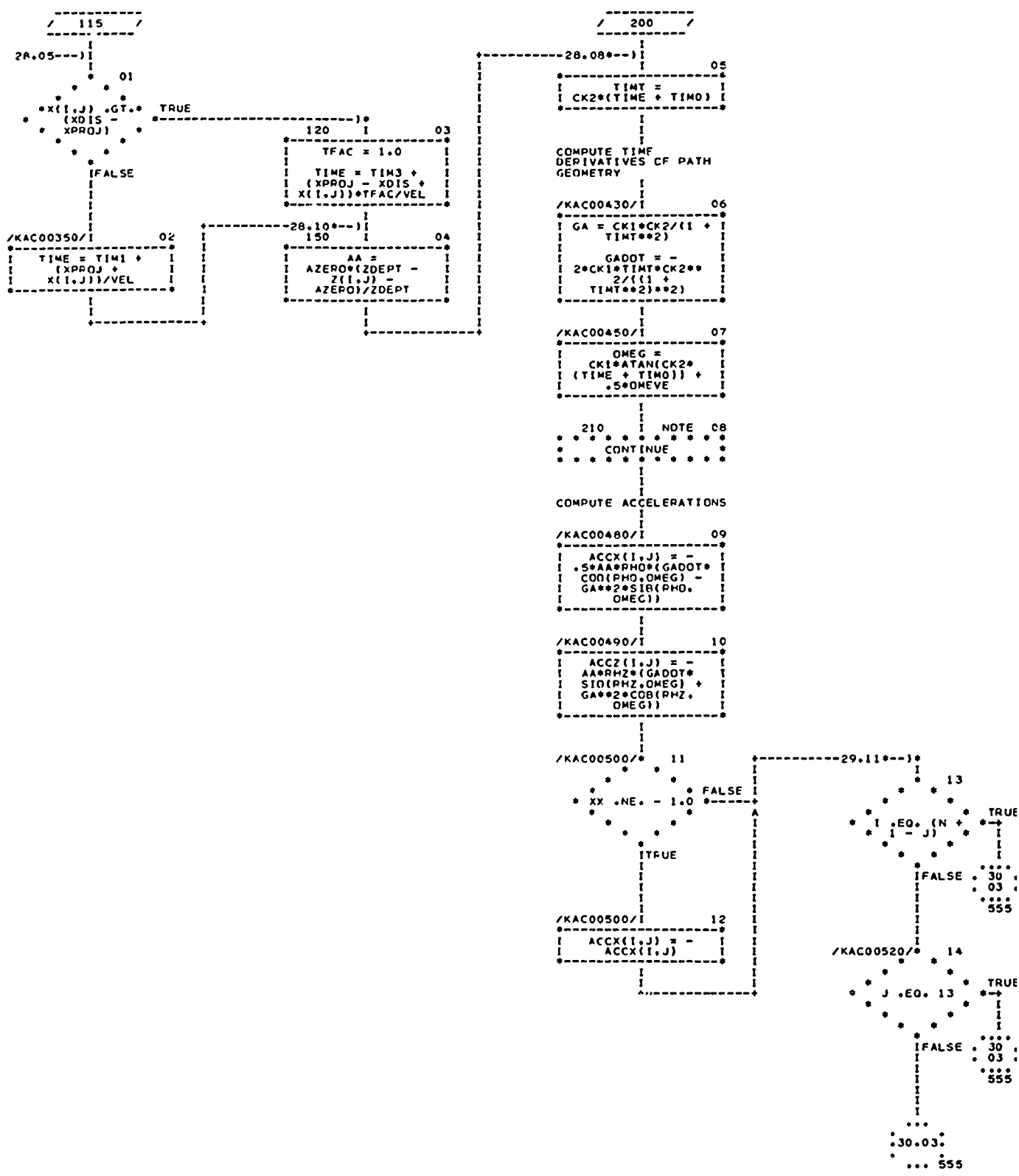

CHART TITLE - SUBROUTINE ACCE

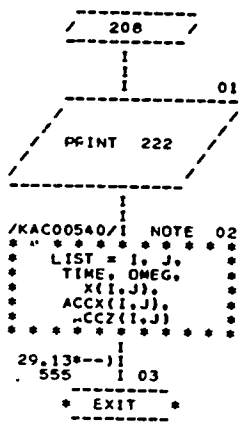

CHART TITLE - SUBROUTINE PLOTSL

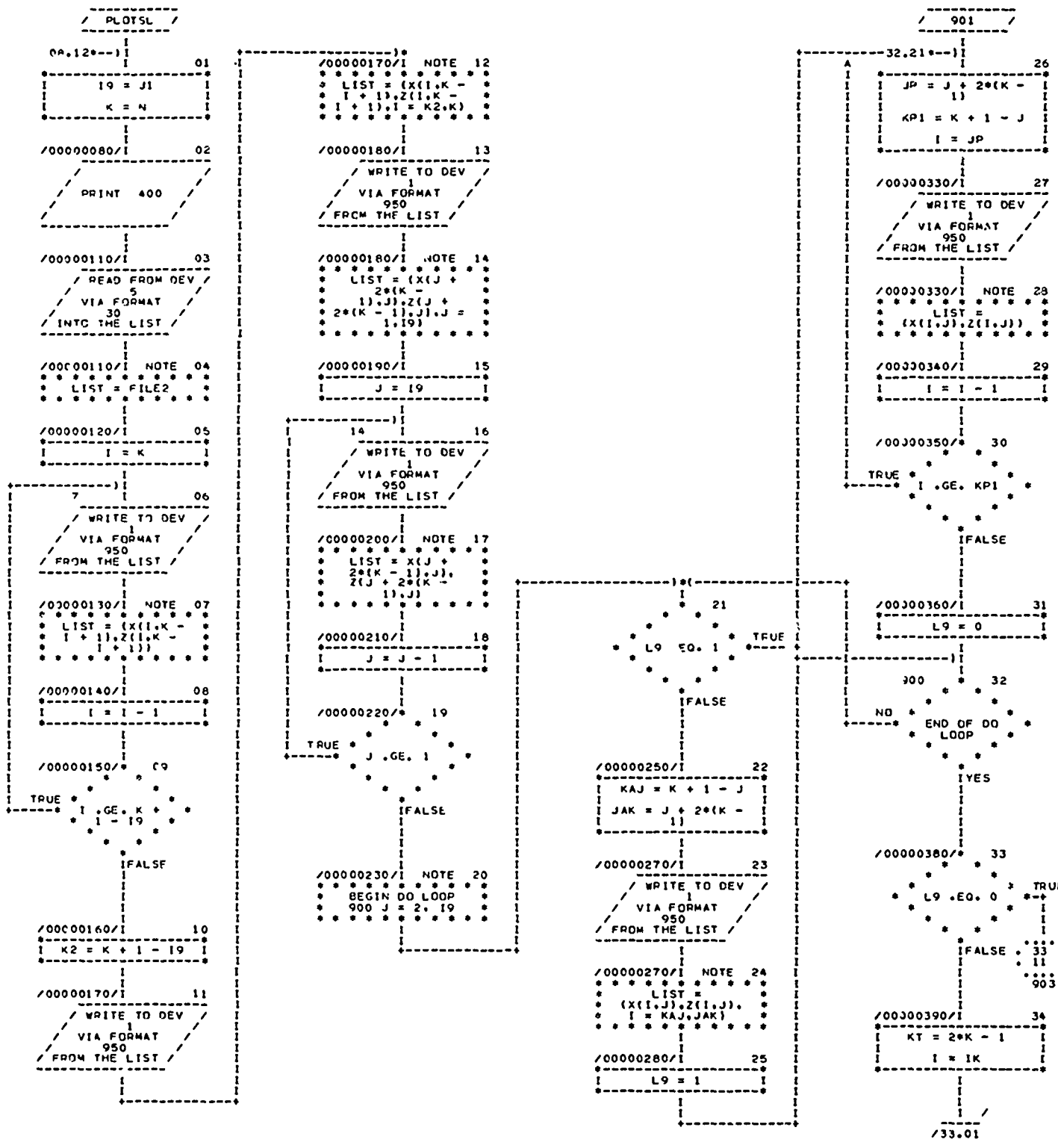

CHART TITLE - SUBROUTINE PLOTSL

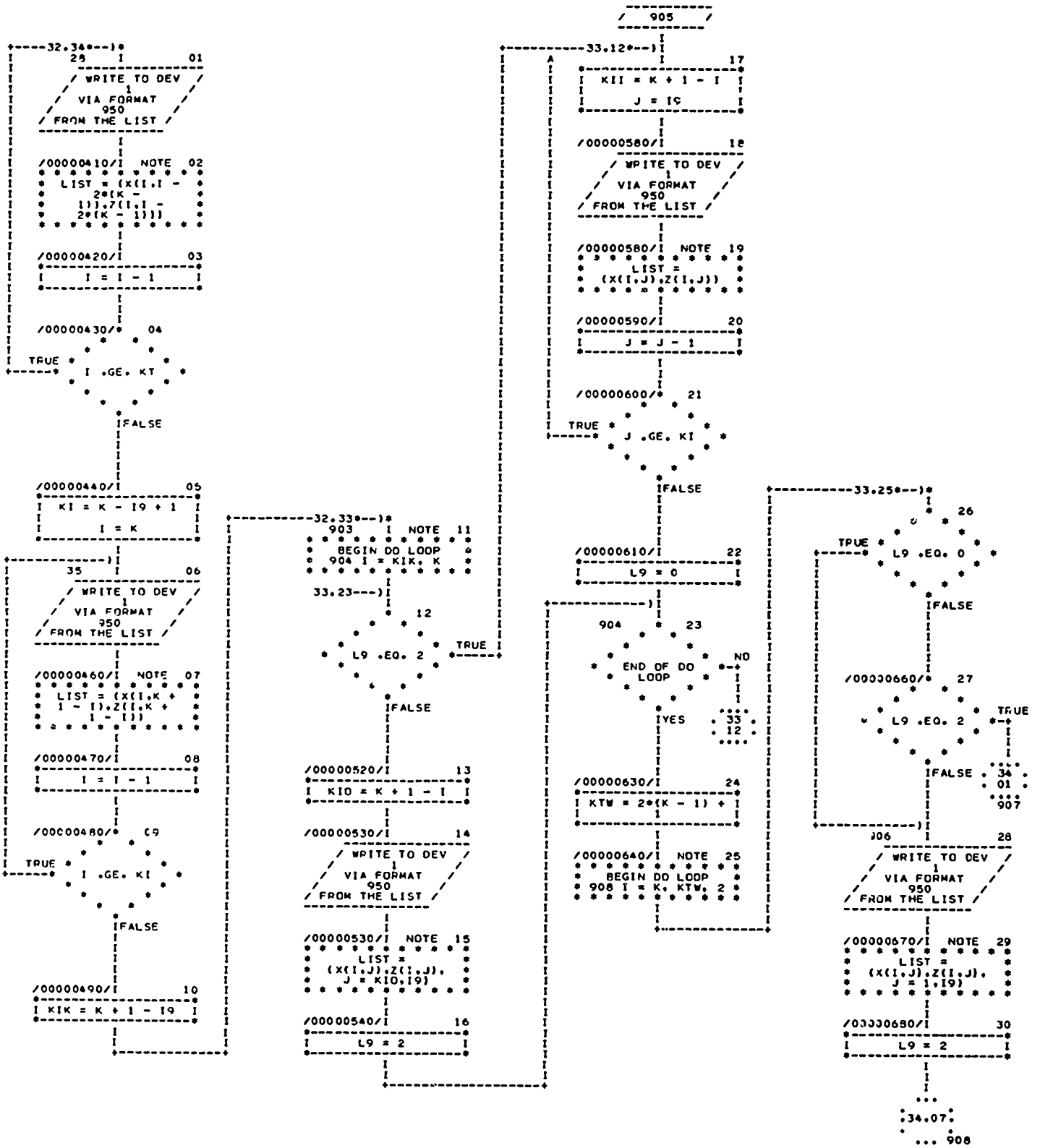

CHART TITLE - SUBROUTINE PLOTSL

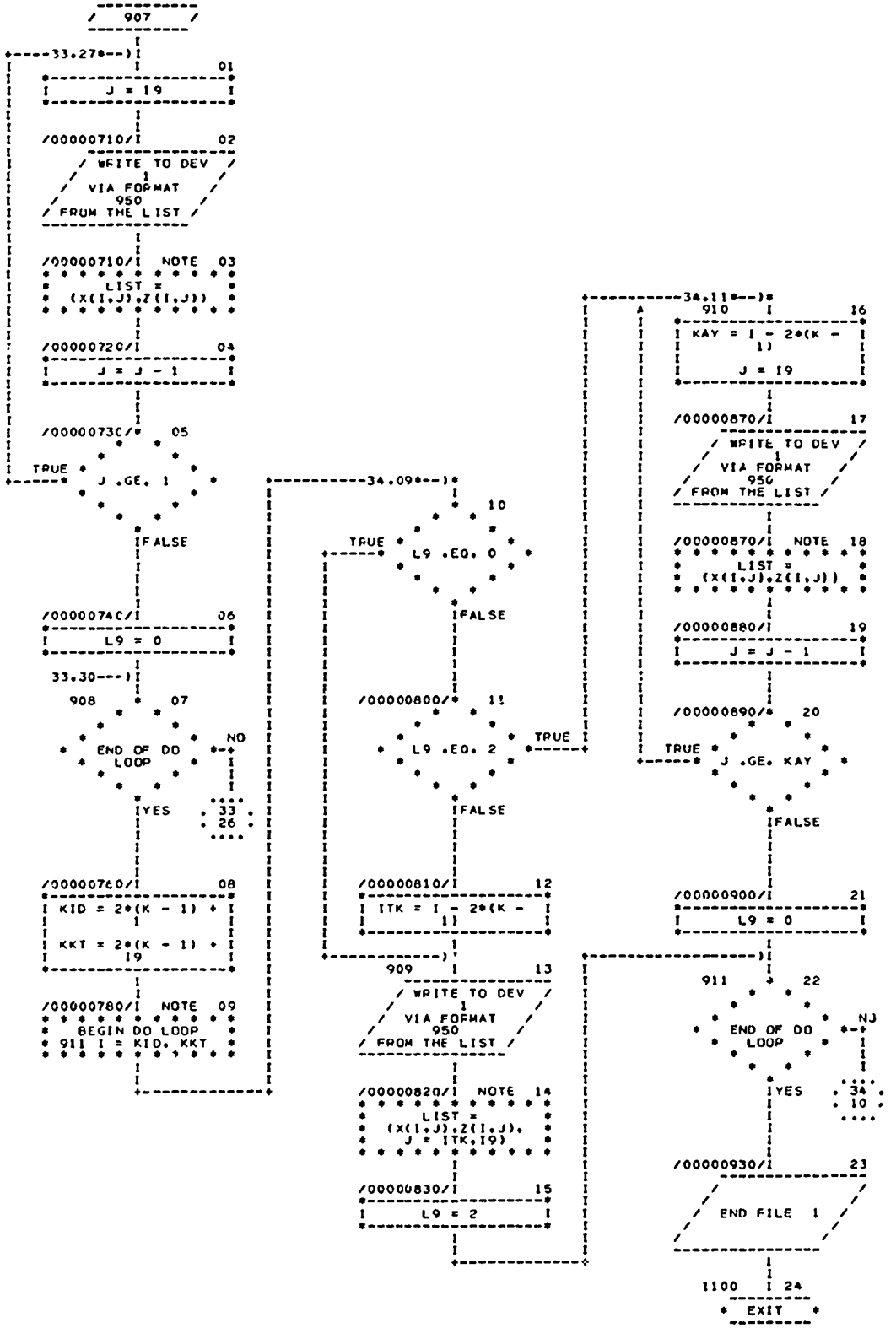

APPENDIX C

COMPUTER PROGRAM FLOW CHART FOR COMPUTATION OF TOWED FORCE COEFFICIENTS FOR PNEUMATIC TIRES

(Page 17 omitted)

CHART TITLE - INTRODUCTORY COMMENTS

THIS PROGRAM COMPUTES THE TOWING FORCE FOR INPUT VALUES READ
FROM DATA FILES IN THE FOLLOWING ORDER
CGR (CONE INDEX GRADIENT IN LBS/CU IN)
CI (CONE INDEX IN LBS/SQ IN)
RA (TIRE RADIUS IN FT)
OO (TIRE WIDTH IN FT)
LG (TIRE LOAD IN LBS)
PO (TIRE LIMIT PRESSURE IN LBS/SQ IN)
DE (DEFLECTION COEFFICIENT EPSILON)
DFAC (RATIO OF MAX. INTERF. FRICTION ANGLE TO FRICTION ANGLE)
AF (REAR ANGLE, INITIAL VALUE ASSUMED AS 10 DEGREES)
TAUFAC (FACTOR DEFINING ZERO SHEAR STRESS LOCATION)
CF (COHESION IN FRONT FIELD)
CR (COHESION IN REAR FIELD LBS/SQ FT)
FF (FRICTION ANGLE IN FRONT FIELD)
FR (FRICTION ANGLE IN REAR FIELD IN DEGREES)
GF (UNIT WEIGHT IN FRONT FIELD IN LBS/CU FT)
GR (UNIT WEIGHT IN REAR FIELD IN LBS/ CU FT)
MAIN VARIABLE DESIGNATIONS ARE
AAO= ENTRY ANGLE IN RADIANS
AAN= SEPARATION ANGLE IN RADIANS
AP= REAR ANGLE IN DEGREES
BI= BETA COEFFICIENT FOR LOG. SPIRAL
DI= INTERFACE FRICTION ANGLE IN RADIANS
PL= LIMITING PRESSURE IN LBS/SQ FT
RO= DEFORMED TIRE RADIUS
BNF= COMPUTED LOAD
BTP= COMUTED TOWING FORCE
BTT= COMPUTED TORQUE
MM(N) = CENTRAL ANGLE AT POINT N IN DEGREES
QQ(N) = NORMAL STRESS AT POINT N IN LBS/SQ FT
EE(N) = SHEAR STRESS AT POINT N IN LBS/SQ FT
UU(N) = X COORDINATE OF POINT N WITH REFERENCE TO TIRE AXIS
VV(N) = Z COORDINATE OF POINT N WITH REFERENCE TO TIRE AXIS
MAIN VARIABLE DESIGNATIONS IN THE SUBROUTINE ARE
X(I,J) = X COORDINATES OF POINT I,J
Z(I,J) = Z COORDINATES OF POINT I,J
S(I,J) = SIGMA AT POINT I,J
T(I,J) = THETA AT POINT I,J
A(J) = TANGENT OF DEFORMED CENTERLINE AT POINT J
D(J) = INTERFACE FRICTION ANGLE AT POINT J

CHART TITLE - PROCEDURES

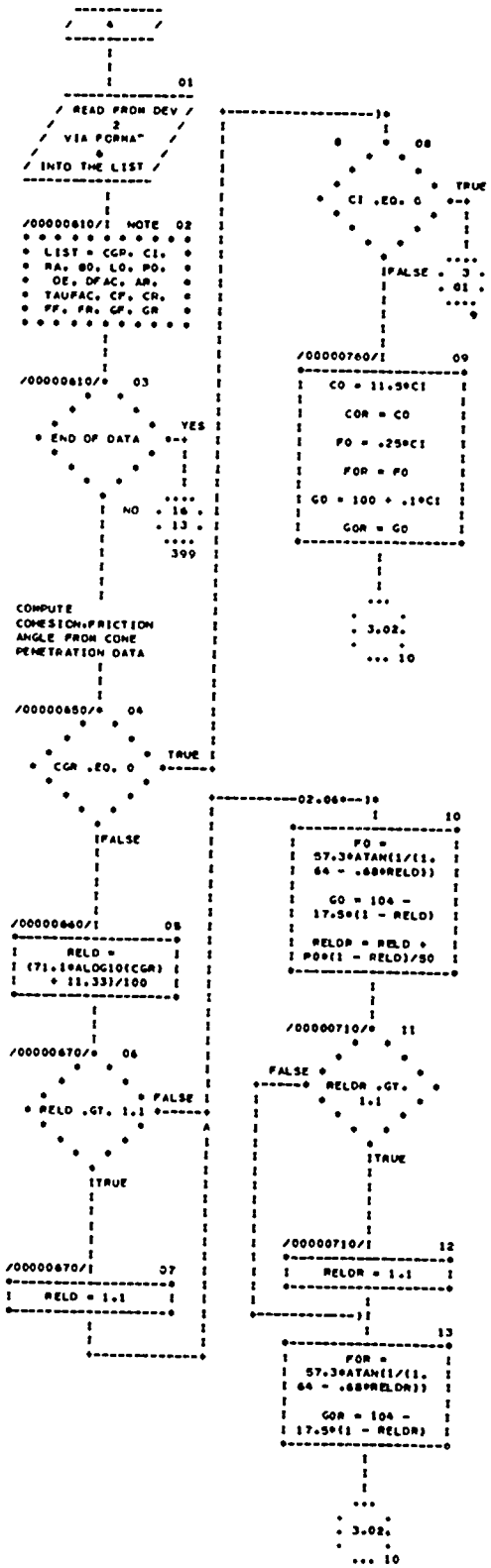

CHART TITLE - PROCEDURES

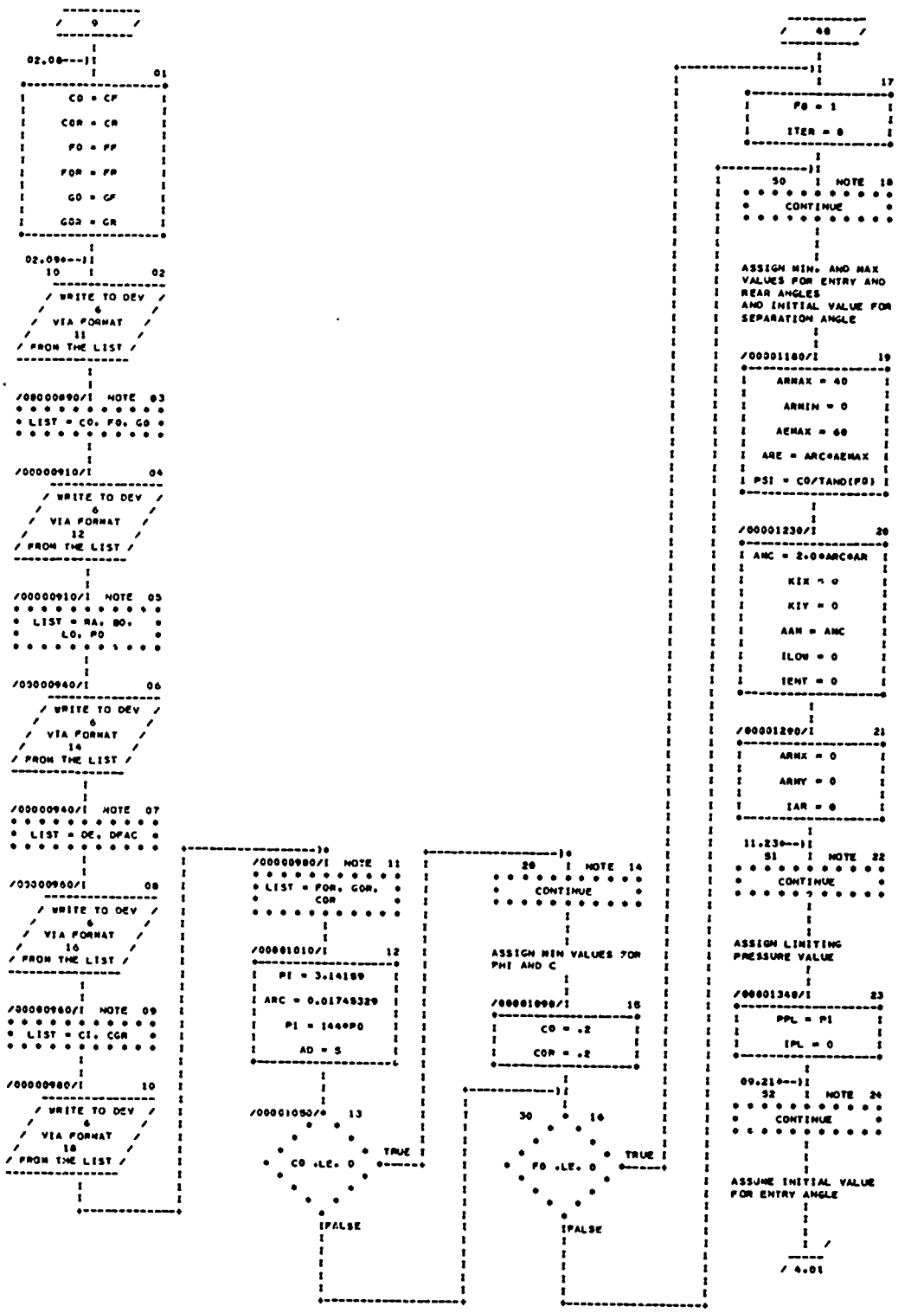

CHART TITLE - PROCEDURES

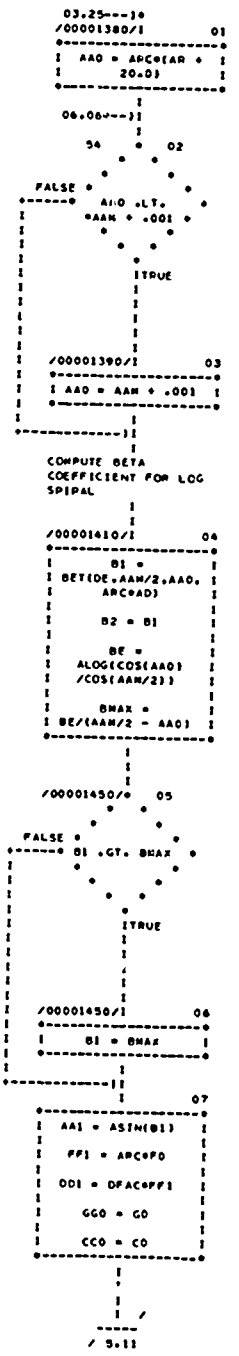

CHART TITLE - PROCEDURES

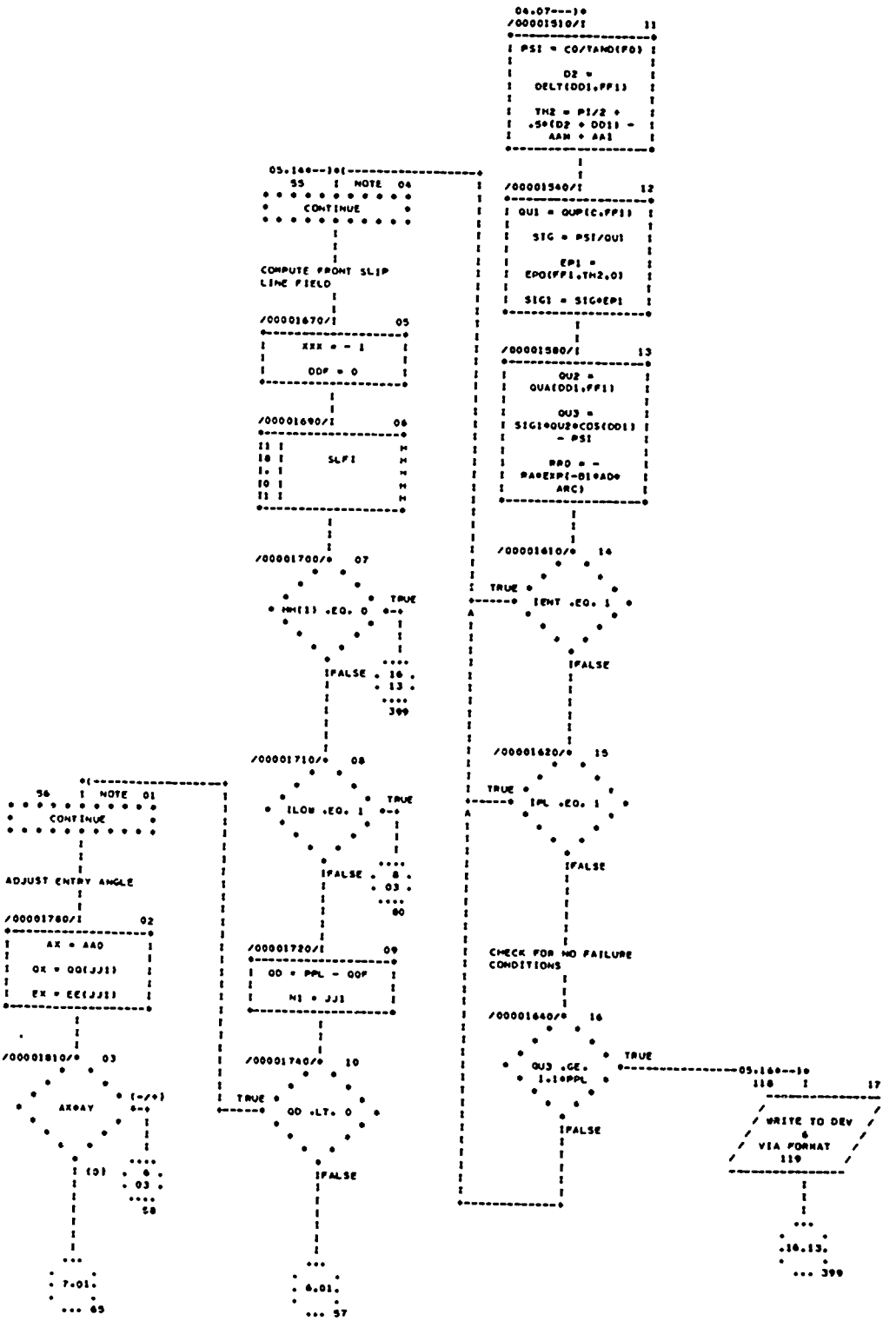

CHART TITLE - PROCEDURES

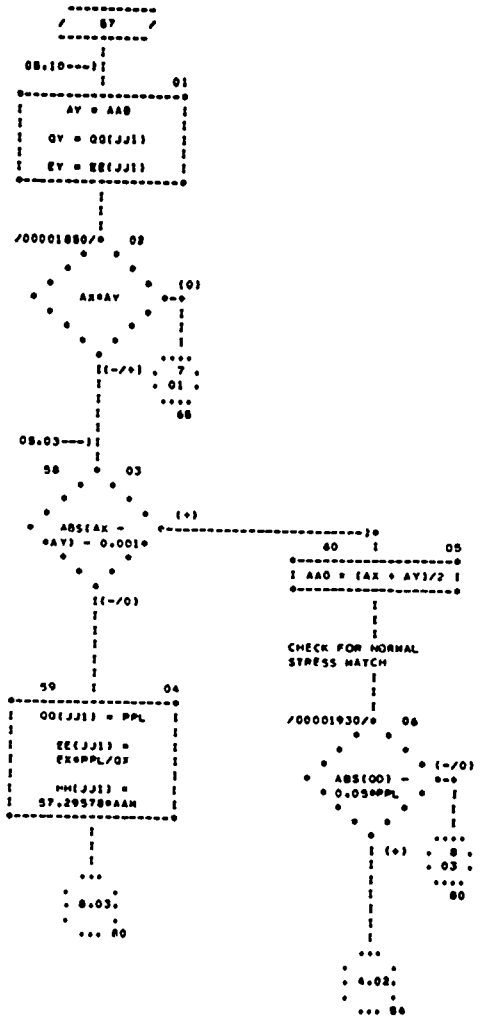

CHART TITLE - PROCEDURES

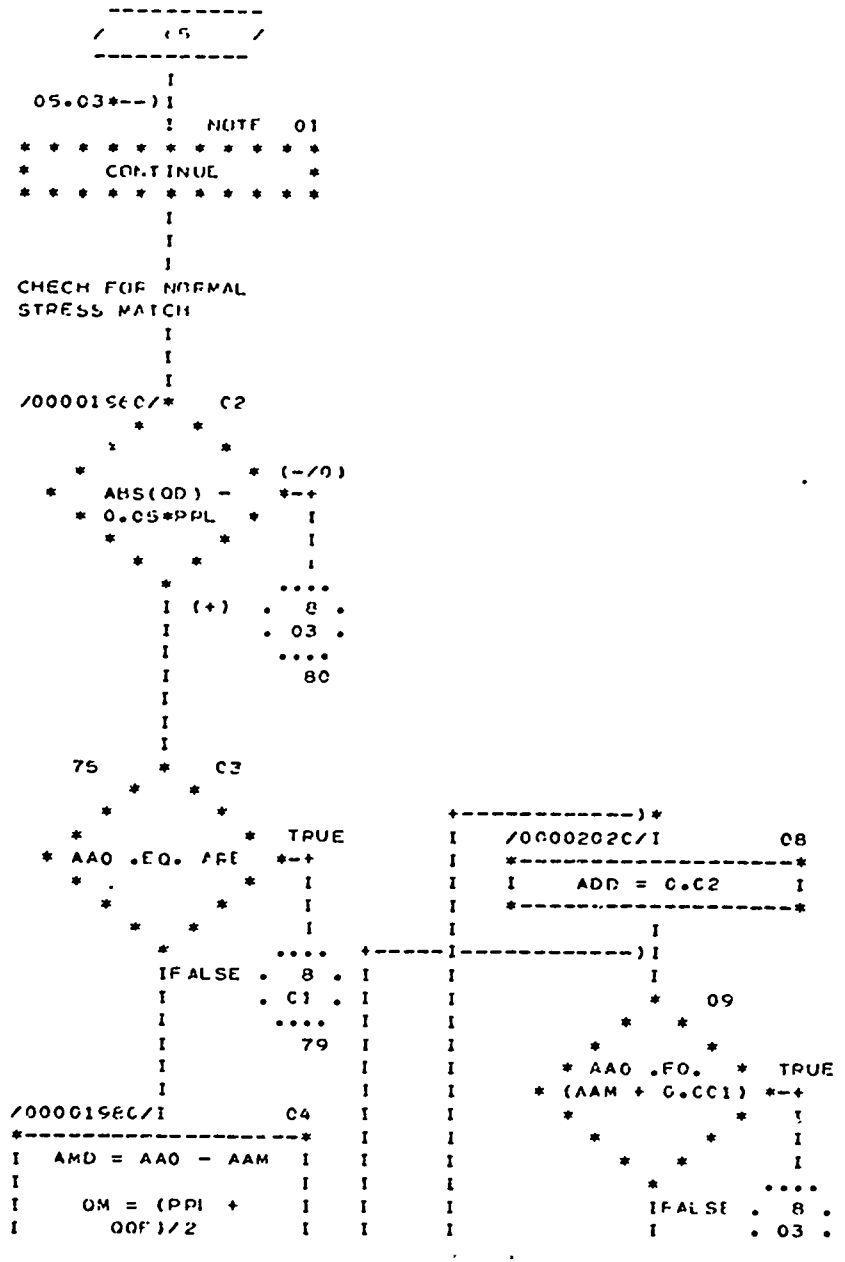

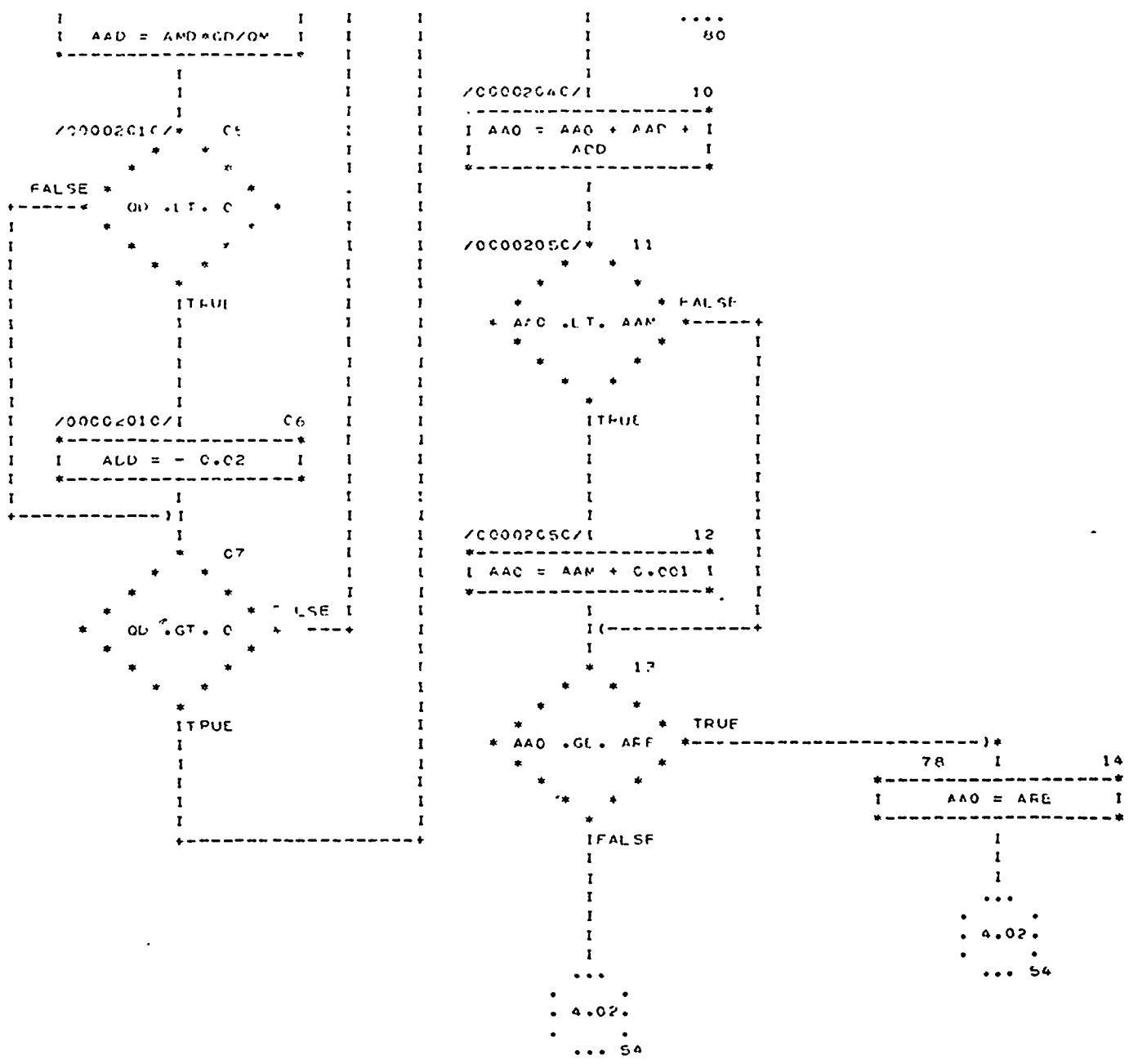
AAD = AMD*GD/DM
C5
FALSE
QD .LT. C
TRUE
C6
ALD = - C.02
C7
FALSE
QD .GT. C
TRUE
80
10
AAO = AAO + AAD + ACD
11
FALSE
A/C .LT. AAM
TRUE
12
AAC = AAM + C.001
13
TRUE
AAO .GE. ARE
78
14
AAO = ARE
4.02
54
4.02
54

CHART TITLE = PROCEDURES

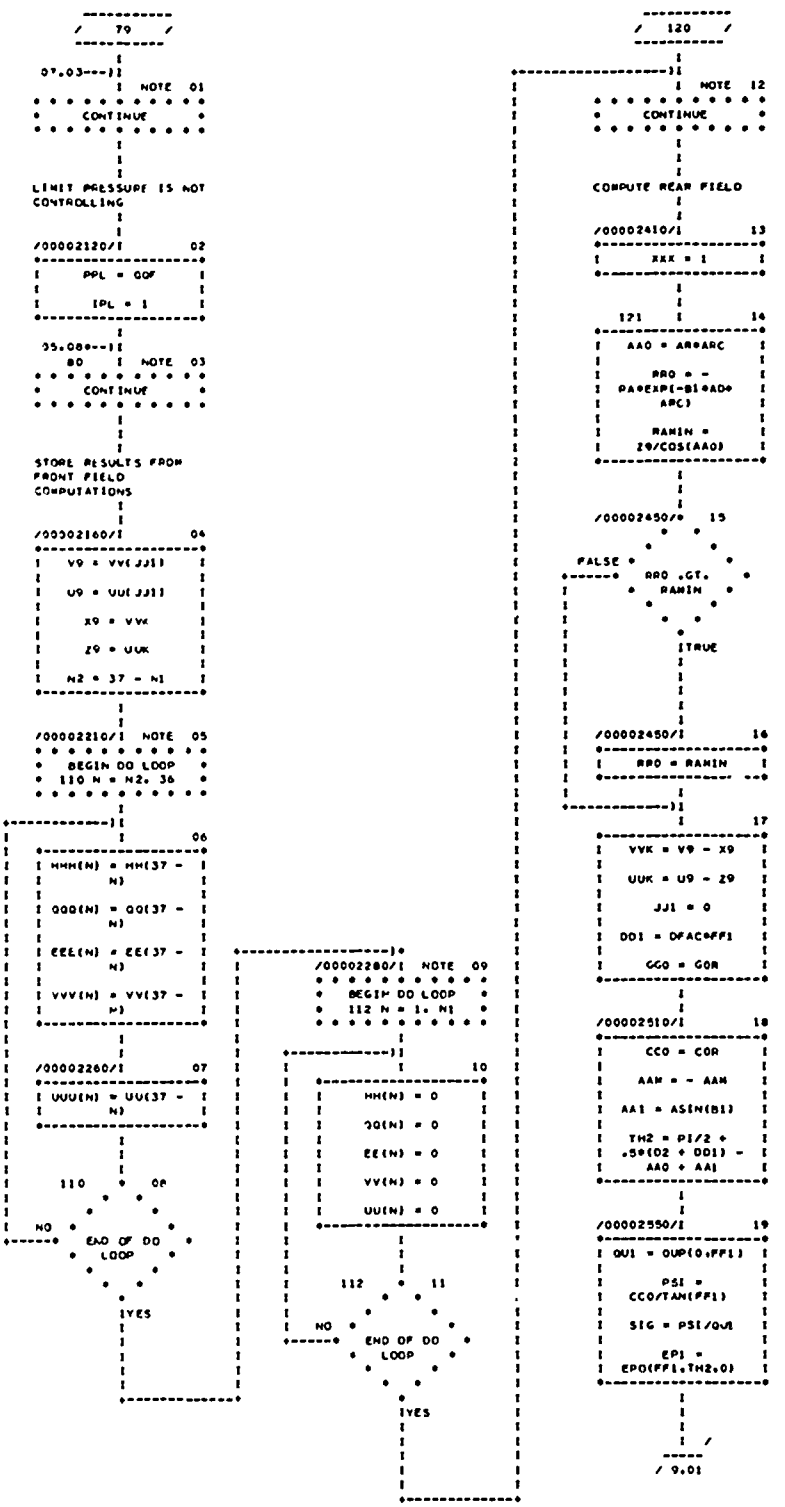

CHART TITLE - PROCEDURES

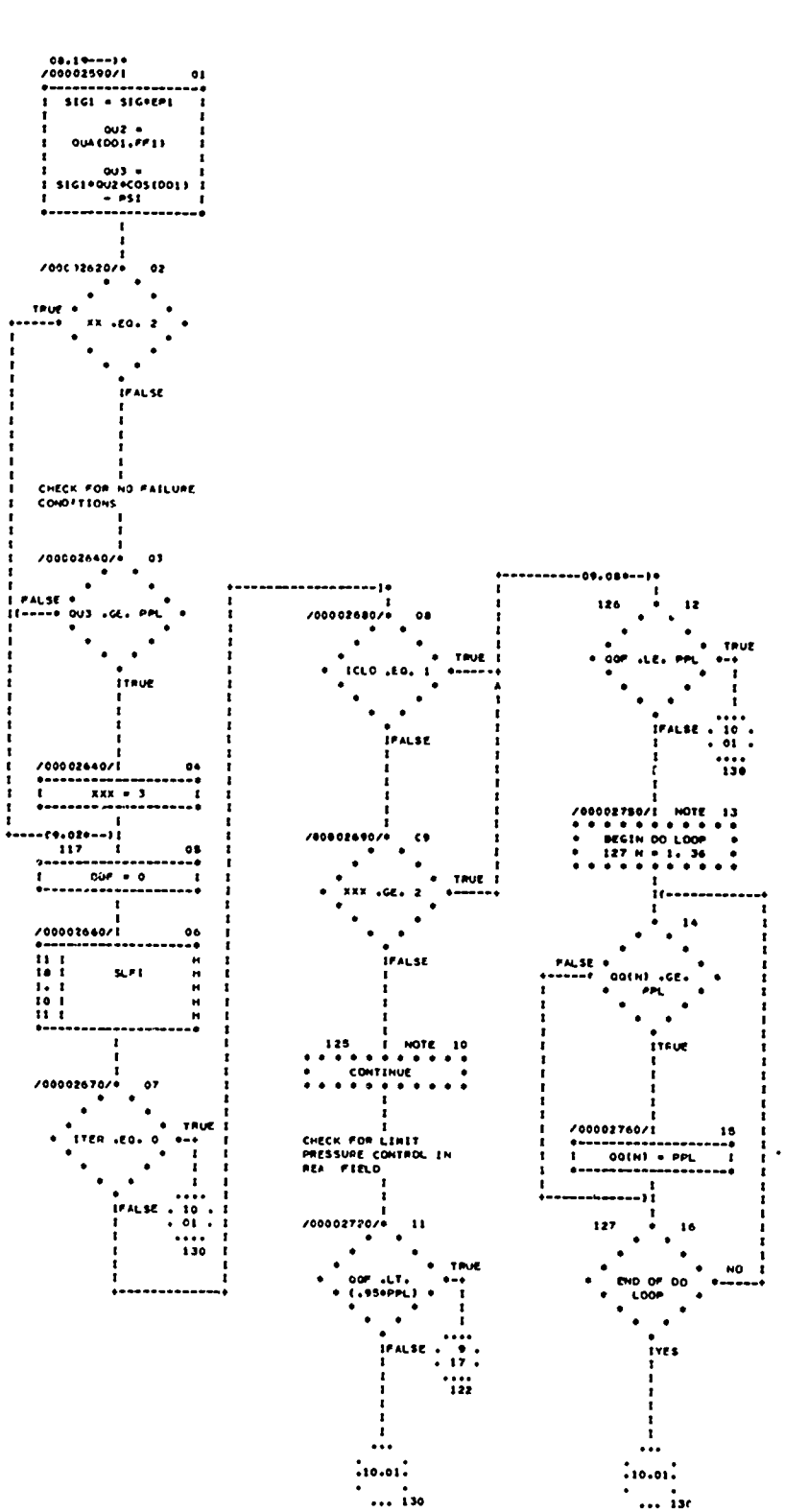

CHART TITLE - PROCEDURE$

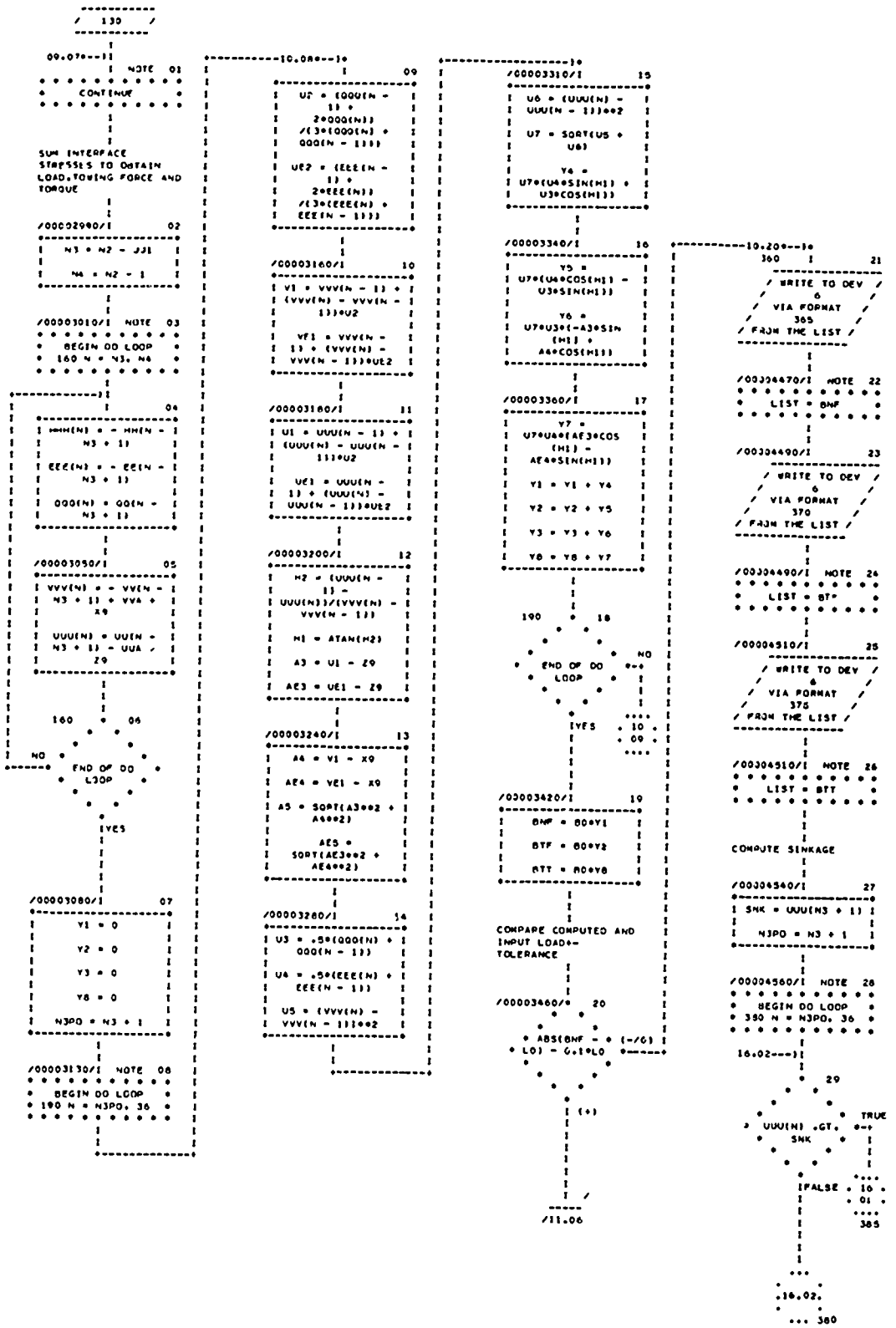

CHART TITLE - PROCEDURES

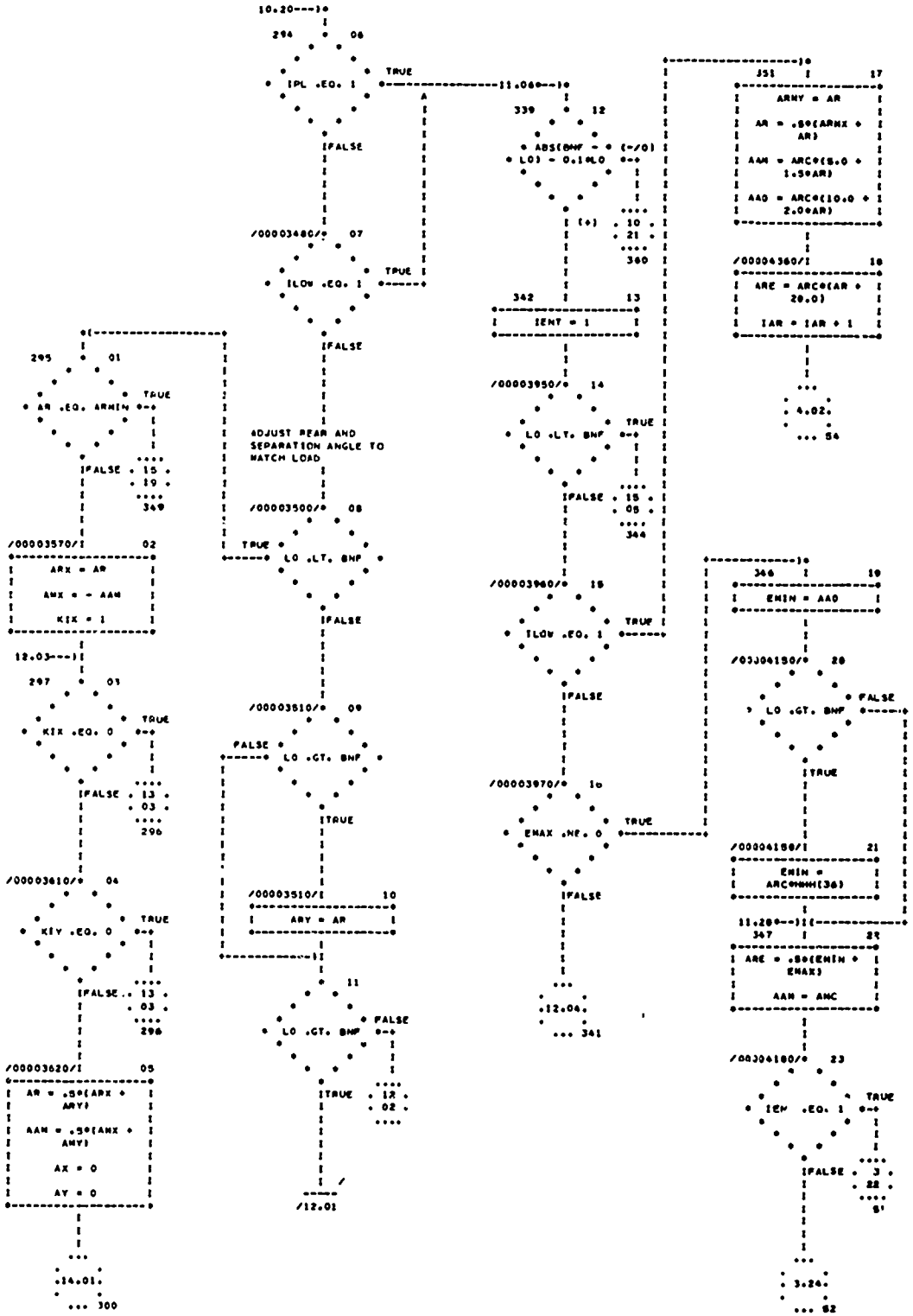

CHART TITLE - PROCEDURES

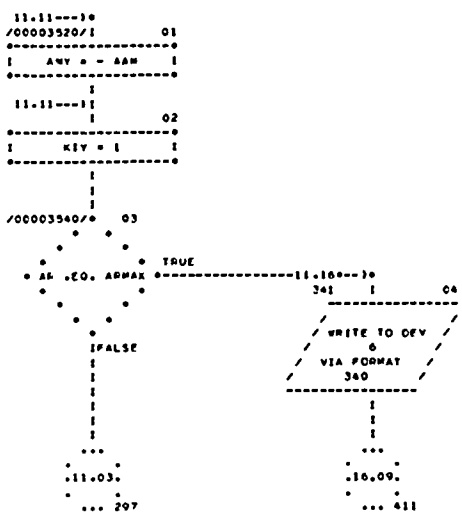

CHART TITLE - PROCEDURES

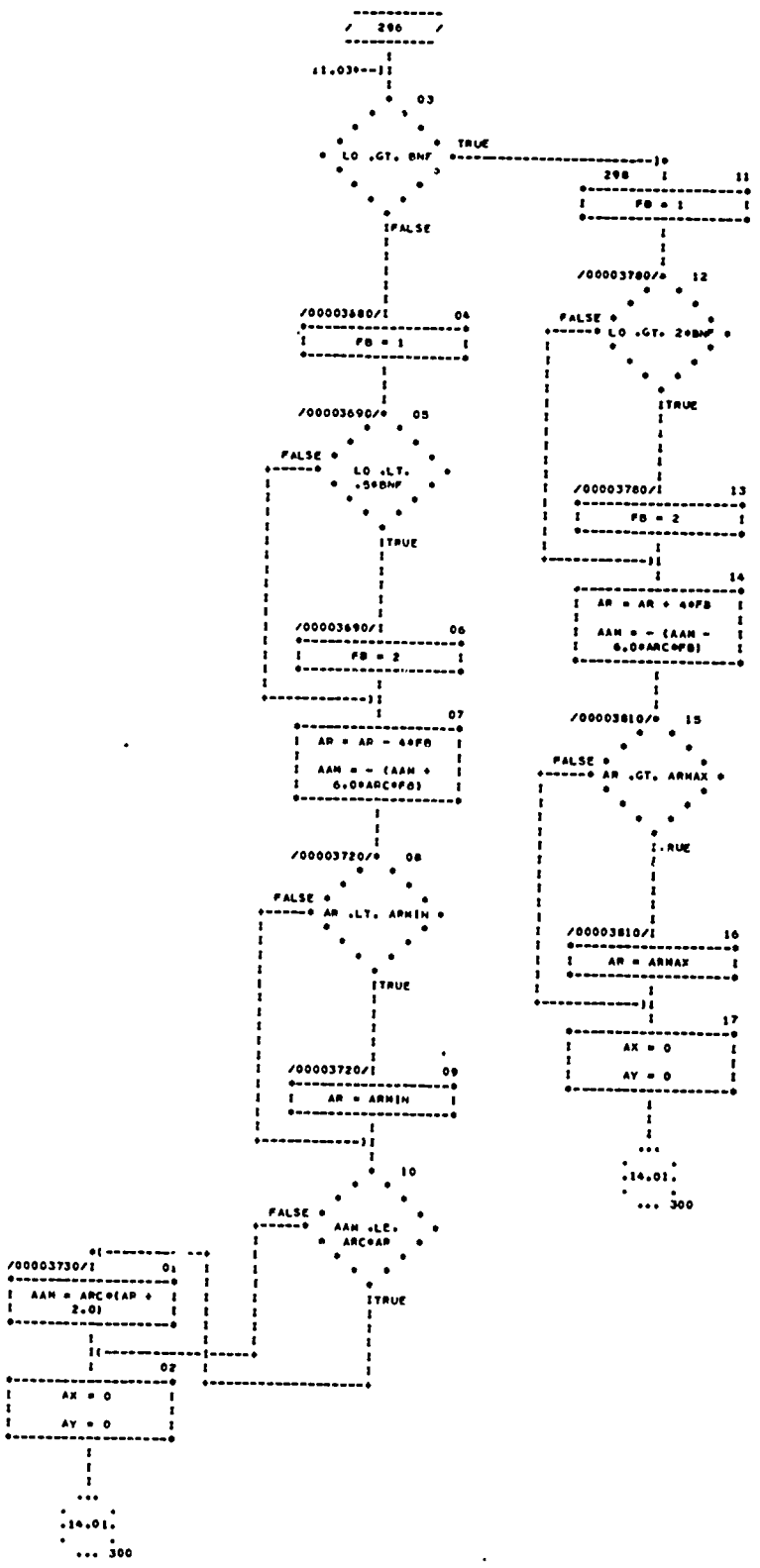

CHART TITLE = PROCEDURES

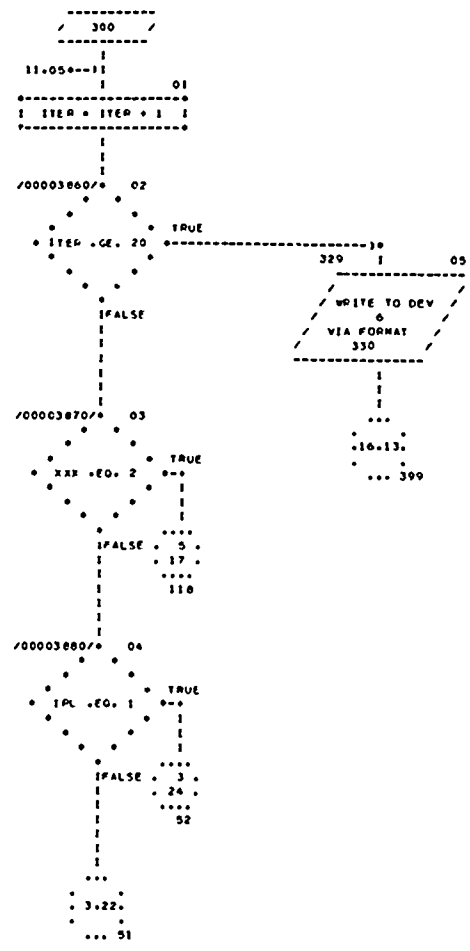

CHART TITLE - PROCEDURES

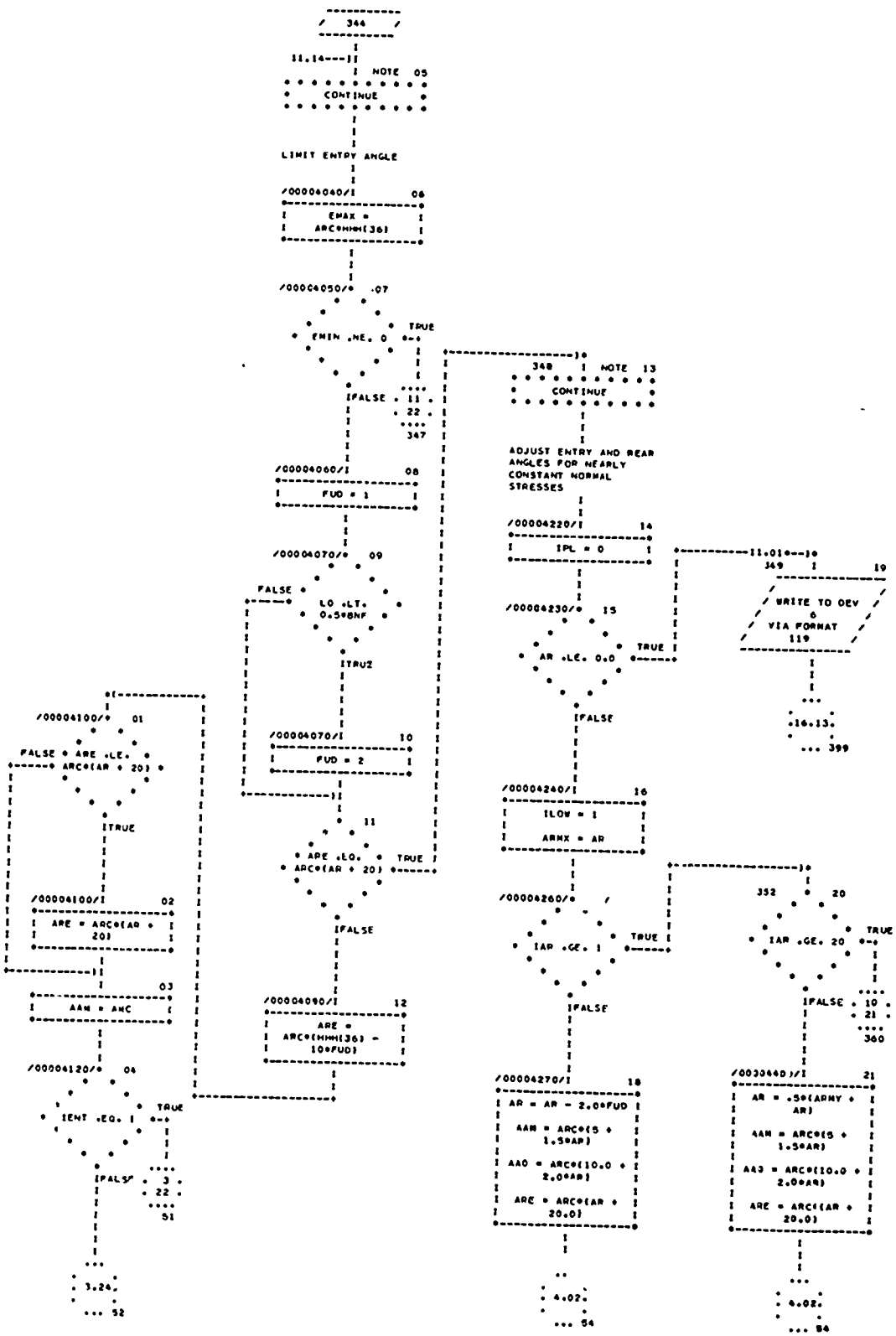

CHART TITLE - PROCEDURES

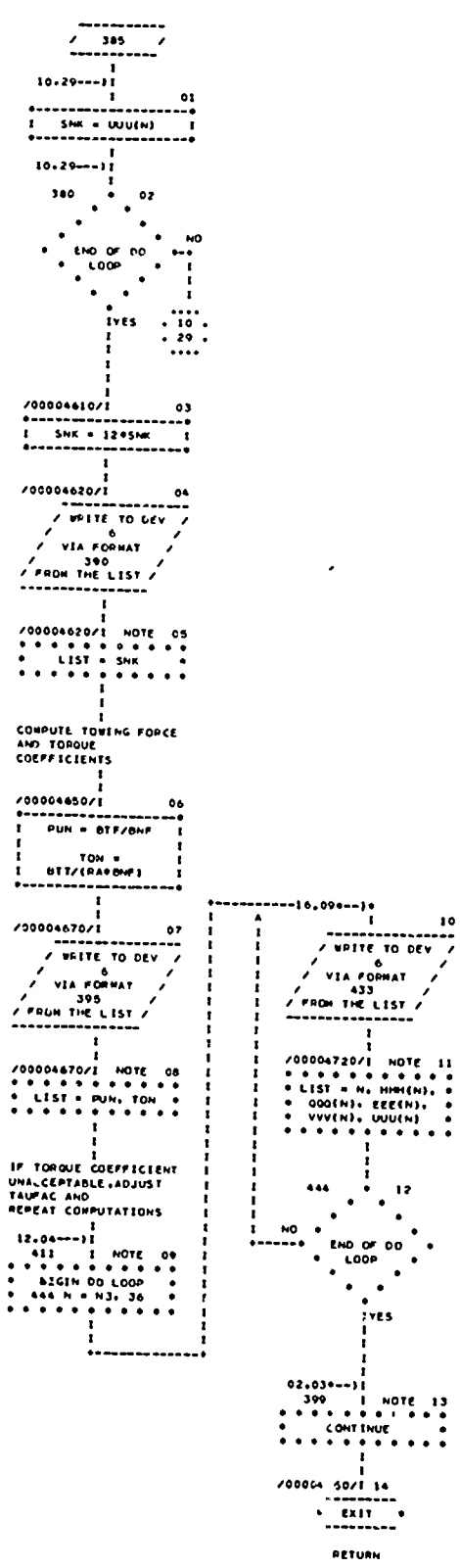

CHART TITLE - SUBROUTINE SLFI

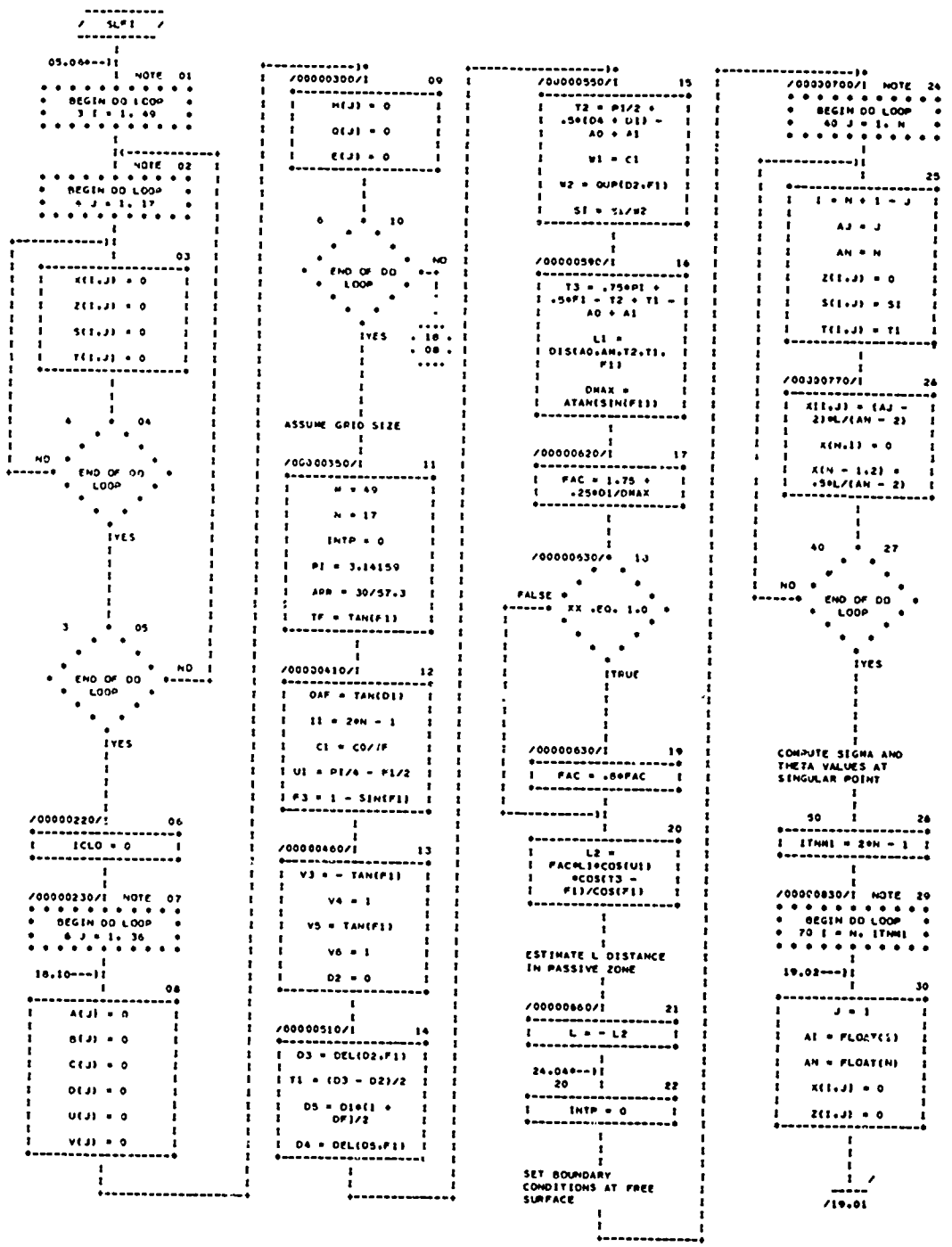

CHART TITLE - SUBROUTINE SLP1

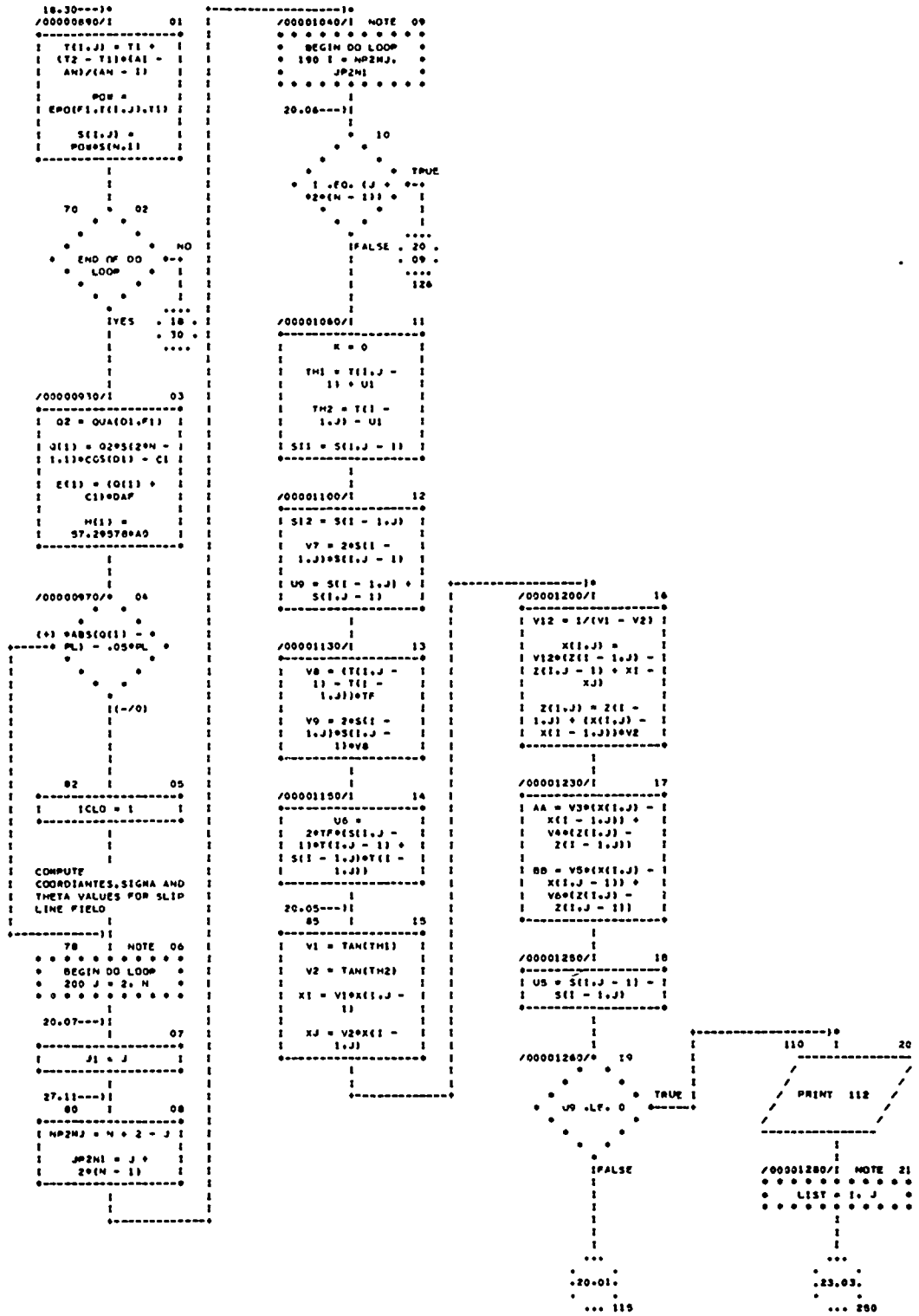

CHART TITLE = SUBROUTINE SLPI

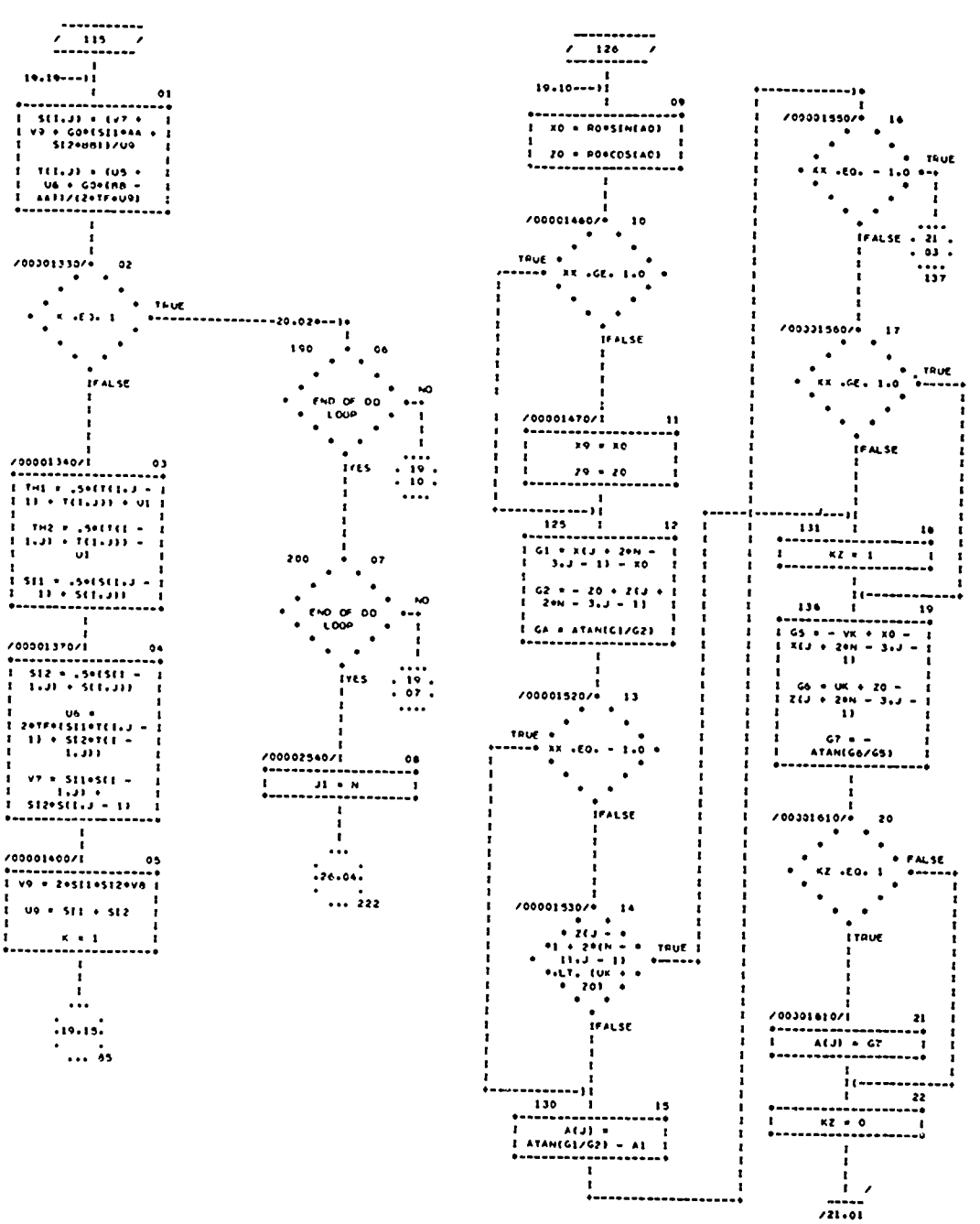

CHART TITLE - SUBROUTINE SLPI

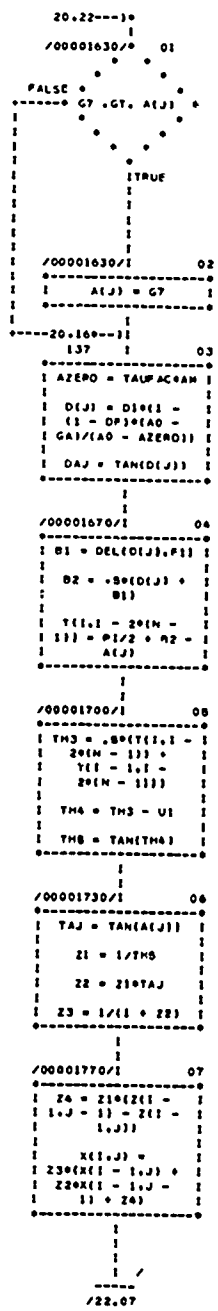

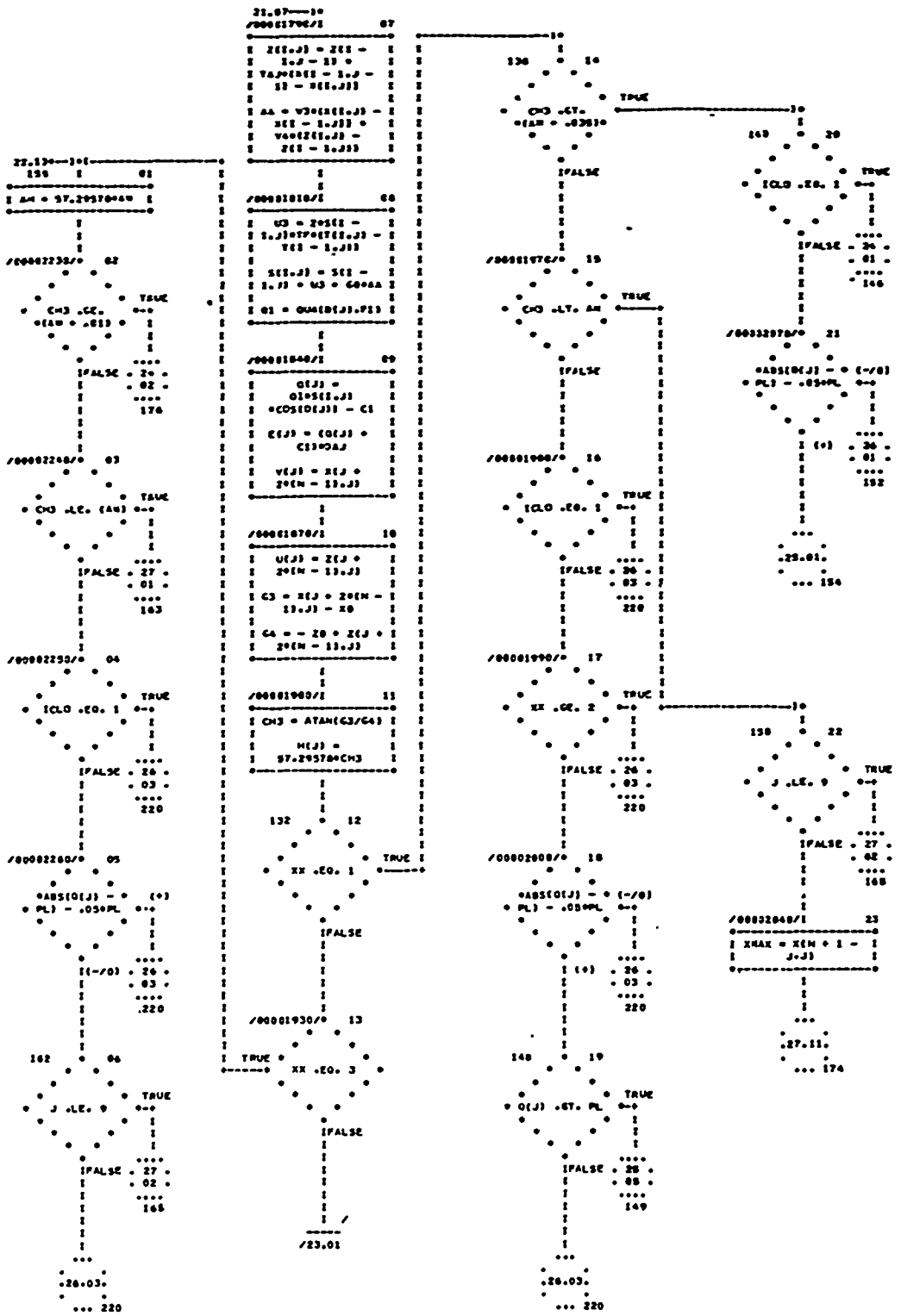

CHART TITLE - SUBROUTINE SLP1

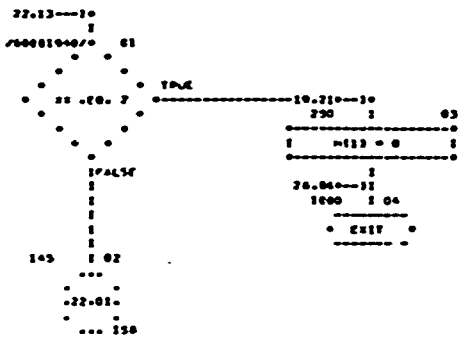

CHART TITLE - SUBROUTINE SLP1

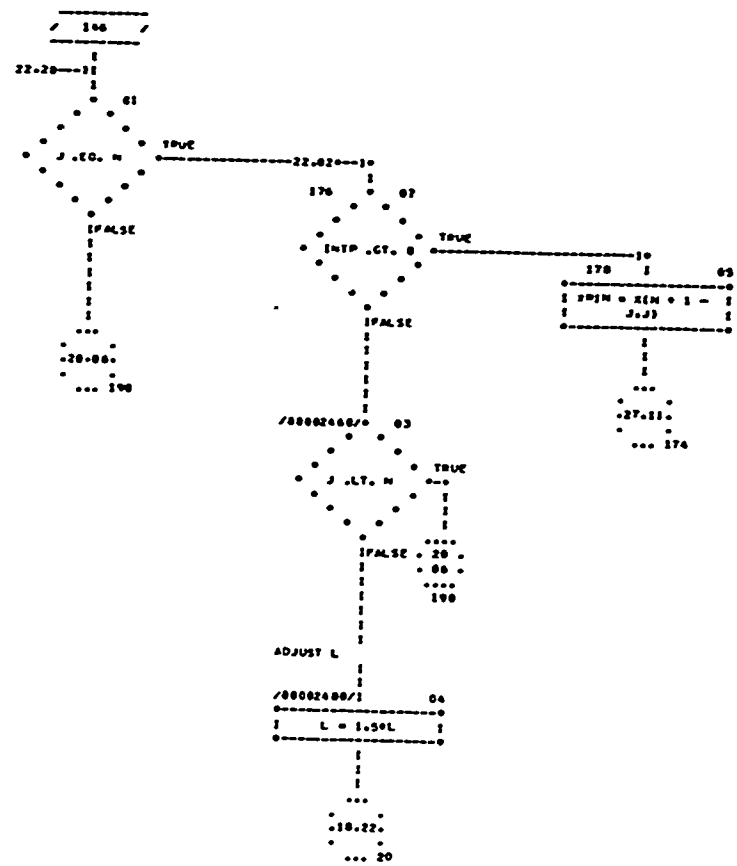

CHART TITLE = SUBROUTINE SLP1

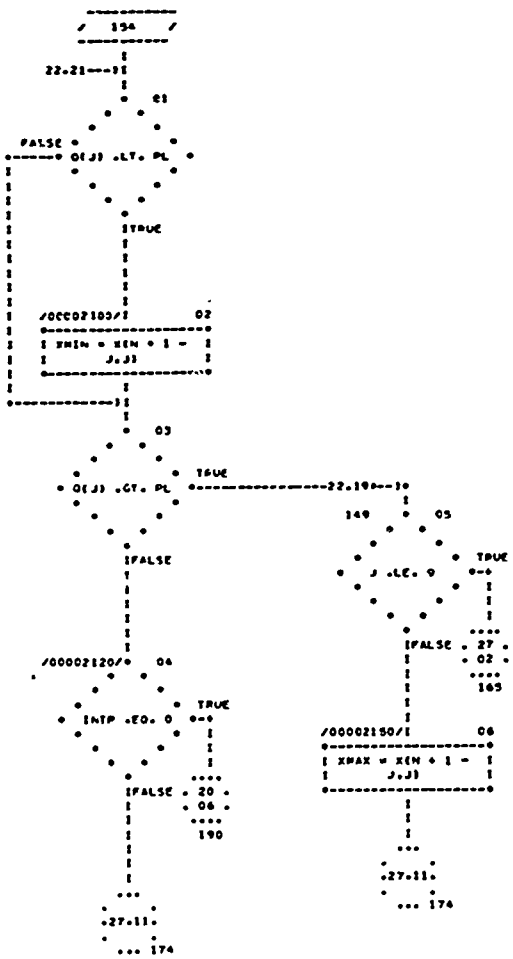

CHAR[illegible] - SUM[illegible] SIPI

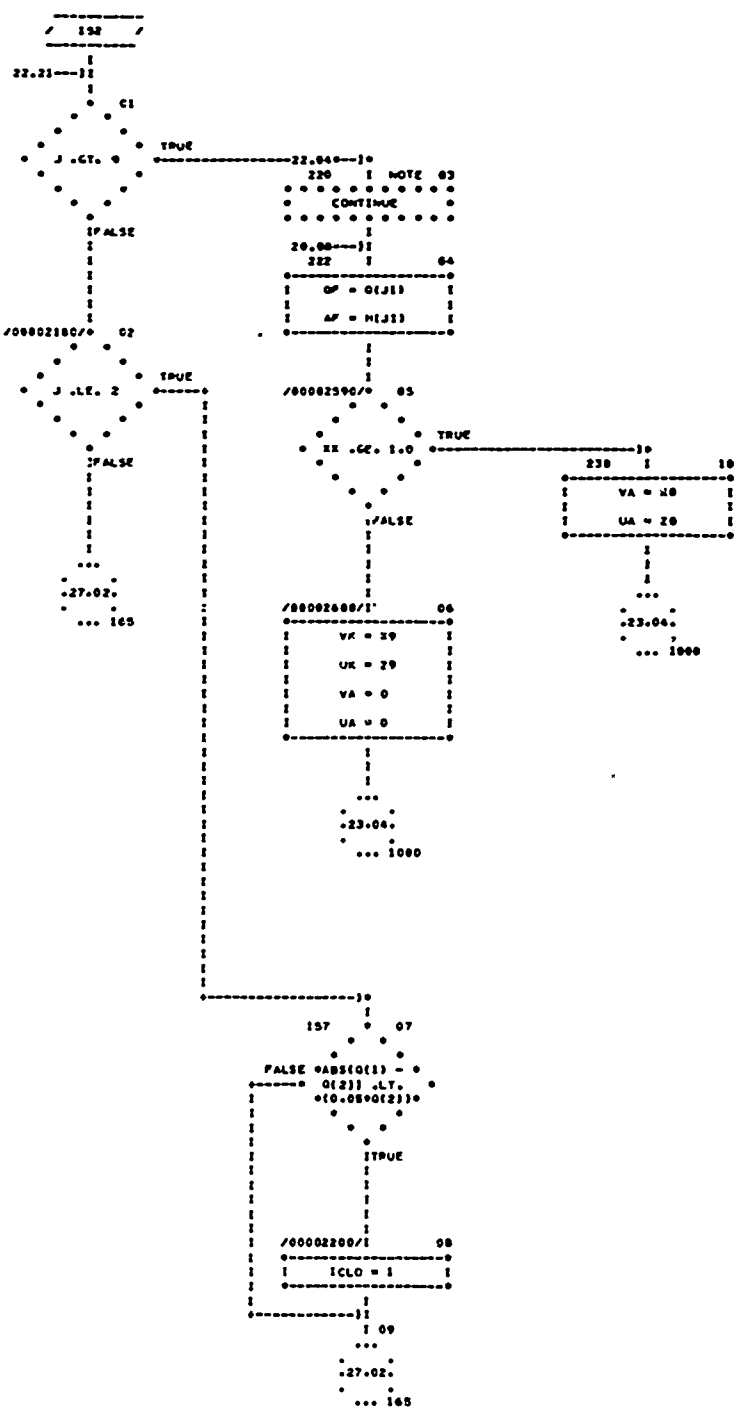

CHART TITLE - SUBROUTINE SLP1